The elucidation of the modes of action of moenomycin and corallorazine A

Dissertation

zur

Erlangung des Doktorgrades (Dr. rer. nat.)

der

Mathematisch-Naturwissenschaftlichen Fakultät

der

Rheinischen Friedrich-Wilhelms-Universität Bonn

vorgelegt von

Lisa Fritz

aus

Neuss

Bonn, 2023

Angefertigt mit Genehmigung der Mathematisch-Naturwissenschaftlichen Fakultät der

Rheinischen Friedrich-Wilhelms-Universität Bonn

1. Gutachterin: Prof. Dr. Tanja Schneider

2. Gutachter: Prof. Dr. Waldemar Vollmer

Tag der Promotion: 14.06.2024

Erscheinungsjahr: 2024

Meiner Oma und Gero, die niemals so ganz gegangen sind.

Abstract

Antimicrobial resistance poses a serious threat to public health worldwide. To overcome this global problem and ensure the supply of effective antibiotics for the therapy of infectious diseases in the future requires to develop innovative anti-infectives with unprecedented and resistance-breaking mechanisms of action and a thorough understanding of their antimicrobial effect on the molecular level. This work investigates the modes of action of two natural product antibiotics, moenomycin and corallorazine A, that target highly conserved structures located on different sites of the bacterial membrane.

The first part of this thesis is devoted to the phosphoglycolipid antibiotic moenomycin, a well-known, potent inhibitor of peptidoglycan glycosyltransferases. Here, it is shown for the first time that the antibiotic possesses an extended target spectrum in *Staphylococcus aureus* comprising LytR-CpsA-Psr (LCP) enzymes that catalyze the attachment of anionic glycopolymers, such as wall teichoic acids (WTAs) or capsular polysaccharides, to peptidoglycan in Gram-positive bacteria. I showed that LcpA, PBP4, and likely PBP2 are recruited to the septum of moenomycin-treated cells in response to the presumed accumulation of WTA precursors at the division site. Moreover, the combination of moenomycin and β-lactams was synergistic in MSSA1112 wildtype and the TarO-deprived SA113 strain but not in the MSSA1112 Δ*lcpABC* triple mutant, suggesting that moenomycin reduces the amount of WTAs and/or their attachment to the cell wall. Besides the identification of a so far unknown moenomycin off-target, the results provide new insights into the temporal and spatial coordination of the peptidoglycan and WTA biosynthesis pathways in moenomycin-treated *S. aureus* cells and could contribute to the development of novel, moenomycin-based antibiotics.

The second part of this thesis focuses on the recently discovered lipodipeptide corallorazine A, a bioactive secondary metabolite synthesized by the myxobacterium *Corallococcus coralloides*. Using whole cell analysis and *in vitro* test systems, this work reveals that corallorazine A inhibits the bacterial transcription by targeting the β'-subunit of the DNA-dependent RNA polymerase, a conserved target for antibiotics in prokaryotes. Corallorazine A displayed good antimicrobial activity against Gram-positive bacteria, including methicillin-resistant *S. aureus*, and could serve as an urgently required broad-spectrum antibiotic.

In summary, this work significantly enhances our understanding of how the antibiotics moenomycin and corallorazine A target relevant bacterial cellular structures.

Acknowledgments

First and foremost, I have to thank my thesis adviser, Prof. Dr. Tanja Schneider, for her invaluable patience, understanding, and outstanding feedback. I would also like to express my profound gratitude to Prof. Dr. Waldemar Vollmer for his unlimited support and invaluable advice throughout my PhD journey. Moreover, I would like to acknowledge my committee, including Prof. Dr. Haas and Prof. Dr. Kubitschek.

This endeavor would not have been possible without the generous support from the Jürgen Manchot Foundation, the German Research Foundation, and the German Center for Infection Research, who financed my research.

It has been an honor and privilege to work in this lab along with my colleagues and friends, to all of whom I owe gratitude: Dr. Marvin Rausch and Dr. Julia Deisinger for taking me under their wings when I started my journey as an inexperienced student, Dr. Christian Fritz Otten for keeping my head up high, Dr. Stefania De Benedetti for her empathy, patience, and deep friendship, Dr. Anna Müller for her tenacity and perseverance, Dr. Fabian Grein, our radiation protection commissioner, Karina Boltersdorf for moral support and advice, our lab-technicians and fellow students, particularly my lab-mates Martin Daniel, Julia Dannenberg, and Kevin Ludwig for their great humor.

Thanks also to Dr. Daniela Vollmer, Master Dr. Jacob Biboy, and the rest of the Vollmer lab family for treating me like one of their own and making my research stays in Newcastle unforgettable.

I would like to thank our collaborators and their research fellows, especially Dr. Max Crüsemann, Prof. Dr. Gabriele Bierbaum, Prof. Dr. Matthias Geyer, Prof. Dr. Dirk Menche, Prof. Dr. Tomoya Tsukazaki, and all members of the Institute for Microbiology and Biotechnology of the University of Bonn for their passionate support and input.

I am deeply thankful for the supervision of many diligent students over the years and I hope to have encouraged them to pursue a scientific career.

Finally, I must thank my parents, grand-parents, and friends, particularly Gero Wilbring, Alina Dietrich, and Farah Hussain for having my back when no one else did.

Abbreviations

°C	degree Celsius
2YT	double-strength yeast extract-tryptone broth
A	ampere
A_X	absorbance at X nm
aa	amino acids
ABC	ATP-binding cassette
ACAD	acyl-CoA dehydrogenase
ACP	acyl carrier protein
AM	amidase
anhydroMur*N*Ac	1,6-anhydro-*N*-acetylmuramic acid
approx.	approximately
APS	ammonium peroxodisulfate
Asp	aspartic acid
ATP	adenosine 5'-triphosphate
BDP	BODIPY (boron-dipyrromethene)
BGC	biosynthetic gene cluster
Bis-Tris	2-[bis(2-hydroxyethyl)amino]-2-(hydroxymethyl)propane-1,3-diol
bp	base pair
BSA	bovine serum albumin
BuOH/PyrAc	*n*-butanol/pyridine acetate
C	condensation domain
C_{55}-OH	undecaprenol
C_{55}-P(P)	undecaprenyl (pyro)phosphate
CAL	acyl-CoA ligase
CAMP	cationic antimicrobial peptide
cat	catalytic domain
CDP	cytidine 5'-diphosphate
CFU	colony forming unit(s)
Ci	Curie
CLSI	Clinical and Laboratory Standards Institute
Cm^R	resistant to chloramphenicol
CoA	coenzyme A
CP	capsular polysaccharide
ctrl	control
CWSS	cell wall stress stimulon
Da	dalton
DDM	*n*-dodecyl β-D-maltoside
DEAE	diethylethanolamine
Dha	dehydroalanine
DMSO	dimethyl sulfoxide
DNA	deoxyribonucleic acid

DNase	deoxyribonuclease
dNTPs	deoxynucleoside 5’-triphosphates
DOPG	1,2-dioleoyl-*sn*-glycero-3-phospho-(1'-rac-glycerol)
DTT	dithiothreitol
e.g.	from Latin *exempli gratia*, meaning “for example”
EDTA	ethylenediaminetetraacetic acid
Em^R	resistant to erythromycin
et al.	from Latin *et alii*, meaning “and others”
Ex	elution fraction number x
FA	fluorescence anisotropy
FIC	fractional inhibitory concentration
FITC	fluorescein isothiocyanate
FR	fluorescent ratio
(D/L-)Fuc*N*Ac	*N*-acetyl-D/L-fucosamine
g	gram
g	standard gravity
GFP	green fluorescent protein
(D-)Glc*N*Ac	*N*-acetyl-D-glucosamine
Gly	glycine
GM	glucosaminidase
h	hour(s)
HEPES	2-[4-(2-hydroxyethyl)piperazin-1-yl]ethane-1-sulfonic acid
HF	hydrofluoric acid
His-	hexahistidine tagged
HPLC	high-performance liquid chromatography
HRMS	high-resolution mass spectrometry
i.e.	from Latin *id est*, meaning “that is to say”
IC_{50}	half maximal inhibitory concentration
IPTG	isopropyl β-D-1-thiogalactopyranoside
kb	kilobase
K_D	dissociation constant
l	liter
L	lateral membrane
LB	Luria Bertani
LCP	LytR-CpsA-Psr
$LcpX_{short}$	hexahistidine-tagged *S. aureus* LcpX without transmembrane domain
LDS	lithium dodecyl sulfate
lipid I	undecaprenyl-pyrophosphoryl-*N*-acetylmuramyl-(pentapeptide)
lipid I_{cap}	undecaprenyl-pyrophosphoryl-*N*-acetyl-D-fucosamine
lipid II	undecaprenyl-pyrophosphoryl-*N*-acetylmuramyl-(pentapeptide)-*N*-acetylglucosamine
lipid III_{WTA}	undecaprenyl-pyrophosphate-*N*-acetyl-D-glucosamine
LPS	lipopolysaccharide

LTA	lipoteichoic acid
M	mol/liter
m	meter
(D-)ManAcA	*N*-acetyl-D-mannosaminuronic acid
(D-)Man*N*Ac	*N*-acetyl-D-mannosamine
Mc^R	resistant to methicillin
Mc^S	sensitive to methicillin
MeGly	*N*-methylglycine
MES	2-(*N*-Morpholino)-ethane sulphonic acid
MH(A/B)	Mueller-Hinton (agar/broth)
MIC	minimal inhibitory concentration
min	minute(s)
MOE	moenomycin
MOPS	3-(*N*-morpholino)propanesulfonic acid
MRSA	methicillin-resistant *Staphylococcus aureus*
MSSA	methicillin-sensitive *Staphylococcus aureus*
(D-)Mur*N*Ac	*N*-acetyl-D-muramic acid
MW(CO)	molecular weight (cutoff)
NAD(P)H	nicotinamide adenine dinucleotide (phosphate)
n.d.	not determined
Ni-NTA	nickel-nitrilotriacetic acid
NM	*S. aureus* Newman
NMR	nuclear magnetic resonance spectroscopy
nMT	*N*-methyl transferase
NRPS	nonribosomal peptide synthetase
ns	not significant
NTP	nucleoside triphosphate
OD_{600}	optical density at 600 nm
PBP	penicillin-binding protein
PBS	phosphate-buffered saline
PCR	polymerase chain reaction
PDB	Protein Data Bank
P	probability
PG	peptidoglycan
pH	from Latin *pondus hydrogenii*; hydrogen ion concentration
Pro	proline
ref.	reference number
Rif^R	resistant to rifampin
RF	replicative form
RFU	relative fluorescence unit(s)
RLU	relative light unit(s)
(m/t)RNA	(messenger/transfer) ribonucleic acid
RNAP	DNA-dependent RNA polymerase
RNase	ribonuclease
RP-HPLC	reversed-phase HPLC

rpm	rounds per minute
s	second(s)
S	septum
SD	standard deviation
SDS(-PAGE)	sodium dodecyl sulfate (polyacrylamide gel electrophoresis)
SEC	size-exclusion chromatography
Ser	serine
Spec	spectinomycin
Sp^R	resistant to spectinomycin
T	thiolation domain
TAE buffer	buffer solution containing Tris-base, acetic acid and EDTA
TD	terminal reduction domain
TEMED	*N*,*N*,*N*′,*N*′-tetramethylethane-1,2-diamine
TLC	thin layer chromatography
TM	transmembrane
Tn^R	resistant to tetracycline
Tris	tris(hydroxymethyl)-aminomethane
TSA/B	tryptic soy agar/broth
UDP	uridine 5’-diphosphate
UV	ultraviolet light
V	volt
v/v	volume/volume percent
Van^R	resistant to vancomycin
VIS	visible light
VISA	vancomycin-intermediate *Staphylococcus aureus*
VRE	vancomycin-resistant *Enterococcus*
VRSA	vancomycin-resistant *Staphylococcus aureus*
w/v	weight/volume percent
WHO	World Health Organization
WT	wildtype
WTA	wall teichoic acid
X-gal	5-bromo-4-chloro-3-indolyl-D-galactoside
YFP	yellow fluorescent protein
αCTD	C-terminal domain of α subunit
αNTD	N-terminal domain of α subunit
λmax	wavelength of the most intense UV/VIS absorption

Index of figures

Figure 1: Schematic representation of the cell envelope in Gram-positive bacteria. 2

Figure 2: Scheme of the peptidoglycan (left) and wall teichoic acid (right) biosyntheses in *S. aureus*. 6

Figure 3: The functions of wall teichoic acids in Gram-positive bacteria. 8

Figure 4: The structure of wall teichoic acids in *S. aureus*. 11

Figure 5: Structural features of the LytR-CpsA-Psr (LCP) enzyme family members in *S. aureus*. 15

Figure 6: Genetic organization of *lcpA*, *lcpB*, and *lcpC* in the *S. aureus* N315 genome. 16

Figure 7: Chemical structures of selected moenomycins. 20

Figure 8: Structure of corallorazine A, B, and C as derived from NMR and HRMS experiments (Schmitz *et al*., 2014). 23

Figure 9: (A) Genetic organization of the 16.5 kb corallorazine biosynthetic gene cluster (BGC) and (B) the predicted corallorazine biosynthesis pathway. 24

Figure 10: Schematic of checkerboard assay. 42

Figure 11: Schematic representation of how down-regulation of the target gene expression by antisense RNA can affect the bacterial cell susceptibility towards an inhibitor (modified from Singh *et al*., 2007). 44

Figure 12: Example standard curve for BSA. 54

Figure 13: Example phosphate standard curve. 59

Figure 14: Determination of the fluorescent ratio (FR). 64

Figure 15: Example muropeptide profile of *S. aureus*. 67

Figure 16: Example standard curve for *N*-acetylglucosamine (Glc*N*Ac). 68

Figure 17: Example HPLC chromatogram of *S. aureus* membrane lipids. 70

Figure 18: The LcpA-catalyzed hydrolysis of [^{14}C]-lipid III_{WTA} *in vitro* is inhibited by moenomycin. 72

Figure 19: *S. aureus* LcpA hydrolyzes lipid II *in vitro* and is thereby inhibited by moenomycin. 73

Figure 20: LcpA is the only lipid II-hydrolyzing LCP enzyme in *S. aureus*. 74

Figure 21: HPLC separation of membrane lipids from *S. aureus* Newman wildtype and the Δ*lcpA* mutant. 75
Figure 22: Amount of the PG precursor lipid II as determined by HPLC for *S. aureus* Newman wildtype and the Δ*lcpA* mutant per 30 ml cell culture at OD_{600} 1.2. 76
Figure 23: The effect of moenomycin on the growth of *S. aureus* Newman *lcp* mutant strains. 78
Figure 24: Spot dilution assays comparing the susceptibilities of *S. aureus* MSSA1112 wildtype and *lcp* mutant strains to moenomycin. 78
Figure 25: Moenomycin shows a delayed bactericidal effect against *S. aureus* MSSA1112. 79
Figure 26: LCP enzymes interact with MOE-BDP in a direct binding assay regardless of their transmembrane domain. 81
Figure 27: FA measurements on *S. aureus* LCP proteins and PG glycosyltransferases using MOE-BDP. 83
Figure 28: Competitive binding assay of *S. aureus* LCP proteins and PG glycosyltransferases. 84
Figure 29: MSSA1112 wildtype checkerboard assay examining the antibiotic activity of moenomycin in the presence of different cell wall-active antibiotics. 87
Figure 30: MSSA1112 Δ*lcpABC* checkerboard assay examining the antibiotic activity of moenomycin in the presence of different cell wall-active antibiotics. 88
Figure 31: SA113 Δ*tarO* checkerboard assay examining the antibiotic activity of moenomycin in the presence of different cell wall-active antibiotics. 89
Figure 32: RP-HPLC profiles of mutanolysin-digested peptidoglycan of *S. aureus* MSSA1112 and the respective Δ*lcpABC* triple mutant. 91
Figure 33: Bocillin FL-labeled PBPs of *S. aureus* MSSA1112 wildtype and the Δ*lcpABC* triple mutant separated by SDS-PAGE. 92
Figure 34: RP-HPLC profiles of mutanolysin-digested peptidoglycan of *S. aureus* Newman pretreated with DMSO or moenomycin. 93
Figure 35: PBP4 is recruited to the division septum in the presence of moenomycin. 94
Figure 36: Quantification of cell envelope components of DMSO- and moenomycin-treated *S. aureus* Newman cells. 95

Figure 37: Localization of MOE-BDP in LCP-deprived *S. aureus* Newman and control strains. 97
Figure 38: The MSSA1112 Δ*lcpA* mutant shows decreased binding of MOE-BDP. 98
Figure 39: Localization of PBPs in LCP-deprived *S. aureus* Newman and control strains. 99
Figure 40: Localization of rhodamine B-labeled ramoplanin in LCP-deprived *S. aureus* Newman and control strains. 100
Figure 41: Localization of FITC-labeled vancomycin in LCP-deprived *S. aureus* Newman and control strains. 101
Figure 42: Localization of GFP-labeled LcpA in *S. aureus* RN4220 depending on the exposition to different cell wall-active antibiotics. 102
Figure 43: Localization of GFP-labeled LcpB in *S. aureus* RN4220 depending on the exposition to different cell wall-active antibiotics. 103
Figure 44: Localization of GFP-labeled LcpC in *S. aureus* RN4220 depending on the exposition to different cell wall-active antibiotics. 104
Figure 45: Localization of GFP-labeled PBP2 in *S. aureus* RN4220 depending on the exposition to different cell wall-active antibiotics. 105
Figure 46: Zymogram of *S. aureus* MSSA1112 and respective LCP-deprived mutant strains. 107
Figure 47: Corallorazine A interferes with the bacterial RNA biosynthesis pathway. 109
Figure 48: Corallorazine A inhibits the *E. coli* DNA-dependent RNA polymerase (RNAP)-catalyzed *in vitro* transcription. 111
Figure 49: Structural prediction for full-length LcpA and the binding of lipid III_{WTA} to truncated LcpA from *S. aureus*. 114
Figure 50: Crystal structures of truncated PBP2 and LcpA from *S. aureus* with moenomycin. 115
Figure 51: Model for the cellular localization of membrane proteins in *S. aureus* wildtype in comparison to the Δ*lcpABC* and Δ*tarO* null mutants. 119
Figure 52: Structural prediction for the binding of moenomycin to truncated LcpA from *S. aureus*. 123

Figure 53: Model for the cellular localization of membrane proteins in *S. aureus* before and after exposure to moenomycin. 125
Figure 54: Structures of (A) phenylahistin, (B) its biosynthesis byproduct, and (C) cyrmenin A, which possess structural resemblance to corallorazine A. 131
Figure 55: Structure of the bacterial RNAP. 133
Figure 56: Structures of the RNAP inhibitors (A) rifampin and (B) fidaxomicin, which are approved for medical use, and the drug candidate (C) corallopyronin A. 134
Figure 57: Inhibitor target sites of the bacterial RNAP. 135
Figure 58: *In vitro* activity test of purified full-length SgtA and SgtB. 138
Figure 59: SDS-PAGE of purified proteins used for FA experiments. 158
Figure 60: The effect of moenomycin in combination with different class antibiotics against methicillin-resistant *S. aureus* (MRSA) strains. 140
Figure 61: Amino acid sequence analysis of *S. aureus* N315 CapA1. 141

Index of tables

Table 1: SDS-PAGE gel recipe for 1 gel. 60

Table 2: MIC values of *S. aureus* MSSA1112, Newman, and SA113 strains for moenomycin and other cell wall targeting antibiotics. 77

Table 3: Binding affinities of *S. aureus* LCP enzymes and PG glycosyltransferases for MOE-BDP determined in FA assays. 85

Table 4: Checkerboard assay results of moenomycin in combination with cell wall-active antibiotics against *S. aureus* MSSA1112 wildtype and Δ*lcpABC*, as well as SA113 Δ*tarO*. 86

Table 5: MIC values of corallorazine A against selected Gram-positive and Gram-negative bacteria. 108

Table 6: Selected clones with reduced expression of genes involved in transcription and translation exhibit an increased susceptibility to corallorazine A. 110

Table 7: MIC values of *S. aureus* Newman for fluorescently labeled cell wall targeting antibiotics. 139

Table 8: MIC values of *S. aureus* RN4220 strains producing GFP-tagged LCP and PBP enzymes for moenomycin and other cell wall targeting antibiotics. 139

Table 9: Checkerboard assay results of moenomycin in combination with antibiotics of other classes against the MRSA strains USA300 and COL. 139

Table of contents

1. Introduction 1

Chapter 1: The attachment of wall teichoic acids to the peptidoglycan scaffold by LCP enzymes in Staphylococcus aureus is an attractive antibiotic target 1

1.1 The well-armed major human pathogen *Staphylococcus aureus* 1

1.2 The function and relevance of the bacterial cell wall 2

1.3 The structure and composition of peptidoglycan 3

1.4 The peptidoglycan biosynthesis in *S. aureus* 4

1.5 The function of wall teichoic acids 7

1.6 The structure and composition of wall teichoic acids 10

1.7 The wall teichoic acids biosynthesis in *S. aureus* 12

1.8 The discovery of the LytR-CpsA-Psr (LCP) enzyme family 13

1.9 The LCP enzymes of *S. aureus* 15

1.10 Moenomycin family antibiotics 20

Chapter 2: The discovery and characterization of corallorazines 22

Aims of this thesis 25

2. Materials and Methods 26

2.1 Materials 26

2.1.1 Chemicals 26

2.1.2 Other materials 28

2.1.3 Laboratory equipment 29

2.1.4 Antibiotics 32

2.1.5 Molecular weight markers 33

2.1.6 Kits 33

2.1.7 Proteins 33

2.1.8 Bacterial strains 34

2.1.9 Growth media 36

2.1.10 Plasmids and oligonucleotides 36

2.2 Microbial methods 38

2.2.1 Sterilization procedure of media, equipment and bacterial cultures 38

2.2.2 Bacterial storage and growth 38

2.2.3 Optical density measurement of cell populations 38
2.2.4 Preparation of chemo-competent *E. coli* 39
2.2.5 Preparation of electro-competent *S. aureus* 39
2.2.6 Isolation of plasmid DNA from *E. coli* 39
2.2.7 Isolation of genomic DNA from *S. aureus* 39
2.2.8 Transformation of chemo-competent *E. coli* cells 40
2.2.9 Transformation of electro-competent *S. aureus* 40
2.2.10 Minimal inhibitory concentration (MIC) 40
2.2.11 Synergy checkerboard assay 41
2.2.12 Spot dilutions of *S. aureus* strains 42
2.2.13 Killing kinetics 43
2.2.14 β-galactosidase reporter assays 43
2.2.15 Susceptibility profile of *S. aureus* antisense recombinant strains 44
2.3 Molecular biological methods 45
2.3.1 DNA amplification via polymerase chain reaction (PCR) 45
2.3.2 Analysis of DNA fragments using agarose gel electrophoresis 46
2.3.3 Purification of DNA fragments 46
2.3.4 Photometrical determination of DNA concentration and purity 46
2.3.6 DNA sequencing 47
2.4 Protein purification methods 47
2.4.1 Protein overproduction 47
2.4.2 Size-exclusion chromatography (SEC) 53
2.5 Protein analysis methods 53
2.5.1 Sodium dodecyl sulfate-polyacrylamide gel electrophoresis (SDS-PAGE) 53
2.5.2 Determination of protein concentration in solution 54
2.6 Protein biochemical methods 55
2.6.1 Purification of UDP-D-Mur*N*Ac-pentapeptide 55
2.6.2 Purification of *Micrococcus luteus* DSM 1790 membranes 55
2.6.3 *In vitro* synthesis of lipid II 56
2.6.4 *In vitro* synthesis of [^{14}C]-lipid III_{WTA} 57
2.6.5 *In vitro* LcpA assay 57
2.6.6 Thin layer chromatography (TLC) 58

2.6.7 Phosphate determination 58
2.6.8 *In vitro* transcription 59
2.6.9 Zymographic analysis 60
2.6.10 MOE-BDP binding assay 61
2.6.11 Bocillin binding assay 61
2.6.12 Fluorescence anisotropy 62
2.6.13 Fluorescence microscopy 63
2.7 Peptidoglycan and cytoplasmic membrane analysis methods 65
2.7.1 Isolation of cell wall from *S. aureus* 65
2.7.2 Sodium dodecyl sulphate test by Hyashi 66
2.7.3 Isolation, digestion and analysis of peptidoglycan from *S. aureus* 66
2.7.4 Quantification of peptidoglycan 68
2.7.5 Extraction of wall teichoic acids 69
2.7.6 Purification and HPLC analysis of membrane lipids 69
3. Results 71
Chapter 1: S. aureus LCP enzymes are targeted by moenomycin 71
3.1.1 Moenomycin inhibits the hydrolytic activity of LcpA 71
3.1.2 *Lcp* single and double mutants are less susceptible to moenomycin 76
3.1.3 Moenomycin-induced killing is time-delayed in *S. aureus* cells 79
3.1.4 LCP enzymes directly interact with moenomycin 80
3.1.5 The combination of moenomycin and other cell wall-active antibiotics shows synergistic antibacterial activity against MSSA1112 wildtype but not the LCP-deficient strain 85
3.1.6 PG cross-linking is increased in cells lacking LCP enzymes 90
3.1.7 Moenomycin treatment reduces the PG and WTA content 95
3.1.8 LcpA-deprived mutants bind significantly less MOE-BDP *in vitro* 96
3.1.9 Moenomycin stimulates the recruitment of LcpA to the cell division site 102
3.1.10 Deletion of LCP enzymes affects the autolytic activity 106
Chapter 2: Corallorazine A targets the DNA-dependent RNA polymerase 108
3.2.1 Corallorazine A shows antibacterial activity 108
3.2.2 Corallorazine A inhibits the transcription 109

4. Discussion 112

Chapter 1: Moenomycin offers more than the inhibition of PG glycosyltransferases 112

4.1.1 Elucidation of the LCP enzyme acceptor substrate 112

4.1.2 The interruption of the WTA biosynthesis pathway at various stages affects the cell wall homeostasis differently 118

4.1.3 How moenomycin interacts with LCP enzymes in *S. aureus* 121

4.1.4 Unraveling the effect of moenomycin on *S. aureus* cells 124

Chapter 2: Corallorazine A extends the small portfolio of RNAP inhibitors 130

4.2.1 Corallorazines form a new group of natural product antibiotics 130

4.2.2. Corallorazine A in comparison with other RNAP inhibitors 132

5. Appendix 138

5.1 Supplementary figures and tables 138

6. References 142

1. Introduction

Chapter 1: The attachment of wall teichoic acids to the peptidoglycan scaffold by LCP enzymes in *Staphylococcus aureus* is an attractive antibiotic target

1.1 The well-armed major human pathogen *Staphylococcus aureus*

Staphylococcus aureus is a commensal Gram-positive bacterium and opportunistic pathogen that colonizes the human nasal mucosa in approximately 30% of the population and constitutes a serious threat for difficult-to-treat community- and healthcare-associated infections worldwide (Laux *et al*., 2019, Antimicrobial Resistance Collaborators, 2022, Lade & Kim, 2023). It is a major cause of bacteremia, infective endocarditis, as well as osteoarticular, skin and soft tissue, respiratory, surgical, and device-related infections (Tong *et al*., 2015). To aggravate the eradication, *S*. *aureus* has the outstanding ability to quickly acquire resistance to nearly every antibiotic approved for human medication (Chambers & Deleo, 2009). The finesse in developing resistance seems to be inexhaustible and comprises, among others, the enzymatic inactivation of the compound, the introduction of efflux mechanisms, the modification of an existing target or the acquisition of an alternative target to reduce the drug affinity, and the fortification of the surrounding cell envelope (Foster *et al*., 2017). Beginning with the introduction of penicillin in 1941, *S*. *aureus* has developed resistance mechanisms to virtually every antibiotic class, including β-lactams, macrolides, aminoglycosides, tetracycline, chloramphenicol, fusidic acid, rifampin, lincosamides, glycopeptides, and fluoroquinolones (Rammelkamp & Maxon, 1942, Finland, 1955, Brumfitt & Hamilton-Miller, 1989, Howden *et al*., 2010, Foster, 2017). Moreover, the prevalence of multi-drug resistant MRSA (methicillin-resistant *S*. *aureus*) strains reduces the treatment options enormously and causes excessive healthcare expenditures (Stryjewski & Corey, 2014, Turner *et al*., 2019). In 2019, approximately five million deaths worldwide were associated with bacterial antimicrobial resistance and *S*. *aureus* was highlighted as the second leading pathogen (Antimicrobial Resistance Collaborators, 2022). The World Health Organization (WHO) classifies methicillin- and vancomycin-resistant *S*. *aureus* as high priority pathogens, because they are a major cause of global morbidity and mortality (WHO, 2017). International research efforts urgently need to address the containment and the combat of multidrug-resistant *S*. *aureus*.

Therefore, the development of novel antibiotics or the chemical modification of existing antimicrobials is of high importance. This requires to gain a deeper understanding of how anti-infectives work.

1.2 The function and relevance of the bacterial cell wall

The bacterial cell wall is a crucial structure in free-living bacteria, because it maintains the integrity and characteristic shape of a cell. The cell wall plays a key role in the uptake of nutrients and forms a barrier to counteract environmental threats and hostile conditions (Silhavy *et al*., 2010). A bacterial cell maintains a functional cell wall during growth and cell division through its constant assembly, dismantling, and remodeling (Typas *et al*., 2012, Egan *et al*., 2020).

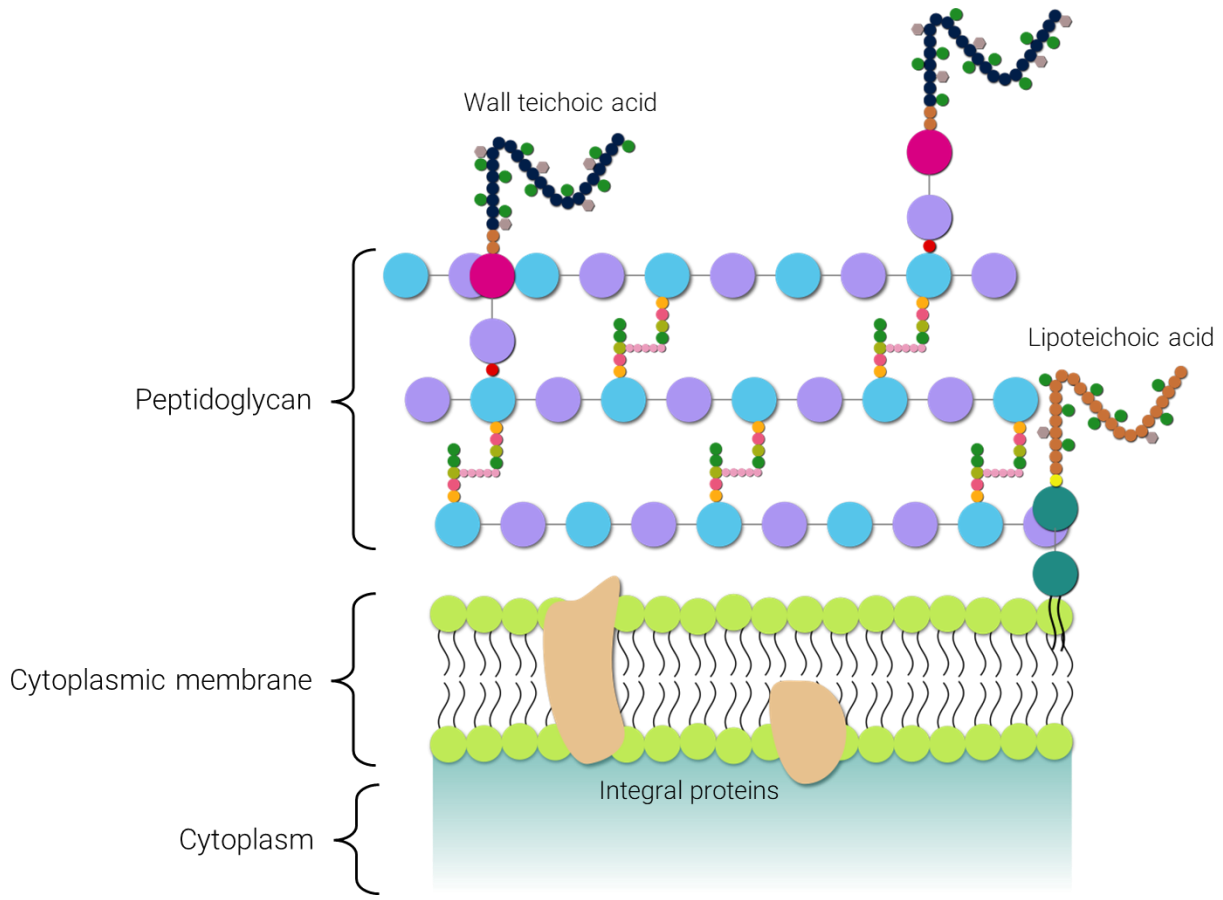

Figure 1: Schematic representation of the cell envelope in Gram-positive bacteria. The cytoplasmic membrane is surrounded by a thick peptidoglycan layer that is decorated with anionic glycopolymers, such as wall teichoic acids (WTAs). WTAs are directly linked to the peptidoglycan sacculus, while the structurally related lipoteichoic acids (LTAs) are anchored to the cell membrane.

A main component of the bacterial cell wall is the peptidoglycan (PG, also called murein) sacculus, which fulfils multiple requirements. On one hand, it has to be rigid to structurally support the cytoplasmic membrane, especially to withstand osmotic differences and the force exerted by protruding appendages such as flagella and pili, and to provide mechanical strength. On the other hand, the mesh-like structure needs to be flexible enough to enable cellular growth and the attachment of various cell envelope components including proteins (Ou & Marquis, 1970, Chevance & Hughes, 2008, Dramsi *et al*., 2008). Maintaining the sacculus is a highly dynamic process requiring PG synthases and specific PG hydrolases to enable the incorporation of newly synthesized glycan strands into existing PG layers, which are cross-linked to expand the scaffolding structure or to repair damages (Höltje, 1998).

The cell wall in Gram-positive and Gram-negative bacteria differs substantially. Both groups possess a cytoplasmic membrane, but the PG is thicker in Gram-positive bacteria (Vollmer & Seligman, 2010). In addition, the PG sacculus of these bacteria is decorated with wall teichoic acids (WTAs), contributing to an average thickness of the PG-WTA cell wall of 10 to 40 nm (Figure 1) (Neuhaus & Baddiley, 2003, Ward, 1981, Vollmer & Seligman, 2010). In contrast, the mostly single-layered PG sacculus of Gram-negative bacteria is 3 to 6 nm thick and surrounded by an outer membrane (Vollmer & Seligman, 2010). Some Gram-positive and Gram-negative bacteria can surround themselves with a capsule to prevent desiccation and enhance pathogenicity (Roberson & Firestone, 1992, Ophir & Gutnick, 1994, Nilsson *et al*., 1997, Thakker *et al*., 1998). Indeed, capsular polysaccharides (CPs) facilitate the adherence to host cells and constitute a protective shield against host defense mechanisms, *e.g*., opsonophagocytic killing and antimicrobials (Pöhlmann-Dietze *et al*., 2000, Wilkinson & Holmes, 1979, Taylor & Roberts, 2005, Campos *et al*., 2004, Spinosa *et al*., 2007). Like WTAs, some Gram-positive bacteria attach the capsule covalently to the PG scaffold (Chan *et al*., 2014). Because the cell wall is of major importance for cell viability, it represents a popular and effective target for antibiotics (Schneider & Sahl, 2010a).

1.3 The structure and composition of peptidoglycan

The PG forms an essential three-dimensional scaffold within the bacterial cell envelope and consists of linear glycan chains made of alternating β-(1,4)-linked *N*-acetylmuramic acid (Mur*N*Ac)

and *N*-acetylglucosamine (Glc*N*Ac) residues that are connected by short peptides (Rogers *et al*., 1980). The average chain length is 18 disaccharide units in *S*. *aureus* (Tipper *et al*., 1967). A pentapeptide stem is attached to the D-lactoyl group of each Mur*N*Ac residue and varies among different species. In *S*. *aureus*, the oligopeptide is composed of L-alanine, D-glutamic acid, L-lysine, and the terminal dipeptide D-alanyl-D-alanine, whereas the sequence in *E*. *coli* and most Gram-negative bacteria contains *meso*-diaminopimelic acid at the third position (Vollmer *et al*., 2008).

In most Gram-positive bacteria, the cross-linking of glycan strands occurs between the side-chain amino group of the residue at position 3 of one stem peptide and the carboxyl group of the D-alanine at position 4 of another stem peptide, sometimes via an interpeptide bridge. The nature of the interpeptide bridge can differ between bacteria. In *S*. *aureus*, it consists of five glycine residues, whereas the structure in other species includes, *e*.*g*., L-alanine-L-alanine in *Enterococcus faecalis* or a complete stem peptide in *Micrococcus luteus* (Schleifer & Kandler, 1972).

In *S*. *aureus*, 35 to 90% of the Mur*N*Ac residues are further modified by *O*-acetylation, which contributes to lysozyme resistance (Ghuysen & Strominger, 1963, Snowden *et al*., 1989, Bera *et al*., 2005). Other secondary modifications in *S*. *aureus* are the covalent attachment of surface polysaccharides, *i*.*e*., teichoic acids and a capsule (Kojima *et al*., 1985, Kawai *et al*., 2011, Rausch *et al*., 2019), and the amidation of the iso-D-glutamate at position 2 of the peptide (Figueiredo *et al*., 2012, Münch *et al*., 2012).

1.4 The peptidoglycan biosynthesis in *S*. *aureus*

PG biosynthesis steps occur in three different compartments: the cytoplasm, the inner leaflet of the cytoplasmic membrane, and the cell exterior (Figure 2) (Barreteau *et al*., 2008, Bouhss *et al*., 2008, Sham *et al*., 2014). In general, nucleotide-activated sugars and amino acids are synthesized in the cytoplasm and transferred onto the carrier lipid at the inner face of the cytoplasmic membrane (Walsh, 1989, Marquardt *et al*., 1992, Benson *et al*., 1993). Subsequently, the lipid-linked precursor is flipped across the membrane, glycan chains are polymerized, and peptides are cross-linked to form the PG mesh that is further modified by *O*-acetylation or the attachment of secondary polymers (Kojima *et al*., 1985, Bera *et al*., 2006, Kawai *et al*., 2011, Rausch *et al*., 2019).

In detail, the biosynthesis of PG is initiated in the cytoplasm by the MurA and MurB-catalyzed formation of UDP-Mur*N*Ac from UDP-Glc*N*Ac and phosphoenolpyruvate (Marquardt *et al*., 1992, Benson *et al*., 1993). The stem peptide is then built on the lactoyl moiety of UDP-Mur*N*Ac. ATP-dependent amino acyl ligases MurC, MurD, and MurE add sequentially the amino acids L-alanine, D-glutamic acid, and L-lysine (Walsh, 1989, Bouhss *et al*., 1997, Patin *et al*., 2010). L-Alanine is racemized to D-alanine by Alr and then dimerized to form D-alanyl-D-alanine by Ddl. MurF ligates the dipeptide to the growing peptide in an ATP-consuming reaction, resulting in the formation of UDP-Mur*N*Ac-pentapeptide that is also referred to as Park's nucleotide (Park, 1952, Walsh, 1989).

The next stage of PG biosynthesis occurs at the inner face of the cytoplasmic membrane. Phospho-Mur*N*Ac-pentapeptide is transferred onto the carrier lipid undecaprenyl phosphate (C_{55}-P) by the integral membrane protein MraY forming lipid I (undecaprenyl-pyrophosphoryl-*N*-acetylmuramyl-(pentapeptide)) (Pless & Neuhaus, 1973, Bouhss *et al*., 2004, Chung *et al*., 2013). The membrane-bound glycosyltransferase MurG adds Glc*N*Ac to the Mur*N*Ac moiety of lipid I, generating lipid II (undecaprenyl-pyrophosphoryl-*N*-acetylmuramyl-(pentapeptide)-*N*-acetylglucosamine) (Hu *et al*., 2003, Mengin-Lecreulx *et al*., 1991). In *S*. *aureus*, the oligopeptide is further modified by the sequential addition of one, two, and two glycine residues by FemX, FemA, and FemB, respectively, using glycyl-tRNA donors (Maidhof *et al*., 1991, Henze *et al*., 1993, Rohrer *et al*., 1999, Schneider *et al*., 2004). The bi-enzyme complex MurT/GatD amidates the α-carboxyl group of D-glutamic acid to yield D-isoglutamine (Figueiredo *et al*., 2012, Münch *et al*., 2012). The ultimate PG precursor is then translocated across the cytoplasmic membrane by the integral membrane protein MurJ (Ruiz *et al*., 2008, Inoue *et al*., 2008, Sham *et al*., 2014).

Upon translocation to the outer face of the cytoplasmic membrane, the glycan chains are polymerized and the peptides are cross-linked by penicillin-binding proteins (PBPs) (Blumberg & Strominger, 1974, Sauvage *et al*., 2008). Overall, *S*. *aureus* has four different PBPs. PBP2 is the only bifunctional PBP (class A) in *S*. *aureus* containing a glycosyltransferase domain for the polymerization of glycan strands and a transpeptidase domain to cross-link the peptides (Murakami *et al*., 1994, Goffin & Ghuysen, 1998). PBP1 and PBP3 are class B PBPs consisting of only a transpeptidase domain to form cross-links (Pinho *et al*., 2000, Pereira *et al*., 2007). The only

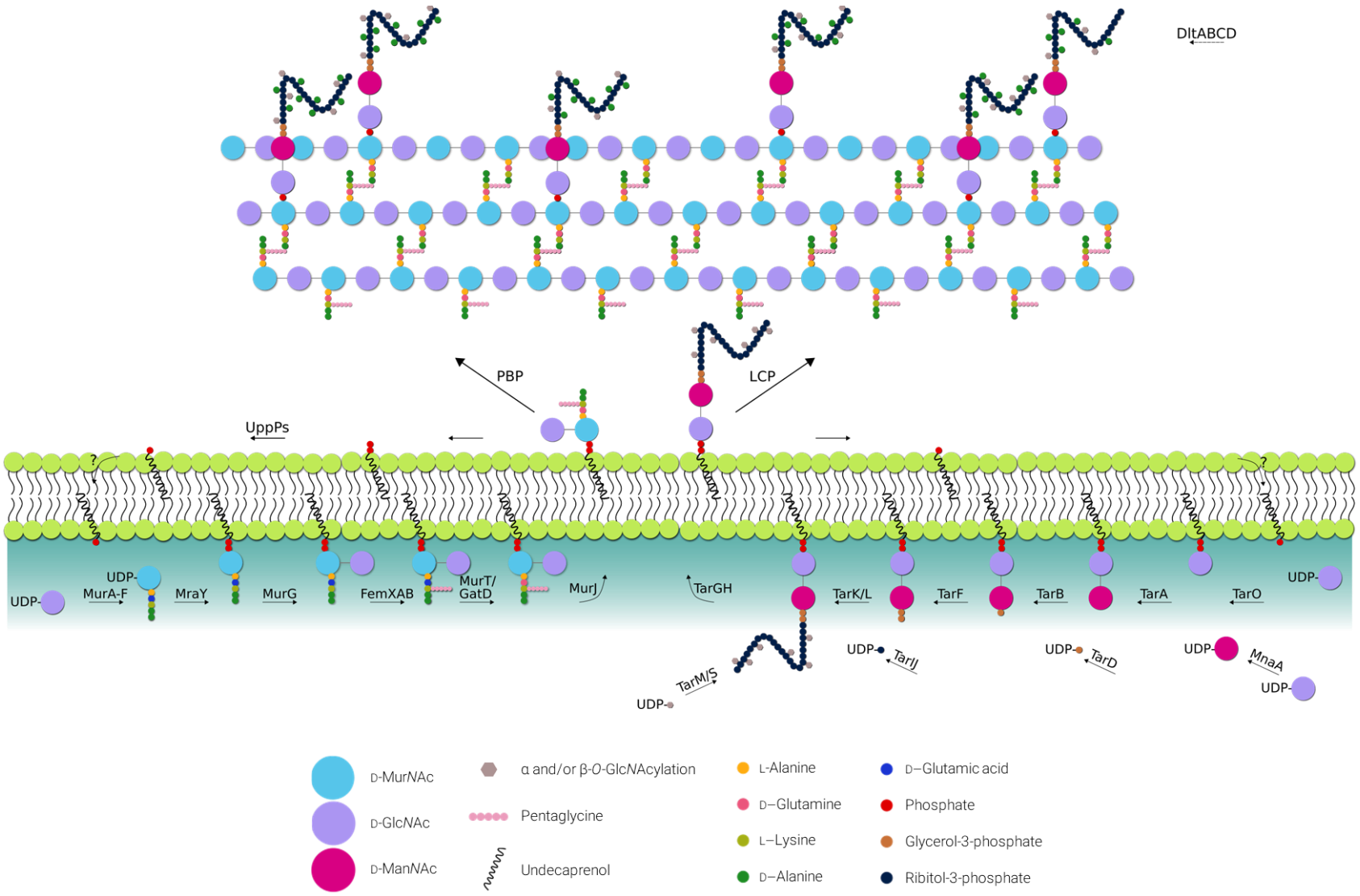

Figure 2: Scheme of the peptidoglycan (left) and wall teichoic acid (right) biosyntheses in *S. aureus*. The precursors of both pathways are stepwise assembled at the lipid carrier C_{55}-P and then translocated to the outer face of the cytoplasmic membrane by an individual flippase. Polymerization of glycan strands and cross-linking of the peptides are achieved by penicillin-binding proteins (PBPs), while the resulting peptidoglycan sacculus is decorated with wall teichoic acids (WTAs) by members of the LytR-CpsA-Psr (LCP) enzyme family.

low molecular mass PBP in *S. aureus*, PBP4, is of particular importance, because it possesses a dual function. It has the capability to act both as a carboxypeptidase, hydrolyzing the terminal D-alanine of the stem peptide to restrict transpeptidation, and as a transpeptidase, producing highly cross-linked PG (Henze & Berger-Bächi, 1995, Wyke *et al*., 1981). In addition, MRSA strains produce an additional PBP, *e.g*., the transpeptidase PBP2a, with low affinity for β-lactam antibiotics (Song *et al*., 1987, Zapun *et al*., 2008). Moreover, *S. aureus* has two monofunctional glycosyltransferases, SgtA and SgtB, to polymerize glycan chains and the SEDS proteins FtsW and RodA that work in concert with their cognate class B PBP to incorporate PG into the sidewall and septum (Reed *et al*., 2011, Taguchi *et al*., 2019, Reichmann *et al*., 2019). Once the phosphorylated carrier lipid undecaprenyl pyrophosphate (C_{55}-PP) is released as a byproduct of the polymerization reaction, it is immediately converted to C_{55}-P by UppP and other phosphatases and flipped back to the inner face of the membrane by a yet unknown translocase to enter a new cycle as a shared carrier lipid (El Ghachi *et al*., 2004 & 2005, Bouhss *et al*., 2008). The PG scaffold is further modified by *O*-acetylation and the attachment of anionic glycopolymers to the Mur*N*Ac residues (Kojima *et al*., 1985, Bera *et al*., 2005, Kawai *et al*., 2011, Rausch *et al*., 2019).

PG biosynthesis is essential in most bacteria and represents a highly conserved process that is effectively targeted by many antibiotics (Vollmer *et al*., 2008, Schneider & Sahl, 2010a & b). Especially the C_{55}-P and C_{55}-P-containing lipid intermediates are of utmost importance for the cell, because the carrier lipid supply is limited and the distribution among PG, WTA, and capsule biosynthesis must be tightly regulated (Bouhss *et al*., 2008, Brown *et al*., 2013, Rausch *et al*., 2019).

1.5 The function of wall teichoic acids

Gram-positive bacteria possess different types of teichoic acids that are either anchored to the cytoplasmic membrane via a glycolipid and called lipoteichoic acids (LTAs) or covalently linked to the PG scaffold as wall teichoic acids (WTAs). In *S. aureus*, the synthesis machinery of LTAs differs substantially from that of PG-attached WTAs (Percy & Gründling, 2014). The zwitterionic charged LTAs are, in contrast, essential for viability in *S. aureus*, but both kinds of teichoic acids seem to perform similar tasks in the cellular context of protection and structural integrity, such as the

accurate positioning of components involved in cell division (Weidenmaier *et al*., 2004, Gründling & Schneewind, 2007, Xia *et al*., 2010a). Since no functional connection is known between LCP enzymes, that are responsible for the covalent attachment of WTAs to PG, and the linkage of LTAs to the cytoplasmic membrane (Chan *et al*., 2014, Heß *et al*., 2017, Flores-Kim *et al*., 2019), this work mainly focusses on WTAs.

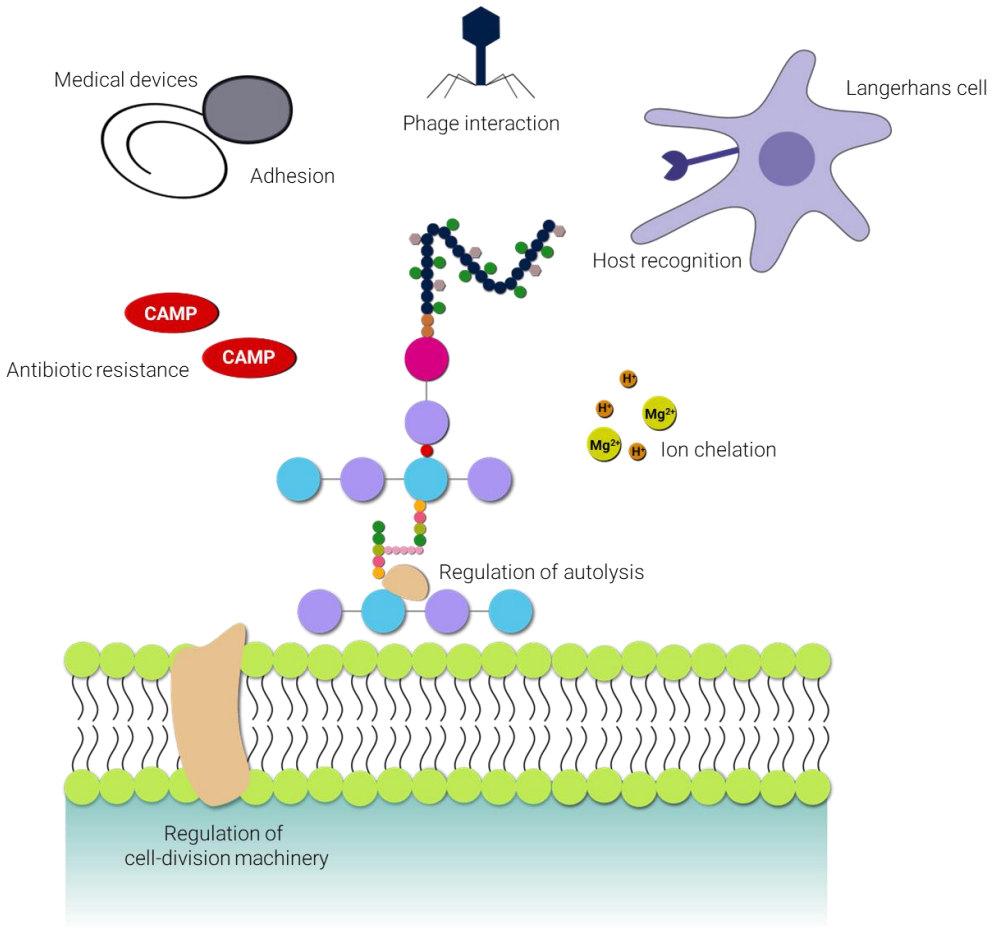

Figure 3: The functions of wall teichoic acids in Gram-positive bacteria. The anionic glycopolymers contribute to adhesion and biofilm formation, *e.g*., on medical devices, mediation of interactions with phages and immune cells, cation homeostasis, antibiotic resistance to cationic antimicrobial peptides (CAMPs), and the regulation of autolytic activity and septal placement.

WTAs are anionic glycopolymers decorating the PG of Gram-positive bacteria. They are covalently attached to PG and, depending on their attachment site, frequency, and charge, fulfill numerous functions including the regulation of cell division and autolysis, ion chelation, antibiotic resistance, interactions with host immune cells and phages, and surface adhesion as described below

(Figure 3) (Heptinstall *et al*., 1970, Peschel *et al*., 1999 & 2000, Gross *et al*., 2001, Campbell *et al*., 2011, Biswas *et al*., 2012).

Under laboratory conditions, WTAs are not essential for cell viability of *S*. *aureus* (Weidenmaier *et al*., 2004, D'Elia *et al*., 2006a & b). However, WTA-deficient *S*. *aureus* mutant strains (genetic deletion of *tarO*, encoding the first glycosyltransferase of the WTA biosynthesis pathway, see section 1.7) display major cell division defects that include misplaced, duplicated, and often uncompleted septa, leading to clusters of unseparated cells (Campbell *et al*., 2011). Consistent with these findings, some enzymes involved in WTA biosynthesis have been shown to colocalize with PG synthesizing proteins (Formstone *et al*., 2008).

Atl is the major autolysin in S. *aureu*s and crucial for the separation of daughter cells by catalyzing the hydrolysis of PG. The preproprotein is modularly organized (signal peptide, propeptide, amidase, three repeat units, and glucosaminidase) and proteolytically cleaved after secretion. The cleavage sites are located on both ends of the propeptide and after the second repeat unit that separates the amidase domain (AM, approx. 62 kDa) and the glucosaminidase (GM, approx. 51 kDa) domain (Oshida *et al*., 1995). While the amidase hydrolyzes the amide bond between the peptide and the *N*-acetylmuramic acid residue in PG, the glucosaminidase cleaves the glycosidic bonds within the PG sugar backbone between the Mur*N*Ac and Glc*N*Ac moieties (Zoll *et al*., 2010, Büttner *et al*., 2014, Nega *et al*., 2020). The zwitterionic characteristics of WTAs, based on negatively charged phosphate groups and positively charged free amino groups within attached D-alanine moieties (see section 1.6) (Neuhaus & Baddiley, 2003, Weidenmaier & Peschel, 2008), allow the formation of an acidic micromilieu by attracting protons with their negatively charged phosphate backbone to modulate the activity of enzymes situated in the bacterial cell wall. Biswas *et al*. (2012) proposed that the activity of Atl, which is mainly active at a neutral pH, is therefore inhibited in close proximity to the glycopolymers. In the absence of WTAs, Atl-derived autolysins do not localize at the septal division site anymore but are distributed all over the cell surface. Concomitantly, the cells become more susceptible to autolysis (Oshida *et al*., 1995, Heilmann *et al*., 1997). WTAs have been shown to chelate magnesium and manganese ions with high affinity and could also positively affect the regulation of cell wall enzymes (Heptinstall *et al*., 1970, Kern *et al*., 2010).

WTAs are one of the first structures of the cell to encounter harmful substances, such as antibiotics and effectors released by the host immune defense system. The zwitterionic properties of the glycopolymers contribute to the resistance to cationic antimicrobial peptides (CAMPs, *e.g.*, defensins and protegrins), lytic enzymes including lysozyme, cationic antibiotics (*e.g.*, vancomycin), and bacteriocins (Peschel *et al.*, 1999 & 2000, Collins *et al.*, 2002, Bera *et al.*, 2007). In addition, WTAs provide protection against immoderate environmental conditions, including heat stress (Vergara-Irigaray *et al.*, 2008).

Due to their cell surface exposition and chemical properties, WTAs play a pivotal role in the adherence to surfaces (inert, *e.g.*, polystyrene and glass, as well as animal tissue) and in biofilm formation (Gross *et al.*, 2001). *In vivo*, the glycopolymers have been shown to be crucial for nasal colonization and induce abscess formation in animal models (Weidenmaier *et al.*, 2004, Tzianabos *et al.*, 2001). WTAs directly interact with host receptors and are major targets of the host defense system (Van Dalen *et al.*, 2020). Conversely to the exploitation of host receptors for nasal colonization, WTAs themselves can serve as ligands for bacteriophages (Chatterjee, 1969, Park *et al.*, 1974, Weidenmaier *et al.*, 2004).

Taken together, WTAs represent attractive targets for novel antimicrobial agents due to the spatio-temporal interplay of WTA and PG machineries and their function in bacteria-host interaction and biofilm formation.

1.6 The structure and composition of wall teichoic acids

WTAs decorate approximately every nineth Mur*N*Ac moiety and represent a main component of the Gram-positive cell wall, comprising up to 60% of the cell wall dry mass (Ellwood, 1970, Kojima *et al.*, 1985, Tomita *et al.*, 2010). WTA chains are composed of two structural domains: the disaccharide linkage unit and a polymer of repeating polyol phosphate units (Figure 4) (Neuhaus & Baddiley, 2003). The former is composed of Man*N*Ac(β-1,4)Glc*N*Ac with one to three glycerol phosphate units linked via the C_4 hydroxyl of the Man*N*Ac moiety (Kojima *et al.*, 1985, Araki & Ito, 1989, Neuhaus & Baddiley, 2003). The linkage unit is mostly conserved among Gram-positive bacteria and covalently attached via a phosphodiester bond to the C_6 hydroxyl of the Mur*N*Ac residue in PG (Ward, 1981, Neuhaus & Baddiley, 2003). In contrast, the length and composition of

the adjoining polyol phosphate repeats, which are also phosphodiester-linked, can vary among different bacteria and even within one species (Naumova *et al*., 2001, Neuhaus & Baddiley, 2003, Vinogradov *et al*., 2006). In most *S*. *aureus* strains, the linkage unit comprises two glycerol phosphate residues and is connected to a poly(ribitol phosphate) chain (Baddiley *et al*., 1962, Brown *et al*., 2013). However, the *S*. *aureus* species ST395 lineage possesses poly(glycerol phosphate) WTAs as commonly found in coagulase-negative staphylococci and *B*. *subtilis* 168 (Endl *et al*., 1984, Lazarevic *et al*., 2002, Winstel *et al*., 2014).

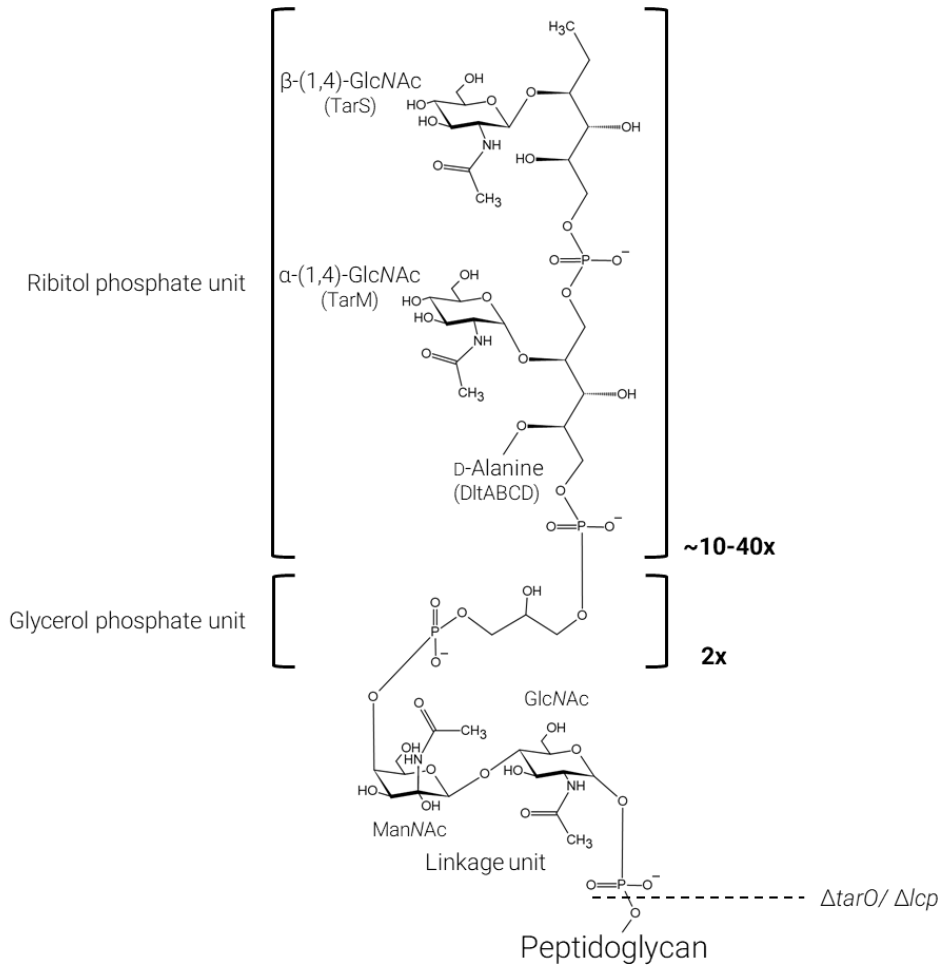

Figure 4: The structure of wall teichoic acids in *S*. *aureus*. The common WTAs found in the majority of *S*. *aureus* strains possess a ribitol phosphate backbone substituted by D-alanine as well as α-(1,4)-GlcNAc and/or β-(1,4)-GlcNAc residues.

The WTA polymer is variably substituted with D-alanine esters at the C_2 hydroxyl of ribitol depending on growth factors, including temperature, medium pH, and salt concentration

(Neuhaus & Baddiley, 2003). The degree of D-alanylation can modulate the net anionic charge of WTAs that is crucial for the function in, *e.g.*, ion homeostasis, resistance to cationic antibiotics, and regulation of autolysins (Neuhaus & Baddiley, 2003). Further modifications of WTAs in *S. aureus* include the glycosylation of the ribitol C_3 or C_4 hydroxyl with Glc*N*Ac in α- and/or β-configuration (Figure 4). Substitutions in exclusively one configuration or mixtures can occur and are highly dynamic depending on environmental influences (Torii *et al.*, 1964, Nathenson *et al.*, 1966, Gerlach *et al.*, 2018, Mistretta *et al.*, 2019).

1.7 The wall teichoic acids biosynthesis in *S. aureus*

The complete WTA biosynthetic pathway takes place in three cellular compartments, *i.e.*, the cytoplasm, the inner leaflet of the cytoplasmic membrane, and the exterior of the cell (Figure 2). The same carrier lipid as in PG biosynthesis, C_{55}-P, is used for the biosynthesis of WTAs, emphasizing the importance of a functional carrier recycling for cell wall maintenance. Due to the formation of poly(ribitol phosphate) WTAs, genes involved in *S. aureus* WTA biosynthesis carry the prefix *tar* for "teichoic acid ribitol", whereas biosynthetic genes required for poly(glycerol phosphate) WTAs are annotated *tag* genes. Since both types of WTAs are found in different *S. aureus* strains with poly(ribitol phosphate) WTAs as primarily occurring variant, the *tar* term is used in this work (Weidenmaier & Lee, 2017).

WTA biosynthesis in *S. aureus* begins in the cytoplasm with the transfer of phospho-D-Glc*N*Ac from UDP-D-Glc*N*Ac to the membrane-anchored carrier lipid C_{55}-P, resulting in the formation of the first precursor, lipid III_{WTA} (undecaprenyl-pyrophosphate-*N*-acetyl-D-glucosamine). This reaction is catalyzed by the integral glycosyltransferase TarO and can be inhibited by the natural product tunicamycin that also targets the hexose-1-phosphate transferase MraY of PG biosynthesis, albeit to a lesser extent (Soldo *et al.*, 2002a, Campbell *et al.*, 2011). Following the stereochemical inversion of UDP-D-Glc*N*Ac at position C_2 to UDP-D-Man*N*Ac by the cytoplasmic epimerase MnaA, the membrane-embedded transferase TarA attaches Man*N*Ac to the Glc*N*Ac residue of lipid III_{WTA} via a β-glycosidic linkage to complete the core component of the WTA linkage unit (Soldo *et al.*, 2002b, D'Elia *et al.*, 2009b).

The glycerol-3-phosphate cytidylyltransferase TarD catalyzes the formation of CDP(cytidine diphosphate)-glycerol that serves as a substrate for the stepwise addition of two phosphoglycerol units to the C_4 hydroxyl of Man*N*Ac by the transferases TarB and TarF, completing the linkage unit (Badurina *et al*., 2003, Bhavsar *et al*., 2005, Ginsberg *et al*., 2006, Brown *et al*., 2010). The complete ribitol phosphate polymer, consisting of about 10 to 40 1,5-connected units, is gradually assembled by the bifunctional enzymes TarK and TarL (Ginsberg *et al*., 2006, Brown *et al*., 2008, Meredith *et al*., 2008, Pereira *et al*., 2008).

While still embedded in the cytoplasmic leaflet of the membrane, the WTA precursor is substituted with α- and/or β-linked Glc*N*Ac residues by the enzymes TarM and/or TarS, respectively (Figure 4) (Xia *et al*., 2010b, Brown *et al*., 2012). Following glycosylation, the ultimate WTA precursor is translocated across the membrane to the external face by the ATP-binding cassette (ABC) transporter system TarGH, which is specifically targeted by the antibiotic targocil, and esterified with D-alanine moieties (Lazarevic & Karamata, 1995, Neuhaus & Baddiley, 2003, Campbell *et al*., 2012). The origin of the D-alanine substrate, however, has not yet been determined although it has been speculated that D-alanine is transferred to WTAs from alanylated LTAs (Koch *et al*., 1985, Reichmann *et al*., 2013). Subsequently, the glycopolymer is covalently attached to the C_6 Mur*N*Ac hydroxyl of the murein sacculus by members of the LytR-CpsA-Psr (LCP) enzyme family (Kawai *et al*., 2011, Eberhardt *et al*., 2012). The distinct identity of the acceptor substrate, either intermediate lipid II, nascent (uncross-linked) or mature (cross-linked) PG, however, is controversially discussed (Chan *et al*., 2013, Schaefer *et al*., 2017, Rausch *et al*., 2019).

1.8 The discovery of the LytR-CpsA-Psr (LCP) enzyme family

The LytR-CpsA-Psr (LCP) enzyme family is a group of transferases that is responsible for the attachment of anionic glycopolymers, such as WTAs (Kawai *et al*., 2011, Chan *et al*., 2013, Gale *et al*., 2017, Schaefer *et al*., 2017), CPs (Hanson *et al*., 2012, Chan *et al*., 2014, Rausch *et al*., 2019), and arabinogalactan (Baumgart *et al*., 2016, Grzegorzewicz *et al*., 2016, Harrison *et al*., 2016), to PG in Gram-positive bacteria. The acronym “LCP” originates from the three proteins LytR (lytic repressor of *B. subtilis*), CpsA (capsular polysaccharide expression regulator of *S. pneumoniae*),

and Psr (PBP5 synthesis repressor of *Enterococcus hirae*) (Lazarevic *et al*., 1992, Massidda *et al*., 1996, Rossi *et al*., 2003).

Genes encoding for members of the LCP enzyme family have been almost exclusively discovered in Gram-positive bacteria except for the cell wall-lacking order *Mollicutes*, indicating that they may be involved in maintenance of the Gram-positive cell wall (Hübscher *et al*., 2008). All examined strains belonging to the Gram-positive phylum *Firmicutes* possessed at least one gene encoding for a member of the LCP protein family, and a maximum of 11 genes were found in the actinobacterium *Streptomyces coelicolor*. The occurrence of multiple LCP enzymes in different species could refer to functional specificity and/or redundancy in the LCP family (Hübscher *et al*., 2008, Eberhardt *et al*., 2012). LCP proteins share a common structure consisting of a short intracellular N-terminal sequence, a single transmembrane helix, and the catalytic extracellular LCP domain. Crystal structures of CpsA from *S*. *pneumoniae* reveal a catalytic magnesium ion that is coordinated by aspartate residues within the LCP domain (Kawai *et al*., 2011).

In search of the missing transferase that attaches the WTA polymer covalently to PG in *B*. *subtilis*, Kawai *et al*. (2011) purified MreB, whose assembly products build the bacterial cytoskeleton and are associated with WTA biosynthetic proteins (Yokoyama *et al*., 1989, Graumann, 2009, Kawai *et al*., 2011). The three LCP proteins YwtF, LytR, and YvhJ, later renamed to TagT, TagU, and TagV, were co-purified and stood out due to their transmembrane (TM) topology, phylogenetic distribution, and the gene localization close to that of known WTA biosynthetic genes (Kawai *et al*., 2011). A Δ*tagTUV* mutant was not viable under normal growth conditions but could be rescued by simultaneous disruption of *tarO*, the first gene involved in WTA biosynthesis. The amounts of WTAs in double mutant variants and a conditional Δ*tagTUV* triple mutant were strikingly reduced and these results confirmed, for the first time, the direct involvement of LCP proteins in WTA biosynthesis (Kawai *et al*., 2011). The work group further revealed that the crystal structure of heterologously expressed *S*. *pneumoniae* ΔTM-Cps2A contains a polyisoprenyl (pyro)phosphate lipid bound to the conserved LCP domain with a magnesium ion perfectly aligned between the two phosphate residues. Unless magnesium was absent or complexed by ethylenediaminetetraacetic acid (EDTA), ΔTM-Cps2A catalyzed the hydrolysis of the phosphodiester bond in the nestled pyrophosphate lipid. In 2017, Schaefer *et al*. reconstituted the capacity of soluble *S*. *aureus* LCP homologs LcpA, LcpB, and LcpC to transfer WTA precursors

to PG oligomers *in vitro*. The work group prepared the radiolabeled WTA precursors C_{30}-lipid IV_{WTA} (hexaprenyl-pyrophospho-Glc*N*Ac-Mur*N*Ac) and C_{30}-lipid V_{WTA} (hexaprenyl-pyrophospho-Glc*N*Ac-Mur*N*Ac-phosphoglycerol) containing a truncated lipid chain and were able to show the glycopolymer ligation to PG oligomers by polyacrylamide gel electrophoresis autoradiography. Moreover, the capacity of ΔTM-LcpA to link the disaccharide unit from lipid IV_{WTA} to nascent PG produced from C_{20}-lipid II was confirmed by high-resolution mass spectrometry. Hence, the first biochemical evidence that LCP proteins are directly entangled in the ligation of WTAs to PG was provided.

1.9 The LCP enzymes of *S. aureus*

The *S. aureus* genome codes for three LCP proteins named LcpA/MsrR/SA1195, LcpB/SA0908, and LcpC/SA2103, with a common topology consisting of a short N-terminal cytoplasmic linker, a single transmembrane α-helix encompassing around 20 amino acids (aa), and an extracellular LCP domain (Figure 5). In contrast to LcpA (327 aa) and LcpC (315 aa), LcpB (405 aa) possesses a remarkably elongated C-terminal region of unknown function. The predicted 3D structure of LcpB provided by Alphafold (identifier AF-A0A0H3JTR6-F1, date accessed April 19, 2023, Jumper *et al*., 2021, program developed by DeepMind, London, UK) reveals an unstructured domain with a minor per-residue confidence score.

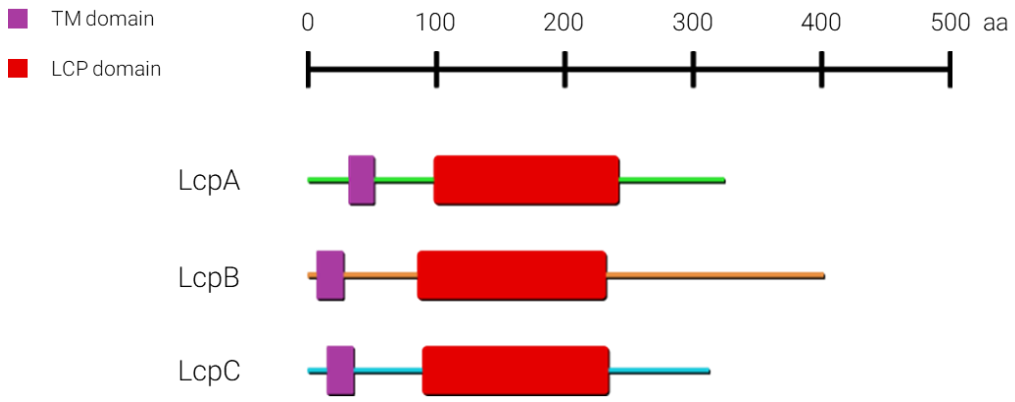

Figure 5: Structural features of the LytR-CpsA-Psr (LCP) enzyme family members in *S. aureus*. The typical domain organization includes a short N-terminal tail followed by a transmembrane (TM) domain and the C-terminal LytR-CpsA-Psr (LCP) domain.

So far, only the crystal structure of soluble LcpA complexed with C_{40}-lipid III_{WTA} (octaprenyl-pyrophospho-Glc*N*Ac) has been solved, showing that the LCP domain consists of a six-stranded β-sheet superimposed by a number of α-helices and double-stranded β-sheets (Li *et al*., 2020). A striking feature is the large hydrophobic lipid binding pocket with a slim opening that expands towards the base. The active site of LcpA is located at the entrance of the pocket with a positively charged region favourable to interact with the pyrophosphate residue of the donor lipid. It encompasses several conserved arginine residues and is surrounded by four loops (regions A to D) that structurally differ from LCP proteins found in other Gram-positive species (Li *et al*., 2020).

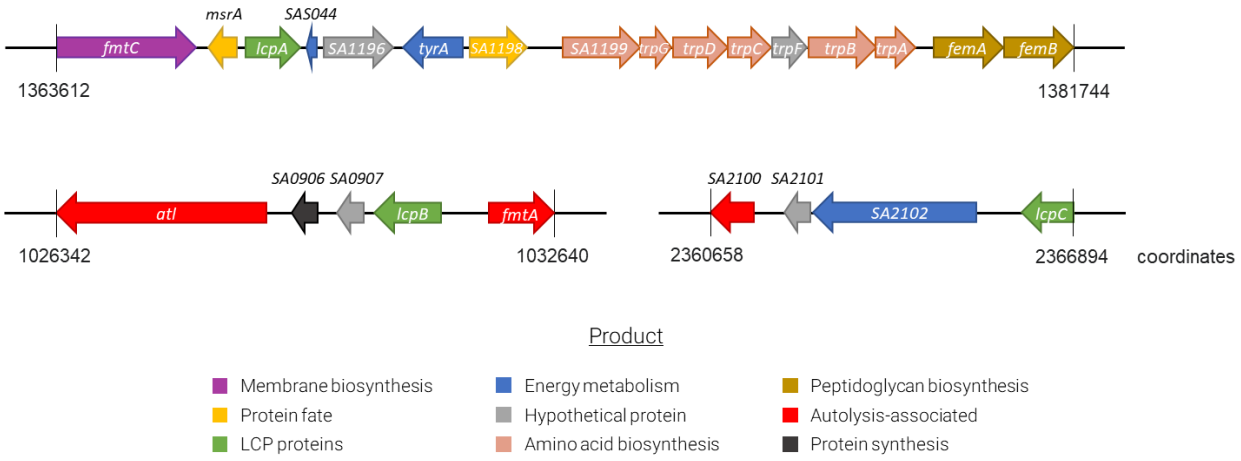

Figure 6: Genetic organization of *lcpA*, *lcpB*, and *lcpC* in the *S. aureus* N315 genome.

While the three LCP genes in *B. subtilis* are encoded within a 50 kb DNA segment that encompasses almost every WTA biosynthetic gene (Kawai *et al*., 2011), the *S. aureus lcp* genes are dispersed within the genome but localized in proximity of genes associated with the modulation of the cell envelope (Figure 6). The *fmtC*/*mprF* gene, encoding for a protein involved in the biosynthesis of the cytoplasmic membrane component lysylphosphatidylglycerol (Staubitz *et al*., 2004), is located upstream of *lcpA*, while the genes encoding for the Fem enzymes, which are responsible for the attachment of the pentaglycine residue to the ultimate PG precursor lipid II (Schneider *et al*., 2004), are found in the downstream region. Interestingly, *lcpB* is indirectly flanked by genes encoding for the major autolysin in *S. aureus*, Atl, and the teichoic acid D-alanine esterase FmtA that is thought to modulate the teichoic acid charge depending on environmental conditions (Rahman *et al*., 2016). *lcpC* lies in close proximity to *SA2100*, a proposed homolog of

the amidase domain of *Staphylococcus epidermidis* autolysin E (Heilmann *et al*., 1997, Over *et al*., 2011).

The LCP genes are part of the cell wall stress stimulon which is induced by cell wall-active antibiotics and, in consequence, causes the disruption of genes encoding for crucial cell envelope biosynthesis enzymes. The depletion of one, two, or all LCP proteins activates the cell wall stress response, emphasizing the importance of this enzyme family for cell wall integrity (Dengler *et al*., 2012).

LCP proteins are suggested to play semi-redundant roles in the linkage of anionic glycopolymers to PG (Eberhardt *et al*., 2012, Chan *et al*., 2013 & 2014, Schaefer *et al*., 2017). In LCP-deficient strains, WTA attachment is restored by complementation with each LCP enzyme, indicating that LcpA, LcpB, and LcpC have WTA ligase activity (Chan *et al*., 2013). This could be confirmed by *in vitro* reconstitution conducted by Schaefer *et al*. (2017). However, the deletion of *lcpA* or *lcpB* results in a more pronounced reduction of cell wall-associated WTAs compared to *lcpC* (Dengler *et al*., 2012, Chan *et al*., 2013). The capsule is covalently linked to the C_6 hydroxyl of PG Mur*N*Ac by LCP enzymes and thus competes with WTAs for this attachment site. Accordingly, as seen in *S*. *pneumoniae*, the amounts of each polymer are negatively correlated (Kim & Weiser, 1998, Yother, 2011, Eberhardt *et al*., 2012). Capsule attachment is completely suppressed in LCP-depleted *S*. *aureus* cells but restored when plasmid-encoded LcpA, LcpB, and LcpC are expressed in *trans*. However, the deletion of neither *lcpA* nor *lcpB* affects CP attachment, while Δ*lcpC* single and Δ*lcpAC* and Δ*lcpBC* double mutants display a distinct reduction in CP anchoring (Chan *et al*., 2014). Rausch *et al*. (2019) could confirm the CP ligase activity of LcpC by *in vitro* reconstitution. The aforementioned results highlight the functional semi-redundancy of LCP enzymes in *S*. *aureus*. Yet, LcpA is supposed to play a leading role in WTA attachment, while LcpC is thought to be the major CP ligase (Chan *et al*., 2013 & 2014, Schaefer *et al*., 2017, Rausch *et al*., 2019).

The disruption of all three *lcp* genes in *S*. *aureus* impairs the growth rate, especially at higher temperatures, and results in severe morphological damages, including enlarged, widely deformed cells with multiple, misplaced septa (Over *et al*., 2011). Each LCP protein is able to restore growth, although to a different extent: complementation with *lcpA* restores the phenotype almost completely, while cells complemented with *lcpB* or *lcpC* still exhibit abnormalities. However, *lcpB* better compensates growth and deformities than *lcpC*. Single knockout mutants of *lcpB* and *lcpC*

have no distinguishable effect on cell size and septum placement, whereas the deletion of only *lcpA* results in enlarged cells and septal irregularities (Hübscher *et al*., 2009, Over *et al*., 2011). The latter phenotype strongly resembles that of the WTA-deficient Δ*tarO* strain and cells treated with the TarO inhibitor tunicamycin (Campbell *et al*., 2011).

To ensure an ordered cell wall maintenance and division, autolysins need to be firmly regulated. The disruption of *lcpA* and/or *lcpC* does not affect triton X-100-induced autolysis, while Δ*lcpB* single and double mutants display a strongly enhanced autolytic activity (Over *et al*., 2011). This result may be associated with the genetic organization of *lcpB* and the downstream gene *atl* (Figure 6), which encodes for the major autolysin in *S*. *aureus*, suggesting an interplay between both proteins. In the absence of WTAs, cells become more susceptible to detergent-induced autolysis due to an increased adherence of autolysins to the cell wall (Schlag *et al*., 2010).

When *lcpA* is deleted in MRSA strains, the cells become susceptible to the β-lactam oxacillin and resistance can be restored by complementation of *lcpA* in *trans* (Rossi *et al*., 2003, Schaefer *et al*., 2017). The disruption of *lcpB* causes a similar but less pronounced effect in different MRSA background strains, whereas Δ*lcpC* knockout mutants were not tested by Schaefer *et al*. (2017). In staphylococci, β-lactam resistance primarily occurs through the production of a β-lactamase and/or the expression of *mecA* or *mecC*, which both encode for a PBP with low affinity for most β-lactam antibiotics (Hartman & Tomasz, 1984, Matsuhashi *et al*., 1986, Ballhausen *et al*., 2014, Nomura *et al*., 2020). In addition, the equipment of the *S*. *aureus* cell wall with WTAs is required for β-lactam resistance (Brown *et al*., 2012, Farha *et al*., 2013). Accordingly, the TarO inhibitor tunicamycin has been shown to act synergistically with oxacillin in MRSA strains (Campbell *et al*., 2011). It has been suggested that WTAs scaffold proteins involved in PG biosynthesis and turnover (Schlag *et al*., 2010, Atilano *et al*., 2010, Campbell *et al*., 2011, Frankel & Schneewind, 2012) that could include enzymes conferring resistance to β-lactams. In line with this assumption, the interaction of PBP2a and WTA glycopolymers could be confirmed by Qamar & Golemi-Kotra (2012). The Δ*tarO* and Δ*lcpA* single and double mutants are equally sensitive to oxacillin, emphasizing the importance of LcpA in WTA ligation (Schaefer *et al*., 2017).

The abrogation of WTA biosynthesis affects the nasal colonization of *S*. *aureus* strains in human and cotton rats (Weidenmaier *et al*., 2004). Moreover, the virulence of *lcpA*-inactivated single and double mutants of *S*. *aureus* MSSA1112 is strongly reduced in *Caenorhabditis elegans* killing

assays. The nematodes exhibit a slightly enhanced survival rate upon infection with the Δ*lcpB* mutant compared to the wildtype strain, while the disruption of *lcpC* does not affect virulence (Over *et al*., 2011). Hübscher *et al*. (2009) also confirmed in a rat endocarditis model that the absence of LcpA decreases virulence.

Notably, LCP-deficient *S*. *aureus* strains release minimal amounts of WTA glycopolymers in the culture medium. This effect is abolished in the presence of the TarO inhibitor tunicamycin (Chan *et al*., 2013). Moreover, Δ*lcpC* single and double mutants as well as the Δ*lcpABC* triple mutant release CPs to the growth medium, indicating that WTA and CP biosyntheses are continued to a certain degree in the absence of LCP enzymes, but no attachment occurs (Chan *et al*., 2013 & 2014). Although the late-stage genes involved in WTA biosynthesis and translocation of the ultimate precursor across the cytoplasmic membrane are essential for cell growth, *S*. *aureus* cells lacking all three LCPs are viable but affected in their growth behavior (D'Elia *et al*., 2006a, Over *et al*., 2011). This observation raises the question of how WTA and CP precursors are cleaved from their carrier lipid after translocation to the outer face of the cytoplasmic membrane if the hydrolytic activity of LCP enzymes is completely abrogated. The hypersusceptibility of the LCP-depleted MSSA1112 strain to bacitracin, an antibiotic known to complex C_{55}-PP and thereby interfering with recycling of the carrier lipid (Qi *et al*., 2008, Dengler *et al*., 2012, Economou *et al*., 2013), contradicts the hypothesis that the precursors are still cleaved in the absence of LCPs. Since CPs and WTAs are attached to PG via a phosphodiester bond, the PG biosynthesis pathway is the only one releasing C_{55}-PP. If the glycopolymers stay attached to the carrier lipid after translocation in the mutant strain, the hypersensitivity to bacitracin may be caused by a carrier shortage for the essential PG biosynthesis (Dengler *et al*., 2012).

Taken together, it can be assumed that, in *S*. *aureus*, LCP enzymes may have semi-redundant roles, with LcpA acting as the major WTA ligase and LcpC being mainly responsible for CP attachment. The precise role for LcpB is less obvious, as this protein is able to link both types of glycopolymers to PG and, in addition, seems to be particularly involved in the protection from autolysis (Over *et al*., 2011, Chan *et al*., 2013 & 2014, Schaefer *et al*., 2017, Rausch *et al*., 2019). Since MRSA strains devoid of WTAs become susceptible to β-lactam antibiotics (Rossi *et al*., 2003, Wang *et al*., 2013, Schaefer *et al*., 2017), LCP enzymes could be attractive targets for new antimicrobial therapeutics.

1.10 Moenomycin family antibiotics

Moenomycins are natural product antibiotics derived from the bacterial genus *Streptomyces* and are known to inhibit bacterial PG biosynthesis by targeting PG glycosyltransferases (van Heijenoort & van Heijenoort, 1980, Chen *et al*., 2003, Halliday *et al*., 2006). Discovered in 1965, moenomycin A was the first identified member of this antibiotic family comprising only phosphoglycolipids (Wallhausser *et al*., 1965, Huber *et al*., 1965, Lenoir *et al*., 1969).

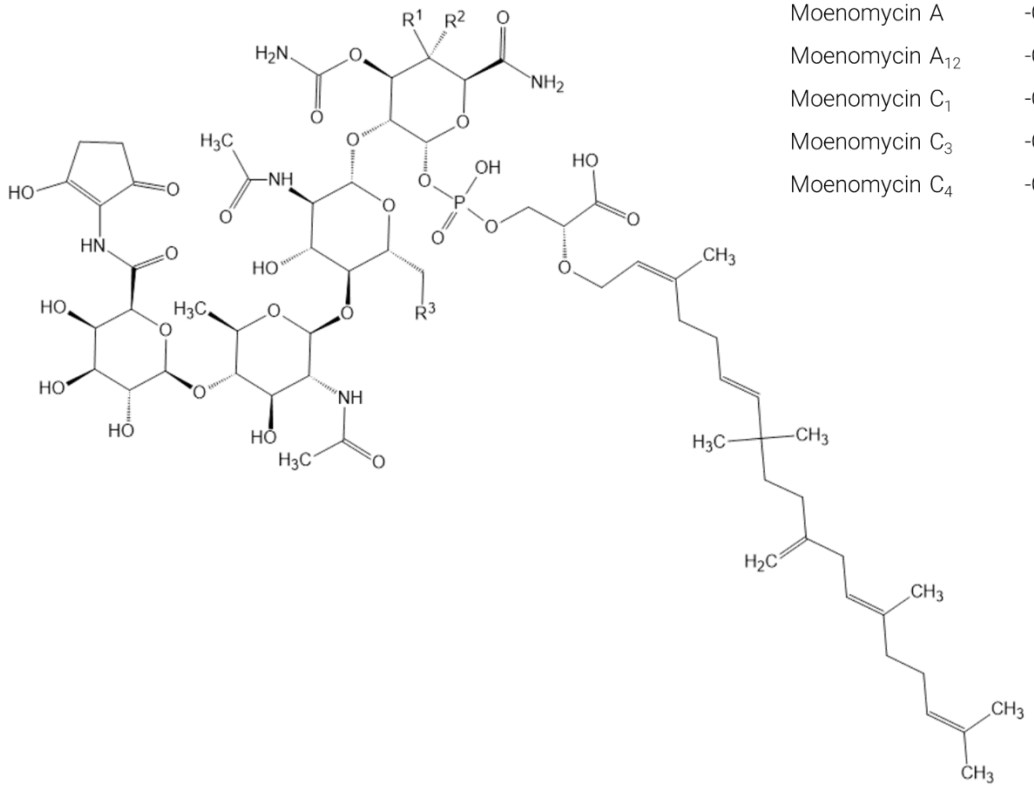

Component	R^1	R^2	R^3
Moenomycin A	$-CH_3$	-OH	-OGlc
Moenomycin A_{12}	$-CH_3$	-H	-OGlc
Moenomycin C_1	$-CH_3$	-H	-H
Moenomycin C_3	$-CH_3$	-OH	-H
Moenomycin C_4	$-CH_3$	-OH	-OH

Figure 7: Chemical structures of selected moenomycins.

Moenomycins share a common basic structure consisting of a 3-phosphoglyceric acid core that is linked via a phosphodiester bond to a complex tetrasaccharide and tethered to an exceptional C_{25}-isoprenoid chain with its C_2 hydroxyl (Figure 7). The structure of the lipid isomer as well as diverse substitutions of the tetrasaccharide unit vary among different members of the moenomycin family (Ostash & Walker, 2010). In Gram-positive bacteria, minimal inhibitory concentrations (MICs) between 1 to 100 ng/ml have been determined and a high potency against

MRSA and vancomycin-resistant *S. aureus* (VRSA) strains has been observed (Ostash & Walker, 2010). To achieve the same bactericidal effect against Gram-negative bacteria requires 100 to 1000-fold higher moenomycin concentrations to facilitate the uptake across the outer membrane. Accordingly, some Gram-negative strains with an increased permeability of the outer membrane, such as *Neisseria*, are highly susceptible to the phosphoglycolipid (Torikata *et al*., 1977, Parenti *et al*., 1978, van Heijenoort *et al*., 1987, Baizman *et al*., 2000, Ostash & Walker, 2010, Yang *et al*., 2022).

Crystal structures of PG glycosyltransferases complexed with neryl- or full-length moenomycin A reveal that the compound binds to the donor site in the catalytic cavity, which is normally occupied by the elongating lipid-linked glycan chain, whereas the substrate lipid II binds to the acceptor site. Thus, the polymerization of glycan chains is inhibited which ultimately leads to cell death (Lovering *et al*., 2007, Yuan *et al*., 2008, Heaslet *et al*., 2009, Sung *et al*., 2009). The binding of moenomycin A to PG glycosyltransferases is reversible and the compound does not compete with the substrate lipid II (Stembera *et al*., 2002, Chen *et al*., 2003, Cheng *et al*., 2008).

Moenomycins have served as animal growth promotors for decades. Although a widespread prevalence of acquired moenomycin-resistance in animal livestock has not been reported, their use as feed additives has officially been prohibited in the European Union since 2006, while the application in the United States is still approved (Pfaller, 2006, Gallo *et al*., 2010, Ostash & Walker, 2010). The phosphoglycolipids are not therapeutically used in human medicine due to their poor pharmacokinetic properties. Presumably caused by the isoprenoid chain, they form micelle-like structures in aqueous solutions and have a long half-life in the bloodstream. In addition, moenomycins show hemolytic activity and no bioavailability when administered orally (Volke *et al*., 1997, Graves-Woodward & Pratt, 1999, Anikin *et al*., 1999, Pfaller, 2006, Adachi *et al*., 2006). The shortening of the lipid chain, however, has been demonstrated to reduce the antibiotic activity (Vogel *et al*., 2001a & b, Welzel, 2005, Ostash *et al*., 2009). Nevertheless, moenomycins are potent inhibitors and can serve as a powerful template for the development of structurally related compounds for the treatment of human infections.

In this work, if not stated otherwise, the annotation “moenomycin” is used for a mixture of the moenomycins A, A_{12}, C_1, C_3, and C_4.

Chapter 2: The discovery and characterization of corallorazines

The ubiquitous, soil-dwelling Myxobacteria of the order Myxococcales exhibit an exceptional multicellular way of living expressed by aggregation into swarms, quorum sensing, fruiting-body formation, and preying on a vast array of bacteria and fungi (Pérez *et al*., 2016, Arias Del Angel *et al*., 2017, Livingstone *et al*., 2017). Myxobacteria possess the largest genomes of prokaryotes known so far. They are a rich source of secondary metabolites, including potent antimicrobials of novel structural classes with innovative modes of action that are urgently needed to overcome the ascending antibiotic crisis (Wenzel & Müller, 2009, Weissman & Müller, 2010).

Corallorazines were first discovered by Schmitz *et al*. (2014) as a novel set of secondary metabolites synthesized by the myxobacterium *Corallococcus coralloides* B035. The organism was originally isolated from a Belgian soil sample in the 1980s (Irschik *et al*., 1985) and is known to produce corallopyronin A, a potent DNA-dependent RNA polymerase inhibitor that is effective against Gram-positive and intracellular Gram-negative bacteria and currently undergoing preclinical trials (Schäberle *et al*., 2014b, Krome *et al*., 2022).

Corallorazines are classified as lipodipeptides and comprise three structurally related compounds, corallorazine A, corallorazine B, and corallorazine C (Figure 8). Corallorazine A is the major metabolite and contains a core piperazine ring composed of *N*-methylglycine and dehydroalanine (Dha) that are cyclized via a hemiaminal. Additionally, the Dha residue is acylated with the rare branched fatty acid (2*E*, 4*Z*)-iso-octa-2,4-dienoic acid. Corallorazine B and C have been suggested to form intermediates of the corallorazine biosynthesis pathway, because the latter is lacking the *N*-methyl group and the glycine residue is absent in both compounds. Deduced from high-resolution mass spectrometry (HRMS) and nuclear magnetic resonance spectroscopy (NMR) experiments, corallorazine A has a molecular formula of $C_{15}H_{22}N_2O_3$ with a molar mass of 278.35 g/mol. The UV maximum was detected at λmax = 267 nm. The hemiaminal functionality enables the formation of enantiomers with a ratio of 44:56, as judged from high-performance liquid chromatography (HPLC) results (Schmitz *et al*., 2014).

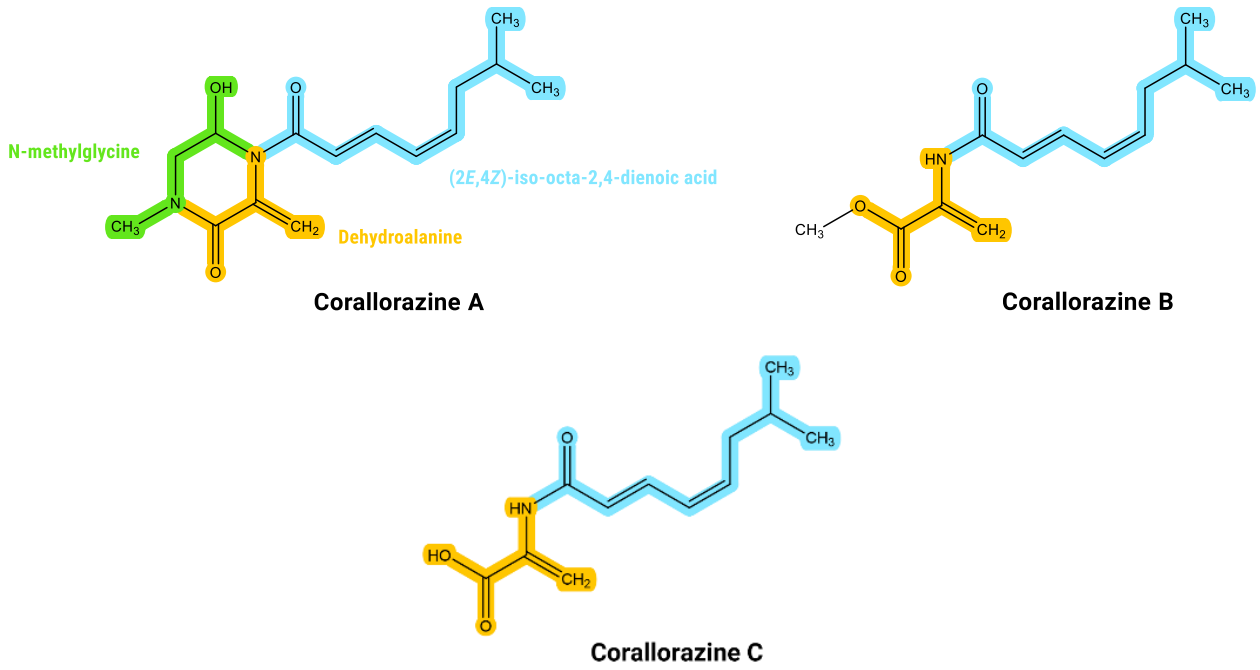

Figure 8: Structure of corallorazine A, B, and C as derived from NMR and HRMS experiments (Schmitz *et al*., 2014). Homologous residues are highlighted in similar colors. All of these compounds contain an acylated dehydroalanine backbone (yellow) and a rare branched fatty acid (blue). The structure of corallorazine A includes additionally an *N*-methylglycine residue (green), while corallorazine B bears a supplementary methyl group.

Dreckmann *et al*. (manuscript in preparation) identified the corallorazine nonribosomal peptide synthetase (NRPS) biosynthetic gene cluster (BGC) *crz* (Figure 9) and reconstituted the biosynthesis pathway *in vitro* to produce a corallorazine A derivative with an altered acyl chain. The corallorazine BGC of *C. coralloides* belongs to a supercluster and comprises 16.5 kb that can be divided into eight biosynthetic *crz* genes. *crz7* and *crz8* encode a cytochrome P450 oxygenase and the associated flavine mononucleotide reductase, respectively. However, for the enzymatic biosynthesis of corallorazine A, these proteins seem to be irrelevant, because the complete structure of the compound can be derived from functional predictions of Crz1-6. The biosynthesis pathway appears to commence with the formation of the rare acyl chain (2*E*,4*Z*)-iso-octa-2,4-dienoic acid from isovaleryl-CoA and a second yet unknown substrate. Crz4 and Crz5 are acyl-CoA dehydrogenases that presumably incorporate double bonds into the acyl chain while *crz3* encodes for an acyl-CoA-ligase transferring the CoA-bearing precursor onto the acyl carrier protein Crz6. *crz1* encodes for the megaenzyme Crz1 that assembles into a bimodular NRPS system together with Crz2. It is suggested to add an L-serine to the acyl chain in a lipoinitiation reaction and to catalyze its dehydration to dehydroalanine. In a next step, a glycine molecule is

methylated and attached to the precursor, forming the dipeptidic Dha-*N*-methyl-Gly backbone. By consuming NAD(P)H, the product is cyclized and released as completed corallorazine A (Dreckmann *et al*., manuscript in preparation).

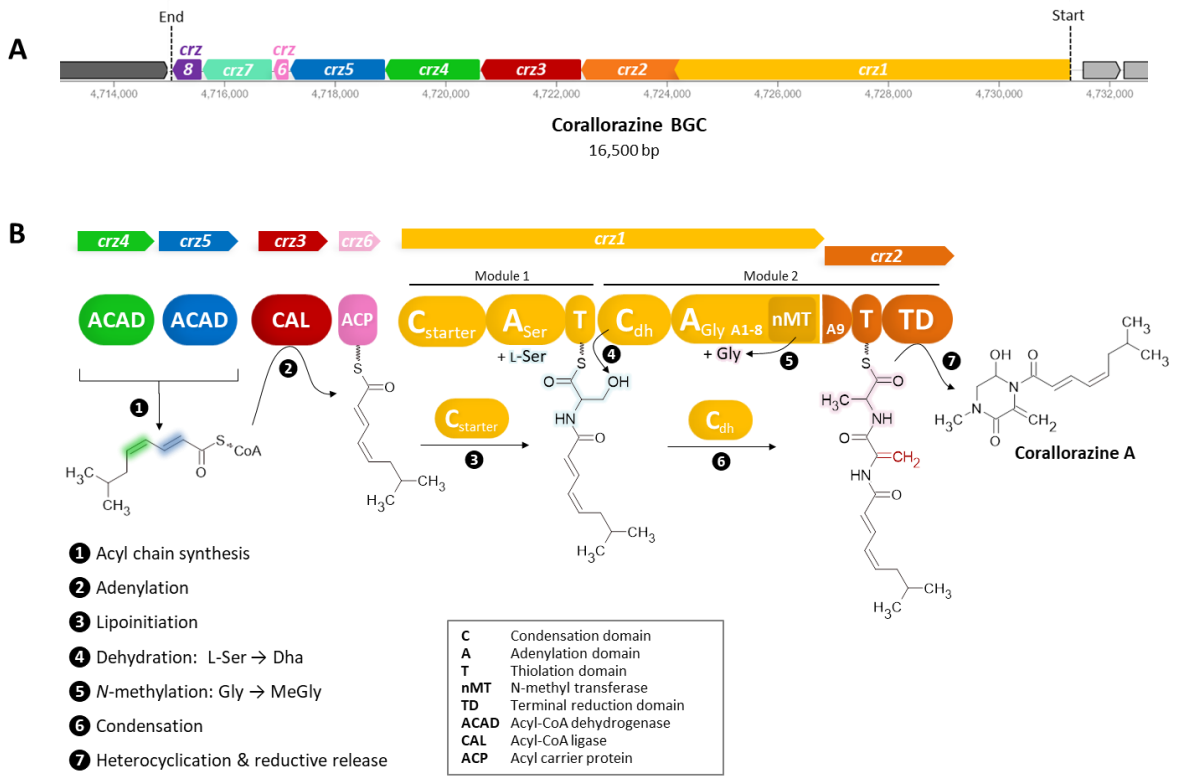

Figure 9: (A) Genetic organization of the 16.5 kb corallorazine biosynthetic gene cluster (BGC) and (B) the predicted corallorazine biosynthesis pathway. Isovaleryl-CoA and a second yet unknown substrate are used to build the rare acyl chain (2*E*,4*Z*)-iso-octa-2,4-dienoic acid. Crz4 and Crz5 are acyl-CoA dehydrogenases supposed to introduce double bonds into the acyl precursor. In the next step, the acyl-CoA-ligase Crz3 connects the acyl chain to the acyl carrier protein Crz6 before it is further modified by the bimodular NRPS consisting of Crz1 and Crz2. The amino acid L-serine is connected to the acyl chain and dehydrated into dehydroalanine. A glycine molecule is methylated and subsequently attached to the growing acyl precursor. After heterocyclization, the product is reductively released, forming completed corallorazine A (figure originating from Dreckmann *et al*., manuscript in preparation).

Corallorazine A has been demonstrated to be unable to inhibit leukocyte elastase, a serine protease secreted by neutrophils during inflammation. Moreover, the compound shows no affinity for cannabinoid receptors, which are involved in the regulation of multiple physiological functions in the human body (Belaaouaj *et al*., 2000, Howlett, 2002, Schmitz *et al*., 2014). To conclude, no biological activity has been detected for corallorazine A so far.

Aims of this thesis

The prevalence of multi-resistant *S. aureus* strains causes increasing numbers of difficult-to-treat, often life-threatening infections, and is a serious issue for healthcare worldwide. While antibiotics once were considered a convenient magic bullet in curing bacterial diseases, the doctor's armamentarium of effective antimicrobials has become depleted. Apart from the development of novel antibiotics with unprecedented mechanisms of action, a detailed knowledge about how anti-infective substances function is indispensable for a potent drug design to outpace the ascending antibiotic crisis. Therefore, the aim of this thesis is to answer the following questions:

- Are LCP proteins off-targets of moenomycin and how does their inhibition contribute to bacterial killing?
- Does corallorazine A have an antibiotic activity and, if so, what is its mode of action?

2. Materials and Methods

2.1 Materials

2.1.1 Chemicals

Chemical/ Reagent	Manufacturer/ Supplier
Acetic acid	Carl Roth, Karlsruhe, Germany
N-Acetylglucosamine	Sigma Aldrich, St. Louis, USA
40% Acrylamide/Bisacrylamide 29:1	PanReac AppliChem, Darmstadt, Germany
Agar	Carl Roth
Agarose	Carl Roth
Ammonium bicarbonate	Sigma Aldrich
Ammonium heptamolybdate	Carl Roth
Ammonium hydroxide	Honeywell, Morristown, USA
Ammonium peroxodisulfate (APS)	PanReac AppliChem
L-Arabinose	Carl Roth
L-Ascorbic acid	Carl Roth
Aqua ad iniectabilia	B. Braun, Melsungen, Germany
5-Bromo-4-chloro-3-indolyl β-D-galactopyranoside (X-gal)	Sigma Aldrich
N-Butanol	Merck, Darmstadt, Germany
C_{55}-P (undecaprenyl-phosphate)	Larodan, Solna, Sweden
Calcium chloride	Merck
Cerium(IV) sulfate	Merck
Chloroform	Thermo Fisher, Waltham, USA
Copper(II) sulfate pentahydrate	Merck
Deoxynucleoside triphosphates (dNTPs)	New England Biolabs, Ipswich, UK
Dimethyl sulfoxide (DMSO)	Sigma Aldrich
1,2-Dioleoyl-*sn*-glycero-3-phospho-(1'-rac-glycerol) (DOPG)	Avanti Polar Lipids, Alabaster, USA
Dipotassium hydrogen phosphate	Carl Roth
Disodium hydrogen phosphate	Carl Roth
Dithiothreitol (DTT)	Carl Roth
N-Dodecyl β-D-maltoside (DDM)	Carl Roth
Double-distilled water	Carl Roth
Ethanol	PanReac AppliChem
Ethylenediaminetetraacetic acid (EDTA)	Merck
Folin-Ciocalteu phenol reagent	Merck
Gel Loading Dye, 6x, purple	New England Biolabs
GelRed nucleic acid stain 10000X water	Biotium, Fremont, USA
Glycerol	Carl Roth

Chemical/ Reagent	Manufacturer/ Supplier
Glycine	Carl Roth
Hydrochloric acid	Carl Roth
2-[4-(2-Hydroxyethyl)piperazin-1-yl]ethane-1-sulfonic acid (HEPES)	Merck
Imidazole	Sigma Aldrich
Iodine	Merck
Isopropanol	Avantor, Radnor, USA
Isopropyl-β-D-thiogalactopyranoside (IPTG)	Thermo Fisher
N-Lauroylsarcosine	Sigma Aldrich
Lithium chloride	Carl Roth
Magnesium chloride	Carl Roth
Magnesium sulfate	Merck
β-Mercaptoethanol	Carl Roth
Methanol	Thermo Fisher
Methylene blue	Sigma Aldrich
2-(*N*-Morpholino)-ethane sulphonic acid (MES)	Carl Roth
Mueller-Hinton broth	Thermo Fisher
Nucleoside triphosphates (NTPs)	Thermo Fisher
NuPAGE LDS sample buffer (4X)	Thermo Fisher
PageBlue protein staining solution	Thermo Fisher
Perchloric acid	Merck
Phosphomolybdic acid	Sigma Aldrich
Phosphoric acid	Merck
Phusion GC Buffer	New England Biolabs
Pierce protease inhibitor mini tablets, EDTA-free	Thermo Fisher
Potassium chloride	Merck
Potassium dihydrogen phosphate	Carl Roth
Potassium hydroxide	Merck
Potassium sodium tartrate tetrahydrate	Merck
Protein assay dye reagent concentrate	Bio-Rad Laboratories, Hercules, USA
Pyridine	Merck
2x RNA loading dye	Thermo Fisher
SOC outgrowth	New England Biolabs
Sodium acetate	Sigma Aldrich
Sodium azide	Sigma Aldrich
Sodium bicarbonate	Honeywell
Sodium borate	bioWORLD, Dublin, USA
Sodium borohydride	Sigma Aldrich
Sodium carbonate	Sigma Aldrich
Sodium chloride	Carl Roth
Sodium dihydrogen phosphate dihydrate	Merck
Sodium dodecyl sulphate	Carl Roth
Sodium hydroxide	Merck
Sodium sulfate	Sigma Aldrich

Chemical/ Reagent	Manufacturer/ Supplier
Sucrose	Carl Roth
Sulfuric acid	Carl Roth
N,*N*,*N*′,*N*′-Tetramethylethane-1,2-diamine (TEMED)	Avantor
Tricine SDS running buffer (10X)	Thermo Fisher
Tris-(hydroxymethyl)-aminomethane hydrochloride	Carl Roth
Tris-MOPS-SDS	GenScript, Piscataway, USA
Triton X-100	Thermo Fisher
Tryptic soy broth	Merck
Tryptone	MP Biomedicals, Eschwege, Germany
UDP-D-[^{14}C]Glc*N*Ac	Hartmann Analytic, Braunschweig, Germany
UDP-D-Glc*N*Ac	Sigma Aldrich
Xylose	Sigma Aldrich
Yeast extract	Carl Roth

2.1.2 Other materials

Utensil/ Reagent	Manufacturer/ Supplier
384-well polystyrene microplate with flat bottom (non-binding, black, ref. 781900)	Greiner Bio One, Frickenhausen, Germany
50 mL conical centrifuge tubes	Corning, Corning, USA
50 mL conical centrifuge tubes, skirt	Greiner Bio One
96-well polystyrene microplate with flat bottom (medium-binding, white, ref. 655075)	Greiner Bio One
96-well polystyrene microplate with flat bottom (transparent, ref. 655161)	Greiner Bio One
96-well polystyrene microplate with U-bottom (sterile, transparent, ref. 650161)	Greiner Bio One
Acrodisc syringe filters (pore size 0.2 µm)	Pall Corporation, Port Washington, USA
Autoclave tape	VWR, Radnor, USA
Axygen 0.2 mL thin wall PCR tubes	Corning
Axygen 80 µm AxySeal sealing film	Corning
BD DISCARDIT II disposable syringes	Becton Dickinson, Franklin Lakes, USA
Cover glass 18 x 18 mm, thickness 0.13-0.17 mm	Engelbrecht, Edermünde, Germany
Cryotubes with attached screw cap	Brand, Wertheim, Germany
Cuvettes (10 x 4 x 45 mm)	Sarstedt, Nümbrecht, Germany
Disposable 5 ml polypropylene columns	Thermo Fisher
Disposal bags	Sarstedt
Electroporation cuvette (1 mm)	Bio-Budget Technologies, Krefeld, Germany

Utensil/ Reagent	Manufacturer/ Supplier
Filtropur BT 50 (pore size 0.2 µm)	Sarstedt
HiTrap DEAE sepharose FF column	Cytiva, Marlborough, USA
Immersol immersion oil 518F	Carl Zeiss, Oberkochen, Germany
Inoculation loop, 1 & 10 µl	Sarstedt
Invitrogen Novex 10-20% tricine gels	Thermo Fisher
Lid with condensation rings, polystyrene (ref. 656171)	Greiner Bio One
Microscope slide 76 x 26 mm (0.95-1.05 mm)	Engelbrecht
Microtube 1.5 ml & 2 ml	Sarstedt
Microtube with Snap-on Seal Closure	Thermo Fisher
NuPAGE 4-12% Bis-Tris acrylamide gel	Thermo Fisher
Nunc OmniTray single-well plates (ref. 140156)	Thermo Fisher
Oligonucleotides	Microsynth, Balgach, Switzerland
Parafilm PM996 wrap	Bemis, Neenah, USA
PCR SoftTubes, 0.5 ml	Biozym, Hessisch Oldendorf, Germany
Peha-soft nitrile white disposable gloves	Hartmann, Heidenheim, Germany
Petri dish (94/16 mm, polystyrene)	Greiner Bio One
pH indicator rod pH 0–14	Carl Roth
Pipette tip 5 ml, 1000 µl, 200 µl & 10 µl	Sarstedt
Protino Ni-NTA agarose	Macherey-Nagel, Düren, Germany
Safe-Lock reaction tubes 1.5 & 2 ml	Eppendorf, Hamburg, Germany
Sensor Chip CM5	Cytiva
Slide-A-Lyzer mini dialysis unit (7 kDa MWCO)	Thermo Fisher
Sterican needles	B. Braun
Superdex Increase 75 10/300 column	Cytiva
TLC Silica gel 60 F_{254} plate	Merck
Tube 15 ml, conical bottom	Greiner Bio One
Vivaspin 500 centrifugal concentrator (10 kDa MWCO)	Sartorius, Göttingen, Germany
Vivaspin Turbo 15 centrifugal concentrator (10 kDa MWCO)	Sartorius
Zeba Spin desalting columns (0.5 ml, 7 kDa MWCO)	Thermo Fisher
ΦX174 replicative form (RF) DNA	Promega, Madison, USA

2.1.3 Laboratory equipment

Equipment	Manufacturer/ Supplier
Agilent 1260 Infinity II LC system	Agilent Technologies, Santa Clara, USA
ÄKTA Prime+ system	Cytiva
Amersham Typhoon biomolecular imager	Cytiva

Equipment	Manufacturer/ Supplier
Alpha 1-2 LDplus freeze dryer	Martin Christ Gefriertrocknungsanlagen, Osterode am Harz, Germany
Avanti JXN-26 centrifuge (JA-25.50 fixed-angle rotor, J-LITE JLA-8.1000 fixed-angle aluminum rotor)	Beckman Coulter, Brea, USA
Axio Observer Z1 microscope (equipped with HXP 120 C lamp, AxioCam MRm camera, αPlan-APOCHROMAT 100×/1.46 oil immersion objective, Carl Zeiss filter set 38)	Carl Zeiss
Axio Observer Z1 microscope (equipped with X-Cite Xylis LED Lamp, Teledyne Photometrics Prime BSI express camera, αPlan-APOCHROMAT 100×/1.46 oil immersion objective, Carl Zeiss filter set 38)	Carl Zeiss
B3D1020 mini 3D mixer	Benchmark Scientific, Sayreville, USA
Bead Ruptor 12	Omni International, Kennesaw, USA
Biometra UV-Transilluminator TI 1	Biometra, Göttingen, Germany
Bransonic CPXH digital ultrasonic bath	Branson
CN 4713-22 fridge-freezer	Liebherr, Bulle, Switzerland
Contamination monitor LB 124	Berthold Technologies, Bad Wildbad, Germany
Desiccator	VWR
Dry block feater QBH2	Grant, Shepreth, UK
Multichannel pipette 200 µl	VWR
EV231 electrophoresis power supply	Consort, Turnhout, Belgium
FiveEasy F20 pH/mV meter	Mettler Toledo, Columbus, USA
Flake ice machine AF 80	Scotsman, Milano, Italy
Gilson HPLC system	Gilson, Madison, USA
GraphPad Prism V9.5.1.733 software	GraphPad Software
Heating magnetic stirrer AREC	VELP Scientifica, Usmate, Italy
Heraeus Fresco 21 (24 x 1.5/2.0 ml rotor)	Thermo Fisher
Heraeus Megafuge 40R (X-750 rotor with round buckets)	Thermo Fisher
Heraeus Megafuge 8R (HIGHConic III fixed angle rotor)	Thermo Fisher
Heraguard ECO clean bench	Thermo Fisher
Heratherm Compact microbiological incubator	Thermo Fisher
HLC Heating-ThermoMixer MHL 23	Ditabis, Pforzheim, Germany
i-control V3.9.1.0 software	Tecan Group, Männedorf, Switzerland
Image eraser	Cytiva
Image Lab software V5.2	Bio-Rad Laboratories
ImageJ V1.53k software	National Institutes of Health, Bethesda, USA
ImageQuant TL V8.2.0.0. software	Cytiva

Equipment	Manufacturer/ Supplier
Infinite 200 PRO microplate reader	Tecan Group
Infors HT Ecotron incubator shaker	Infors HT, Bottmingen, Switzerland
Julabo MWB mini water bath	Julabo, Seelbach, Germany
Laboratory pump VP 820	VWR
Laura software	LabLogic Systems, Koblenz, Germany
MicroPulser Electroporator	Bio-Rad Laboratories
Microwave Micromat	Electrolux, Stockholm, Sweden
MiniSpin micro centrifuge (F-45-12-11 rotor)	Eppendorf
MiniStar silverline microcentrifuge	VWR
Molecular Imager Gel Doc XR+ system	Bio-Rad Laboratories
MultoHigh-Bio-300-C4 reversed-phase column (5 µM, 125 x 4 mm)	CS Chromatographie, Langerwehe, Germany
Mupid One electrophoresis system	Nippon Genetics, Düren, Germany
NanoPhotometer NP80	Implen, Munich, Germany
Novaspec III+ spectrophotometer	Biochrom, Cambridge, UK
NU-543-300S class II, Type A2 biosafety cabinet	NuAire, Plymouth, USA
Nutrient media steriliser MediaClave 10	Integra Biosciences, Zizers, Switzerland
OpenLab CDS V2.6 software	Agilent Technologies
PCB 6000-1 precision balance	Kern & Sohn, Balingen-Frommern, Germany
peqSTAR thermocycler	VWR
Personal contamination monitor LB 147	Berthold Technologies
Premium Line 1800 ceramic HD 3700 hair dryer	Grundig, Fürth, Germany
ProntoSIL 120-3-C1 250x4.6mm HPLC Column	Bischoff, Leonberg, Germany
PZ 28-1 Präzitherm precision hot plate	Harry Gestigkeit, Düsseldorf, Germany
Rainin Pipet-Lite XLS+ 2 µl, 20 µl, 200 µl & 1000 µl	Mettler Toledo
Research plus 5 ml pipette	Eppendorf
Rotavapor R-100, interface I-100, vacuum pump V-100, heating bath B-100	Büchi Labortechnik, Flawil, Switzerland
Sartorius BCE64I-1S Entris II analytical balance	Sartorius
Sartorius M3P micro balance	Sartorius
Savant SPD101B-120 speed vac concentrator	Thermo Fisher
Scan 1200 automatic colony counter	Interscience, Saint Nom la Bretèche, France
Scan 1200 V8.6.12.0 v3.4 software	Interscience
Scanlaf Mars 1200 Runner safety workbench	LaboGene, Allerød, Denmark
SFX 250 digital sonifier with 0.5-inch horn	Branson, Brookfield, USA
SHP Laboclav 135-MSLV	SHP Steriltechnik, Haldensleben, Germany
Sorvall MTX 120 micro-ultracentrifuge (S55A2 rotor)	Thermo Fisher
Spark 10M microplate reader	Tecan Group
SparkControl V3.1 SP1 software	Tecan Group
Storage phosphor screen	Cytiva

Equipment	Manufacturer/ Supplier
Storm 820 phosphor imager	Cytiva
Storm Scanner control V5.03 software	Cytiva
SureCast glass plates & gel spacers	Thermo Fisher
TDE40086FV -80 °C upright freezer	Thermo Fisher
Thermal Shake lite thermal shaker	VWR
ThermoStat C thermoblock	Eppendorf
Trilution LC V2.1 software	Gilson
UCSF Chimera V1.17.1 software	University of California, USA
Ultracentrifuge LE-80K (70Ti rotor)	Beckman Coulter
Unicorn V5.11	Cytiva
Universal oven UF260	Memmert, Schwabach, Germany
Vortex Genie 2	Scientific Industries, New York, USA
Water heating bath	Gesellschaft für Labortechnik, Burgwedel, Germany
XCell SureLock mini-cell electrophoresis system	Thermo Fisher
ZEN blue V3.6.095.03000 software	Carl Zeiss

2.1.4 Antibiotics

Antibiotic	Solvent	Reference/ Source
Ampicillin	water	Carl Roth
Bocillin FL	water	Thermo Fisher
Cefoxitin	water	Carl Roth
Chloramphenicol	ethanol	Carl Roth
Ciprofloxacin	water	Fagron, Rotterdam, Netherlands
Clindamycin	ethanol	Cayman Chemical
Corallorazine A	DMSO	AG Crüsemann, University of Bonn
Erythromycin	ethanol	Carl Roth
Kanamycin	water	Carl Roth
Moenomycin	DMSO	Cayman Chemical, Ann Arbor, USA
Moenomycin-BODIPY	DMSO	Menche Lab, University of Bonn
Oxacillin	water	Sigma Aldrich
Ramoplanin	water	Sigma Aldrich
Rhodamine B-Ramoplanin	water	Sigma Aldrich
Rifampin	methanol	Merck
Targocil	DMSO	GLPBio, Montclair, USA
Teixobactin	water	NovoBiotic, Cambridge, USA
Tunicamycin	DMSO	Sigma Aldrich
Vancomycin	water	Hikma Pharmaceuticals, London, UK
Vancomycin-FITC	water	Sigma Aldrich

2.1.5 Molecular weight markers

Molecular weight marker	Manufacturer/ Supplier
GeneRuler 1kb DNA ladder	Thermo Fisher
PageRuler Plus prestained protein ladder	Thermo Fisher
Quick-Load 1 kb DNA Ladder	New England Biolabs

2.1.6 Kits

Kit	Manufacturer/ Supplier
Amine Coupling Kit	Cytiva
In-Fusion HD Cloning Kit	Takara, Kyoto, Japan
Monarch DNA Gel Extraction Kit	New England Biolabs
Monarch Plasmid Miniprep Kit	New England Biolabs
NucleoSpin Microbial DNA Mini Kit	Macherey-Nagel

2.1.7 Proteins

Protein	Description	Reference/ Source
His-Colicin M	MH_6GS-Colicin M-KLN	This work
His-LcpA	MGSSH_6SSGLVPRGSH-LcpA	This work
His-LcpB	MGSSH6SSGLVPRGSH-LcpB	This work
His-LcpC	MGSSH6SSGLVPRGSH-LcpC	This work
$LcpA_{short}$-His	MA-$LcpA_{58-327}$-LEH_6	This work
$LcpB_{short}$-His	MA-$LcpB_{31-405}$-LEH_6	This work
$LcpC_{short}$-His	MA-$LcpC_{30-315}$-LEH_6	This work
PBP2-His	MAS-PBP2-LEH_6	This work
PBP4-His	MAS-PBP4-LEH_6	This work
SgtA-His	SgtA-$ALEH_6$	This work
SgtB-His	MGSS-SgtB-LEH_6	This work
WbpL-His	MDIGINSDP-WbpL-$KLAAALEH_6$	This work
Benzonase nuclease		Sigma Aldrich
Bovine serum albumin (BSA)		Carl Roth
DNase I (bovine pancreas)		PanReac AppliChem
Lysostaphin (*Staphylococcus simulans*)		Sigma Aldrich
Lysozyme (chicken egg white)		Carl Roth
Mutanolysin (*Streptomyces globisporus*)		Sigma Aldrich
Phusion High-Fidelity DNA Polymerase		New England Biolabs
RNA polymerase holoenzyme (*E. coli*)		New England Biolabs

Protein	Description	Reference/ Source
RNase A (bovine pancreas)		Sigma Aldrich
Trypsin (porcine pancreas)		Carl Roth

2.1.8 Bacterial strains

Strain	Characteristics	Reference/ Source
Staphylococcus aureus		
Newman	MSSA, Mc^s, capsular serotype 5, *saeRS* constitutively expressed by SaeS T53C substitution, *fnbA* and *fnbB* mutated	Duthie & Lorenz, 1952
Newman Δ*lcpA*	Newman, *SA1195*::*spec*, Sp^r	Chan *et al*., 2014
Newman Δ*lcpB*	Newman, markerless *SA0908* deletion mutant	Chan *et al*., 2014
Newman Δ*lcpC*	Newman, *SA2103*::*ermB*, Em^r	Chan *et al*., 2014
Newman Δ*lcpBC*	Newman, markerless *SA0908* deletion, *SA2103*::*ermB*, Em^r	Chan *et al*., 2014
Newman Δ*lcpA* p*lcpA*	Newman, *SA1195*::*spec*, Sp^r, plasmid-encoded *msrR*, Em^r	This work
MSSA1112	Clinical isolate, *bla*, Mc^s Pen^r	Entenza *et al*., 1997
MSSA1112 Δ*lcpA*	MSSA1112, Δ*msrR*::*ermB*, Em^r	Hübscher *et al*., 2009
MSSA1112 Δ*lcpB*	MSSA1112, markerless *SA0908* deletion mutant	Over *et al*., 2011
MSSA1112 Δ*lcpC*	MSSA1112, markerless *SA2103* deletion mutant	Over *et al*., 2011
MSSA1112 Δ*lcpABC*	MSSA1112, *SA2103*/*SA0908*/*msrR* triple mutant, Em^r	Over *et al*., 2011
MSSA1112 Δ*lcpAB*	MSSA1112, *msrR*/*SA0908* double mutant, Em^r	Over *et al*., 2011
MSSA1112 Δ*lcpAC*	MSSA1112, *msrR*/*SA2103* double mutant, Em^r	Over *et al*., 2011
MSSA1112 Δ*lcpBC*	MSSA1112, *SA0908*/*SA2103* double mutant	Over *et al*., 2011
RN4220	Laboratory strain, restriction-deficient derivative of NCTC 8325-4	Kreiswirth *et al*., 1983
SG511	MSSA, Mc^s	Sass & Bierbaum, 2009
HG003	Derivative of NCTC 8325, *rsbU* repaired, *tcaR* repaired	Herbert *et al*., 2010
Mu50	Clinical isolate, VISA, Rif^R	Kuroda *et al*., 2001
COL	MRSA, Mc^r, *agr*, lacks ΦSA3, which integrates in *hlb*	Dyke *et al*., 1966

Strain	Characteristics	Reference/ Source
AS-091	RN4220, pEPSA5-antisense *infA*	Forsyth *et al*., 2002
AS-306	RN4220, pEPSA5-antisense *rpoC*	Forsyth *et al*., 2002
AS-329	RN4220, pEPSA5-antisense sig*A*	Forsyth *et al*., 2002
AS-089	RN4220, pEPSA5-antisense *rpsE*	Forsyth *et al*., 2002
NCTC 8325	MSSA, *rsbU*, *tcaR*, Mc^S	Novick *et al*., 1967
SA113	Derivative of NCTC 8325	Iordanescu & Surdeanu, 1976
SA113 Δ*tarO*	SA113 Δ*tarO*::*ermB*, Em^r	Weidenmaier *et al*., 2004
Staphylococcus simulans		
ATCC 12559		Kloos & Schleifer, 1975
Escherichia coli		
I-112768		Keio collection
MB5746	MG1655, *tolC*::Tn10, Tn^r	Kodali *et al*., 2005
DH5α	Non-expression strain	New England Biolabs
DC10β	Non-expression strain	Monk *et al*., 2012
LOBSTR	Expression strain	Andersen *et al*., 2013
BL21 (DE3)	Expression strain	New England Biolabs
C43 (DE3)	Expression strain	Miroux & Walker, 1996
Bacillus subtilis		
W168	Wildtype, *trpC2*	Kunst *et al*., 1997
W168 pAC6-P_{yheI}	Cm^r	Harms *et al*., 2018
W168 pAC6-P_{ypuA}	Cm^r	Harms *et al*., 2018
W168 pAC6-P_{yvgS}	Cm^r	Harms *et al*., 2018
W168 pAC6-P_{yorB}	Cm^r	Harms *et al*., 2018
Enterococcus faecalis		
BM4223 pIP819	VRE, Van^r	Leclercq *et al*., 1989
Micrococcus luteus		
DSM 1790		Wieser *et al*., 2002

2.1.9 Growth media

Culture medium	Ingredients
Tryptic soy broth (TSB, Merck)	17 g/l peptone from casein, 3 g/l peptone from soymeal, 2.5 g/l D(+)-glucose monohydrate, 5 g/l NaCl, 2.5 g/l K_2HPO_4
Tryptic soy broth agar (TSA, Merck)	17 g/l peptone from casein, 3 g/l peptone from soymeal, 2.5 g/l D(+)-glucose monohydrate, 5 g/l NaCl, 2.5 g/l K_2HPO_4, 15 g/l agar
Luria Bertani (LB) broth	10 g/l tryptone, 10 g/l NaCl, 5 g/l yeast extract
Luria Bertani (LB) agar	10 g/l tryptone, 10 g/l NaCl, 5 g/l yeast extract, 15 g/l agar
Mueller-Hinton broth (MHB, Thermo Fisher)	0.3 g/l dehydrated infusion from beef, 0.0175 g/l casein hydrolysate, 0.0015 g/l starch, pH 7.3 ± 0.1
Mueller-Hinton agar (MHA, Thermo Fisher)	0.3 g/l dehydrated infusion from beef, 0.0175 g/l casein hydrolysate, 0.0015 g/l starch, 15 g/l agar, pH 7.3 ± 0.1
SOC outgrowth (New England Biolabs)	2% (w/v) vegetable peptone, 0.5% (w/v) yeast extract, 10 mM NaCl, 2.5 mM KCl, 10 mM $MgCl_2$, 10 mM $MgSO_4$, 20 mM glucose
2x YT	16 g/l tryptone, 10 g/l yeast extract, 5 g/l NaCl

2.1.10 Plasmids and oligonucleotides

Plasmid	Properties	Reference/ Source
pET28a-*lcpA*	Overproduction of His-LcpA	Dr. Anna Müller[1]
pET28a-*lcpB*	Overproduction of His-LcpB	Dr. Anna Müller[1]
pET28a-*lcpC*	Overproduction of His-LcpC	Dr. Anna Müller[1]
pET21b-$lcpA_{175-984}$	Overproduction of $LcpA_{short}$-His	Dr. Anna Müller[1]
pET21b-$lcpB_{94-1218}$	Overproduction of $LcpB_{short}$-His	Dr. Anna Müller[1]
pET21b-$lcpC_{91-948}$	Overproduction of $LcpC_{short}$-His	Dr. Anna Müller[1]
pET28b-*sgtA*	Overproduction of SgtA-His	This work
pET28b-*sgtB*	Overproduction of SgtB-His	This work
pET2430-*cma*	Overproduction of His-Colicin M	Barreteau *et al*., 2010
pCQ11-*gfp-lcpA*	Microscopic localization study of GFP-LcpA	Dr. Anna Müller[1]
pCQ11-*gfp-lcpB*	Microscopic localization study of GFP-LcpB	This work
pCQ11-*gfp-lcpC*	Microscopic localization study of GFP-LcpC	Dr. Anna Müller[1]
pCQ11-*gfp-pbp2*	Microscopic localization study of GFP-PBP2	This work
pCQ11-*pbp4-yfp*	Microscopic localization study of PBP4-YFP	Jan-Samuel Puls[1]
pVll002-*wbpL*	Overproduction of WbpL-His	Project work (2016)
pET21b-*pbp4*	Overproduction of PBP4-His	Dr. Kevin Ludwig[1]
pCQ11-*ery-lcpA*	Complementation of *S. aureus* Newman Δ*lcpA*	This work
pET21b-*pbp2*	Overproduction of PBP2-His	Christian Körner (2006)[1]

[1] Institute for Pharmaceutical Microbiology, University of Bonn, Germany

Primer	Sequence (5′-3′)	Used to generate
pET28b-*sgtB*-FW	CTC GAG CAC CAC CAC CAC	pET28b-*sgtB*
pET28b-*sgtB*-RV	GCT GCT GCC CAT GGT ATA TCT C	
sgtB-FW	ACC ATG GGC AGC AGC ATG AAA AGA AGC GAT AGG TAC TCA AAC T	
sgtB-RV	GTG GTG GTG CTC GAG ACG ATT TAA TTG TGA CAT AGC CTG TTG ATA TT	
pET28b-*sgtA*-FW	GCA CTC GAG CAC CAC	pET28b-*sgtA*
pET28b-*sgtA*-RV	GGT ATA TCT CCT TCT TAA AGT TAA ACA AAA	
sgtA-FW	AGA AGG AGA TAT ACC ATG ACG AAT CAA GAC AAC AAT CA	
sgtA-RV	GTG GTG CTC GAG TGC ACG CTT TTT TCG ATT TAA CAA ATG	
open-pCQ11-*gfp*-FW	GGC GCG CCT ATT CTA AAT	pCQ11-*gfp-lcpB*
open-pCQ11-*gfp*-RV	GCT AGC TGC TTT GTA TAG TTC	
lcpB-FW	TAC AAA GCA GCT AGC ATG AAT AAA TTT TTA AAA TAC TTT TTG ATC CTT CTA G	
lcpB-RV	TAG AAT AGG CGC GCC TTA ATT TAC AAC ACC ATT TTG GTT ATT TGA AG	
open-pCQ11-*gfp*-FW	GGC GCG CCT ATT CTA AAT	pCQ11-*gfp-pbp2*
open-pCQ11-*gfp*-RV	GCT AGC TGC TTT GTA TAG TTC	
pbp2-FW	TAC AAA GCA GCT AGC ATG ACG GAA AAC AAA GGA TCT	
pbp2-RV	TAG AAT AGG CGC GCC TTA GTT GAA TAT ACC TGT TAA TCC ACC G	
open-pCQ11-FW	CGC GCC TAT TCT AAA TGC A	pCQ11-*ery-lcpA*
open-pCQ11-RV	CGA TAT CAA GCT TAA TTG TTA TCC G	
lcpA-FW	TTA AGC TTG ATA TCG ATG GAT AAA GAA ACT AAT GAC AAC	
lcpA-RV	TTT AGA ATA GGC GCG TTA ATC TTC ATC TAA AAA GTC TT	

2.2 Microbial methods

2.2.1 Sterilization procedure of media, equipment and bacterial cultures

Glassware was sterilized in a dry heat-sterilizer (Universal oven UF260, Memmert, Schwabach, Germany) at 200 °C for 4 h. Plasticware, including pipette tips, culture media, and solutions, were autoclaved at 121 °C for 20 min (SHP Laboclav 135-MSLV, SHP Steriltechnik, Haldensleben, Germany, or, alternatively for culture media, MediaClave 10, Integra Biosciences, Zizers, Switzerland). Acrodisc Syringe Filters (pore size 0.2 µm, Pall Corporation, Port Washington, USA) were used to sterilize heat-labile solutions, such as antibiotic stocks. For decontamination, bacterial cultures and labware were autoclaved at 134 °C for 20 min (SHP Laboclav 135-MSLV, SHP Steriltechnik).

2.2.2 Bacterial storage and growth

S. aureus strains were cultivated in tryptic soy broth (TSB) or on tryptic soy agar (TSA) or Mueller Hinton (MH) agar plates, depending on the experiment, at 37 °C. *E. coli* strains were grown in Luria Bertani (LB) liquid medium or on LB agar plates at 37 °C. Alternatively, SOC outgrowth liquid medium (New England Biolabs) was used for freshly transformed *E. coli* strains and 2x YT liquid medium for certain protein overproductions. *B. subtilis* strains were cultivated in MH broth or on MH agar plates at 30 °C. To promote growth, liquid cultures were incubated with orbital shaking at 120 rpm. Strains carrying a resistance cassette were cultivated in the presence of the appropriate selection antibiotic. Plates were incubated overnight and stored up to four weeks at 4 °C. For long-term storage, overnight cultures were mixed with sterile glycerol to a final concentration of 10% (v/v) and stored at -70 °C.

2.2.3 Optical density measurement of cell populations

Bacterial growth was monitored by determining the optical density at 600 nm (OD_{600}) spectrophotometrically (Novaspec III+ spectrophotometer, Biochrom, Cambridge, UK). Sterilized medium was used as blank.

2.2.4 Preparation of chemo-competent *E. coli*

500 ml LB medium was inoculated with 1% (v/v) overnight culture and cells were grown to an OD_{600} of 0.5 at 37 °C with gentle shaking. Cells were harvested via centrifugation (4,415 x *g*, 15 min, 4 °C) and resuspended in 10 ml sterilized ice-cold 0.1 M $CaCl_2$ solution prior to incubation for 30 min on ice. Subsequently, cells were pelleted and resuspended in 500 µl sterilized ice-cold 0.1 M $CaCl_2$ with supplemented glycerol (15% v/v). After a 60 min incubation period in ice, the suspension was aliquoted (50 µl) and immediately used for transformation or stored long-term at -70 °C.

2.2.5 Preparation of electro-competent *S. aureus*

Electro-competent *S. aureus* cells were prepared as described by Monk *et al*. (2012) with minor modifications. Briefly, 100 ml TSB medium was inoculated with 1% (v/v) of an overnight culture. Cells were grown to an OD_{600} of 0.5 at 37 °C with gentle shaking and incubated for another 30 min. The culture was placed in an ice bath for 10 min. All further steps were conducted at 4 °C on ice. Cells were pelleted at 4,000 x *g* for 10 min and resuspended in 100 ml sterilized ice-cold water. After repeating this step, cells were resuspended in 1/10, 1/25, and 1/200 the initial culture volume of sterile ice-cold 10% (v/v) glycerol. Aliquots of 50 µl were either used immediately for electroporation or frozen at -70 °C.

2.2.6 Isolation of plasmid DNA from *E. coli*

Plasmid DNA was purified from *E. coli* cells using the Monarch Plasmid Miniprep Kit (New England Biolas, Ipswich, UK) as per the manufacturer's instructions.

2.2.7 Isolation of genomic DNA from *S. aureus*

Genomic DNA was purified from *S. aureus* cells using the NucleoSpin Microbial DNA Mini Kit (Macherey-Nagel, Düren, Germany) as per the manufacturer's instructions.

2.2.8 Transformation of chemo-competent *E. coli* cells

An aliquot of chemo-competent *E. coli* cells (20-50 µl) was thawed on ice for about 5 min, before 200 µg of purified plasmid DNA or 5 µl ligation mix was added. After 15 min incubation on ice, cells were heat shocked at 42 °C for 90 s and, subsequently, placed back on ice for 2 min. 1 ml SOC outgrowth medium (New England Biolabs) was added to freshly transformed cells prior to incubation for 1 h at 37 °C with gentle shaking. The cells were spun down by centrifugation at 12,300 x *g* for 2 min. The supernatant medium was decanted and the cells were resuspended in the remaining liquid, which was plated on LB agar plates containing the respective selection antibiotic. Plates were incubated at 37 °C overnight.

2.2.9 Transformation of electro-competent *S. aureus*

The electroporation of electro-competent *S. aureus* cells was performed as described previously by Monk *et al*. (2012) with minor modifications. An aliquot of 50 µl competent cells was thawed on ice for 5 min and further allowed to reach room temperature. Cells were spun down by centrifugation at 12,300 x *g* for 1 min and resuspended in the same volume of buffer A (10% (v/v) glycerol, 500 mM sucrose, filter sterilized) to which 5 µg plasmid DNA purified from *E. coli* strain DC10β was added. The mixture was transferred into an electroporation cuvette (1 mm, Bio-Budget Technologies, Krefeld, Germany) and pulsed at 1.8 kV for 2.5 ms. 1 ml TSB medium with 500 mM sucrose (filter sterilized) was added prior to incubating at 37 °C for 1 h with gentle shaking. The suspension was centrifuged at 12,300 x *g* for 2 min and the supernatant medium was decanted. Electroporated cells were resuspended in the remaining liquid and plated on TSA containing the appropriate selection antibiotic. Plates were incubated at 37 °C overnight.

2.2.10 Minimal inhibitory concentration (MIC)

The minimal inhibitory concentration is defined as the lowest concentration of an antibiotic that inhibits visible growth (EUCAST, 1998). MICs were performed in sterile, transparent 96-well polystyrene microplate with U-bottom (Greiner Bio One, ref. 650161, Frickenhausen, Germany).

The test compound was serially diluted in Mueller-Hinton broth (MHB) in a final volume of 50 µl. To prepare the inoculum, the test strains were grown in MHB until OD_{600} 0.5 - 1.0 and the cell concentration was adjusted to approximately 1 x 10^6 cells/ml. 50 µl of this cell suspension was added to 50 µl of the respective antibiotic serial dilution to obtain a final concentration of 0.5 x 10^5 cells/ml according to the Clinical and Laboratory Standards Institute (CLSI) guidelines (CLSI, 2019). Appropriate controls (growth control of test strain, sterile controls for medium and antibiotic) were included with every batch of MIC determination. Microplates were incubated at 37 °C for 20 h without agitation.

2.2.11 Synergy checkerboard assay

To evaluate the antibacterial effect of two combined antibiotics, two-dimensional microdilution checkerboard assays were performed. In this assay, the concentration of each drug is tested alone and in combination against the microorganism of interest. Agent A was serially diluted in MHB starting 4-fold higher concentrated than the desired highest concentration. Each column of a transparent 96-well polystyrene microplate with U-bottom (Greiner Bio One, ref. 650161) was filled with 25 µl of a different dilution of agent A. In parallel, agent B was equally diluted and 25 µl of each dilution were transferred, in each row, into the wells already containing agent A. Both times, the last column (agent A) or row (agent B) was skipped and instead filled with 25 µl MHB to determine the MIC of the single agent. The test strain was grown in MHB to an OD_{600} of 0.5 - 1.0 and the cell concentration was adjusted to approximately 1 x 10^6 cells/ml. 50 µl of cell suspension was transferred into each well. Microplates were covered with a non-breathable plastic film and incubated for 20 h at 37 °C. To assess if the antibiotics act synergistically when combined, the fractional inhibitory concentration (FIC) index value was determined using the following equation:

$$\frac{A}{MIC_A} + \frac{B}{MIC_B} = FIC_A + FIC_B = FIC\ index\ value$$ Hall *et al.*, (1983)

Where A and B denote the MIC of both compounds in combination and MIC_A and MIC_B are the individually determined MIC of each agent. Synergy is defined by an FIC index value less than 0.5, additive or indifference between 0.5 and 4 and antagonisms with a value greater than 4 (Figure 10) (Lorian, 2005).

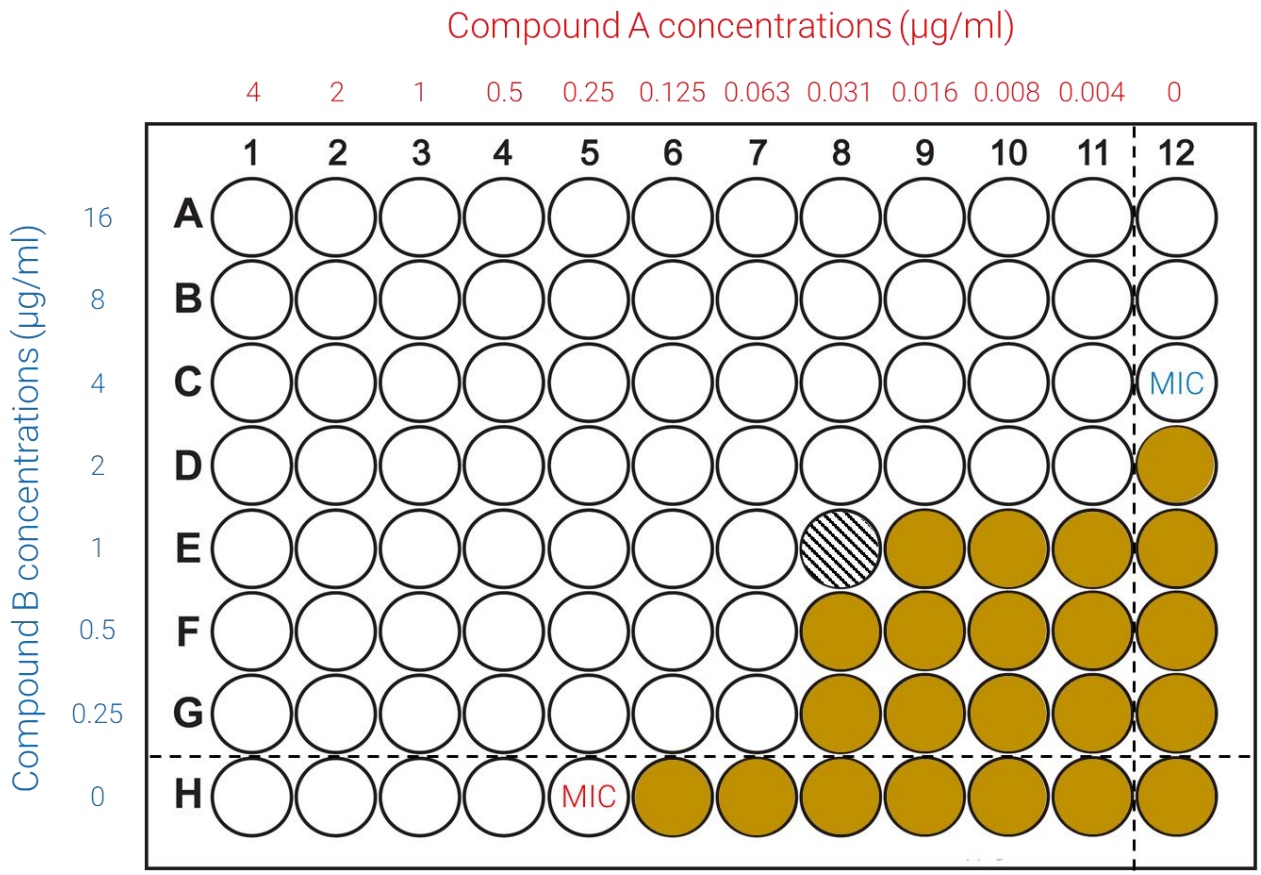

Figure 10: Schematic of checkerboard assay. Compound A is serially diluted along the abscissa while compound B is diluted sequentially along the ordinate. Column 12 and row H each contain the serial dilutions of one compound alone to determine the MIC values. Well H12 represents the medium control. White circles denote "no growth", whereas yellow circles represent "growth". A synergistic effect of both compounds (FIC < 0.5) is depicted by black stripes.

2.2.12 Spot dilutions of *S. aureus* strains

S. aureus MSSA1112 wildtype and Δ*lcp* deletion mutant strains were grown in 20 ml TSB at 37 °C with shaking until OD_{600} of 1.0. Each culture was serially diluted (10x) and plated on TSA supplemented with different concentrations of moenomycin. Plates were incubated at 37 °C overnight and documented with a Scan 1200 automatic colony counter and the associated Scan 1200 V8.6.12.0 v3.4 software (Interscience, Saint Nom la Bretèche, France).

2.2.13 Killing kinetics

To study the effect of moenomycin on *S. aureus* MSSA1112 wildtype over time, time-kill kinetic assays were performed. Cells were grown in 10 ml MH at 37 °C with gentle shaking until an OD_{600} of 0.5 and diluted 1:100 in the same medium. 0.125 µg/ml moenomycin (1x MIC) (1 mg/ml stock solution moenomycin in DMSO) or the equivalent amount of DMSO was added to the 1:100 diluted stock culture and the cells were continued to grow at 37 °C. Serial dilutions (10x) of the bacterial cultures were prepared at 0, 1, 2, 3, 4, and 24 h after antibiotic addition and 50 µl of each dilution was plated on half an MHA plate. Plates were incubated at 37 °C overnight and colony-forming units (CFU) per milliliter were determined. Only plates containing 20 to 300 colonies were considered.

2.2.14 β-galactosidase reporter assays

β-galactosidase reporter assays were performed as previously described (Harms *et al*., 2018) to examine the interference of the test compound with major biosynthesis pathways in *B. subtilis* 168 and to identify its mode of action. The bioreporter strains harbor the hybrid plasmids pAC6-P_{yorB}, pAC6-P_{yvgS}, pAC6-P_{yheI} or pAC6-P_{ypuA}, in which the *lacZ* gene encoding for a β-galactosidase is fused to the respective promoter that is induced if the test compound affects the particular biosynthesis pathway (DNA (P_{yorB}), RNA (P_{yvgS}), protein (P_{yheI}), or cell wall (P_{ypuA})). Upon expression of the reporter gene, the inhibition zone in disc diffusion assays in surrounded by a blue circle resulting from the hydrolysis of the X-gal (5-bromo-4-chloro-3-indolyl-D-galactoside) substrate.

The *B. subtilis* reporter strains were grown to an OD_{600} of 0.5 in MHB containing 5 µg/ml chloramphenicol at 30 °C with shaking at 120 rpm. 40 ml of MHA was heated to 55 °C and supplemented with 5 µg/ml chloramphenicol and 150 µg/ml (cell wall reporter), 250 µg/ml (DNA reporter), and 500 µg/ml (RNA and protein reporter) X-gal, respectively. The agar was inoculated with the respective reporter strain according to the following formula:

$$\frac{40\ \text{ml [agar]} \times 10^7}{\text{OD}_{600} \times 2 \times 10^9} = \text{x ml [of preparatory culture]}$$ (Harms *et al*., 2018)

The mixture was then poured into sterile, non-treated, clear Nunc OmniTray single-well plates (ref. 140156, Thermo Fisher, Waltham, USA). Following solidification, 6 µg test compound was spotted on the agar plate and allowed to dry before overnight incubation at 30 °C. Antibiotics already known to induce or not induce the respective promoters were used as positive controls (0.3 µg ciprofloxacin for P_{yorB}, 6 µg rifampin for P_{yvgS}, 3 µg clindamycin for P_{yhel}, and 6 µg vancomycin for P_{ypuA}) or negative controls (3 µg clindamycin for P_{yorB}, P_{yvgS}, and P_{ypuA}, 6 µg vancomycin for P_{yhel}), respectively.

2.2.15 Susceptibility profile of *S. aureus* antisense recombinant strains

Antisense RNA was used to investigate the impact of an antibiotic on a biosynthesis pathway in *S. aureus*. Here, the expression of the respective genes involved in the targeted process was down-regulated by the transcription of an antisense RNA that hybridizes specifically to its cognate mRNA and inhibits its translation into protein (Figure 11). If, after treatment, the strain becomes more susceptible, one can assume that the compound most likely targets the affected pathway (Forsyth *et al*., 2002, Donald *et al*., 2009).

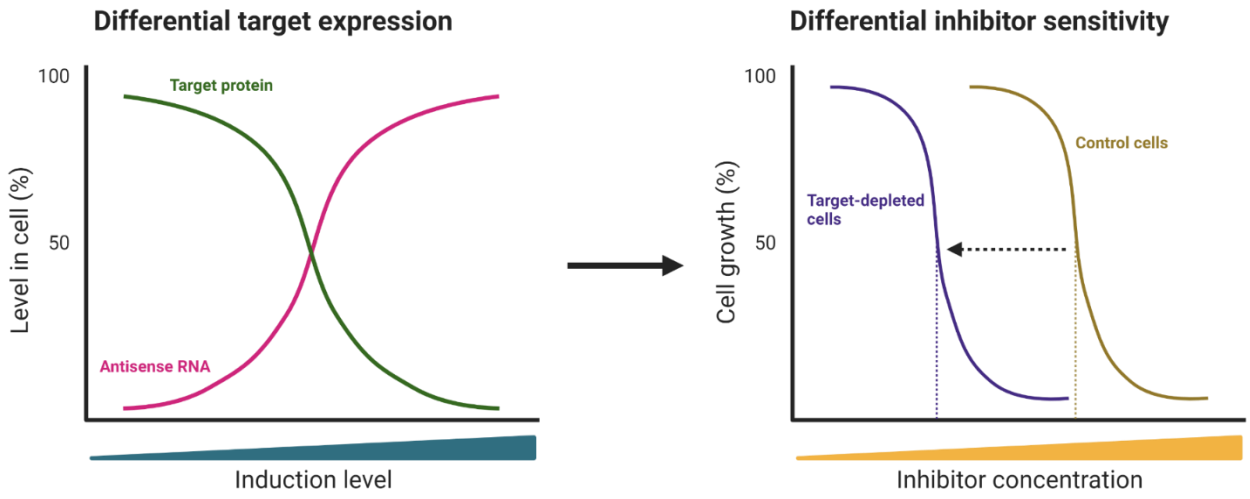

Figure 11: Schematic representation of how down-regulation of the target gene expression by antisense RNA can affect the bacterial cell susceptibility towards an inhibitor (modified from Singh *et al.*, 2007). Upon induction of antisense RNA transcription, the production of the targeted protein is reduced and the target-depleted cells become increasingly susceptible to the inhibitor in case it is directed against the specific pathway.

The procedure to obtain a susceptibility profile of recombinant *S. aureus* antisense strains was performed as previously described (Chiriac *et al*., 2015). Overnight cultures of *S. aureus* RN4220 antisense strains harboring a xylose-inducible plasmid that encodes for the antisense RNA were grown in LB medium supplemented with 5 µg/ml chloramphenicol at 37 °C with shaking. Cultures were freshly grown until an OD_{600} of 0.6 - 0.8 and subsequently diluted to an OD_{600} of 0.005. After separating into four flasks, xylose was added 1-fold, 0.5-fold, and 0.25-fold the MIC (the MIC for xylose was determined as described above, see section 2.2.10). No xylose was added to the control flask. After 210 min of incubation, the cultures were again diluted to an OD_{600} of 0.005 in medium containing twice the xylose concentration and 75 µl of this solution was transferred into each well of a medium-binding, white 96-well polystyrene chimney well microplate (Greiner Bio One, ref. 655075). The compound of interest was serially diluted in LB supplemented with 5 µg/ml chloramphenicol and the same volume (75 µl) was added to the wells prior to incubating the plate at 37 °C with shaking every 15 min at 1,440 rpm while the OD_{600} was monitored in a Spark 10M microplate reader with SparkControl V3.1 SP1 software (Tecan Group) for 20 h.

To ascertain the IC_{50} value, the percentage of growth inhibition induced by the compound in relation to the untreated control without added xylose was plotted against the MIC and a linear trend line was inserted. The susceptibility was finally determined by dividing the IC_{50} of the untreated control by the IC_{50} of the xylose-induced culture.

2.3 Molecular biological methods

2.3.1 DNA amplification via polymerase chain reaction (PCR)

Amplification of DNA fragments and vector DNA linearization was performed by polymerase chain reaction (PCR) (Mullis *et al*., 1986) in a peqSTAR Thermocycler (VWR, Radnor, USA) using Phusion High-Fidelity DNA polymerase (New England Biolabs) as per the manufacturer's instructions. Oligonucleotide primers were synthesized by Microsynth (Balgach, Switzerland) and are listed in section 2.1.10. Deoxynucleotides (dNTPs) were purchased from New England Biolabs. Amplified DNA was evaluated by agarose gel electrophoresis and subsequent UV visualization as described in section 2.3.2.

2.3.2 Analysis of DNA fragments using agarose gel electrophoresis

To separate DNA fragments according to their size for visualization and purification, horizontal agarose gel electrophoresis was conducted using a Mupid One Electrophoresis System (Nippon Genetics, Düren, Germany). In an electric field, DNA molecules move towards the positively charged anode due to their negatively charged phosphate backbone. The agarose gel operates as a molecular sieve that allows smaller fragments to pass faster and, therefore, ensures the separation of DNA molecules by length (Sambrook & Russell, 2001). Samples were mixed with Gel Loading Dye (6X, purple, New England Biolabs) prior to being loaded onto a 1% (w/v) agarose gel that had been prepared in TAE buffer (40 mM Tris/HCl, 20 mM glacial acetic acid, 1 mM EDTA, pH 8) and supplemented with 0.5 µg/ml GelRed Nucleic Acid Gel Stain (Biotium, Fremont, USA). GeneRuler 1kb DNA Ladder (250-10000 bp, Thermo Fisher) or Quick-Load 1 kb DNA Ladder (500-10000 bp, New England Biolabs) were used as length standards. The electrophoresis was performed in TAE as running buffer at 100 V for approximately 45 min. DNA fragments were visualized under ultraviolet (UV) light and documented using the Molecular Imager Gel Doc XR+ system with Image Lab V5.2 software (Bio-Rad Laboratories, Hercules, USA).

2.3.3 Purification of DNA fragments

DNA fragments were excised from the agarose gel with a scalpel and purified using Monarch DNA Gel Extraction Kit (New England Biolabs) as per the manufacturer's instructions.

2.3.4 Photometrical determination of DNA concentration and purity

The concentrations of genomic DNA, plasmid DNA, and DNA fragments, were determined spectrophotometrically at 260 nm using a NanoPhotometer NP80 (Implen, München, Germany). For assessment of purity and exclusion of contaminations, *e.g.*, with protein, the ratios of the absorbances at 260 and 280 nm ($A_{260/280}$) and at 260 and 230 nm ($A_{260/230}$) were ascertained.

2.3.5 In-fusion seamless cloning

Cloning of PCR fragments was performed using the In-Fusion HD Cloning Kit (Takara, Kyoto, Japan) as per the manufacturer's instructions. Briefly, PCR amplified inserts with 15 bp overlaps complementary to the PCR-linearized vector were incubated in a 3:1 molar ratio with In-Fusion enzyme for 15 min. Chemo-competent *E. coli* cells were transformed with the reaction mixture (as described in 2.2.8) and plated on selective agar plates.

2.3.6 DNA sequencing

The creation of recombinant plasmid DNA without unintended mutations was confirmed by Sanger sequencing (Sanger *et al.*, 1977) provided by Microsynth (Balgach, Switzerland) or Eurofins Genomics (Ebersberg, Germany).

2.4 Protein purification methods

2.4.1 Protein overproduction

2.4.1.1 LCP enzymes

E. coli C43 (DE3) containing the appropriate over-expression plasmid (see section 2.1.10) was grown overnight in LB buffer under selective conditions for plasmid retention. 2 l of 2YT broth with appropriate antibiotic was inoculated with 1% (v/v) of an overnight pre-culture and grown at 30 °C with shaking to an OD_{600} of 0.6. Protein over-production was induced with 1 mM isopropyl-β-D-thiogalactopyranoside (IPTG) for 16 h at 20 °C. Cells were harvested by centrifugation (10,000 x *g*, 12 min, 4 °C) and resuspended in 15 ml of buffer 1 (50 mM Tris/HCl, 300 mM NaCl, 30% (v/v) glycerol, pH 7.5). All the following steps were carried out on ice with ice-cold buffers. 7 mg/l RNase A (bovine pancreas, Sigma Aldrich, St. Louis, USA), 35 mg/l DNase I (bovine pancreas, PanReac AppliChem, Darmstadt, Germany), 0.7 g/l lysozyme (chicken egg white, Carl Roth, Karlsruhe, Germany), and 1 tablet of EDTA-free Pierce protease inhibitor tablets

(Thermo Fisher) were added to the resuspended cells prior to disruption of cells with an SFX 250 digital sonifier (0.5-inch horn, Branson, Brookfield, USA) with 6 x 2.5 min cycles of pulsed ultrasonics (20 s on time, 30 s off time, with increasing amplitude from 10% to 60%). Lysate was centrifuged (20,000 x *g*, 20 min, 4 °C), the supernatant discarded and the pellet resuspended in 10 ml buffer 1 followed by another centrifugation step (4,415 x *g*, 20 min, 4 °C). Proteins were solubilized by resuspending the pellet in 10 ml of buffer 2 (50 mM Tris/HCl, 300 mM NaCl, 30% (v/v) glycerol, 29 mM DDM, pH 7.5) and subsequent incubation with gentle agitation for 45 min. Cell debris were removed by centrifugation (20,000 x *g*, 20 min, 4 °C) and the supernatant was then added to 500 µl of pre-equilibrated Ni-NTA agarose bead resin (Macherey-Nagel). After stirring for 1.5 h, the suspension was poured into a 5 ml polypropylene column (Thermo Fisher). Beads were washed with 5 ml of buffer W1 (50 mM Tris/HCl, 300 mM NaCl, 20 mM imidazole, 30% (v/v) glycerol, pH 7.5) and 5 ml of buffer W2 (50 mM Tris/HCl, 300 mM NaCl, 40 mM imidazole, 30% (v/v) glycerol, pH 7.5) prior to elution with 5 x 500 µl elution buffer (50 mM Tris/HCl, 300 mM NaCl, 300 mM imidazole, 30% glycerol, pH 7.5). Glycerol was added to a final concentration of 40% (v/v) and samples were stored at -20 °C until further use.

For interaction studies, the proteins were further purified by size-exclusion chromatography (SEC, as described in section 2.4.2). Fractions containing the respective enzyme were concentrated using Vivaspin Turbo 15 centrifugal concentrators (10 kDa MWCO, Sartorius, Göttingen, Germany) according to the manufacturer's instructions and the protein purity was assessed by SDS-PAGE (as described in section 2.5.1). Additionally, the protein concentration was determined (as detailed in section 2.5.2) and the samples were stored at -20 °C.

2.4.1.2 LCP short variants

The protein overproduction and purification procedure of the LCP short variants were performed as detailed in section 2.4.1.1 with minor changes. After cell lysis by sonication, cell debris were centrifuged (20,000 x *g*, 20 min, 4 °C) and the clear supernatant was added to equilibrated Ni-NTA agarose bead resin. Elution fractions were additionally purified using size-exclusion chromatography as described in section 2.4.2 on a Superdex Increase 75 10/300 column (Cytiva, Marlborough, USA) pre-equilibrated with buffer 3 (50 mM Tris/HCl, 300 mM NaCl, 10% (v/v)

glycerol, pH 7.5). Protein purity was assessed by SDS-PAGE (section 2.5.1). Appropriate fractions were pooled, concentrated using Vivaspin Turbo 15 centrifugal concentrators (10 kDa MWCO, Sartorius), and further Vivaspin 500 centrifugal concentrators (10 kDa MWCO, Sartorius) as per the manufacturer's instructions. The protein concentration was determined (as detailed in section 2.5.2) and the samples were stored at -20 °C.

To prepare $LcpA_{short}$-His for X-ray crystallography, the protein solution was dialyzed overnight against 2 l of buffer 4 (50 mM Tris/HCl, 300 mM NaCl, pH 7.5) in Slide-A-Lyzer mini dialysis units (7 kDa MWCO, Thermo Fisher). The sample was mixed with moenomycin A in a 1:1 molar ratio and sent to our collaborators Philipp Hendricks, Gregor Hagelüken, and Matthias Geyer at the Institute of Structural Biology of the University of Bonn to obtain protein crystals.

2.4.1.3 PBP2 and PBP4

For overexpression of PBPs, 2 l of LB media supplemented with 100 µg/ml ampicillin was inoculated with a 1:100 diluted overnight culture of *E. coli* C43 (DE3) strain containing either the plasmid pET21b-*pbp2* or pET21b-*pbp4* and grown at 37 °C with shaking until an OD_{600} of 0.6. Protein over-production was induced with 1 mM IPTG for 4 h. Cells were pelleted by centrifugation (10,000 x *g*, 12 min, 4 °C), washed in 20 ml of buffer 1 (50 mM Tris/HCl, 500 mM NaCl, pH 7.5), and resuspended in 20 ml buffer 2 (50 mM Tris/HCl, 500 mM NaCl, 1% (v/v) Triton X-100, 10 mM imidazole, pH 7.5) with 10 mg/l RNase A (bovine pancreas, Sigma Aldrich), 50 mg/l DNase I (bovine pancreas, PanReac AppliChem), 1 mg/l lysozyme (chicken egg white, Carl Roth), 1 tablet of EDTA-free Pierce protease inhibitor tablets (Thermo Fisher), and 0.5% (v/v) *N*-lauroylsarcosine. After incubating for 60 min on ice, cells were disrupted by sonication using an SFX550 digital sonifier (0.5-inch horn, Branson) with 6 x 2.5 min cycles of pulsed ultrasonics (20 s on time, 30 s off time, with increasing amplitude from 10% to 60%) and centrifuged at 20,000 x *g* for 30 min at 4 °C. The supernatant was added to 500 µl pre-washed Ni-NTA agarose bead resin (Macherey-Nagel) and the slurry was tumbled for 2 h at 4 °C prior to transferring into a 5 ml polypropylene column (Thermo Fisher). Beads were washed with 7.5 ml of buffer 2, 7.5 ml of buffer 3 (50 mM Tris/HCl, 500 mM NaCl, 1% (v/v) Triton X-100, 20 mM imidazole, pH 7.5), and protein was finally eluted with 6 x 500 µl of elution buffer (50 mM Tris/HCl, 500 mM NaCl, 1% (v/v)

Triton X-100, 200 mM imidazole, pH 7.5). Elution fractions were stored at -20 °C in a final concentration of 30% (v/v) glycerol.

For interaction studies, the proteins were further purified by size-exclusion chromatography (as described in section 2.4.2). Fractions containing the respective enzyme were concentrated using Vivaspin Turbo 15 centrifugal concentrators (10 kDa MWCO, Sartorius) according to the manufacturer's instructions and the protein purity was assessed by SDS-PAGE (as described in section 2.5.1). Additionally, the protein concentration was determined (as detailed in section 2.5.2) and the samples were stored at -20 °C.

2.4.1.4 SgtA and SgtB

2 l LB broth supplemented with 50 µg/ml kanamycin was inoculated with a 1:100 diluted overnight pre-culture of *E. coli* LOBSTR harboring either pET28b-*sgtA* or pET28a-*sgtB* and grown at 37 °C with shaking until an OD_{600} of 0.6 at which point protein over-production was induced with 1 mM IPTG for 16 h at 37 °C. Cells were harvested by centrifugation (10,000 x *g*, 12 min, 4 °C), washed (4,415 x *g*, 20 min, 4 °C) in 10 ml of buffer 1 (50 mM Tris/HCl, 500 mM NaCl, pH 7.5) and resuspended in 10 ml of buffer 2 (50 mM Tris/HCl, 500 mM NaCl, 1% (v/v) Triton X-100, 10 mM imidazole, pH 7.5) with 0.5% (v/v) *N*-lauroylsarcosine, 1 µl Benzonase nuclease (Sigma Aldrich), and 1 tablet of EDTA-free Pierce protease inhibitor tablets (Thermo Fisher). After incubation for 1 h at 4 °C with tumbling, cells were disrupted by sonication using an SFX550 digital sonifier (0.5-inch horn, Branson) with 6 x 2.5 min cycles of pulsed ultrasonics (20 s on time, 30 s off time, with increasing amplitude from 10% to 60%). Cell lysate was cleared by centrifugation (20,000 x *g*, 30 min, 4 °C) and added to 500 µl of pre-washed Ni-NTA agarose bead resin (Macherey-Nagel) prior to incubating for 2 h at 4 °C with gentle stirring. The resin slurry was then packed into a disposable 5 ml polypropylene column (Thermo Fisher) and the flow-through fractions were collected. Beads were washed with 5 ml of buffer 2 and 5 ml of buffer 3 (50 mM Tris/HCl, 500 mM NaCl, 1% (v/v) Triton X-100, 20 mM imidazole, pH 7.5) before eluting the protein with 6 x 500 µl elution buffer (50 mM Tris/HCl, 500 mM NaCl, 1% (v/v) Triton X-100, 200 mM imidazole, pH 7.5). Fractions were stored at -20 °C in a final concentration of 30% (v/v) glycerol.

For interaction studies, the proteins were further purified by size-exclusion chromatography (as described in section 2.4.2). Fractions containing the respective enzyme were concentrated using Vivaspin Turbo 15 centrifugal concentrators (10 kDa MWCO, Sartorius) according to the manufacturer's instructions and the protein purity was assessed by SDS-PAGE (as described in section 2.5.1). Additionally, the protein concentration was determined (as detailed in section 2.5.2) and the samples were stored at -20 °C.

2.4.1.5 Colicin M

This protocol was adapted from a previously published method (Barreteau *et al*., 2010). *E. coli* C43 (DE3) strain harboring the recombinant plasmid pET2430-*cma* was grown overnight in LB with 50 µg/ml kanamycin to select for protein retention. This *E. coli* strain is naturally resistant to colicin M because of its functional FhuA protein deficiency (Barreteau *et al*., 2010). The overnight pre-culture was diluted 1:100 into 2 l 2YT broth and grown at 37 °C with shaking to an OD_{600} of 0.8. Protein over-production was induced with 1 mM IPTG for 3 h at 37 °C prior to harvesting by centrifugation (10,000 x *g*, 12 min, 4 °C). All subsequent steps were performed on ice with ice-cold buffers. Cells were washed with 40 ml of buffer 1 (20 mM Tris/HCl, 200 mM NaCl, 10 mM β-mercaptoethanol, 10% (v/v) glycerol, pH 7.4) and resuspended in 6 ml of buffer A prior to disruption of cells with an SFX550 digital sonifier (0.5-inch horn, Branson) with 6 x 2.5 min cycles of pulsed ultrasonics (20 s on time, 30 s off time, with increasing amplitude from 10% to 60%). Cell lysate was ultracentrifuged (150,000 x *g*, 1 h, 4 °C) and the supernatant added to 500 µl of pre-equilibrated Ni-NTA agarose bead resin (Macherey-Nagel). The suspension was incubated for 1 h with gentle stirring before pouring into a 5 ml polypropylene column (Thermo Fisher). Beads were washed with 10 ml buffer W (20 mM Tris/HCl, 200 mM NaCl, 10 mM β-mercaptoethanol, 10% (v/v) glycerol, 20 mM imidazole, pH 7.4) and protein was eluted with 5 x 500 µl elution buffer (20 mM Tris/HCl, 200 mM NaCl, 10 mM β-mercaptoethanol, 10% (v/v) glycerol, 200 mM imidazole, pH 7.4). Elution fractions were supplemented with 30% (v/v) glycerol and the samples were stored at -20 °C.

For interaction studies, the protein was further purified by size-exclusion chromatography (as described in section 2.4.2). Fractions containing the respective enzyme were concentrated using

Vivaspin Turbo 15 centrifugal concentrators (10 kDa MWCO, Sartorius) according to the manufacturer's instructions and the protein purity was assessed by SDS-PAGE (as described in section 2.5.1). Additionally, the protein concentration was determined (as detailed in section 2.5.2) and the samples were stored at -20 °C.

2.4.1.6 WbpL

E. coli C43 (DE3) strain was transformed with plasmid pVll002-*wbpL* expressing the initial glycosyltransferase of A-band lipopolysaccharide biosynthesis in *Pseudomonas aeruginosa*, WbpL, with a C-terminal His_6-tag (Rocchetta *et al*., 1998). Cells were grown in 2 l 2YT broth supplemented with 100 µg/ml ampicillin at 37 °C with shaking to an OD_{600} of 0.6 and expression was induced by the addition of 1 mM IPTG at 25 °C overnight. Cells were collected by centrifugation (10,000 x *g*, 12 min, 4 °C), resuspended in 10 ml buffer 1 (25 mM Tris/HCl, 150 mM NaCl, 2 mM β-mercaptoethanol, 10% (v/v) glycerol, pH 7.5) with 10 mg/l RNase A (bovine pancreas, Sigma Aldrich), 5 mg/l DNase I (bovine pancreas, PanReac AppliChem), and 1 g/l lysozyme (chicken egg white, Carl Roth), and incubated for 30 min on ice. Disruption of cells was achieved by sonication using an SFX550 digital sonifier (0.5-inch horn, Branson) with 6 x 2.5 min cycles of pulsed ultrasonics (20 s on time, 30 s off time, with increasing amplitude from 10% to 60%). Lysate was centrifuged (20,000 x *g*, 30 min, 4 °C) and the pellet was resuspended in 10 ml buffer 2 (25 mM Tris/HCl, 150 mM NaCl, 2 mM β-mercaptoethanol, 10% (v/v) glycerol, 49 mM DDM, pH 7.5) supplemented with 5 mg/l DNase I and 1 g/l lysozyme. After tumbling for 2 h at 4 °C, the lysate was centrifuged at 20,000 x *g* for 30 min at 4 °C to pellet the insoluble material. The supernatant was added to 500 µl of pre-equilibrated Ni-NTA agarose bead resin (Macherey-Nagel) and incubated for 2 h at 4 °C with gentle agitation. Subsequently, the suspension was poured into a 5 ml polypropylene column (Thermo Fisher). After collecting the flowthrough, the resin was washed consecutively with 10 ml of buffer 1 and 10 ml of buffer W (25 mM Tris/HCl, 150 mM NaCl, 2 mM β-mercaptoethanol, 10% (v/v) glycerol, 3.9 mM DDM, pH 7.5) before eluting the protein with 3 x 500 µl of each elution buffer 1 to 3 (25 mM Tris/HCl, 150 mM NaCl, 2 mM β-mercaptoethanol, 10% (v/v) glycerol, 3.9 mM DDM, 100-300 mM imidazole, pH 7.5). Elution fractions were supplemented with 30% (v/v) glycerol and the protein purity was assessed by

SDS-PAGE (as described in section 2.5.1). Additionally, the protein concentration was determined (as detailed in section 2.5.2) and the samples were stored at -20 °C.

2.4.2 Size-exclusion chromatography (SEC)

Size-exclusion chromatography (SEC) was performed using an ÄKTA Prime+ system with a Superdex Increase 75 10/300 column (Cytiva). UV absorbance chromatograms were collected with Unicorn V5.11 software (Cytiva). All buffers were filtered (0.2 µm pore size, Filtropur BT 50, Sarstedt, Nümbrecht, Germany) and degassed before use. Prior to loading the protein, column was equilibrated with at least 1.2 column volume running buffer (50 mM Tris/HCl, 300 mM NaCl, 10% (v/v) glycerol, pH 7.5). Chromatography was performed at a flow rate of 0.5 ml/min and fractions of 1 ml were collected. To assess protein purity and content, fractions were analyzed by SDS-PAGE (see section 2.5.1). Purest fractions were combined and concentrated using Vivaspin Turbo 15 centrifugal concentrator (10 kDa MWCO, Sartorius) as per manufacturer's instructions.

2.5 Protein analysis methods

2.5.1 Sodium dodecyl sulfate-polyacrylamide gel electrophoresis (SDS-PAGE)

To analyze protein samples for content and purity, samples were subjected to discontinuous sodium dodecyl sulfate-polyacrylamide gel electrophoresis (SDS-PAGE). Using this technique, the proteins' intrinsic charge is masked by treatment with sodium dodecyl sulfate (SDS) or lithium dodecyl sulfate (LDS) and β-mercaptoethanol is used to reduce disulfide bonds. The resulting unfolded and negatively charged proteins are separated in an electric field according to their masses by passing a porous acrylamide gel (Laemmli, 1970).

If not stated otherwise, 9.75 µl protein solution was mixed with 4x NuPAGE LDS sample buffer (Thermo Fisher) and 50 mM dithiothreitol (DTT) prior to incubating at 37 °C for 1 h with gentle shaking. Samples were loaded onto a pre-cast NuPAGE 4 -12% Bis-Tris acrylamide gel mounted in a mini-gel tank (Thermo Fisher) and run at 120 V for 1-2 h. As molecular weight marker, 6 µl PageRuler Plus prestained protein ladder (Thermo Fisher) with a range of 10 to 250 kDa was

applied. Tris-MOPS-SDS (Genscript, Piscataway, USA) was used as running buffer. Gels were repeatedly washed with distilled water and subsequently stained overnight with PageBlue protein stain (Thermo Fisher). For destaining, gels were incubated in distilled water until the background was clear. The Molecular Imager Gel Doc XR+ imaging system with the Image Lab V5.2 software (Bio-Rad Laboratories) was used to document the gels by scanning.

2.5.2 Determination of protein concentration in solution

Protein concentrations were determined colorimetrically using the protein assay dye reagent concentrate (Bio-Rad Laboratories) as per the manufacturer's instructions. Under acidic conditions, the absorbance maximum of coomassie brilliant blue G-250 dye shifts from 465 to 595 nm when binding to basic or aromatic amino acid residues. Therefore, the rise in absorbance at 595 nm is proportional to the protein amount in the test sample (Bradford, 1976).

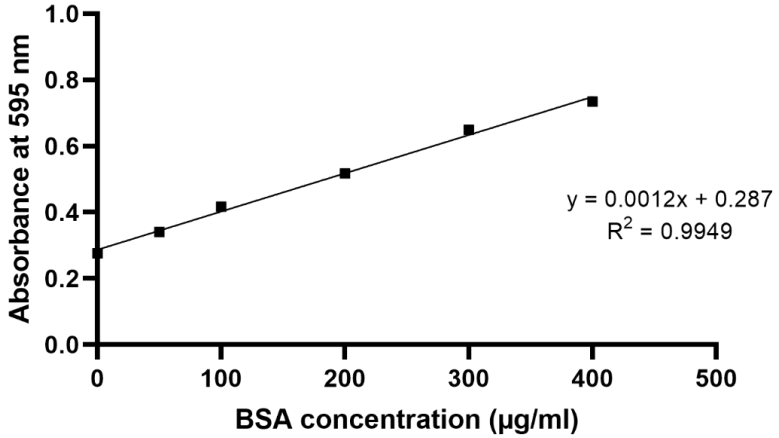

Figure 12: Example standard curve for BSA. The absorbance at 595 nm is plotted against the concentration of BSA.

In short, bovine serum albumin (BSA) solutions with a linear range of 0 µg/ml to 400 µg/ml were prepared as protein standard. 10 µl of each standard and sample solution was transferred in duplicates into a transparent 96-well polystyrene microplate with flat bottom (Greiner Bio One, ref. 655161). 200 µl of diluted dye reagent (1 part dye reagent concentrate mixed with 4 parts distilled water) was added into each well and the mixture was allowed to incubate for 5 min at room temperature. The absorbance at 595 nm was subsequently measured using a Spark 10M

microplate reader with SparkControl V3.1 SP1 software (Tecan Group). A standard curve was plotted using the known BSA concentrations and the sample protein amount was calculated (Figure 12). If the absorbance of protein samples exceeded that of the highest standard solution, samples were diluted accordingly and the measurement was repeated.

2.6 Protein biochemical methods

2.6.1 Purification of UDP-D-Mur*N*Ac-pentapeptide

Staphylococcus simulans 22 cells (ATCC 12559) were grown in 2x 2 l MH at 37 °C with shaking to an OD_{600} of 0.6. At this point, the bacterial culture was supplemented with 130 µg/ml chloramphenicol to suppress the cellular stress response, that would indirectly inhibit the accumulation of UDP-D-Mur*N*Ac-pentapeptide, and further incubated at 37 °C for 15 min. 10 µg/ml vancomycin was added to the culture, which was incubated for another 60 min. Cells were harvested via centrifugation (12,230 x *g*, 20 min, 4 °C) and resuspended in 20 ml of distilled water. The resulting suspension was drop-wise added to 60 ml of boiling distilled water and boiled for a further 15 min. The lysate was then cooled to room temperature and centrifuged at 20,440 x *g* for 30 min at 4 °C. The supernatant was frozen at -70 °C and lyophilized (Alpha 1-2 LDplus, Martin Christ Gefriertrocknungsanlagen, Osterode am Harz, Germany). The crudely purified UDP-D-Mur*N*Ac-pentapeptide was stored long-term at -20 °C. To use for the *in vitro* synthesis of lipid II, the lyophilizate was dissolved in 4 ml of distilled water.

2.6.2 Purification of *Micrococcus luteus* DSM 1790 membranes

2x 2 l TSB was inoculated with *Micrococcus luteus* DSM 1790 and incubated overnight at 30 °C with shaking. Cells were harvested by centrifugation (12,230 x *g*, 15 min, 4 °C) and resuspended in 80 ml of 50 mM Tris/HCl, 10 mM $MgCl_2$, pH 7.5 supplemented with 100 µg/ml DNase I (bovine pancreas, PanReac AppliChem) and 1 mg/ml lysozyme (chicken egg white, Carl Roth) prior to incubating on ice for 1 h with gentle shaking. Cell suspension was heated to 35 °C with agitation

and immediately cooled down on ice. The volume was increased to 700 ml with ice-cold Tris/HCl-$MgCl_2$ (pH 7.5) buffer and cell debris were pelleted by centrifugation (12,230 x *g*, 15 min, 4 °C). Membranes were then washed with 30 ml Tris/HCl $MgCl_2$ (pH 7.5) buffer, centrifuged (20,440 x *g*, 30 min, 4 °C), and resuspended in 8 ml of Tris/HCl $MgCl_2$ (pH 7.5) buffer. Purified membranes were stored long-term at -20 °C.

2.6.3 *In vitro* synthesis of lipid II

The approach described in Schneider *et al*. (2004) was adopted with changes. To find optimal reaction conditions, crudely purified UDP-D-Mur*N*Ac-pentapeptide and *M*. *luteus* membranes (extractions are described in sections 2.6.1 and 2.6.2, respectively) were titrated against each other. 10 nmol of the substrate C_{55}-P was resuspended in 10 µl chloroform and dried *in vacuo*. The reaction mix (100 µl) comprised of 100 mM Tris/HCl, 0.6% (v/v) Triton X-100, 1 mM UDP-D-Glc*N*Ac, 7.6 mM $MgCl_2$, pH 7.5, and various concentrations of UDP-D-Mur*N*Ac-pentapeptide and *M*. *luteus* membranes was incubated for 3 h at 30 °C with gentle shaking. Lipids were extracted by addition of *n*-butanol/pyridine acetate (2:1, v/v) pH 4.2 and separated by TLC (see section 2.6.6). For the synthesis of lipid II in preparative scale, reaction volume was upscaled to 10 ml. Centrifugation steps were performed for 10 min at 8,232 x *g* at 4 °C. Subsequent to lipid extraction, the organic phase was desalted thrice with an equal volume of distilled water pH 4.2 and separated by High-performance liquid chromatography (HPLC). Analysis was performed on a HiTrap DEAE Sepharose FF column (Cytiva) using a Gilson HPLC system operating Trilution LC V2.1 software (Gilson, Madison, USA). Separation of lipid II was achieved with a linear 175 min-gradient from 0 to 300 mM ammonium bicarbonate in 50% (v/v) methanol, 33% (v/v) chloroform with a flow rate of 5 ml/min. Lipid II containing fractions were combined and solvents were removed by evaporation using a Rotavapor R-100 rotary evaporator (Büchi, Flawil, Switzerland). Samples were frozen to -70 °C and lyophilized (Alpha 1-2 LDplus, Martin Christ Gefriertrocknungsanlagen). Before use, 1.5 ml of 1:1 (v/v) chloroform:methanol was added and the obtained solution was centrifuged at 12,300 x *g* for 2 min to pellet precipitated salt. Lipid II concentration was quantified by phosphate determination (see section 2.6.7).

2.6.4 *In vitro* synthesis of [^{14}C]-lipid III_{WTA}

For preparation of radioactive lipid III_{WTA}, 5 nmol of C_{55}-P was resuspended in 10 µl of chloroform and dried *in vacuo*. Reaction buffer composed of 50 mM Tris/HCl, 2.5 mM *n*-lauroylsarcosine, 2.5 mM $MgCl_2$, 100 mM NaCl, 2 mM UDP-D-Glc*N*Ac, and 0.33 mM UDP-[^{14}C]-D-Glc*N*Ac (specific activity 300 mCi/mmol, Hartmann Analytic, Braunschweig, Germany), pH 7.5 was added and briefly vortex mixed. To initiate the reaction, 38 µg of WbpL-His was applied reaching a total reaction volume of 50 µl. Samples were incubated at 30 °C overnight prior to lipid extraction and separation by TLC (see section 2.6.6). Negative control had protein added after addition of extraction solvent. Radiolabeled lipid III_{WTA} was visualized by iodine stain and scraped off the TLC plate. 1 ml of methanol was added to the powdery silica gel and the suspension was vortex mixed overnight. After centrifugation for 2 min at 21,100 x *g*, the supernatant containing the extracted lipid was transferred into a new tube and dried.

2.6.5 *In vitro* LcpA assay

An assay to determine the *in vitro* hydrolysis activity of His-LcpA in a total volume of 50 µl was performed as followed. 2 nmol of lipid II and 18 µg of DOPG (1,2-dioleoyl-*sn*-glycero-3-phospho-(1'-*rac*-glycerol)) were resuspended in 10 µl of chloroform and dried *in vacuo*. Reaction buffer (50 mM MES, 10 mM $MgCl_2$, 0.6% (v/v) DMSO, pH 5.5) was added and briefly vortex mixed. If stated, 100 µM moenomycin was added (Cayman Chemical, Ann Arbor, USA). The reaction was initiated by addition of 3 µg of His-LcpA and samples were incubated at 30 °C for 3 h with gentle shaking. To stop the reaction, lipids were extracted and separated by TLC (see section 2.6.6). In the negative controls, the protein was inactivated by the extraction solvent and added after the incubation period to the reactions.

To test the *in vitro* hydrolysis activity of His-LcpA with [^{14}C]-lipid III_{WTA}, the lipid amount of one synthesis reaction as described in section 2.6.4 was used as substrate. The assay was performed in detail as mentioned for lipid II.

2.6.6 Thin layer chromatography (TLC)

To facilitate the separation and analysis of individual components of a mixture, thin layer chromatography (TLC) was used. Samples are applied on an inert carrier sheet coated with a thin layer of adsorbent material that serves as the stationary phase. When placed in a closed TLC chamber, an organic solvent ascends the plate driven by capillary forces (mobile phase). The migration of the analytes depends thereby on their specific affinity for stationary and mobile phase (Harry *et al*., 1989).

Lipids were extracted in an equal volume of *n*-butanol/pyridine acetate (2:1, v/v) pH 4.2. Samples were then vortex mixed for 1 min and centrifuged for 3 min at 12,300 x *g* until phase separation became visible. The upper lipid-containing organic phase was spotted on a TLC Silica gel 60 F_{254} plate (Merck, Darmstadt, Germany) in 10 µl-steps with intermediate cold blow-drying. The TLC plate was transferred into a glass TLC separation chamber using a mixture of HPLC-grade chloroform/methanol/water/ammonium hydroxide (88:48:10:1, v/v) as mobile phase (Rick *et al*., 1998). As soon as the solvent front almost reached the end of the plate, the TLC plate was heat-dried with a blower to remove any residual mobile phase elutant and dipped in cerium molybdate stain (Hanessian's stain; 2.5% (w/v) phosphomolybdic acid and 1% (w/v) cerium(IV) sulfate in 6% (w/v) sulfuric acid). Upon heating at 130 °C, lipids and other molecules became visible as blue bands. Ionizing radiation of TLCs containing radioactive samples was captured by a phosphor storage screen that was further scanned with a Storm 820 phosphor imager using Storm Scanner control V5.03 software (Cytiva). Signal intensities were calculated using ImageJ V1.53k software (National Institutes of Health, Bethesda, USA).

2.6.7 Phosphate determination

This method was adapted from Rouser *et al*. (1970). An inorganic phosphate standard with a linear range of 0 to 60 nmol/µl was prepared from a 1 mM KH_2PO_4 stock solution. Test samples and standard were assayed in duplicates. Samples were resuspended in phosphate-free glass vials filled with 100 µl of distilled water and dried for 25 min at 140 °C in a heating block. 0.3 ml of 70% (v/v) perchloric acid was added, glass vials were covered with glass marbles, and samples

were hydrolyzed for 90 min at 180 °C. After cooling down the samples to room temperature, 1 ml of distilled water, 0.4 ml of 1.25% (w/v) ammonium heptamolybdate, and 0.4 ml of 5% (w/v) ascorbic acid were added. Samples were briefly vortex mixed and incubated for 5 min at 100 °C while the glass vials were again covered by marbles. Phosphate ions form a blue colored complex with molybdate under acidic conditions, thus the degree of coloration is proportional to the amount of phosphate present in the sample. The absorbance at 797 nm was measured using a Novaspec IIbsI+ spectrophotometer (Biochrom). To create a standard curve, the absorbance determined at 797 nm was plotted against the standard concentration of inorganic phosphate (Figure 13).

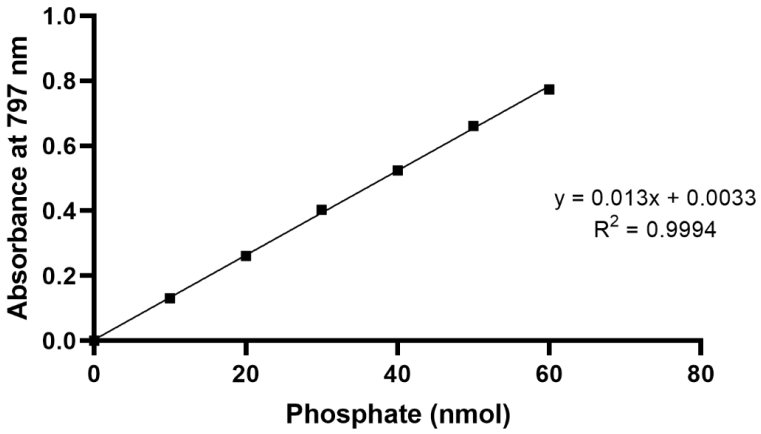

Figure 13: Example phosphate standard curve. The absorbance measured at 797 nm is plotted against the amount of phosphate.

2.6.8 *In vitro* transcription

0.5 µg of ΦX174 replicative form (RF) DNA (Promega, Fitchburg, USA) was added to 1x reaction buffer (40 mM Tris/HCl, 150 mM KCl, 10 mM $MgCl_2$, 1 mM DTT, 0.01% (v/v) Triton X-100, 0.5 mM of each NTP, pH 7.5) containing 0.5 units *Escherichia coli* RNA polymerase holoenzyme (New England Biolabs) and, except where otherwise stated, the respective antibiotic in a total volume of 25 µl. The DNA was transcribed at 37 °C for 2 h. After the addition of 25 µl 2x RNA loading dye (Thermo Fisher), the reaction was incubated at 70 °C for 10 min and immediately cooled down on ice for another 3 min. The samples were loaded onto a 1% (w/v) agarose gel supplemented with

1x GelRed (Biotium) and run for 45 min at 100 V. The gel was imaged using the Molecular Imager Gel Doc XR+ imaging system with Image Lab V5.2 software (Bio-Rad Laboratories).

2.6.9 Zymographic analysis

Zymography is an electrophoretic technique to visualize the hydrolytic activity of enzymes that were priorly separated according to their molecular weight (Vandooren *et al*., 2013). In this work, proteinous cell lysate containing hydrolytic enzymes is used to degrade gel-embedded PG.
50 ml MH was inoculated with *S. aureus* NCTC8325 and grown overnight at 37 °C with shaking. Cells were harvested by centrifugation (4,816 x *g*, 10 min, 4 °C) and washed thrice with an equal volume of distilled water. The pellet was resuspended in 5 ml of distilled water and autoclaved. Stacking and resolving gels were poured as described in Table 1.

Table 1: SDS-PAGE gel recipe for 1 gel

Component	Stacking gel (4%)	Resolving gel (10%)
Acrylamide/Bisacrylamide (40%; 29:1)	400 µl	2.5 ml
Resolving Buffer (3 M Tris/HCl, pH 8.5)	-	1.67 ml
Stacking Buffer (1 M Tris/HCl, 0.8% (w/v) SDS)	480 µl	-
SDS (20%, w/v)	-	70 µl
S. aureus NCTC 8325 autoclaved cells	-	1.5 ml
ddH_2O	3 ml	4.12 ml
APS (40%, w/v)	6.72 µl	6.8 µl
TEMED	3.2 µl	6.7 µl

S. aureus MSSA1112 wildtype and *lcp* deletion mutant strains were grown in 100 ml TSB at 37 °C with shaking until OD_{600} of 1.2. Cells were centrifuged (4,816 x *g*, 10 min, 4 °C) and washed with an equal volume of distilled water. Pellet was resuspended in 400 µl of ice-cold 50 mM Tris/HCl, 3 M LiCl, and 0.1% (v/v) Triton X-100 and incubated on ice for 30 min. Samples were centrifuged (21,100 x *g*, 5 min, 4 °C) and the supernatant was immediately used. 5 µl of the supernatant was combined with 4x NuPAGE LDS sample buffer (Thermo Fisher) and loaded on gel. As molecular

weight marker, 6 µl PageRuler Plus prestained protein ladder (Thermo Fisher) with a range of 10 to 250 kDa was applied and electrophoresis was conducted at 80 V for 1-2 h in a running buffer comprised of 25 mM Tris/HCl, 192 mM glycine, and 0.1% (w/v) SDS. Gels were washed twice in distilled water first for 5 min and then for 1 h followed by overnight incubation at 37 °C in zymogram buffer (50 mM Tris/HCl, 100 mM NaCl, 0.1% (v/v) Triton X-100, pH 7.5) with gentle shaking. The gel was rinsed in distilled water, stained with 0.1% (w/v) methylene blue and 0.01% (w/v) potassium hydroxide for 5 min, and destained with gentle agitation in distilled water until signal bands were cleared prior to documentation using the Molecular Imager Gel Doc XR+ imaging system with Image Lab V5.2 software (Bio-Rad Laboratories).

2.6.10 MOE-BDP binding assay

Approximately 5 µg of protein was incubated in 50 mM MES, 10 mM $MgCl_2$, 0.6% (v/v) DMSO, pH 5.5 with 2.5 mM moenomycin (20 mg/ml stock solution in DMSO) or the same amount of DMSO in a volume of 15 µl at 30 °C for 30 min with gentle shaking at 200 rpm. MOE-BDP (synthesized by the Menche Lab, University of Bonn, according to Hsieh *et al*., 2021) was added to a final concentration of 57.6 µM to the reaction mixtures, which were incubated for another 30 min. Samples were supplemented with 5 µl of 4x NuPAGE LDS sample buffer (Thermo Fisher) and 0.1 µl β-mercaptoethanol prior to boiling at 95 °C for 10 min. After cooling down to room temperature, 15 µl of the mixture was resolved by SDS-PAGE (see section 2.5.1). The gel was scanned with an Amersham Typhoon Biomolecular Imager (Cytiva) using a Cy2 525BP20 filter. Images were analyzed using the associated ImageQuant TL V8.2.0.0. software.

2.6.11 Bocillin binding assay

To visualize *S. aureus* PBPs in membrane preparations, the method described by Zhao *et al*. (1999) was adopted with changes. *S. aureus* MSSA1112 wildtype and the Δ*lcpABC* triple mutant were grown in 50 ml TSB at 37 °C with shaking until an OD_{600} of 0.6. The cells were harvested by centrifugation (4,816 x *g*, 10 min, 4 °C) and resuspended in 1 ml of buffer A (100 mM Tris/HCl, 150 mM NaCl, pH 7.5). In a parallel approach, the wildtype strain was supplemented with either

5x MIC moenomycin (20 mg/ml stock in DMSO) or the equal amount of DMSO and incubated for a further 30 min at 37 °C prior to adjusting the OD_{600} again to 0.6 and cell harvesting. 0.4 mg/ml lysozyme, 2 µg/ml RNase A, 2 µg/ml DNase, and 0.05 mg/ml lysostaphin were added to the resuspended pellet and the suspension was incubated for 1 h at 37 °C with agitation. Cells were disrupted by bead beating at maximum speed (Bead Ruptor 12, Omni International, Kennesaw, USA) 12 times for 30 sec with intermittent cooling on ice for 1 min. Glass beads were removed by centrifugation at 12,000 x *g* for 10 min and the supernatant was subjected to ultracentrifugation at 150,000 x *g* for 40 min at 4 °C. The pellet was resuspended in 200 µl of buffer B (100 mM Tris/HCl, 150 mM NaCl, 20 mM $MgCl_2$, pH 7.5) and 5 µl of the membrane preparation was incubated for 30 min at 35 °C with 7.5 µM Bocillin FL (Thermo Fisher) in a total volume of 15 µl. The negative control was preincubated with 20 mg/ml ampicillin for 30 min at 35 °C prior to the addition of the fluorescently labeled β-lactam. 5 µl of 4x NuPAGE LDS sample buffer (Thermo Fisher) and 0.15 µl β-mercaptoethanol were added to the samples before heat inactivation at 95 °C for 5 min and subsequent resolving by SDS-PAGE as described in section 2.5.1. The gel was scanned with an Amersham Typhoon Biomolecular Imager (Cytiva) using a Cy2 525BP20 filter. Images were analyzed using the associated ImageQuant TL V8.2.0.0. software.

2.6.12 Fluorescence anisotropy

Fluorescence anisotropy (FA) is a technique used to determine the rotational mobility of a fluorophore that is exposed to polarized light. Due to the Brownian motion, the position of the fluorophore changes constantly in solution and the faster the motion, the more depolarized light is emitted. If the fluorophore is bound to a larger molecule, the tumbling becomes slower and the amount of emission is decreased. Hence, FA can be used to study the interaction of fluorophore-coupled molecules with proteins or other ligands (Lakowicz, 2010).

The method was adapted from Boes *et al*. (2020). Reactions were performed in duplicates in a non-binding, black 384-well plate (Greiner Bio One, ref. 781900) in an Infinite 200 PRO microplate reader with i-control V3.9.1.0 software (Tecan Group) equipped with polarization filters with excitation and emission wavelengths of 485 and 535 nm, respectively. Serial dilutions of the proteins (His-LCP enzymes, PBP2-His, SgtA-His, SgtB-His, and negative control His-Colicin M) were

prepared in a reaction mix (30 µl) comprised of 50 mM MES, 10 mM $MgCl_2$, 0.5% (v/v) DMSO, pH 5.5. MOE-BDP was added to a final concentration of 0.33 µM. For competition assays, fixed concentrations of proteins (0.5 µM, approximately 50-80% of FA saturation) and MOE-BDP (0.33 µM) were added to serial dilutions of moenomycin or lipid II prepared in the respective protein reaction buffer (30 µl final volume). Reaction mixtures were incubated for 20 min at room temperature with gentle shaking prior to measuring FA at 20 °C. FA in millianisotropy units (mA) was plotted against the protein concentration in µM for evaluation and normalized. K_D values were determined by nonlinear curve fitting using GraphPad Prism V9.5.1.733 software (GraphPad Software, La Jolla, USA).

2.6.13 Fluorescence microscopy

S. aureus Newman wildtype, *lcp* deletion mutant strains and Δ*lcpA* p*lcpA* complemented strain (50 µg/ml erythromycin for plasmid retention), as well as *S. aureus* SA113 and the respective *tarO* deletion mutant, were grown in 20 ml of TSB at 37 °C with shaking to an OD_{600} of 1.2. The cells were diluted to OD_{600} of 0.7 and 400 µl was then labeled with either 4.93 µM MOE-BDP, 0.32 µM rhodamine B labeled ramoplanin (Sigma Aldrich), 7.5 µM Bocillin FL (Thermo Fisher) or a 1:1 (w/w) mixture of vancomycin and fluorescein-labeled vancomycin at a final concentration of 1 µg/ml and incubated for a further 10 min at 37 °C together with a non-treated control sample. Cells were pelleted at 12,300 x *g* for 2 min and washed thrice in 400 µl of PBS prior to resuspension in 20 µl. Samples were applied on microscope slides coated with 1% (w/v) agarose and examined by fluorescence microscopy using an Axio Observer Z1 microscope equipped with an HXP 120 C lamp, Axio Cam MRm camera, αPlan-APOCHROMAT 100×/1.46 oil immersion objective and filter set 38 (Carl Zeiss, Oberkochen, Germany). Image acquisition, processing, and analysis were performed with ZEN blue V3.6.095.03000 software (Carl Zeiss) and ImageJ V1.53k software. To determine the fluorescent ratio (FR), the fluorescence intensity at the septum was divided by the average fluorescence intensity at the cell poles after deduction of the average background fluorescence (Figure 14) (Atilano *et al*., 2010). Each 50 cells of three independent experiments were used for calculations.

To investigate the localization of green fluorescent protein (GFP)-labeled LCP enzymes or PBP2 and yellow fluorescent protein (YFP)-labeled PBP4 in *S. aureus* RN4220, cells harboring the plasmid pCQ11-*gfp-lcpA*, pCQ11-*gfp*-l*cpB*, pCQ11-*gfp-lcpC*, pCQ11-*gfp-pbp2*, and pCQ11-*pbp4-yfp*, respectively, were grown in 20 ml of TSB supplemented with 50 µg/ml erythromycin and 100 µM IPTG to an OD_{600} of 1.2. After diluting to an OD_{600} of 0.7, a 400 µl suspension was treated with 10x MIC of either moenomycin, vancomycin, teixobactin, ramoplanin or ampicillin (Table 8) and incubated with a non-treated control for a further 10 min at 37 °C. Cells were harvested and washed twice in 400 µl of PBS before resuspension in 20 µl. Fluorescence microscopy was performed as described above.

To visualize the cellular localization of MOE-BDP in *S. aureus* MSSA1112 wildtype and the Δl*cpA* mutant, cells were grown in 20 ml of TSB at 37 °C with shaking to an OD_{600} of 1.2. After diluting to an OD_{600} of 0.7, 400 µl of the cell suspension was labeled with 4.93 µM MOE-BDP and incubated further for 10 min. Cells were pelleted, washed thrice in 400 µl PBS, and finally resuspended in 20 µl of the same buffer. Samples were transferred on a microscopy slide coated with 1% (w/v) agarose for microscopy using an Axio Observer Z1 microscope (equipped with X-Cite Xylis LED Lamp, Teledyne Photometrics Prime BSI express camera, αPlan-APOCHROMAT 100×/1.46 oil immersion objective, filter set 38) and associated ZEN blue V3.6.095.03000 software (Carl Zeiss). Analysis using convolved average projections (CAPs) was conducted by Jan-Samuel Puls from the Institute of Pharmaceutical Microbiology at the University of Bonn (Puls *et al*., 2023).

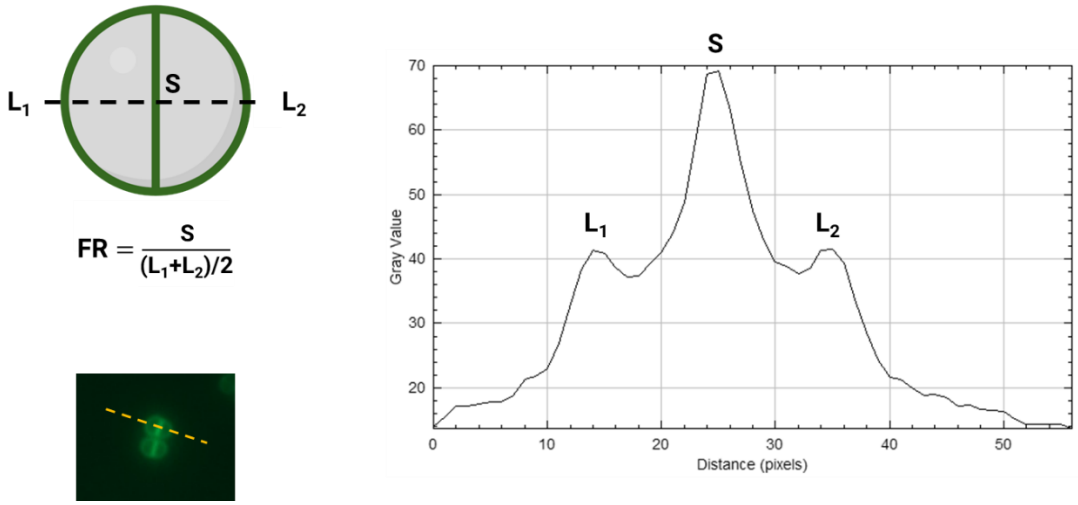

Figure 14: Determination of the fluorescent ratio (FR). After subtracting the average background fluorescence, the fluorescence at the septum (S) was quantified and divided by the average fluorescence measured at the lateral membrane (L). An FR value higher than 2 implies the accumulation of the labeled protein/antibiotic at the cell division septum.

2.7 Peptidoglycan and cytoplasmic membrane analysis methods

2.7.1 Isolation of cell wall from *S. aureus*

The protocol for the isolation of *S. pneumoniae* cell wall (Bui *et al*., 2012) was modified by the Vollmer group (Newcastle University, UK) to isolate cell wall from *S. aureus* (Sutton *et al*., 2022). Overnight pre-cultures of *S. aureus* MSSA1112 wildtype or Δ*lcpABC* were diluted 1:100 into 2 x 2 l TSB and grown at 37 °C with shaking to an OD_{600} of 1.2. The cultures were immediately cooled down on ice for 15 min. For a different experiment, an overnight pre-culture of *S. aureus* Newman was diluted 1:100 into 2 x 2 l TSB and grown at 37 °C with shaking to an OD_{600} of 1.2. Moenomycin (20 mg/ml solution in DMSO) was added to one flask to reach a final concentration of 0.3125 µg/ml (5x MIC). In parallel, the same amount of DMSO was added to the second flask. After another 30 min incubation, the cultures were immediately cooled down on ice for 15 min. For all experiments, the cells were pelleted by centrifugation at 6,800 x *g* for 20 min and resuspended in 80 ml of ice-cold 50 mM Tris/HCl pH 7.0. The suspension was added drop-wise to 240 ml of boiling 5% (w/v) SDS solution while stirring on a magnetic stir plate. After additional 15 min, the samples were cooled down to room temperature and stored at -20 °C.

The lysates were reheated at 80 °C for 30 min and centrifuged at room temperature for 30 min at 12,000 x *g*, until the supernatant was clear. The pellet was washed twice in 20 ml 1 M NaCl and then several times in 20 ml H_2O to get rid of SDS. The successful removal of SDS was confirmed by the Hayashi test as described in section 2.7.2. Finally, the pellet was resuspended in 6 ml H_2O and transferred into a 2 ml-screwcap-tube filled to 1/3 with glass beads. Cells were disrupted by bead beating at maximum speed (Bead Ruptor 12, Omni International, Kennesaw, USA) 12 times for 30 sec with intermittent cooling on ice for 1 min. Glass beads were removed and washed with 10 ml H_2O. The sample was centrifuged for 5 min at 2,000 x *g* and the pellet was washed with 30 ml H_2O. Each supernatant was combined and centrifuged at room temperature for 30 min at 25,000 x *g*. Afterwards, the pellet was resuspended in 10 ml 100 mM Tris/HCl, 20 mM $MgSO_4$, pH 7.5. 10 µg/ml DNase I (bovine pancreas, PanReac AppliChem) and 50 µg/ml RNase A (bovine pancreas, Sigma Aldrich) were added and the reaction proceeded for 2 h while stirring at 37 °C. 10 mM $CaCl_2$ and 100 µg/ml trypsin (porcine pancreas) were added for another 18 h at 37 °C. The

SDS concentration was adjusted to final 1% (w/v) and the total volume was increased to 20 ml with distilled water. After incubation at 80 °C for 15 min, the samples were centrifuged for 30 min at 25,000 x *g* at 25 °C. The pellet was resuspended in 10 ml 8 M LiCl, incubated at 37 °C for 15 min, and centrifuged again. Then the pellet was washed in 10 ml 100 mM EDTA pH 7.0 and centrifuged as described above after another incubation at 37 °C for 15 min. Following two washing steps with 20-30 ml distilled water, the pellets were resuspended in 1 ml distilled water, frozen at -70 °C in a glass vial, and finally lyophilized (Alpha 1-2 LDplus, Martin Christ Gefriertrocknungsanlagen). Samples were stored long-term at -20 °C.

2.7.2 Sodium dodecyl sulphate test by Hyashi

Samples were tested for the presence of SDS by using the Hayashi test as previously described (Hayashi, 1975). 25 µl of 0.7 M sodium phosphate, 1 µl of 0.5% (w/v) methylene blue, and 150 µl of chloroform were mixed with a sample volume of 50 µl by vortexing. SDS forms a water-insoluble complex with methylene blue, which is extracted by chloroform. If the organic phase shows no discoloration, the tested sample is free of SDS.

2.7.3 Isolation, digestion and analysis of peptidoglycan from *S. aureus*

To obtain murein from the purified cell wall, anionic glycopolymers were removed by HF-treatment performed by Dr. Daniela Vollmer (Newcastle University, UK) (Bui *et al*., 2012). For that purpose, the total amount of isolated cell wall of each sample was separated in 5 mg portions, which were then each dissolved in 2.7 ml ice-cold HF and stirred closed with parafilm at 4 °C for 48 h. After centrifugation at 4 °C for 45 min at 200,000 x *g*, the supernatant was discarded and the pellet was washed twice with ice-cold H_2O, once with ice-cold 100 mM Tris/HCl pH 7.0, and finally twice with H_2O. The pellet was resuspended in 500 µl of ice-cold H_2O containing 0.05% (v/v) NaN_3 and stored at 4 °C.

To obtain muropeptides from the purified PG for analysis, 180 µl of the well mixed preparation was stirred with 20 mM $NaPO_4$, 0.00025% (v/v) NaN_3, and 10 µg mutanolysin, pH 4.8 at 37 °C

overnight. The reaction was refreshed with another 10 µg mutanolysin and incubated at the same conditions for another 24 h. The digestion was boiled at 100 °C for 10 min and centrifuged after cooling down to room temperature at 13,000 x *g* for 15 min. The supernatant was stored long-time at -20 °C.

The further procedures including HPLC analysis and evaluation were performed by Dr. Jacob Biboy (Newcastle University, UK) according to de Jonge *et al*. (1992). 50-100 µl of distilled water along with 0.5 M sodium borate pH 9.0 in a ratio of 1:1 (v/v) and a spatula tip of solid sodium borohydride were added to the samples. After incubating for 30 min at room temperature with centrifugation at 2,000 x *g* and ventilation, the pH was adjusted between pH 3.5 and 4.5 by adding 20% (v/v) phosphoric acid. Samples were used directly for HPLC or stored long-term at -20 °C.

The muropeptides were separated by RP-HPLC using a Prontosil (Bischoff, Leonberg, Germany) column (3 µm, particle size, 250 × 4.6 mm, 120 Å pore size) and a linear gradient from 0% to 30% (v/v) methanol in 10 mM NaOH pH 6.0 supplemented with 0.00025% (v/v) NaN_3 at a flow rate of 0.5 ml/min. 30 µl of each sample was mixed with 190 µl of buffer A (10 mM NaOH, 0.00025% (v/v) NaN_3, pH 6.0) and 200 µl was subjected to HPLC analysis (Figure 15). Profiles were quantified with Laura software (LabLogic Systems, Koblenz, Germany).

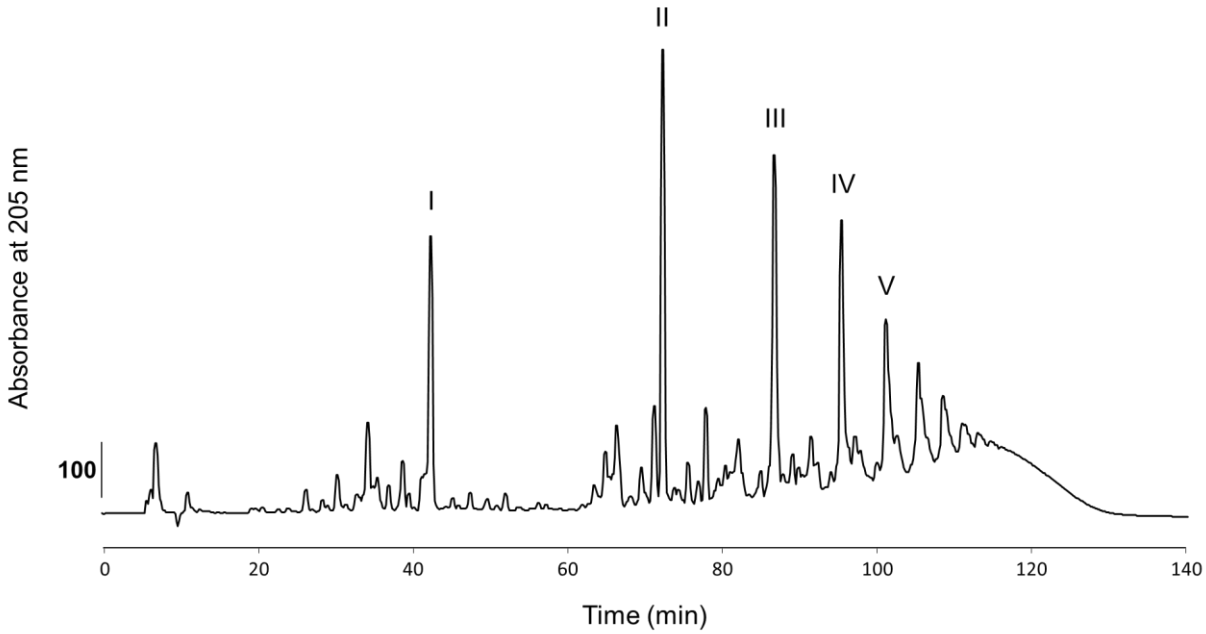

Figure 15: Example muropeptide profile of *S. aureus*. The absorbance at 205 nm is plotted against the time. Muropeptides were separated on a Prontosil column (3 µm, particle size, 250 × 4.6 mm, 120 Å pore size). The numbers indicate commonly found peaks (de Jonge *et al*., 1992) representing monomers (peak I) and oligomers (dimers peak II, trimers peak III, tetramers peak IV, pentamers peak V).

2.7.4 Quantification of peptidoglycan

If not stated otherwise, the quantification of PG was performed by determining the *N*-acetylglucosamine (Glc*N*Ac) concentration according to Arenas *et al*. (2022). Test samples and standard were assayed in duplicates. Briefly, PG was dissolved in water and a sample of 80 µl was mixed with an equal amount of working solution (15% (w/v) $CuSO_4$ diluted 1:25 in 0.236 mM Na_2CO_3, 88.58 mM potassium sodium tartrate tetrahydrate, 0.238 mM $NaHCO_3$, and 1.41 M Na_2SO_4) prior to boiling at 95 °C for 20 min. In parallel, a sugar standard comprising Glc*N*Ac solutions with a linear range of 0 mM to 12.5 mM was processed. After cooling down to room temperature, 320 µl of 1:4 diluted Folin-Ciocalteu phenol reagent (Merck) in 0.5 N HCl was added and vortex mixed. Subsequently, 320 µl of water was added to the samples and the absorbance at 660 nm was measured using a Spark 10M microplate reader with SparkControl V3.1 SP1 software (Tecan Group). To create a standard curve, the absorbance determined at 660 nm was plotted against the concentration of Glc*N*Ac (Figure 16). Since purified PG contains both Glc*N*Ac and *N*-acetylmuramic acid (Mur*N*Ac) and this method cannot differentiate between the type of reducing sugar, the calculated sample concentration must be divided by 2.

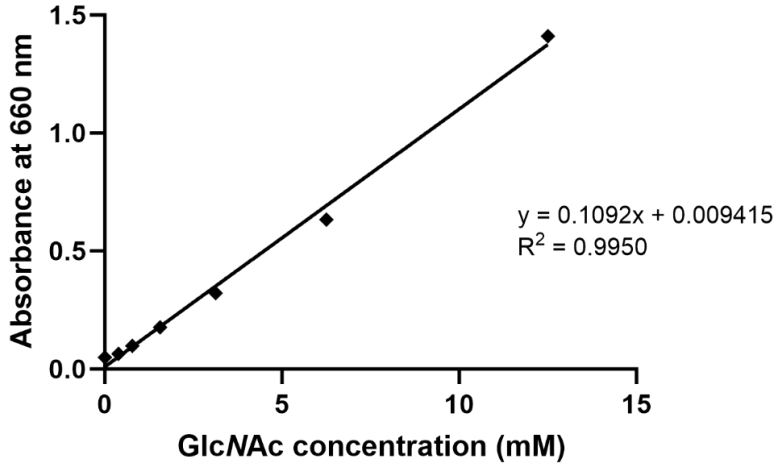

Figure 16: Example standard curve for *N*-acetylglucosamine (Glc*N*Ac). The absorbance at 660 nm is plotted against the concentration of Glc*N*Ac.

2.7.5 Extraction of wall teichoic acids

This protocol was adapted from a previously published method (Sobhanifar *et al*., 2015) with minor changes. *S*. *aureus* Newman cells were grown in 50 ml TSB at 37 °C with shaking until an OD_{600} of 1.2. Bacterial cultures were supplemented with either 5x MIC moenomycin (20 mg/ml stock in DMSO) or the equal amount of DMSO and incubated for a further 30 min at 37 °C. Purified WTAs were desalted using Zeba Spin desalting columns (0.5 ml, 7 kDa MWCO, Thermo Fisher), frozen to -70 °C, and lyophilized (Alpha 1-2 LDplus, Martin Christ Gefriertrocknungsanlagen) for long-term storage at -20 °C. Samples were dissolved in 100 µl water and quantification was performed by phosphate determination (see section 2.6.7).

2.7.6 Purification and HPLC analysis of membrane lipids

The previously described protocols for extraction of membrane lipids from *E*. *coli* (Kato *et al*., 1999, Barreteau *et al*., 2009) were adapted with modifications. *S*. *aureus* Newman wildtype and the Δ*lcpA* knockout mutant were grown in 50 ml TSB at 37 °C with shaking to an OD_{600} of 1.2 prior to the addition of 5x MIC moenomycin (20 mg/ml stock in DMSO) or the equal amount of DMSO and further incubation for 30 min. Cells were harvested by centrifugation (12,300 x *g*, 5 min, 4°C) and washed in ice-cold 0.9% (w/v) NaCl solution. Pellet was resuspended in 500 µl methanol and 250 µl 60% (w/v) potassium hydroxide prior to boiling for 1 h at 65 °C. Samples were then cooled on ice for 5 min and mixed with 200 µl glacial acetic acid, 300 µl phosphate-buffered saline (PBS, pH 7.4), and 700 µl chloroform. After thorough vortex mixing and centrifugation at 12,300 x *g* for 3 min, the organic layer was collected and washed with an equal volume of distilled water. The chloroform layer was transferred into new tube and dried *in vacuo*. Membrane lipids were resuspended in 100 µl of buffer A (3:1:1 (v/v) water/ methanol/ isopropanol supplemented with 10 mM phosphoric acid) and 80 µl was separated on a reversed-phase column (MultoHigh-Bio-300-C4 5 µM, 125 x 4 mm, CS-Chromatographie, Langerwehe, Germany) using an Agilent 1260 Infinity II LC system operating OpenLab CDS V2.6 software (Agilent Technologies, Santa Clara, USA). HPLC was performed with a column temperature of 30 °C at a flow rate of 0.5 ml/min using an isocratic elution with buffer A for 3 min, followed by a linear 32-min gradient from 100%

buffer A to 100% buffer B (0.5:1:1 (v/v) water/ methanol/ isopropanol supplemented with 10 mM phosphoric acid) and an isocratic elution with 100% buffer B for 5 min. Within 2 min, the concentration of buffer A was linearly increased to 100% and run for a further 8 min. Membrane lipids were monitored at 205 nm (Figure 17) (Sidders *et al*., 2023).

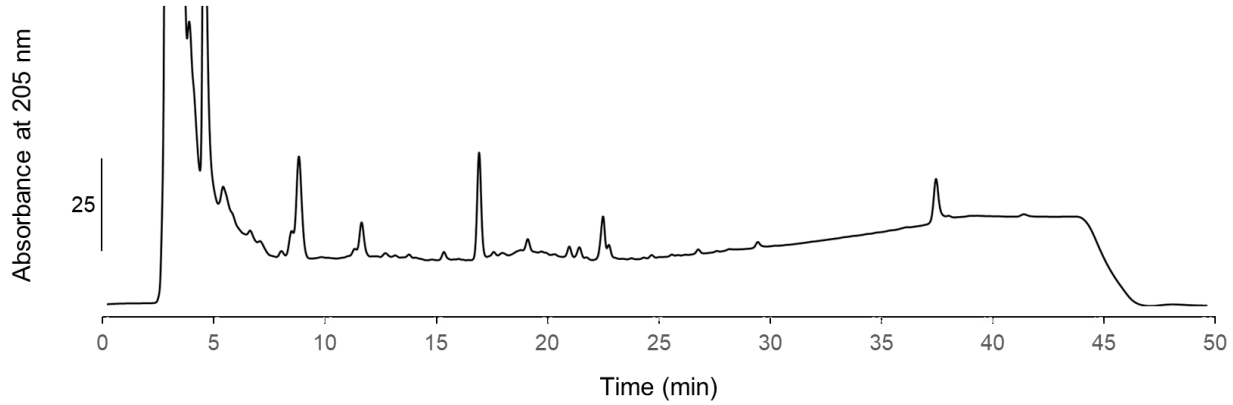

Figure 17: Example HPLC chromatogram of *S*. *aureus* membrane lipids. The absorbance at 205 nm is plotted against the time. Membrane lipids were separated on a MultoHigh-Bio-300-C4 column (5 µM, 125 x 4 mm).

3. Results

Chapter 1: *S. aureus* LCP enzymes are targeted by moenomycin

The LCP enzyme family has been demonstrated to attach WTAs to PG in *S. aureus* (Chan *et al*., 2013, Schaefer *et al*., 2017). Although these anionic glycopolymers are not essential for cell survival, the depletion of WTAs was shown to sensitize MRSA strains to β-lactams (Wang *et al*., 2013) and thus providing options for combinatorial treatment of MRSA infections. While evaluating the role of LCP enzymes for capsule biosynthesis by Rausch *et al*. (2019), our group discovered an inhibitory effect of the phosphoglycolipid antibiotic moenomycin on the hydrolytic activity of *S. aureus* LcpA. This observation required to reinvestigate the mode of action of moenomycin and its possible off-target effect on LCP enzymes.

3.1.1 Moenomycin inhibits the hydrolytic activity of LcpA

To be able to attach anionic glycopolymers to PG, LCP proteins must cleave the ultimate lipid-linked WTA precursor at the outer leaflet of the cytoplasmic membrane. Since WTAs and CPs are coupled via a phosphodiester bond to the C_6 hydroxyl of the PG Mur*N*Ac residue (Kojima *et al*., 1985, Kawai *et al*., 2011, Rausch *et al*., 2019), it is reasonable to assume that LCP enzymes catalyze the hydrolysis of the phosphodiester bond (Figure 18A) to release the carrier lipid C_{55}-P, an essential and limited molecule in PG and cell surface glycopolymer biosynthetic pathways (Manat *et al*., 2014).

To investigate the catalytic properties of full-length *S. aureus* LcpA, the purified enzyme was assayed *in vitro* with the first lipid-linked WTA precursor, lipid III_{WTA}, which had been enzymatically synthesized and radioactively labeled using [^{14}C]-Glc*N*Ac as substrate (Figure 18A). After the extraction with BuOH/PyrAc, the reaction products were separated by TLC and analyzed by autoradiography. If LcpA hydrolyzes [^{14}C]-lipid III_{WTA}, the hydrophilic, radioactively labeled cleavage product phospho-[^{14}C]-Glc*N*Ac should be retained in the aqueous phase that is not applied on the TLC. Thus, the catalytic activity of LcpA can be calculated from the reduction in signal intensity. Indeed, LcpA was shown to hydrolyze [^{14}C]-lipid III_{WTA} and this reaction could be inhibited by addition of the antibiotic moenomycin (Figure 18B & C).

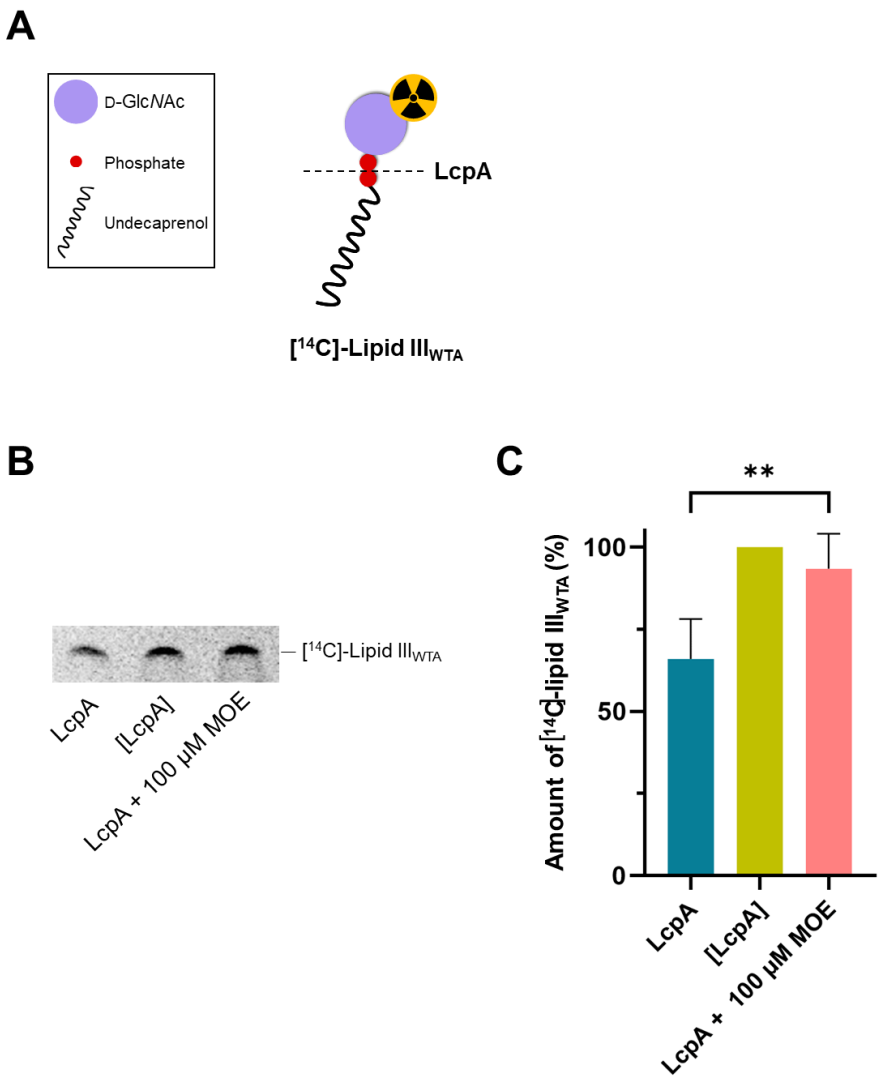

Figure 18: The LcpA-catalyzed hydrolysis of [^{14}C]-lipid III$_{WTA}$ *in vitro* is inhibited by moenomycin. (A) Possible cleavage site of LcpA within enzymatically synthesized [^{14}C]-lipid III$_{WTA}$. (B) Hexahistidine-tagged LcpA was assayed with [^{14}C]-lipid III$_{WTA}$ in the presence or absence of moenomycin. After extraction with BuOH/PyrAc, the samples were separated by TLC and imaged by autoradiography. Hydrolysis was displayed by reduction of the [^{14}C]-lipid III$_{WTA}$ substrate band. In the negative control indicated by brackets, the enzyme was inactivated by organic solvents and added after the incubation period. The addition of moenomycin (MOE) inhibited the *in vitro* hydrolysis of [^{14}C]-lipid III$_{WTA}$ by LcpA. (C) The intensity of the [^{14}C]-lipid III$_{WTA}$ signals on TLC was calculated using ImageJ V1.53k software. Values are presented as the mean ± SD (error bars) of three independent experiments. **P ≤ 0.01 (unpaired t-test, GraphPad Prism V9.5.1.733).

Another enzymatic property of LcpA was discovered while assaying the attachment of WTA precursors to lipid II. With the ultimate PG precursor, the corresponding signal was weaker on TLC and a new band at the level of C_{55}-P was seen (Figure 19B). This result indicated that LcpA was also able to hydrolyze lipid II *in vitro* (Figure 19A). When LcpA was assayed with lipid II in the presence of moenomycin, the intensity of the lipid II-corresponding band was not diminished,

indicating that the hydrolysis of the PG precursor was inhibited by the antibiotic (Figure 19B & C). In contrast to LcpA, purified LcpB and LcpC did not hydrolyze lipid II *in vitro* (Figure 20). Of note, the hydrolytic activity of LcpA prevented the reconstitution of a direct WTA attachment reaction *in vitro* involving lipid III_{WTA} as a donor substrate and lipid II as an acceptor substrate.

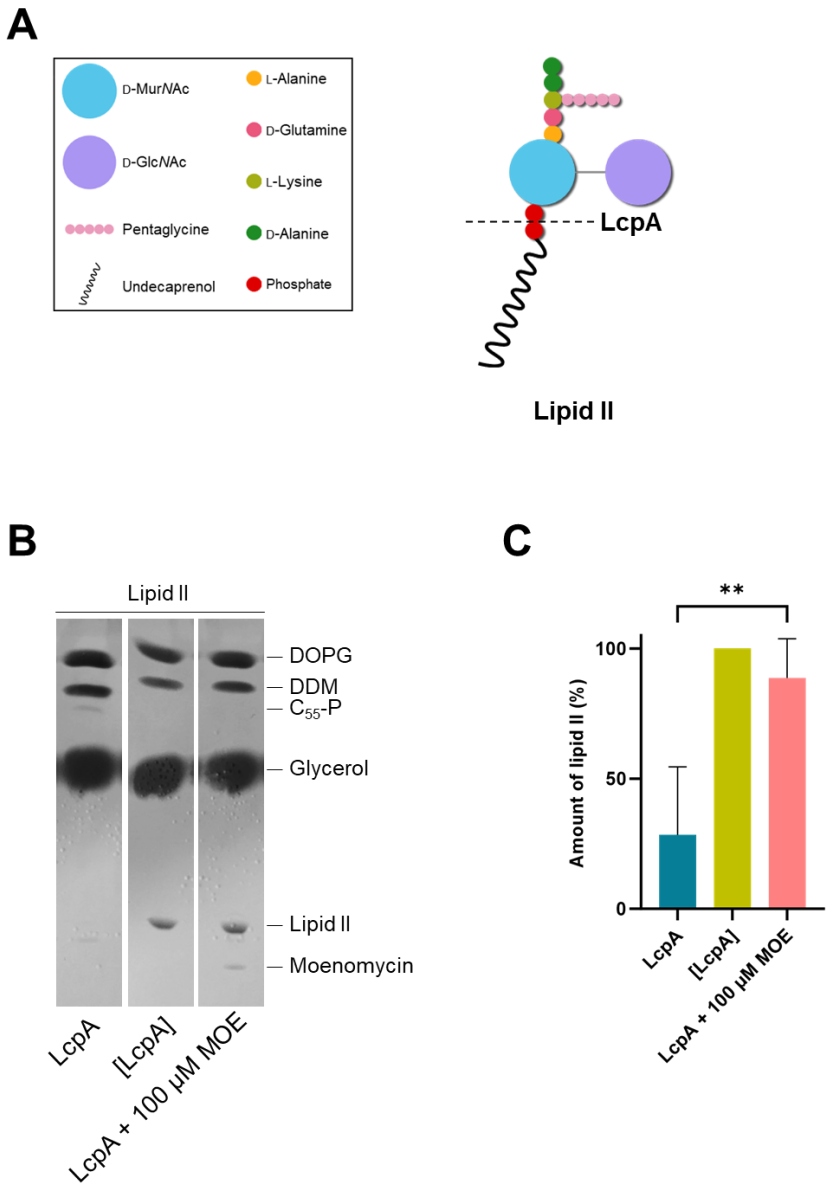

Figure 19: *S. aureus* LcpA hydrolyzes lipid II *in vitro* and is inhibited by moenomycin. (A) Possible cleavage site of LcpA within lipid II. (B) Purified lipid II was incubated with hexahistidine-tagged LcpA and, if stated, moenomycin. Following extraction with BuOH/PyrAc, samples were separated by TLC and developed using Hanessian's stain. Hydrolysis was displayed by reduction of the lipid II substrate band. In the negative control indicated by brackets, the enzyme was inactivated by organic solvents and added after the incubation period. The addition of moenomycin (MOE) inhibited the *in vitro* hydrolysis of lipid II by LcpA. (C) The intensity of the lipid II signals on TLC was calculated using ImageJ V1.53k software. Values are presented as the mean ± SD (error bars) of three independent experiments. **P ≤ 0.01 (unpaired t-test, GraphPad Prism V9.5.1.733).

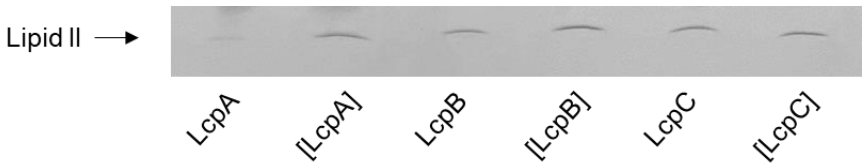

Figure 20: LcpA is the only lipid II-hydrolyzing LCP enzyme in *S. aureus*. Purified lipid II was incubated with hexahistidine-tagged LCP enzymes from *S. aureus*. Following extraction with BuOH/PyrAc, samples were separated by TLC and developed using Hanessian's stain. Hydrolysis was displayed by reduction of the lipid II substrate band. In the negative controls indicated by brackets, the enzyme was inactivated by organic solvents and added after the incubation period. TLC is representative for three independent experiments.

As the uncontrolled hydrolysis of lipid II would be fatal for the bacterial cell, the observed hydrolysis likely represents an *in vitro* artefact. To investigate this, the cellular lipid II content of *S. aureus* Newman wildtype and the corresponding Δ*lcpA* mutant was compared. To this end, the membrane lipids were isolated and separated by HPLC (Figure 21). The analysis of the lipid II peak area (retention time of 29.5 min as identified with a lipid II standard, data not shown) revealed that the Δ*lcpA* single mutant synthesized *de facto* less of the PG precursor (0.1378 nmol per 30 ml culture at OD_{600} 1.2) (Figure 22) than the wildtype strain (0.1627 nmol), suggesting that the property of LcpA to hydrolyze lipid II does not occur *in vivo* or is prevented by other mechanisms within the cell. Noticeably, the membrane lipid profile of the Δ*lcpA* mutant differed from the parental strain by smaller peaks with a retention time of 8.5 min (peak 1) and 11.5 min (peak 2), respectively (Figure 21). With moenomycin, these peaks distinctly accumulate in addition to a third peak with 17 min retention time (peak 3). However, the identity of the corresponding lipids is not known and a topic for future research.

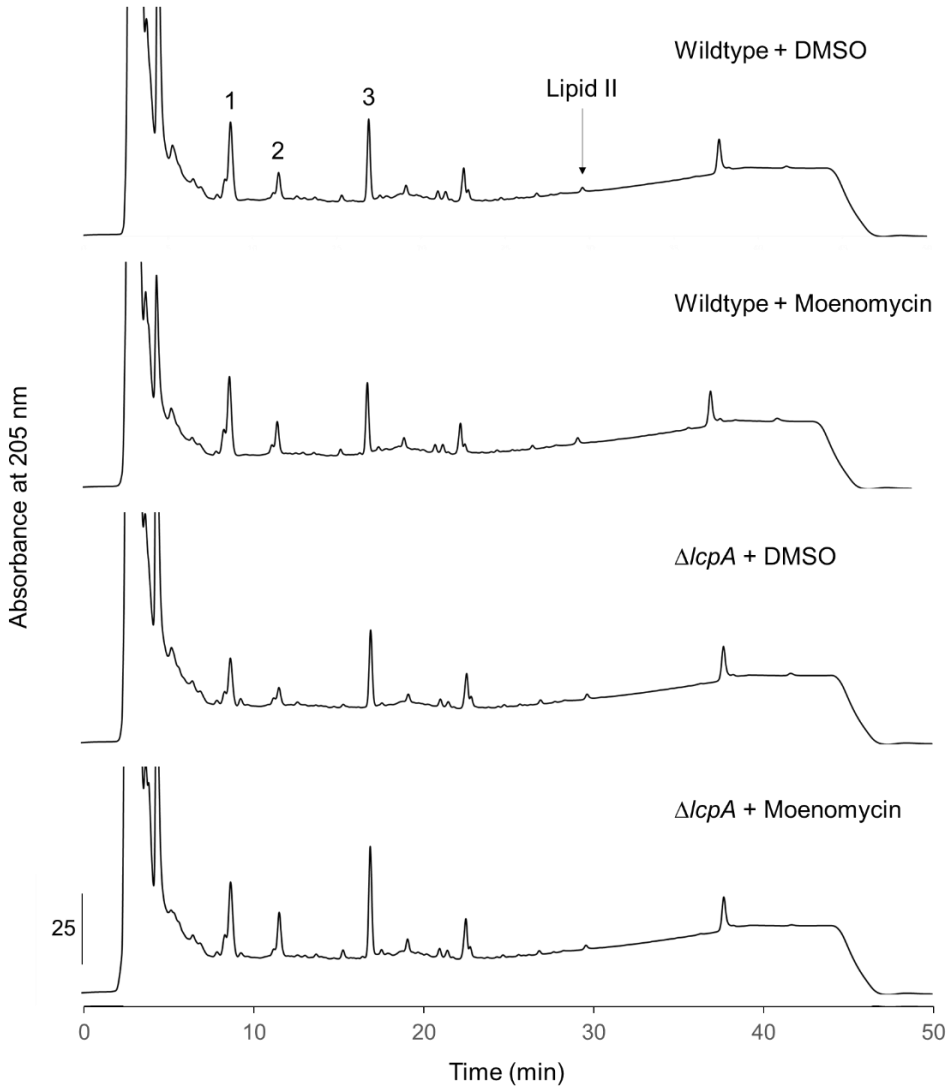

B

Peak	% total peak area			
	Wildtype + DMSO	**Wildtype + MOE**	**Δ*lcpA* + DMSO**	**Δ*lcpA* + MOE**
1	1.96 ± 0.17	1.99 ± 0.11	1.84 ± 0.12	2.01 ± 0.54
2	0.74 ± 0.01	0.75 ± 0.08	0.48 ± 0.04	1.12 ± 0.08
3	1.14 ± 0.19	1.03 ± 0.13	1.26 ± 0.40	1.63 ± 0.10
Lipid II	0.33 ± 0.05	0.34 ± 0.05	0.27 ± 0.02	0.28 ± 0.01

Figure 21: HPLC separation of membrane lipids from *S. aureus* Newman wildtype and the Δ*lcpA* mutant. (A) Cells were grown until OD_{600} of 1.2 and treated with DMSO/5x MIC moenomycin (MOE) before lipid purification. HPLC analysis was performed on a MultoHigh-Bio-300-C_4 column (5 µM, 125 x 4 mm) using a linear 32-min gradient from 100% buffer A (3:1:1 (v/v) water/methanol/isopropanol supplemented with 10 mM phosphoric acid) to 100% buffer B (0.5:1:1 (v/v) water/methanol/isopropanol supplemented with 10 mM phosphoric acid) at 30 °C and a flow rate of 0.5 ml/min. The peak corresponding to lipid II with a retention time of 29.5 min is indicated. The numbers 1 to 3 highlight noticeable peaks whose corresponding lipid structure is not known. (B) Percentage of total peak areas of noticeable peaks as highlighted in the chromatograms. Values are presented as the mean ± SD of three independent experiments.

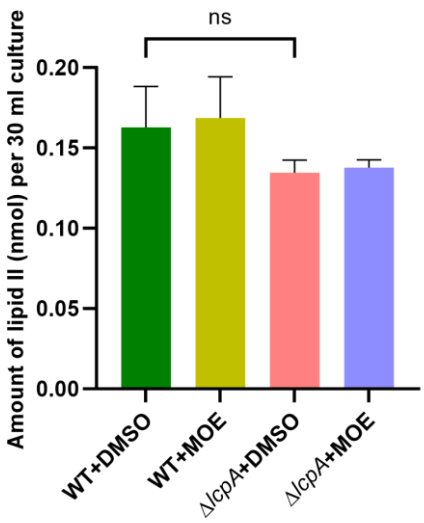

Figure 22: Amount of the PG precursor lipid II as determined by HPLC for *S. aureus* Newman wildtype and the Δ*lcpA* mutant per 30 ml cell culture at OD_{600} 1.2. Although not significant (ns, P > 0.05, unpaired t-test, GraphPad Prism V9.5.1.733), the wildtype showed a higher amount of lipid II than found in the Δ*lcpA* single mutant for the untreated as well as the moenomycin-treated samples. Values are presented as the mean ± SD (error bars) of three independent experiments.

3.1.2 *Lcp* single and double mutants are less susceptible to moenomycin

To investigate the impact of LCP proteins on the growth of *S. aureus* MSSA1112 and Newman in the presence of moenomycin, the MICs against the wildtype and corresponding *lcp*-deleted strains were determined and compared to other cell wall targeting antibiotics (Table 2). Moenomycin showed potent antimicrobial activities with MICs ranging from 0.0625 to 0.25 µg/ml among the tested strains. In line with the hypothesis that LCP enzymes may represent off-targets, the differences between the mutants and their respective parental strain were only moderate. In comparison, the susceptibilities of *S. aureus* SA113 Δ*tarO*, which is like the MSSA1112 Δ*lcpABC* triple mutant devoid of WTAs but affected earlier in the WTA biosynthesis pathway, and SA113 Δ*atlA*, a mutant not expressing the major autolysin Atl of *S. aureus* (Oshida *et al*., 1995), were almost unaffected. The latter was considered in this context since WTA-depleted *S. aureus* cells are more prone to detergent-induced autolysis (Zoll *et al*., 2012), suggesting a possible connection between Atl and the activity of LCP proteins.

Table 2: MIC values of *S. aureus* MSSA1112, Newman, and SA113 strains for moenomycin and other cell wall targeting antibiotics. n.d.: not determined. The table shows representative data of three or more independent experiments.

Strain	MIC (µg/ml)								
	Moenomycin	Vancomycin	Teixobactin	Ramoplanin	Ampicillin	Cefoxitin	Oxacillin	Tunicamycin	Targocil
MSSA1112 wildtype	0.125	4	1	2	4	4	1	128	2
MSSA1112 Δ*lcpA*	0.25	4	1	2	4	2	1	128	2
MSSA1112 Δ*lcpB*	0.125	4	1	2	4	2	1	128	2
MSSA1112 Δ*lcpC*	0.125	4	1	2	4	4	1	64	2
MSSA1112 Δ*lcpABC*	0.0625	4	1	1	1	2	1	16	>16
MSSA1112 Δ*lcpAB*	0.25	4	0.5	1	4	2	1	128	2
MSSA1112 Δ*lcpAC*	0.25	4	1	2	4	4	1	128	2
MSSA1112 Δ*lcpBC*	0.25	2	1	1	4	4	1	128	2
Newman wildtype	0.0625	2	1	2	0.5	2	0.25	n.d.	n.d.
Newman Δ*lcpA*	0.125	2	1	1	1	2	0.25	n.d.	n.d.
Newman Δ*lcpB*	0.125	2	1	1	1	4	0.125	n.d.	n.d.
Newman Δ*lcpC*	0.25	2	1	1	1	4	0.125	n.d.	n.d.
Newman Δ*lcpBC*	0.25	2	1	1	1	2	0.125	n.d.	n.d.
SA113 wildtype	0.125	2	1	2	0.25	2	0.25	32	2
SA113 Δ*tarO*	0.0625	2	1	1	0.5	4	0.25	32	>16
SA113 Δ*atlA*	0.125	2	1	0.5	0.5	1	0.25	16	2

The antibiotic susceptibility profiles for a panel of cell wall-targeting antibiotics were determined to reveal further resistance tendencies in LCP-deficient and related strains. As seen for moenomycin, there were no significant differences in the MICs of the tested compounds among the strains. An exception represents the MSSA1112 Δ*lcpABC* triple mutant, which was more sensitive to ampicillin (1 µg/ml) than the wildtype (4 µg/ml) but resistant to targocil (MIC >16 µg/ml), an antibiotic targeting the WTA biogenesis by inhibiting the flippase TarGH (Campbell *et al*., 2012). A similar MIC for targocil was obtained against *S. aureus* SA113 Δ*tarO*. Furthermore, the triple mutant was more susceptible to tunicamycin compared to the parental strain (16 µg/ml and 128 µg/ml, respectively). In *S. aureus*, the fatty acyl nucleoside antibiotic inhibits TarO, the initial glycosyltransferase of the WTA biosynthesis pathway, and, at higher concentrations, additionally the phospho-*N*-acetylmuramoyl-pentapeptide-transferase of PG biosynthesis, MraY (Campbell *et al*., 2011).

Next, the growth of strains in the presence of moenomycin was followed (Figure 23). The *S. aureus* Newman *lcp* single mutant strains were significantly less susceptible to increasing concentrations of moenomycin compared to the wildtype strain, indicating that LCP enzymes may indeed present off-targets for moenomycin.

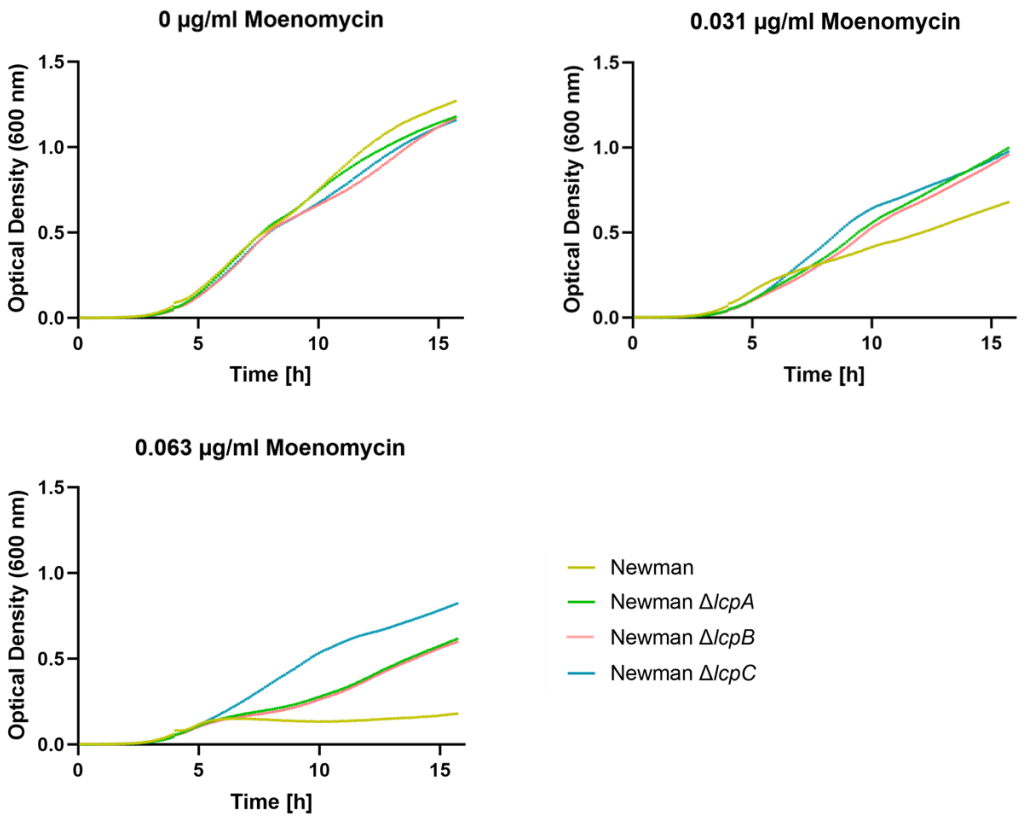

Figure 23: The effect of moenomycin on the growth of *S. aureus* Newman *lcp* mutant strains. Cells were cultured in MH medium with indicated moenomycin concentrations while the growth was monitored using the optical density at 600 nm. Growth curves are representative of three or more independent experiments.

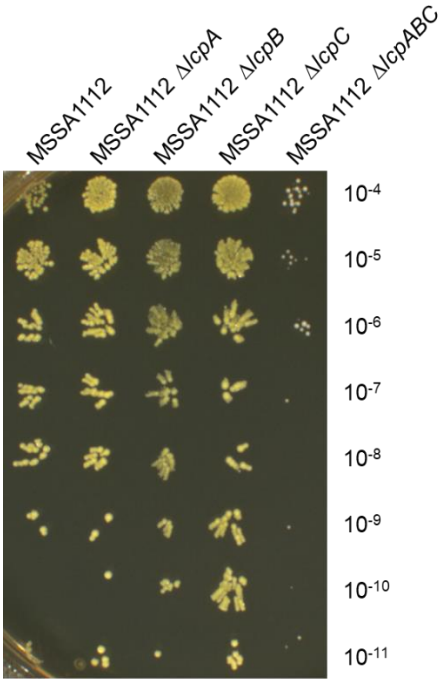

Figure 24: Spot dilution assays comparing the susceptibilities of MSSA1112 wildtype and *lcp* mutant strains to moenomycin. Strains were grown to an OD_{600} of 1.0 were serially diluted and spotted on TSA containing 15.625 ng/ml moenomycin. Numbers indicate the dilution factor. Representative result of three independent experiments.

A spot dilution assay was performed with *S. aureus* MSSA1112 and the respective *lcp* deletion mutants (Figure 24) to exclude that the decreased susceptibility of *lcp* single mutants to moenomycin, as indicated in the growth curves of *S. aureus* Newman (Figure 23), is strain-specific. The wildtype strain grew slightly weaker compared to the single *lcp* mutant strains and the triple mutant showed a reduced growth. Remarkably, also the colony phenotype differed substantially from the other strains. While the pigmentation of the wildtype and single mutants was golden on TSA, the colonies of the Δ*lcpABC* triple mutant were white as also seen in the absence of moenomycin (data not shown). Moreover, the colonies of the LCP-deficient strain had a significantly reduced diameter.

3.1.3 Moenomycin-induced killing is time-delayed in *S. aureus* cells

Next, the moenomycin-induced killing of *S. aureus* MSSA1112 wildtype was followed over time to examine the bactericidal effect (Figure 25). When exposed to moenomycin, the strain showed an initial increase in the viable counts within the first 2 h, indicating that the antibiotic did not cause an immediate loss in viability, but the viable counts declined in the following hours. The exposure to moenomycin also reduced the colony size (data not shown). Overall, this experiment revealed a surprising delay in the bactericidal effect of moenomycin on the *S. aureus* strain MSSA1112.

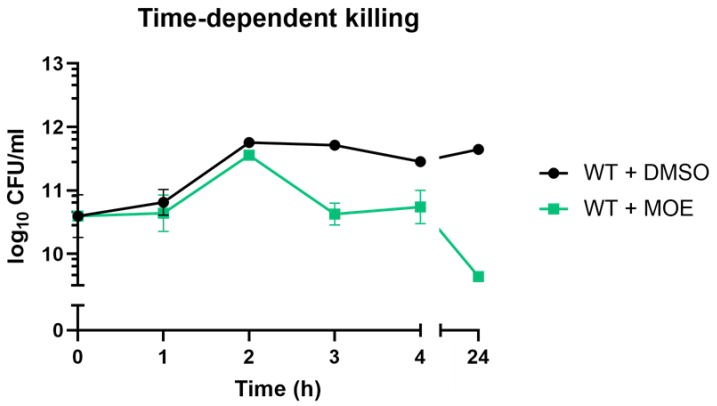

Figure 25: Moenomycin shows a delayed bactericidal effect against *S. aureus* MSSA1112. Cells were grown in MH medium until exponential phase (OD_{600} 0.5) and exposed to 1x MIC of moenomycin (MOE) or the equal amount of DMSO used. At different time points, cells were serially diluted and plated on MHA plates. Time-dependent killing was assessed by determining the colony forming units (CFU) per milliliter. Values are presented as the mean ± SD (error bars) of two independent experiments.

3.1.4 LCP enzymes directly interact with moenomycin

To further investigate the interaction of moenomycin with LCP proteins and to understand the mechanism of enzyme inhibition, different techniques were used to conduct affinity measurements. For that purpose, a moenomycin version carrying the commonly used fluorophore boron-dipyrromethene (BODIPY) on the A-ring was synthesized by the Menche Lab (University of Bonn) (Hsieh *et al*., 2001). Since crystal structures of *S*. *aureus* PBP2 in complex with moenomycin revealed that the A-ring does not directly interact with the glycosyltransferase domain of PBP2 (Lovering *et al*., 2007, Yuan *et al*., 2008), the fluorophore was not expected to affect binding to the cellular target. However, the specific interaction site of moenomycin in LCP enzymes is not known yet. Efforts to obtain high-resolution crystal structures of the complex are ongoing at the time this thesis is written.

In a binding assay, BODIPY-labeled moenomycin (MOE-BDP) was incubated with purified LCP enzymes and PG glycosyltransferases prior to the separation by SDS-PAGE and detection by fluorimaging (Figure 26). As a negative control, the proteins were preincubated with unlabeled moenomycin before the application of the labeled compound. For all purified LCP proteins from *S*. *aureus*, including variants lacking the transmembrane domain, a signal located right above the respective protein band was observed (Figure 26B). Since MOE-BDP is a molecule of approximately 2287 Da and the additional band was not detected in negative control samples, it can be assumed that LCP proteins and the fluorescently labeled antibiotic formed a stable complex. In line with the results of previous publications demonstrating the binding of moenomycin to PG glycosyltransferases (Lovering *et al*., 2007, Yuan *et al*., 2008, Heaslet *et al*., 2009), *S*. *aureus* PBP2 and the monofunctional glycosyltransferases SgtA and SgtB were used as control samples, for which a signal was also detectable (Figure 26A) (see supplementary Figure 58 for activity test of SgtA and SgtB). In the case of PBP2, the intensity was considerably weaker and appeared slightly below the respective protein band. This result was confirmed in independent experiments. For SgtA, a second signal became visible right above the band of the proposed dimer structure. In contrast, no signal was present in a negative control with *S*. *aureus* PBP4 that does not possess a glycosyltransferase domain, suggesting that the assay reliably reports the specific binding of moenomycin to glycosyltransferases.

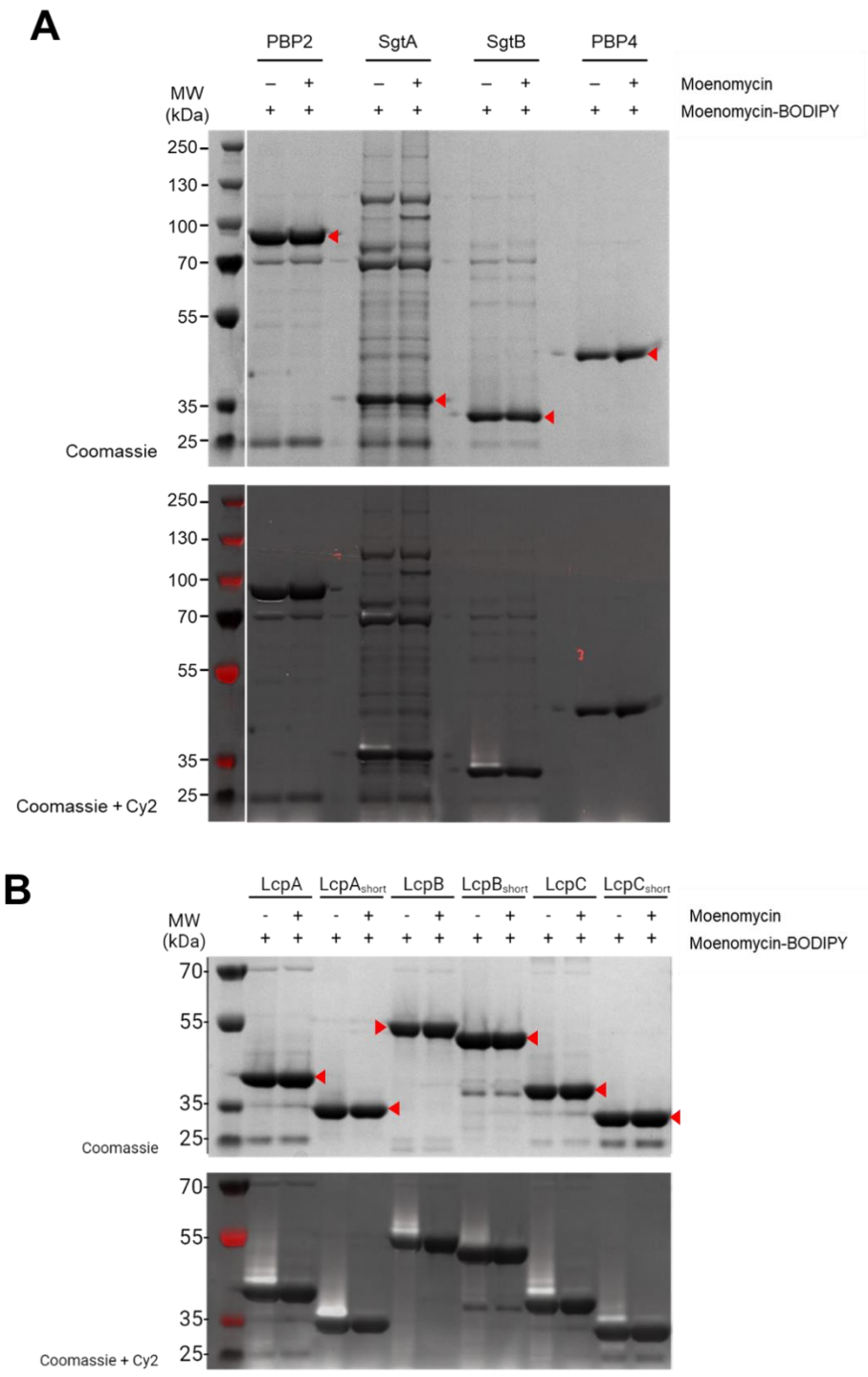

Figure 26: LCP enzymes interact with MOE-BDP in a direct binding assay regardless of their transmembrane domain. Hexahistidine-tagged LCP proteins were purified and incubated in the presence of moenomycin-BODIPY (MOE-BDP) prior to separation by SDS-PAGE. If indicated, samples were pre-incubated with moenomycin before addition of MOE-BDP to occupy the possible binding site. Gels were scanned using a Cy2 filter and stained with coomassie G-250-based PageBlue protein staining solution (Thermo Fisher). $LcpA_{short}$, $LcpB_{short}$, and $LcpC_{short}$: hexahistidine-tagged LCP proteins without transmembrane domain. Arrows indicate the respective protein band. Representative results of three independent experiments.

To confirm the results obtained in the binding assay and to further characterize the interaction between LCP proteins and moenomycin, fluorescence anisotropy (FA) measurements were conducted. Prior to the binding studies, the ideal probe concentration and protein conditions were determined (see supplementary Figure 59 for protein purity). MOE-BDP served as the fluorescent probe and was used in a fixed concentration of 0.33 µM. The results are shown in Figure 27 with the FA signal plotted against the respective protein concentration. *S. aureus* PBP2 and the monofunctional glycosyltransferases SgtA and SgtB showed a high affinity for MOE-BDP, because the FA signal reached saturation at low protein concentrations. The K_D values were calculated to be lower than 0.1 µM (Table 3). For LcpA, LcpB, and LcpC, binding of the fluorescent probe could be detected with weaker affinities. The K_D values were 0.30 ± 0.06 µM, 0.63 ± 0.08 µM, and 0.57 ± 0.15 µM, respectively. No effect on the fluorescent probe could be detected for the negative control colicin M.

To verify the specific binding of fluorescently labeled moenomycin, the probe was challenged by increasing concentrations of unlabeled moenomycin. For these experiments, a fixed protein concentration of 0.5 µM correlating with approximately 50-80% of the FA saturation and 0.33 µM of MOE-BDP were used. The FA signal declined with all three LCP enzymes, PBP2, SgtA, and SgtB, indicating that unlabeled moenomycin replaces the fluorescent probe in the binding site of the respective proteins (Figure 28A). In an additional competition assay, LcpA and fluorescently labeled moenomycin were mixed with the PG precursor lipid II. In the experiments described above (see section 3.1.1), LcpA was shown to hydrolyze lipid II *in vitro*. The FA signal decreased with increasing concentrations of lipid II, suggesting that moenomycin and lipid II occupy the same binding site within LcpA (Figure 28B).

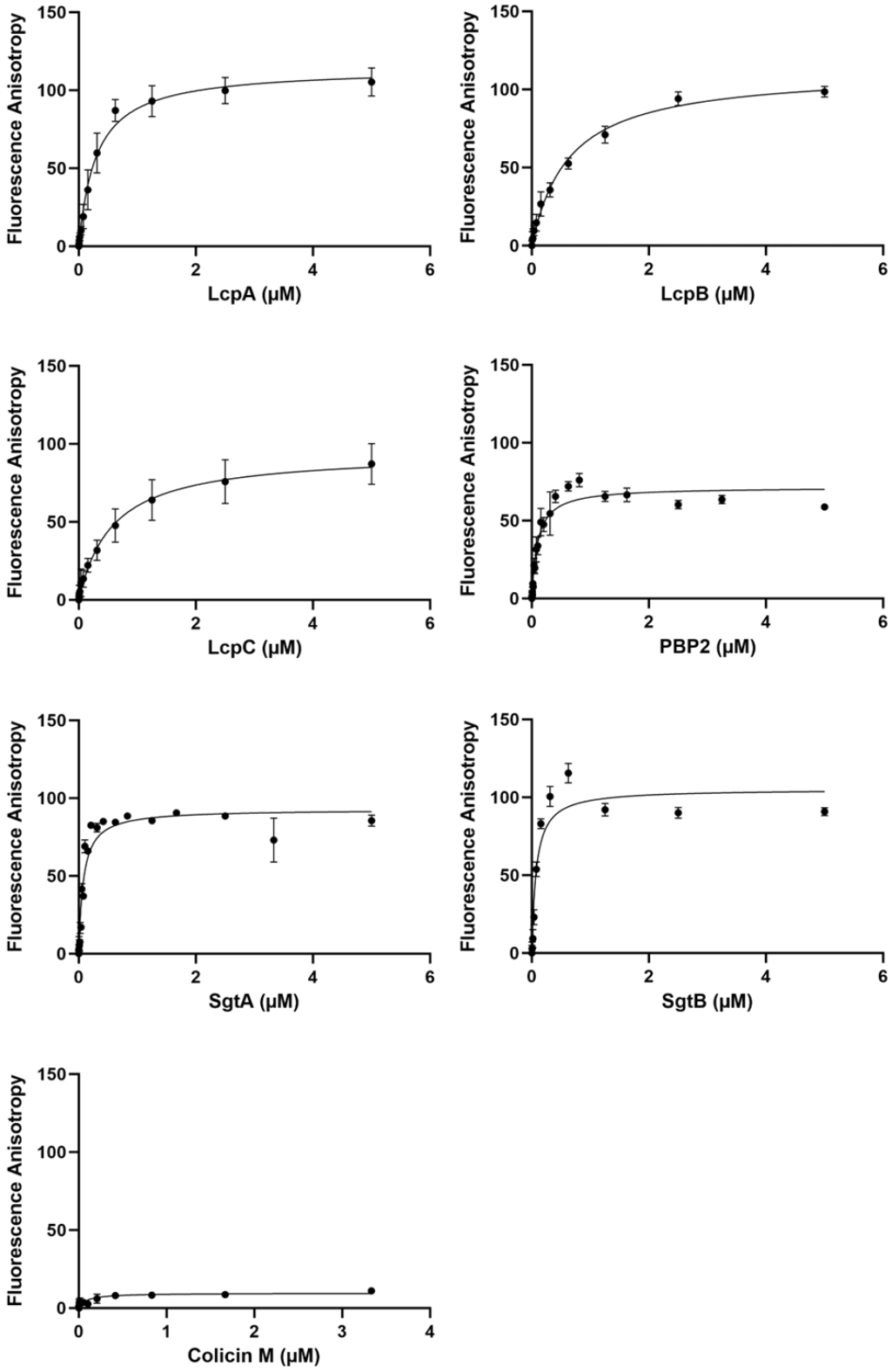

Figure 27: FA measurements on *S. aureus* LCP proteins and PG glycosyltransferases using MOE-BDP. The FA (in mA units) is plotted against the protein concentration. Experiments were performed in triplicates and error bars indicate the mean ± SD. The results suggest a direct binding of MOE-BDP (0.33 µM) to LCP enzymes and glycosyltransferases, while no binding was detectable for colicin M.

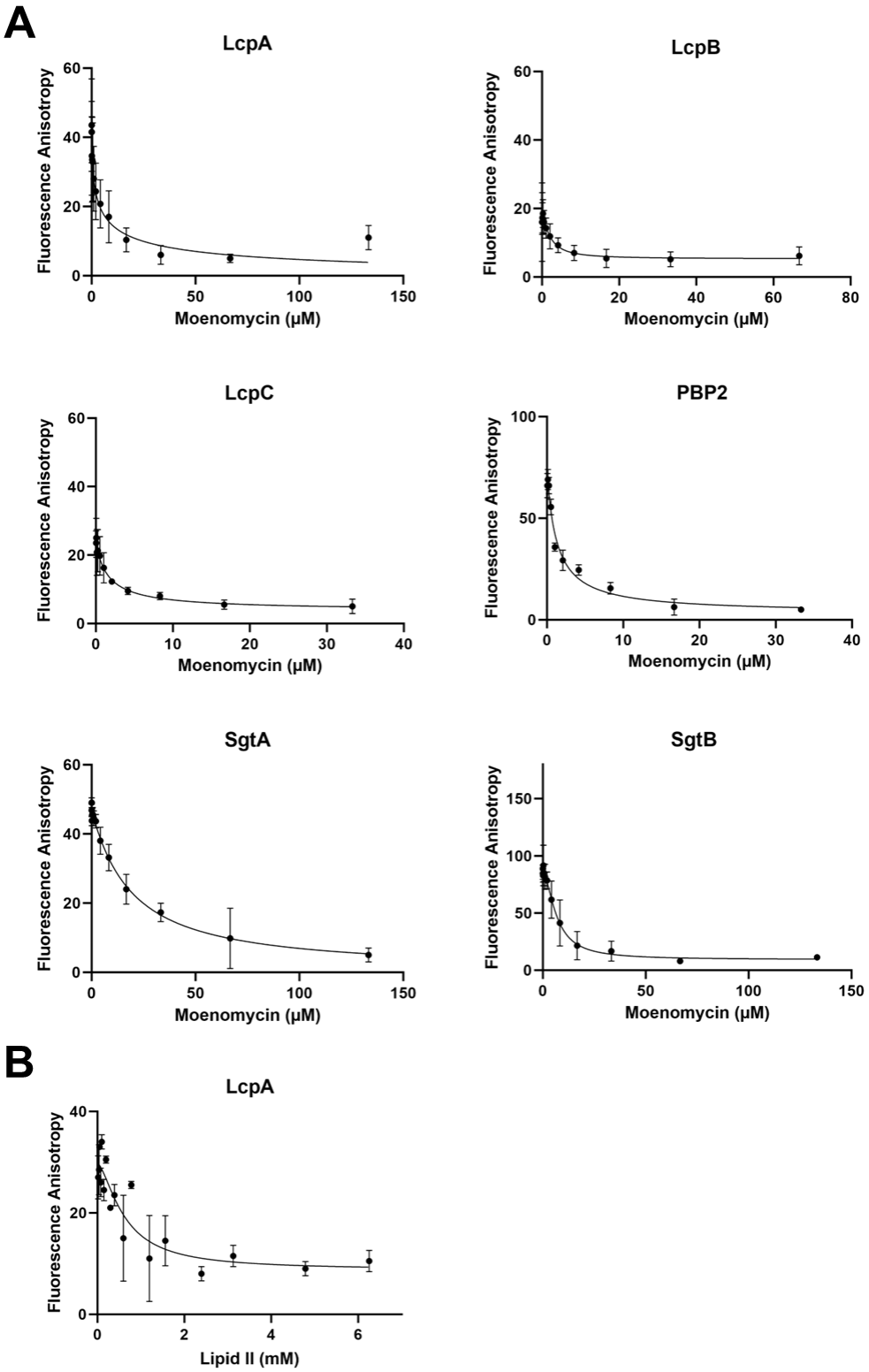

Figure 28: Competitive binding assay of *S. aureus* LCP proteins and PG glycosyltransferases. The FA (in mA units) is plotted against the concentration of unlabeled compound. 0.5 µM protein (approximately 50-80% of FA saturation) was incubated with 0.33 µM MOE-BDP and increasing concentrations of unlabeled compound. Experiments were performed in triplicates and error bars depict the mean ± SD. Moenomycin and lipid II competitively displaced the MOE-BDP probe from LCP enzymes and PG glycosyltransferases.

Table 3: Binding affinities of *S. aureus* LCP enzymes and PG glycosyltransferases for MOE-BDP determined in FA assays. The K_D value is the dissociation constant representing the equilibrium between the enzyme-MOE-BDP complex and the separated constituents. The K_D values are presented as the mean ± SD of three independent experiments performed in duplicates.

Protein	K_D values (MOE-BDP)
LcpA	0.30 ± 0.06 µM
LcpB	0.63 ± 0.08 µM
LcpC	0.57 ± 0.15 µM
PBP2	0.10 ± 0.02 µM
SgtA	0.08 ± 0.04 µM
SgtB	0.08 ± 0.03 µM

3.1.5 The combination of moenomycin and other cell wall-active antibiotics shows synergistic antibacterial activity against MSSA1112 wildtype but not the LCP-deficient strain

To further understand the functional properties of LCP enzymes, checkerboard assays of moenomycin in combination with antibiotics targeting the PG or WTA biosynthesis were conducted with *S. aureus* MSSA1112 wildtype (Figure 29), the respective Δ*lcpABC* triple mutant (Figure 30), and the SA113 Δ*tarO* strain (Figure 31). In all cases, the glycopeptide vancomycin did not shift the MIC for moenomycin, which was differing from the result obtained for the MRSA strain USA300 (supplementary Figure 60 and Table 9). The FIC values were 0.563, 0.531, and 0.75, respectively (Table 4). However, the combination with the β-lactams oxacillin or cefoxitin increased the susceptibility of the MSSA1112 wildtype (FIC values 0.375 and 0.188, respectively) and the TarO-deprived SA113 strain (0.313 and 0.375) to moenomycin but not of the Δ*lcpABC* triple mutant. For the latter strain, the FIC indexes of 0.75 for both compounds were distinctly higher than the critical value of 0.5. Moreover, the antibiotics tunicamycin and targocil, which are known to affect the WTA biogenesis, sensitized MSSA1112 wildtype to the phosphoglycolipid (FIC values 0.266 and 0.281), whereas the susceptibility remained unaffected for the Δ*lcpABC* triple mutant (FIC values both 0.5) and the Δ*tarO* null strain (0.531 and 1.0, respectively). The finding, that the combination of moenomycin and β-lactams are not synergistic in the WTA-depleted

Δ*lcpABC* triple mutant but in the wildtype and the *tarO*-deprived strain, supports the hypothesis that moenomycin affects the attachment activity of LCP enzymes.

Table 4: Checkerboard assay results of moenomycin in combination with cell wall-active antibiotics against *S. aureus* MSSA1112 wildtype and Δ*lcpABC*, as well as SA113 Δ*tarO*. A fractional inhibitory concentration (FIC) of <0.5 indicates synergism while a value of 0.5-4 suggests an unremarkable additive effect or no increase in inhibitory activity when the two compounds are combined (Lorian, 2005). In the MSSA1112 wildtype strain, moenomycin acted synergistically in combination with all antibiotics tested except vancomycin, whereas the MIC of moenomycin against the LCP-deficient strain was not altered by any of the tested compounds. In the SA113 Δ*tarO* null mutant, the combination of the β-lactams oxacillin or cefoxitin with moenomycin revealed a synergistic effect, while the antibiotics vancomycin, tunicamycin, and targocil did not alter the MIC of moenomycin. Representative results of three independent experiments.

Antibiotic	Class	MSSA1112 wildtype		MSSA1112 Δ*lcpABC*		SA113 Δ*tarO*	
		FIC	Interaction	FIC	Interaction	FIC	Interaction
Oxacillin	β-lactam	0.375	synergistic	0.75	indifferent	0.313	synergistic
Cefoxitin	β-lactam	0.188	synergistic	0.75	indifferent	0.375	synergistic
Vancomycin	glycopeptide	0.563	indifferent	0.531	indifferent	0.75	indifferent
Tunicamycin	fatty acyl nucleoside	0.266	synergistic	0.5	indifferent	0.531	indifferent
Targocil	other	0.281	synergistic	0.5	indifferent	1.0	indifferent

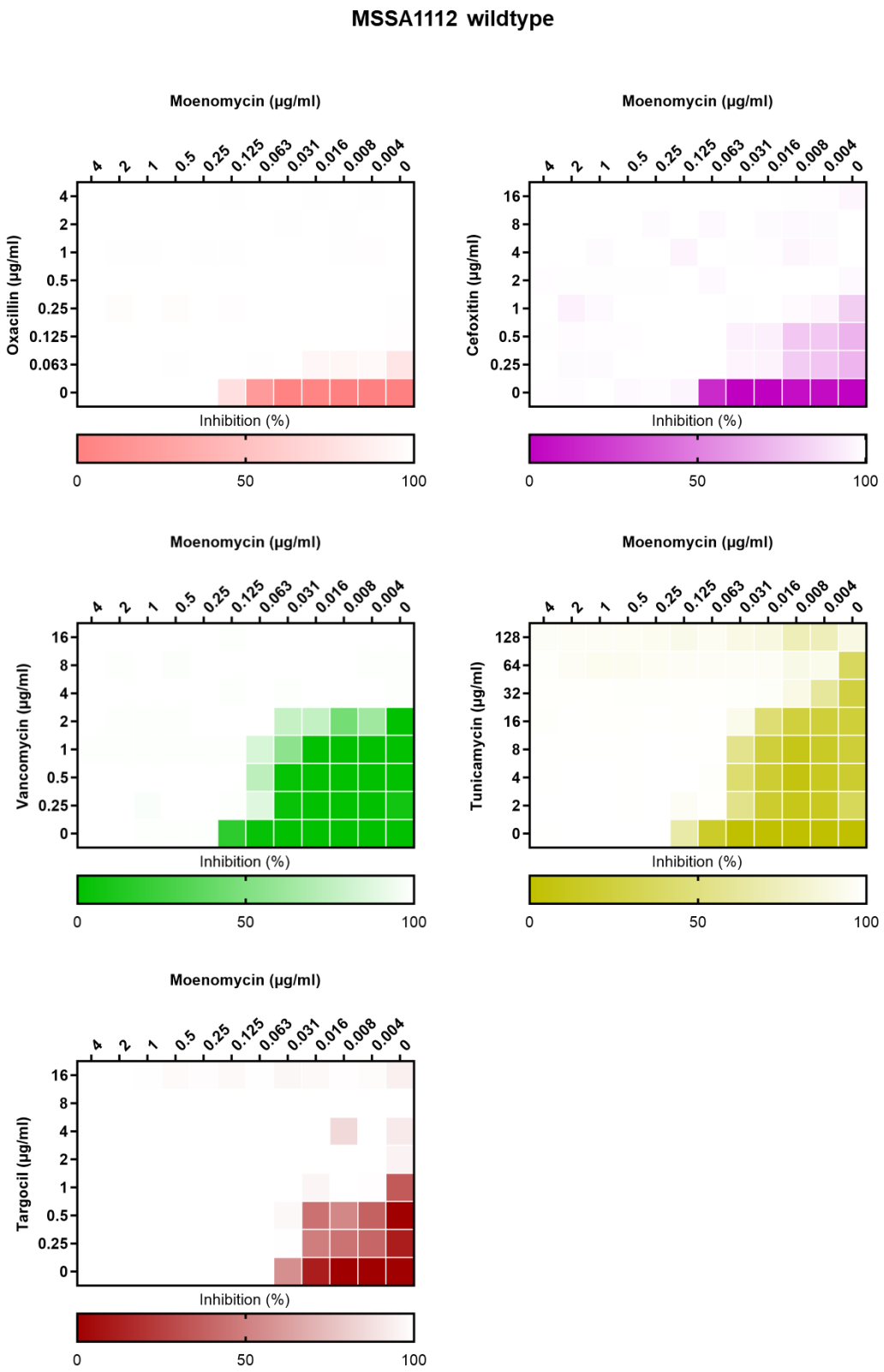

Figure 29: MSSA1112 wildtype checkerboard assay examining the antibiotic activity of moenomycin in the presence of different cell wall-active antibiotics. The combination of moenomycin with oxacillin, cefoxitin, tunicamycin, and targocil had a synergistic effect on *S. aureus* MSSA1112 wildtype, while vancomycin did not alter the MIC for the phosphoglycolipid antibiotic. Representative results of three independent experiments.

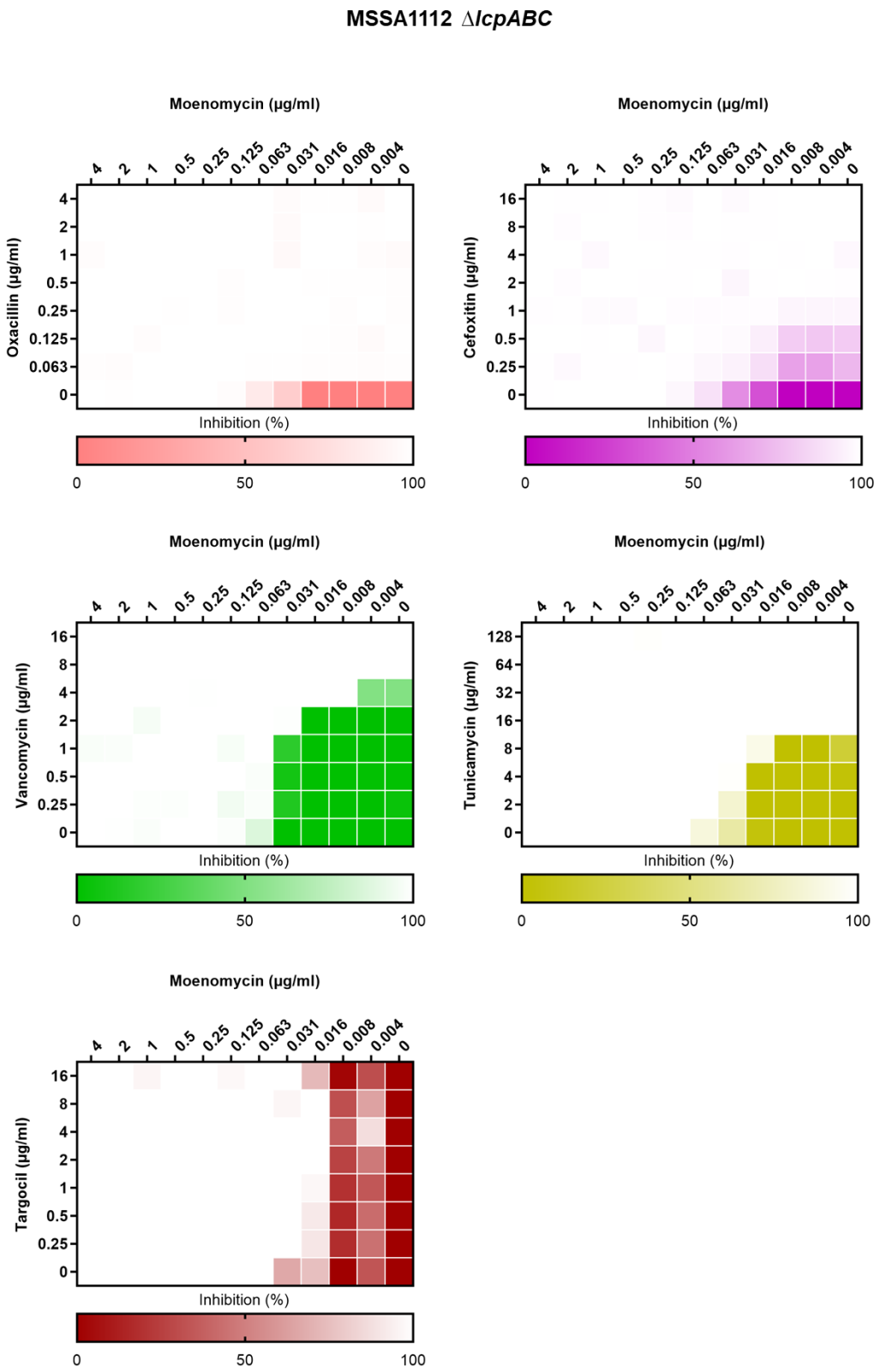

Figure 30: MSSA1112 Δ*lcpABC* checkerboard assay examining the antibiotic activity of moenomycin in the presence of different cell wall-active antibiotics. The combination of moenomycin and selected antibiotics showed no synergistic activity against *S. aureus* MSSA1112 Δ*lcpABC*. Representative results of three independent experiments.

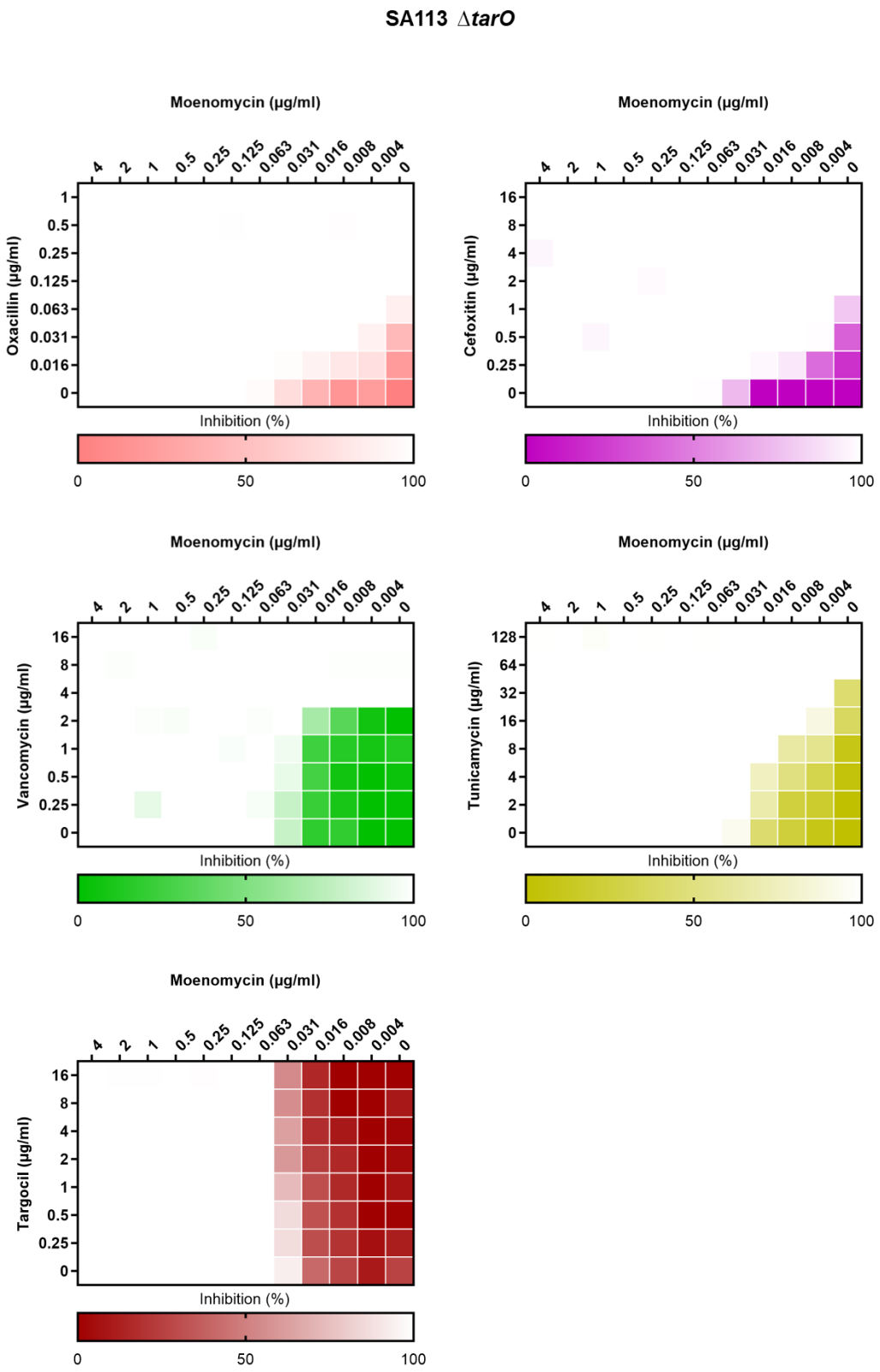

Figure 31: SA1113 Δ*tarO* checkerboard assay examining the antibiotic activity of moenomycin in the presence of different cell wall-active antibiotics. The combination of moenomycin with oxacillin and cefoxitin had a synergistic effect on *S. aureus* SA113 Δ*tarO*, while vancomycin, tunicamycin, and targocil did not alter the MIC for the phosphoglycolipid antibiotic. Representative results of three independent experiments.

3.1.6 PG cross-linking is increased in cells lacking LCP enzymes

In *S. aureus* cells lacking the initial glycosyltransferase of WTA biosynthesis, TarO, the percentage of cross-linked peptides in PG is reduced as seen for the Δ*pbpD* mutant that does not produce PBP4 (Atilano *et al*., 2010). Binding assays harnessing the fluorescent agent Bocillin FL, a penicillin derivate that was shown to covalently bind to all PBPs of *S. aureus* (Jousselin *et al*., 2016), have revealed that the Δ*tarO* strain possesses comparable amounts of PBP4. However, PBP4 loses its septal localization in the Δ*tarO* background and has been found to be dispersed within the cell membrane. Since no direct interaction between PBP4 and TarO was detected, it has been suggested that the recruitment of PBP4 to the septum is driven by the presence of immature WTAs (Atilano *et al*., 2010). To investigate if the deletion of *lcpABC* has a comparable effect on PG cross-linking, muropeptides of *S. aureus* MSSA1112 and the respective Δ*lcpABC* triple mutant were analyzed by HPLC (Figure 32A). The muropeptide profiles revealed that the percentage of cross-linked peptides in the mutant strain (58.49% of total peak area) was higher compared to the parental strain MSSA1112 (48.44%) (Figure 32B). In accordance, the Δ*lcpABC* mutant contained more detectable PBP4 than the wildtype as determined by Bocillin FL-binding (Figure 33A), indicating enhanced transpeptidation since PBP4 is responsible for the high cross-linkage in the *S. aureus* PG (Łeski & Tomasz, 2005, Memmi *et al*., 2008). By contrast, the levels of PBP1, PBP2, and PBP3 were similar in both strains (Figure 33A).

Next, the effect of moenomycin on PG cross-linkage was tested. If moenomycin inhibits LCP enzymes *in vivo*, one may also expect an effect on protein-protein interactions with other cell envelope-embedded enzymes, such as PG transpeptidases. Indeed, when *S. aureus* Newman wildtype cells were exposed to the 5x MIC of moenomycin, the percentage of peptides in cross-links was higher (59.52% of total peak area) than in the DMSO-treated control (53.59%) (Figure 34). The Bocillin FL-binding was enhanced for all PBPs in the moenomycin-treated sample (Figure 33). Notably, when comparing the entirety of membrane proteins produced by the Δ*lcpABC* triple mutant and the wildtype strain exposed to moenomycin, a similar protein of about 40 kDa seemed to be overproduced in both samples (Figure 33B).

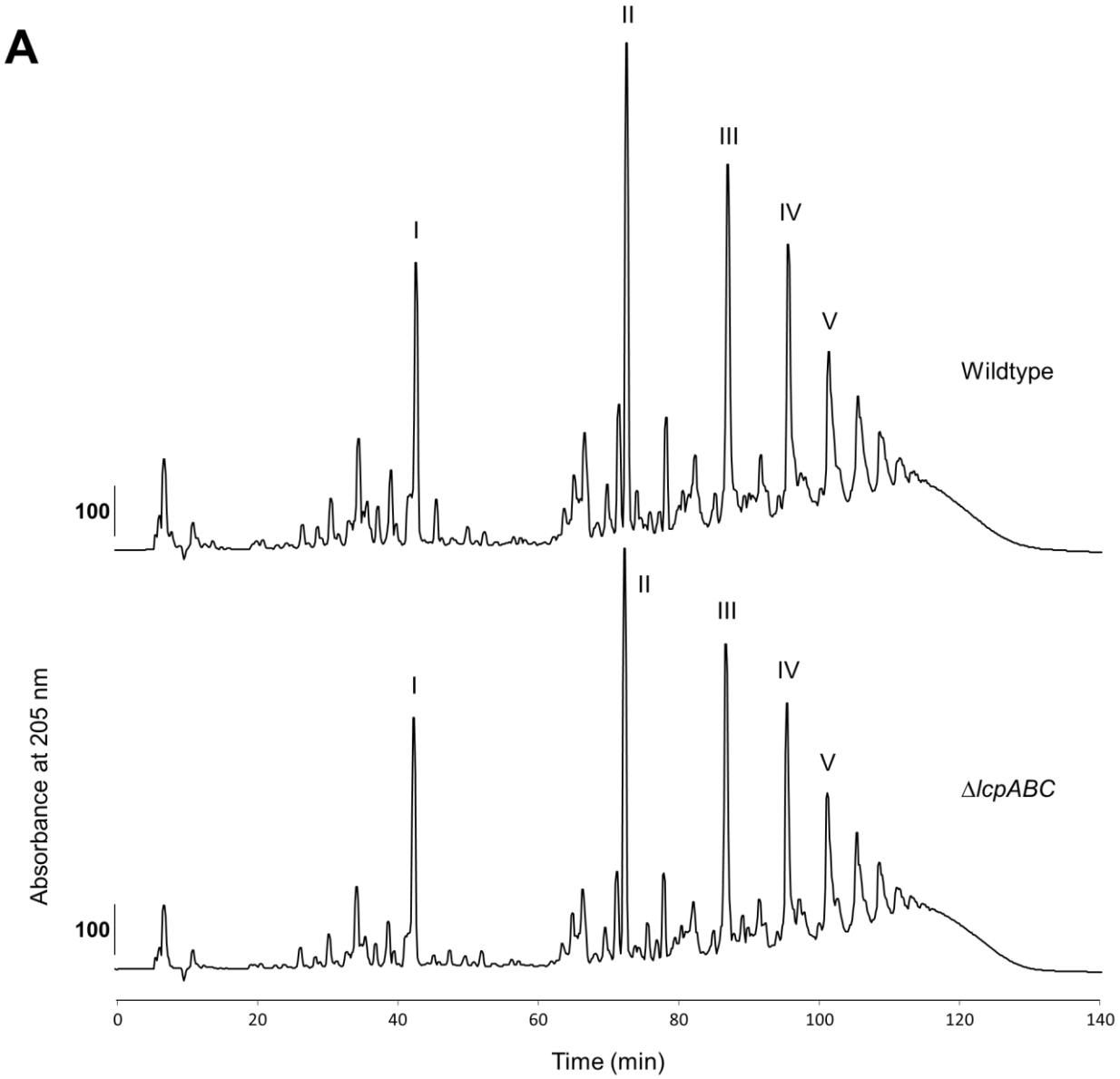

B

Muropeptides/ Property	% total peak area	
	Wildtype	Δ*lcpABC*
Monomers	15.84 ± 0.02	10.85 ± 0.41
Dimers	17.37 ± 1.00	15.45 ± 0.54
Trimers	18.36 ± 0.93	15.22 ± 0.64
> Trimers	48.44 ± 0.05	58.49 ± 1.59
Total	100.0	100.0

Figure 32: RP-HPLC profiles of mutanolysin-digested peptidoglycan of *S. aureus* MSSA1112 and the respective Δ*lcpABC* triple mutant. (A) Muropeptides were reduced and separated on a Prontosil column (de Jonge *et al.*, 1992). (I–V) Muropeptides from monomers to pentamers. (B) Table summarizes the types of muropeptides as calculated from the total peak area in the respective chromatogram. Values are presented as the mean ± SD of two independent experiments. The Δ*lcpABC* triple mutant possessed more highly cross-linked muropeptides than the parental strain MSSA1112.

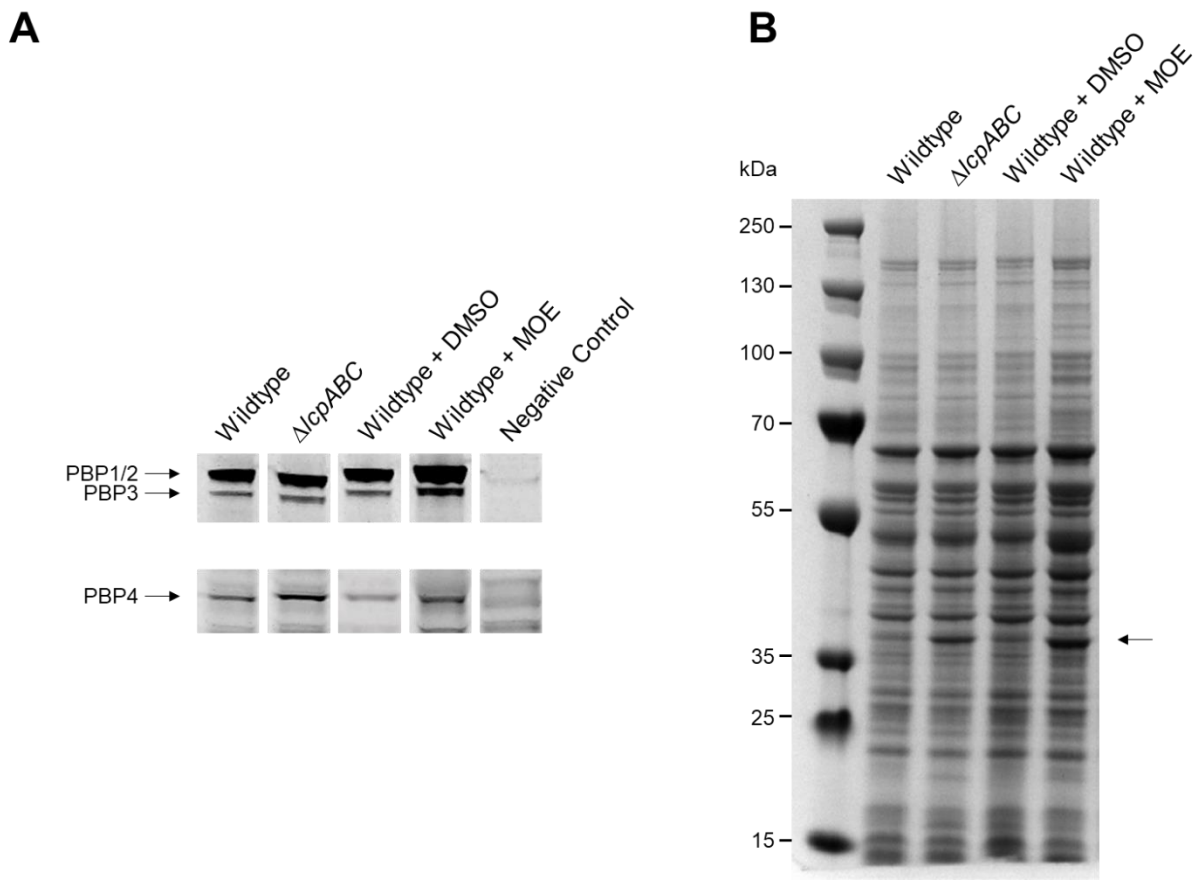

Figure 33: Bocillin FL-labeled PBPs of *S. aureus* MSSA1112 wildtype and the Δ*lcpABC* triple mutant separated by SDS-PAGE. (A) Scan of the acrylamide gel with a Cy2 525BP20 filter. The mutant produced more PBP4 than the wildtype. The same effect was observed after moenomycin (MOE) treatment of the wildtype, that also resulted in a higher production of PBP1-3. The negative control was wildtype membranes blocked by preincubation with ampicillin. (B) Coomassie-stained gel of the membrane preparations. The production of similar length proteins at approximately 40 kDa (indicated by arrow) appeared to be stimulated by both the deletion of *lcpABC* and the treatment with moenomycin. Representative results of three independent experiments.

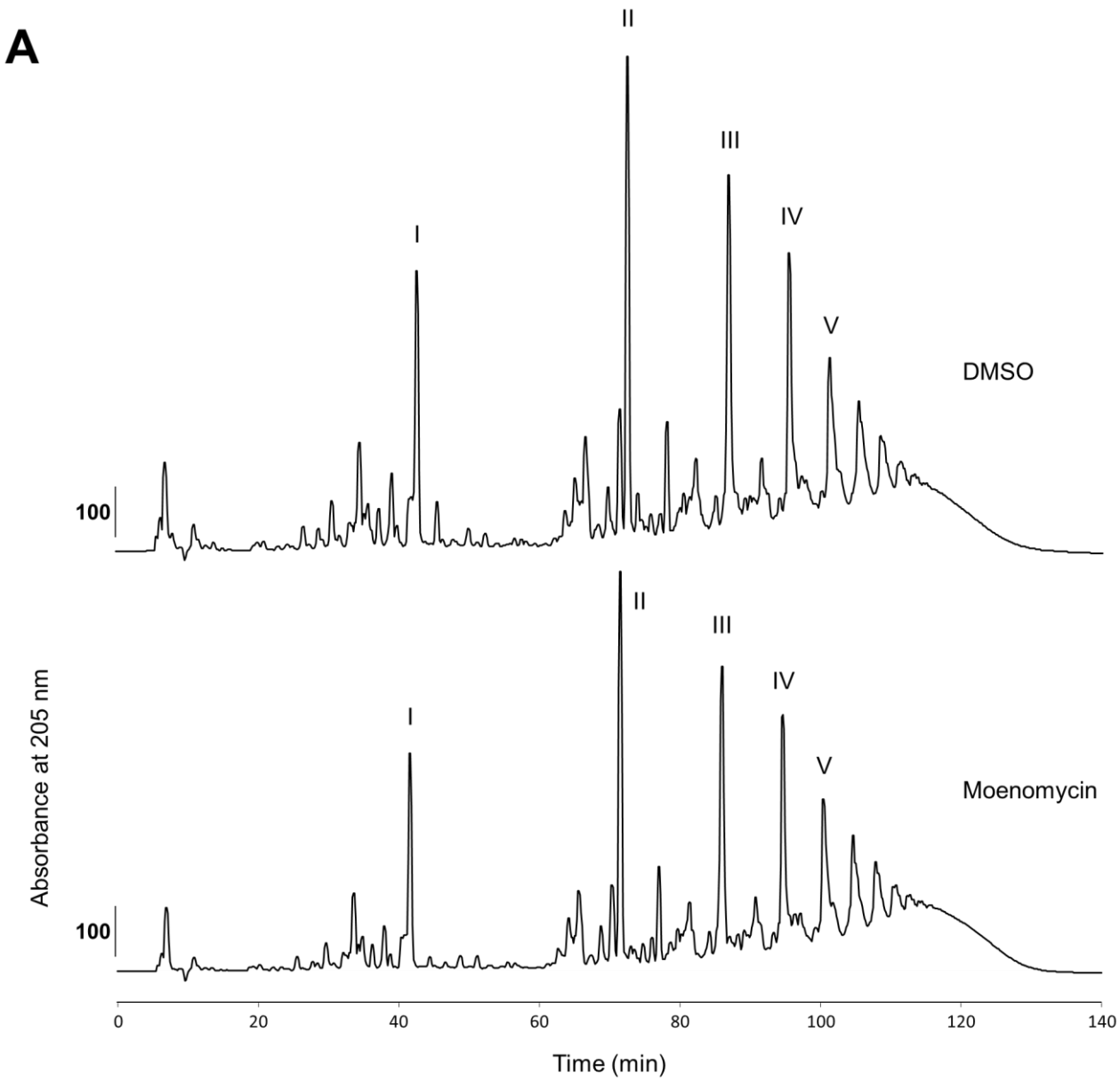

B

Muropeptides/ Property	% total peak area	
	DMSO	Moenomycin
Monomers	12.57 ± 0.30	10.30 ± 0.74
Dimers	16.21 ± 0.41	14.12 ± 0.14
Trimers	17.64 ± 0.88	16.06 ± 0.14
> Trimers	53.59 ± 1.60	59.52 ± 0.74
Total	100.0	100.0

Figure 34: RP-HPLC profiles of mutanolysin-digested peptidoglycan of *S. aureus* Newman pretreated with DMSO or moenomycin. (A) Muropeptides were reduced and separated on a Prontosil column (de Jonge *et al.*, 1992). (I–V) Muropeptides from monomers to pentamers. (B) Table summarizes the types of muropeptides as calculated from the total peak area in the respective chromatogram. Values are presented as the mean ± SD of two independent experiments. Peptidoglycan cross-linkage was enhanced in moenomycin-treated cells compared to the DMSO control.

Localization studies on plasmid-encoded YFP-labeled PBP4 revealed the predominant recruitment of the protein to the division site in the presence of moenomycin (Figure 35). To quantify the dispersion of the fluorophore-attached protein at the septum, the septal versus lateral membrane fluorescence was determined. A ratio exceeding the value 2 implied the concentration of the protein at the division site rather than the dispersion throughout the cell envelope (Atilano *et al.*, 2010). After the exposure to moenomycin, the FR value of 2.08 ± 0.04 was significantly enhanced compared to the non-treated control (1.77 ± 0.04). This further supports the hypothesis that the inhibition of LCPs by moenomycin triggers the accumulation of WTA precursors at the septum, which in turn attracts more PBP4 to the division site.

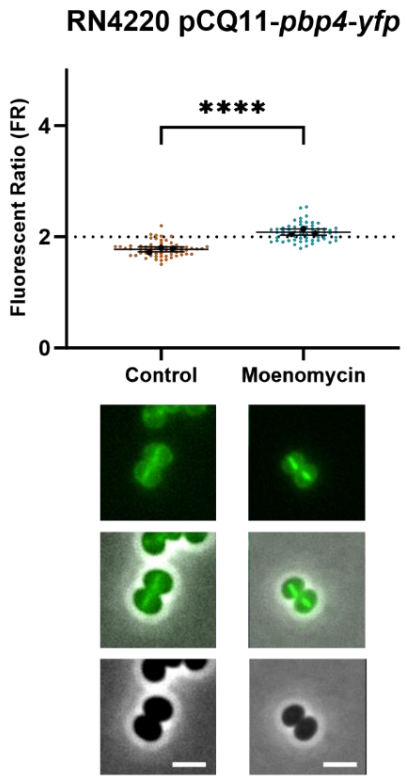

Figure 35: PBP4 is recruited to the division septum in the presence of moenomycin. Cells were grown in TSB medium supplemented with 100 µM IPTG and 50 µg/ml erythromycin until the late exponential phase and then exposed to the 10x MIC of moenomycin for 10 min at 37 °C. 50 cells of three independent experiments were quantified. An FR greater than 2 shows the preferred binding of the fluorescent conjugate to the cell septum while values equal or less than 2 indicate the dissemination throughout the cell surface. Points represent the mean of each individual experiment. The line shows the combined mean of three independent experiments ± SD. ****P ≤ 0.0001 (unpaired t-test, GraphPad Prism V9.5.1.733). In the non-treated control, PBP4-YFP is dispersed throughout the cell membrane. After antibiotic treatment, the fluorescently labeled PBP localized preferentially to the division septum.

3.1.7 Moenomycin treatment reduces the PG and WTA content

To investigate the effect of moenomycin on WTA ligation *in vivo*, the cell walls of antibiotic-treated and untreated *S. aureus* Newman cells were purified and the weight was determined. Covalently coupled anionic glycopolymers were removed by exposure to hydrofluoric acid and the purified PG was quantified by weight measurement and, in addition, by the abundance of the sugar component Glc*N*Ac (Figure 36A).

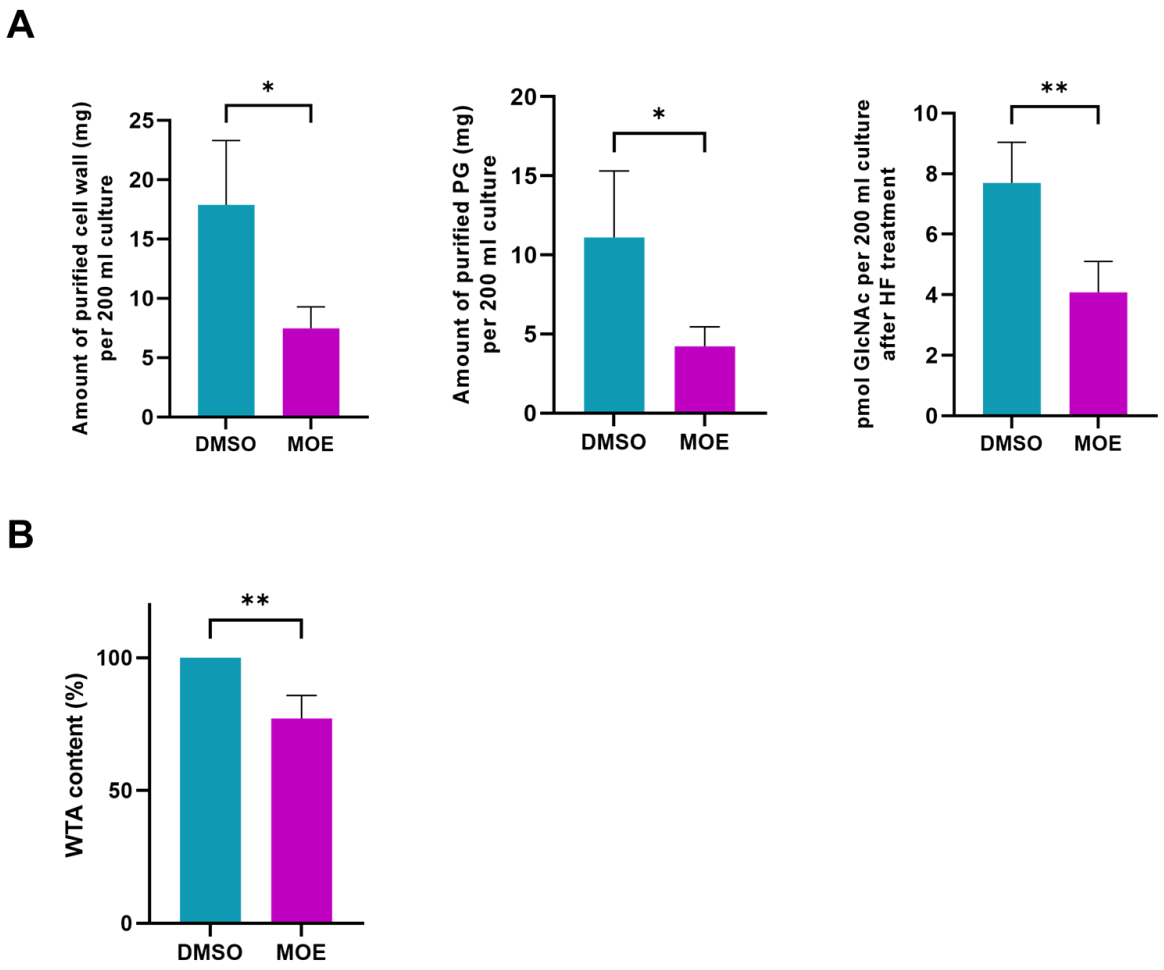

Figure 36: Quantification of cell envelope components of DMSO- and moenomycin-treated *S. aureus* Newman cells. (A) Cells were grown until an OD_{600} of 1.2 and, if stated, exposed to the 5x MIC for moenomycin (MOE) for 30 min. Following purification, the weight of isolated cell wall was determined before and after HF treatment to remove anionic glycopolymers. Aliquots from the same samples were used to quantify the amount of PG by measuring the Glc*N*Ac content. Cells treated with moenomycin showed a reduced amount of PG. (B) The WTA content was determined via phosphate determination. Moenomycin-treated cells possessed less WTAs compared to the control cells, which were exposed to DMSO. Values are presented as the mean ± SD (error bars) of two independent experiments. *P ≤ 0.05, **P ≤ 0.01 (unpaired t-test, GraphPad Prism V9.5.1.733).

Next, the WTAs of antibiotic-treated and untreated cells were purified and quantified by phosphate determination (Figure 36B). When moenomycin was added, the cells produced 22.83 ± 4.34% less WTAs compared to the control. Besides the proposed inhibition of LCP proteins by moenomycin, the phosphoglycolipid is known to inhibit the PG glycosyltransferase PBP2 (Lovering *et al*., 2007). Consistent with this inhibition, the total amount of synthesized PG in antibiotic-treated cells was diminished by 61.94 ± 19.74%. Therefore, the reduction of the WTA content could be an indirect consequence of PG biosynthesis inhibition, as a lower PG amount offers less attachment sites for WTAs. Remarkably, the pellet of *S*. *aureus* cells which were priorly exposed to moenomycin exhibited a reduced cohesiveness that was also observed for WTA-deprived Δ*lcpABC* and Δ*tarO* mutants (data not shown).

3.1.8 LcpA-deprived mutants bind significantly less MOE-BDP *in vitro*

To verify LCPs as a target structure for moenomycin *in vivo*, *S*. *aureus* Newman and the respective *lcp* deletion strains were grown in TSB medium until the late exponential phase prior to the addition of 4.93 µM MOE-BDP for 10 min. This concentration was below the MIC value for the fluorescent agent (supplementary Table 7) to avoid major cellular changes in response to the antibiotic. In all strains tested, except for the Δ*lcpA* single mutant, the FR was distinctly less than the threshold, indicating that MOE-BDP binds to cellular targets that are distributed all over the cell surface (Figure 37A). For the SA113 Δ*tarO* strain, the FR was significantly lower than determined for the parental strain, referring to an accumulation of the probe apart from the division site. The FR could not be calculated for the Δ*lcpA* single mutant due to poor binding of the fluorescently labeled moenomycin, which could not be improved by increasing the MOE-BDP concentration (data not shown). In the complemented strain, *S*. *aureus* Newman Δ*lcpA* harboring the IPTG-inducible plasmid pCQ11-*ery*-*lcpA*, a fluorescence signal in the cell envelope became detectable pointing towards LcpA as a target structure for the fluorescent probe (Figure 37B).

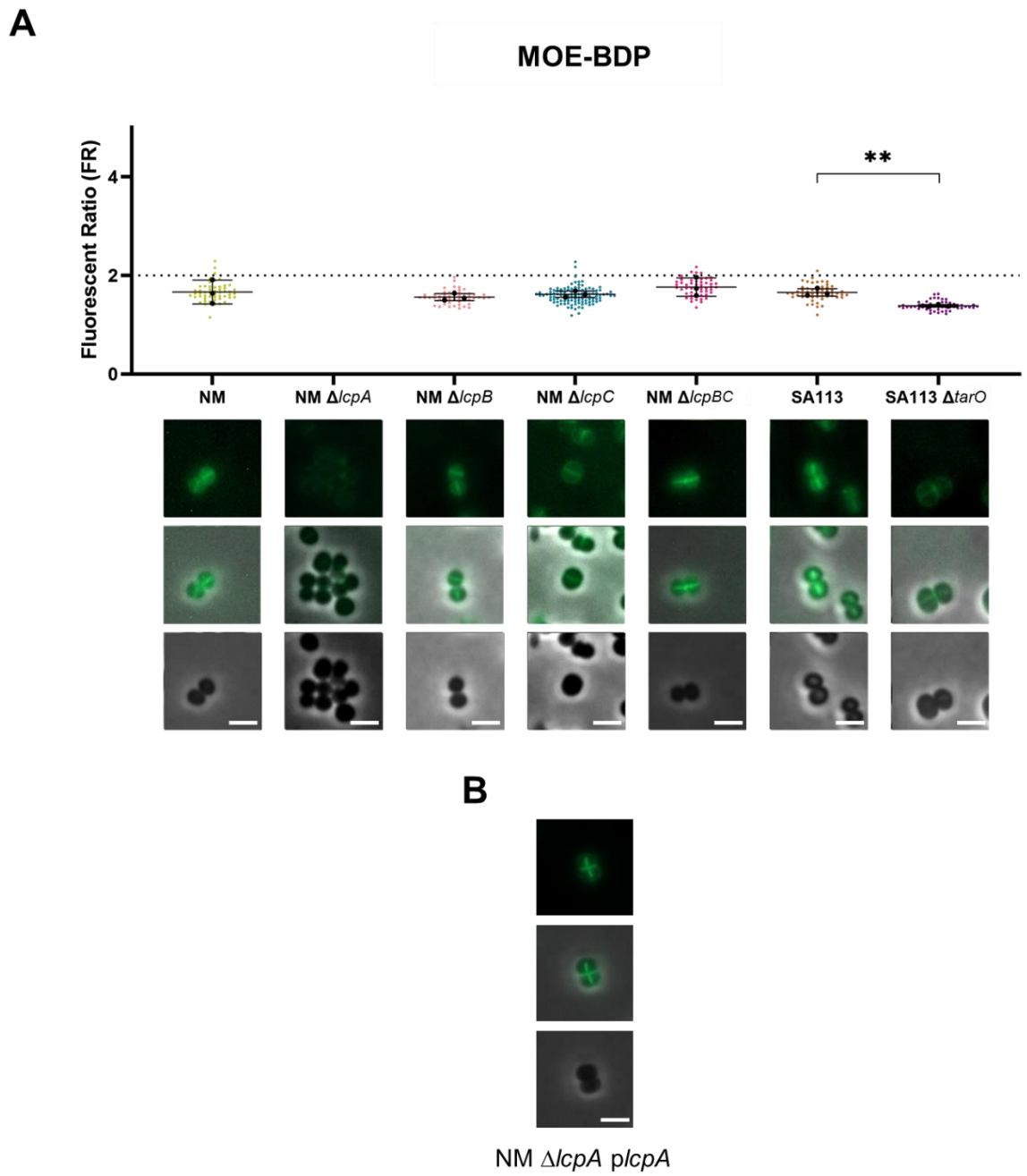

Figure 37: Localization of MOE-BDP in LCP-deprived *S. aureus* Newman and control strains. (A) Cells were grown in TSB medium until the late exponential phase and exposed to 4.93 µM MOE-BDP for 10 min at 37 °C. Per strain, each 50 cells of three independent experiments were examined. An FR greater than 2 shows the preferred binding of the fluorescent conjugate to the cell septum while values equal or less than 2 indicate the dissemination throughout the cell surface. Points represent the mean of each individual experiment. The line shows the combined mean of three independent experiments ± SD. **P ≤ 0.01 (unpaired t-test, GraphPad Prism V9.5.1.733). In the strains tested, MOE-BDP did not accumulate at the septum and was equally dispersed over the cell surface with exception of *S. aureus* Newman (NM) Δ*lcpA*. For this strain, binding was reduced to the point that the FR could not be visually determined. The FR of the Δ*tarO* null mutant was significantly decreased with regard to the control strain SA113, indicating that MOE-BDP binds preferentially to the lateral cell wall than the septal site. (B) When complemented with plasmid-encoded *lcpA*, MOE-BDP bound perceptibly to the septum and cell surface. For these experiments, cells were grown in TSB medium supplemented with 100 µM IPTG and 50 µg/ml erythromycin. Scale bar: 2 µm.

To further investigate the binding of MOE-BDP to *lcpA*-depleted cells, the fluorescence intensities of MOE-BDP-treated *S. aureus* MSSA1112 wildtype and the Δ*lcpA* single mutant were determined (Figure 38, data analysis was performed by Jan-Samuel Puls, Pharmaceutical Microbiology, University of Bonn). For MSSA1112 Δ*lcpA*, binding of MOE-BDP was detectable, but the fluorescence intensity was significantly reduced by 17% compared to the parental strain. This result highlights LcpA as a potential off-target protein for MOE-BDP. Currently ongoing research addresses the question if the complementation of the mutant can reverse this effect and if the occurrence of this effect in the MSSA1112 background is limited to the Δ*lcpA* mutant. Notably, the literature offers no information about the gene expression levels of PG glycosyltransferases and LCP proteins in *S. aureus* that would allow to assess the relation between the fluorescent probe binding and the amount of produced protein. Due to the severe morphological defects, it was not possible to calculate the fluorescence intensity for bound MOE-BDP in the Δ*lcpABC* triple mutant (data not shown).

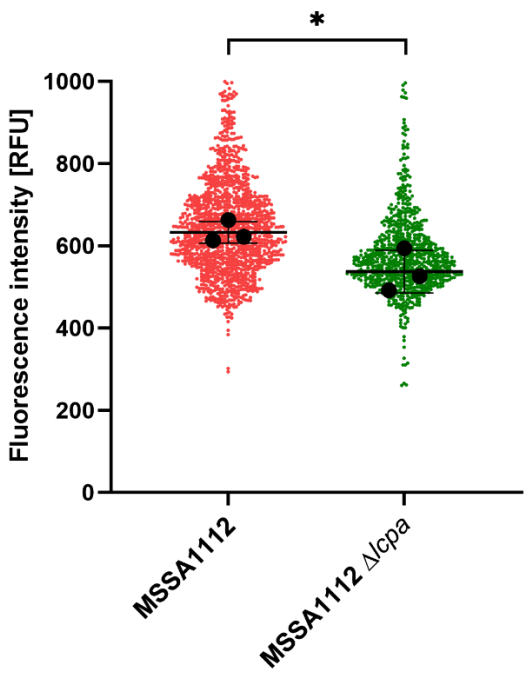

Figure 38: The MSSA1112 Δ*lcpA* single mutant shows decreased binding of MOE-BDP. Quantification of MOE-BDP fluorescence intensities of individual cells in RFU (relative fluorescent units). Per strain, each 300 cells of three independent experiments were examined. Points represent the mean of each individual experiment, the line shows the combined mean of three independent experiments ± SD. *P ≤ 0.05 (unpaired t-test, GraphPad Prism V9.5.1.733). Data analysis was performed by Jan-Samuel Puls (Pharmaceutical Microbiology, University of Bonn). LcpA-depleted *S. aureus* MSSA1112 bound significantly less of the fluorescent moenomycin conjugate with respect to the wildtype strain.

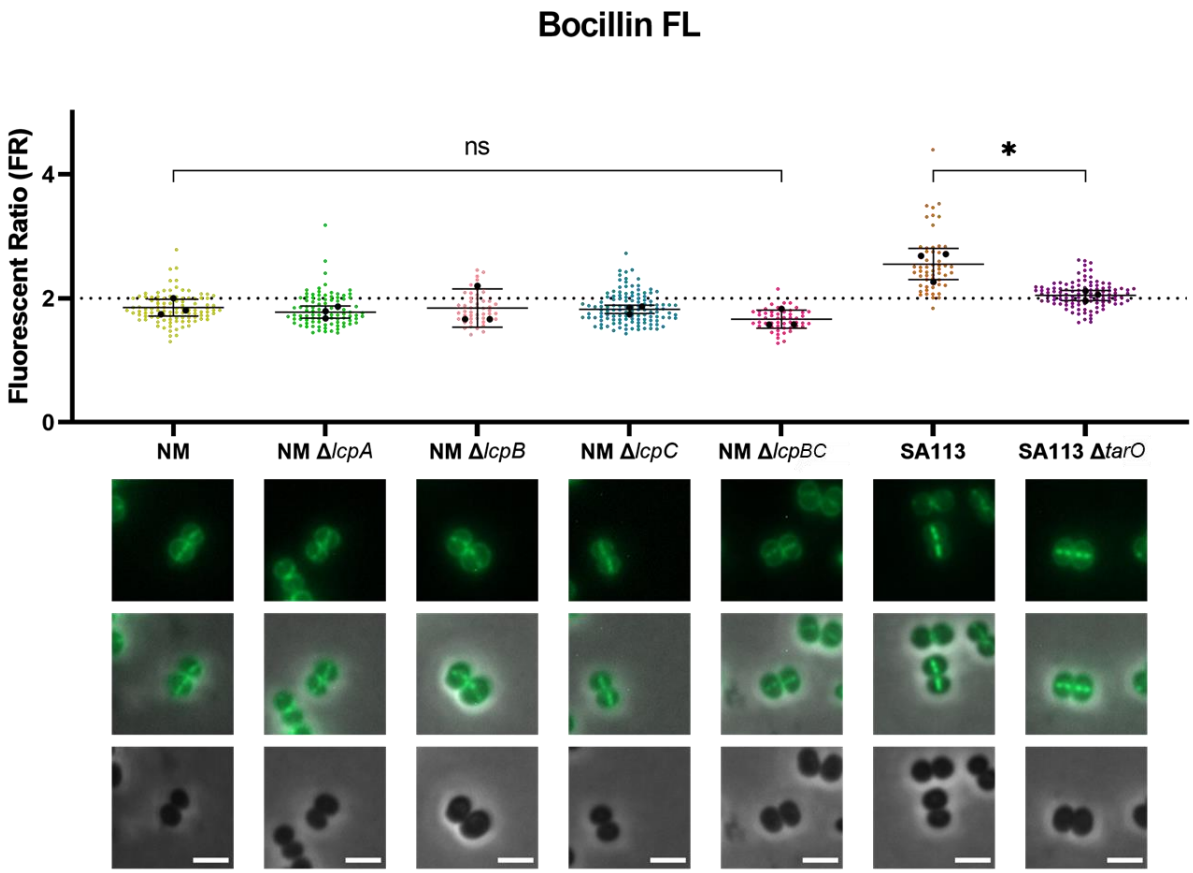

Figure 39: Localization of PBPs in LCP-deprived *S. aureus* Newman and control strains. Cells were labeled with the fluorescent penicillin derivate Bocillin FL which is supposed to bind to the transpeptidase domain of PBPs. Cells were grown in TSB medium until the late exponential phase and exposed to 7.5 µM of the agent for 10 min at 37 °C. Per strain, each 50 cells of three independent experiments were quantified. An FR greater than 2 shows the preferred binding of the fluorescent conjugate to the cell septum while values equal or less than 2 indicate the dissemination throughout the cell surface. Points represent the mean of each individual experiment. The line shows the combined mean of three independent experiments ± SD. ns $P > 0.05$, *$P \leq 0.05$ (unpaired t-test, GraphPad Prism V9.5.1.733). *S. aureus* SA113 exhibited an increased binding to the septum versus cell wall, whereas the fluorescent reagent was significantly more dispersed over the cell envelope in the WTA-deficient strain SA113 Δ*tarO*. Bocillin FL was distributed over the cell membrane in *S. aureus* Newman (NM) and the respective *lcp*-deleted strains. Scale bar: 2 µm.

To further study the interplay between LCP enzymes and PBPs *in vivo*, the LCP-depleted *S. aureus* Newman and control strains were grown until the late exponential phase in TSB medium and exposed to 7.5 µM Bocillin FL for 10 min. The FR ratios in *S. aureus* Newman strains were less than the threshold of 2, indicating that there was no accumulation of PBPs at the division septum (Figure 39). Moreover, the average value for the SA113 wildtype strain was 2.55 ± 0.25, whereas a value of 2.075 ± 0.08 was obtained for the Δ*tarO* mutant, showing that the PBPs were evenly distributed over the cell membrane when WTAs were absent.

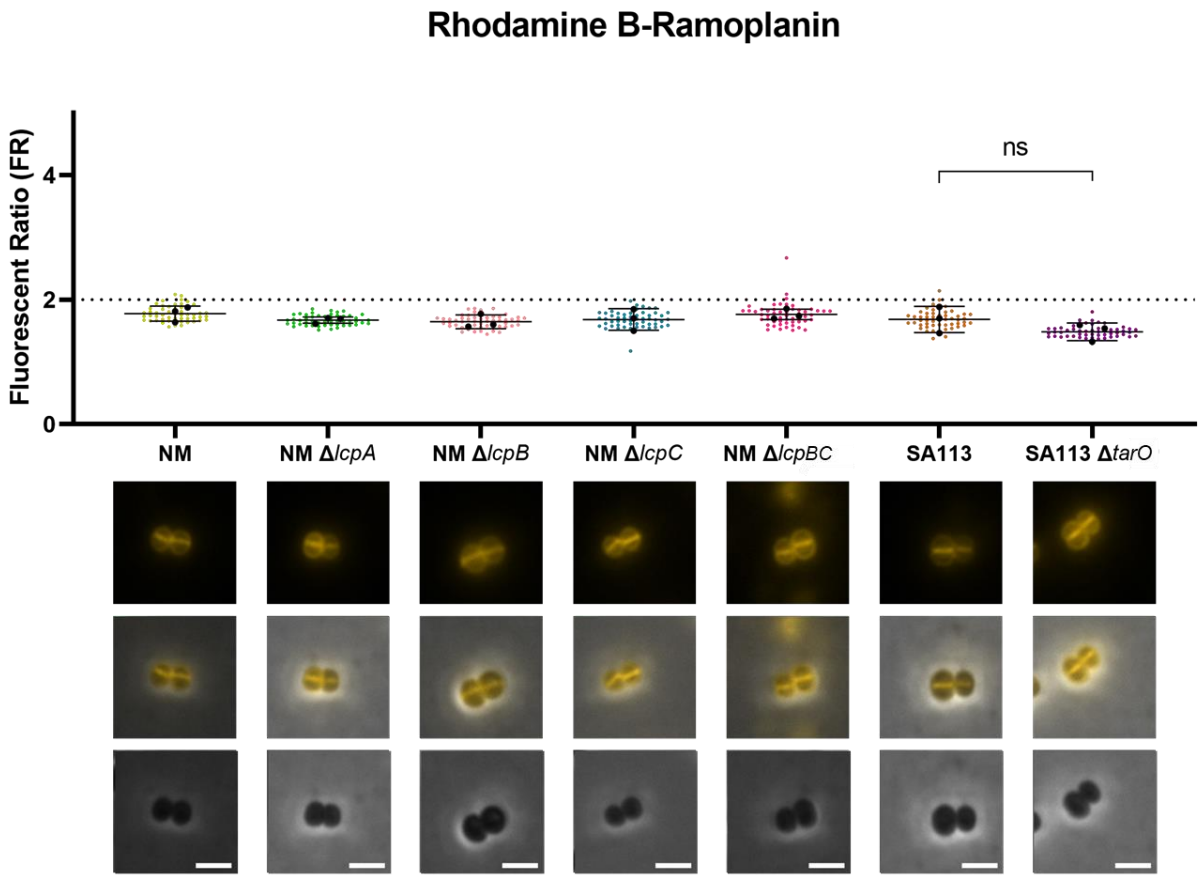

Figure 40: Localization of rhodamine B-labeled ramoplanin in LCP-deprived *S. aureus* Newman and control strains. Ramoplanin is supposed to sequester the pyrophosphate residue of lipid-linked PG, WTA, and capsule precursors. Cells were grown in TSB medium until the late exponential phase and exposed to 0.32 µM fluorescently labeled ramoplanin for 10 min at 37 °C. Per strain, each 50 cells of three independent experiments were quantified. An FR greater than 2 shows the preferred binding of the fluorescent conjugate to the cell septum while values equal or less than 2 indicate the dissemination throughout the cell surface. Points represent the mean of each individual experiment. The line shows the combined mean of three independent experiments ± SD. ns $P > 0.05$ (unpaired t-test, GraphPad Prism V9.5.1.733). Rhodamine B-labeled ramoplanin was equally distributed over the cell surface and the septum in all strains tested. NM: *S. aureus* Newman. Scale bar: 2 µm.

To visualize the location of the PG biosynthesis intermediate lipid II and the carrier lipid C_{55}-PP, the wildtype and *lcp* mutants were treated with 0.32 µM rhodamine B-coupled ramoplanin. Ramoplanin interacts with the pyrophosphate residue of lipid II and C_{55}-PP inhibiting PG transglycosylation and possibly C_{55}-PP dephosphorylation (Fang *et al*., 2006, unpublished results). The average FR for all strains tested did not exceed the threshold, indicating that lipid II did not accumulate at the division site in these strains (Figure 40), although an intensified PG biosynthesis is expected at the cell septum (Pinho *et al*., 2013).

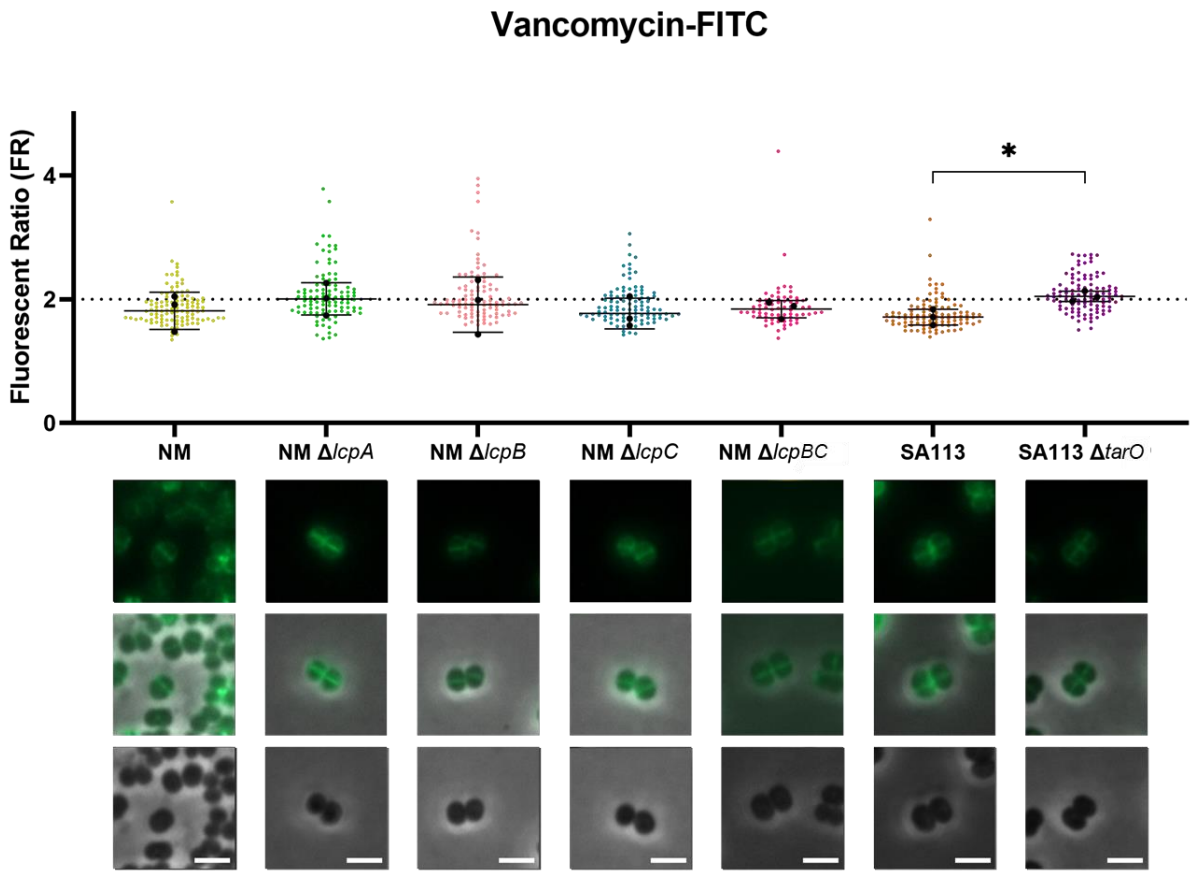

Figure 41: Localization of FITC-labeled vancomycin in LCP-deprived *S. aureus* Newman and control strains. Vancomycin-FITC is supposed to bind to the D-Ala-D-Ala residues of PG and its lipid-linked precursors. Cells were grown in TSB medium until the late exponential phase and treated with a 1:1 (w/w) mixture of vancomycin and fluorescein-labeled vancomycin at a final concentration of 1 µg/ml for 10 min at 37 °C. Per strain, each 50 cells of three independent experiments were quantified. An FR greater than 2 shows the preferred binding of the fluorescent conjugate to the cell septum while values equal or less than 2 indicate the dissemination throughout the cell surface. Points represent the mean of each individual experiment. The line shows the combined mean of three independent experiments ± SD. *P ≤ 0.05 (unpaired t-test, GraphPad Prism V9.5.1.733). In *S. aureus* Newman (NM) and the respective *lcp* deletion mutants, vancomycin-FITC was dispersed throughout the cell wall. In contrast to the Δ*tarO* mutant, the fluorescent conjugate seemed to be recruited away from the division septum in the control strain SA113 according to the significantly decreased FR value. Scale bar: 2 µm.

For tracking PG and its precursor lipid II, the cells were exposed to a 1:1 (w/w) mixture of vancomycin and fluorescein-labeled vancomycin at a final concentration of 1 µg/ml for 10 min. Vancomycin binds to D-Ala-D-Ala residues (Barna & Williams, 1984) and was evenly distributed across the cell surface in the tested strains with an average FR less than or equal to 2, whereby the fluorescent probe rather located to the lateral cell wall in the parental strain SA113 compared to the Δ*tarO* mutant (Figure 41).

3.1.9 Moenomycin stimulates the recruitment of LcpA to the cell division site

The localization of LCP proteins and the bifunctional PBP2 in the presence of different cell wall-targeting antibiotics was visualized by N-terminal GFP-tagging. In the *S. aureus* RN4220 parental background, the plasmid-encoded *gfp*-gene fusions were expressed under the control of an IPTG-inducible promoter. The cells were grown in TSB medium containing 100 µM IPTG until an OD_{600} of 1.2 prior to the addition of 5x the MIC of the respective antibiotic for 10 min (supplementary Table 8). The peptide antibiotic teixobactin was used in addition to the antimicrobials that were already applied as fluorescently labeled agents in the preceded section. Teixobactin targets the pyrophosphate residue in the glycosyltransferase product C_{55}-PP, the PG intermediates lipid I and lipid II, and the WTA precursor lipid III_{WTA} (Ling *et al.*, 2015).

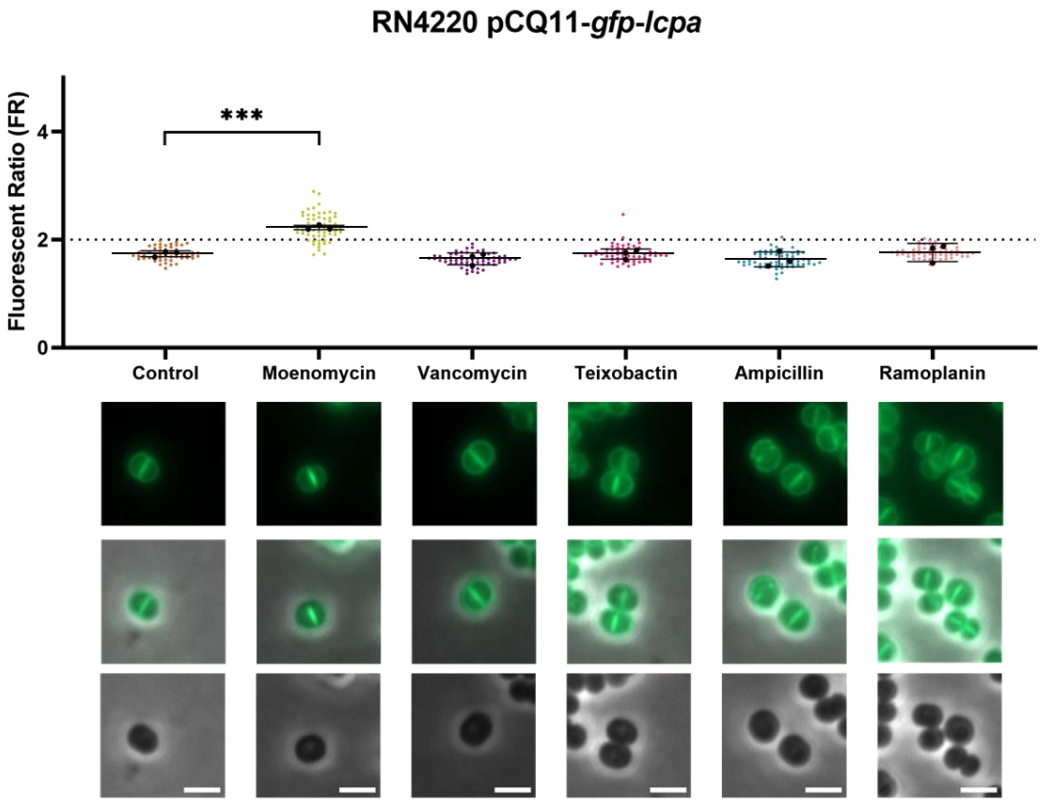

Figure 42: Localization of GFP-labeled LcpA in *S. aureus* RN4220 depending on the exposition to different cell wall-active antibiotics. Cells were grown in TSB medium supplemented with 100 µM IPTG and 50 µg/ml erythromycin until the late exponential phase and then exposed to the 10x MIC of the respective antibiotic for 10 min at 37 °C. Per antibiotic, each 50 cells of three independent experiments were quantified. An FR greater than 2 shows the preferred binding of the fluorescent conjugate to the cell septum while values equal or less than 2 indicate the dissemination throughout the cell surface. Points represent the mean of each individual experiment. The line shows the combined mean of three independent experiments ± SD. ***P ≤ 0.001 (unpaired t-test, GraphPad Prism V9.5.1.733). GFP-LcpA was widely dispersed in the cell wall of the control strain as with vancomycin, teixobactin, ampicillin, and ramoplanin. When treated with moenomycin, GFP-LcpA localized predominantly to the division septum. Scale bar: 2 µm.

The GFP-LcpA fusion protein was recruited to the division site with moenomycin and neither in the control nor with any other tested antibiotic a similar effect was observed (Figure 42). The FR value with moenomycin (2.265 ± 0.06) was significantly enhanced compared to the non-treated control (1.84 ± 0.06).

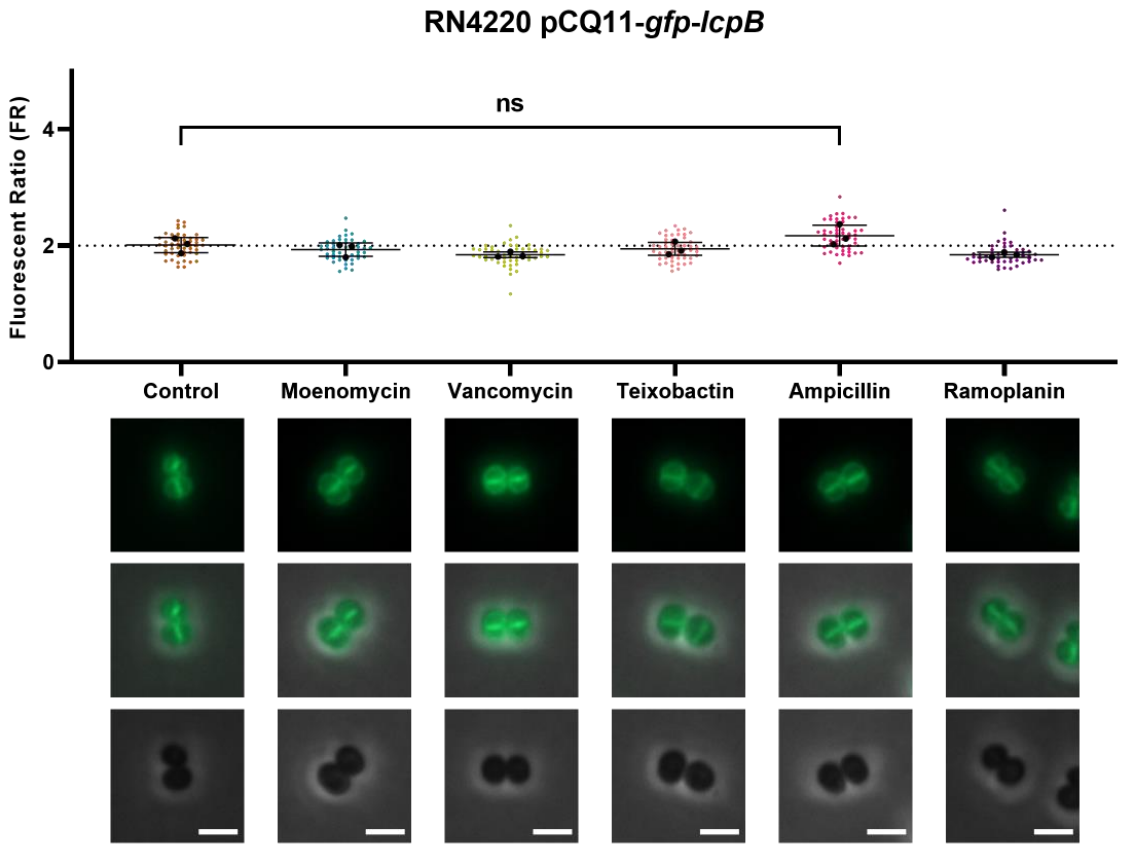

Figure 43: Localization of GFP-labeled LcpB in *S. aureus* RN4220 depending on the exposition to different cell wall-active antibiotics. Cells were grown in TSB medium supplemented with 100 µM IPTG and 50 µg/ml erythromycin until the late exponential phase and then exposed to the 10x MIC of the respective antibiotic for 10 min at 37 °C. Per antibiotic, each 50 cells of three independent experiments were quantified. An FR greater than 2 shows the preferred binding of the fluorescent conjugate to the cell septum while values equal or less than 2 indicate the dissemination throughout the cell surface. Points represent the mean of each individual experiment. The line shows the combined mean of three independent experiments ± SD. ns P > 0.05 (unpaired t-test, GraphPad Prism V9.5.1.733). GFP-LcpB was distributed over the cell surface of the untreated control as with moenomycin, vancomycin, teixobactin, and ramoplanin. When exposed to the β-lactam ampicillin, GFP-LcpB apparently localized to the division septum. However, the FR was not significantly increased with regard to the control sample. Scale bar: 2 µm.

For GFP-LcpB, the average FR value after the exposure to ampicillin was above the threshold (2.18 ± 0.18), but the t-test result showed no significant difference to the FR index of the control (2.02 ± 0.13) (Figure 43). In the presence of the other cell wall-targeting antibiotics used, the GFP fusion protein did not localize to the division septum.

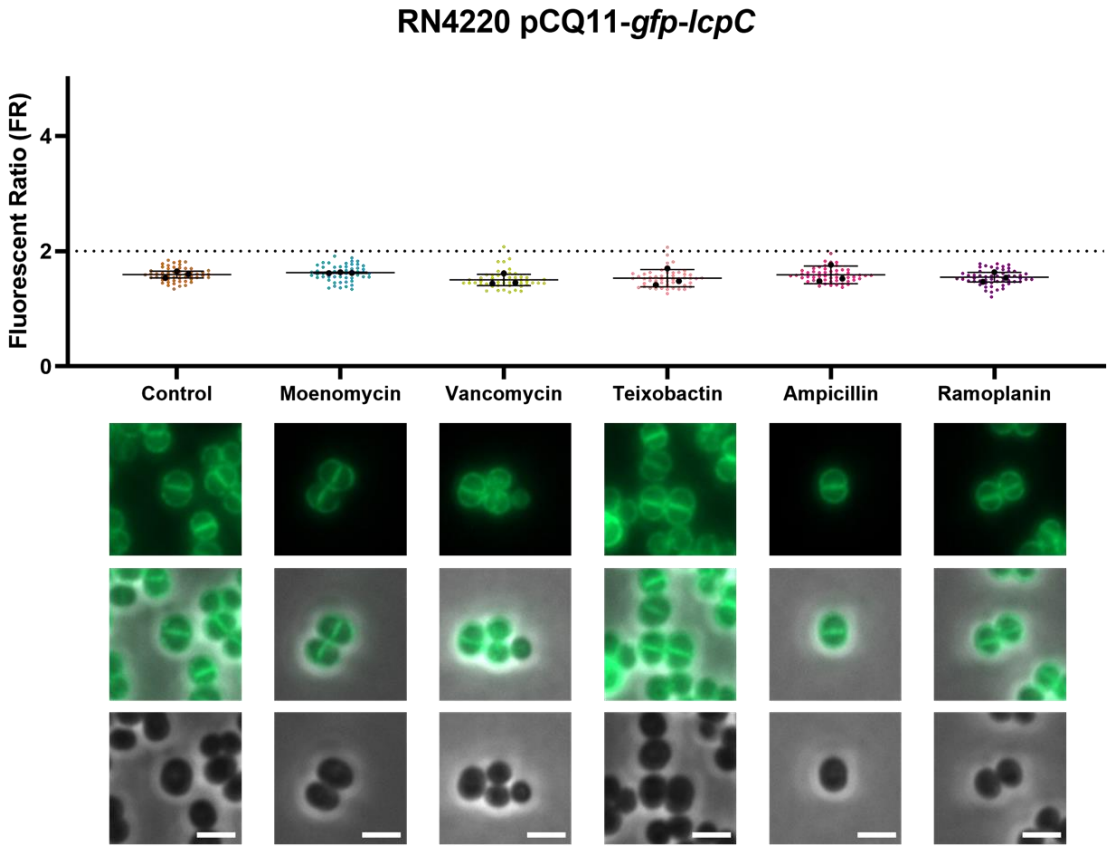

Figure 44: Localization of GFP-labeled LcpC in *S. aureus* RN4220 depending on the exposition to different cell wall-active antibiotics. Cells were grown in TSB medium supplemented with 100 µM IPTG and 50 µg/ml erythromycin until the late exponential phase and then exposed to the 10x MIC of the respective antibiotic for 10 min at 37 °C. Per antibiotic, each 50 cells of three independent experiments were quantified. An FR greater than 2 shows the preferred binding of the fluorescent conjugate to the cell septum while values equal or less than 2 indicate the dissemination throughout the cell surface. Points represent the mean of each individual experiment. The line shows the combined mean of three independent experiments ± SD. GFP-LcpC was equally dispersed on the cell surface regardless of the added antibiotic. The FR was considerably lower than 2 in every approach indicating that GFP-LcpC preferentially localized to the lateral cell wall and not the division site. Scale bar: 2 µm.

GFP-LcpC was also dispersed throughout the cell membrane regardless of the antibiotic used (Figure 44). The average FR values were distinctly lower than the threshold. For the untreated control, an FR of 1.59 ± 0.08 was determined.

To visualize the localization of *S. aureus* PBP2 *in vivo*, Pinho & Errington (2004) inserted the *gfp* gene upstream of the chromosomal *pbp2* locus in *S. aureus* RN4220 under the control of the P_{xyl} promoter. They observed the recruitment of GFP-PBP2 to the division septum which was triggered by the accessibility to its substrate, lipid II. In this thesis, *gfp-pbp2* was encoded on a plasmid under the control of an IPTG-inducible promoter. The FR value of the untreated control strain was 1.94 ± 0.21, indicating that under these conditions, GFP-PBP2 was not preferentially

localized to the septum but widely dispersed over the cell surface (Figure 45). With moenomycin, the average FR value was increased (2.14 ± 0.33) but not significantly enhanced when compared to the control. In the presence of either vancomycin, teixobactin or ampicillin, the fusion protein was almost evenly distributed between the septum and the lateral cell wall with an FR value close to the threshold. For ramoplanin, the FR was lower (1.81 ± 0.08), revealing that GFP-PBP2 was predominantly orientated to the lateral cell wall.

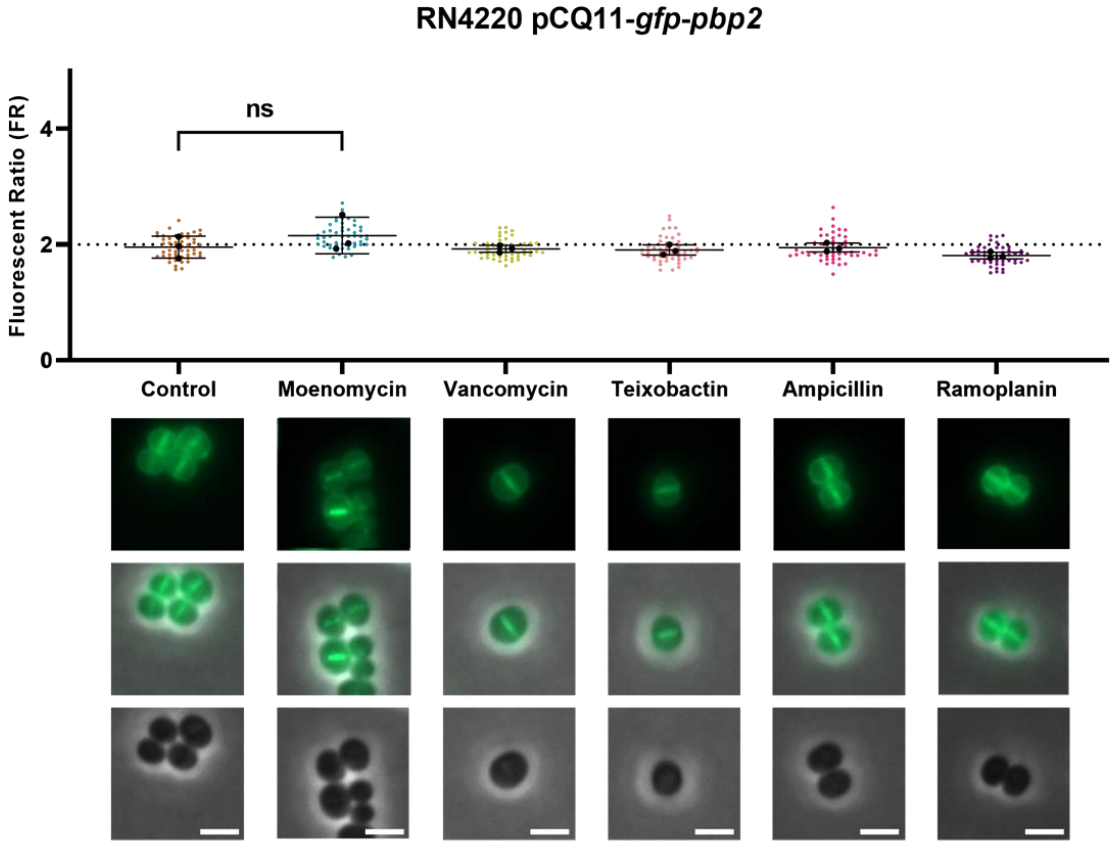

Figure 45: Localization of GFP-labeled PBP2 in *S. aureus* RN4220 depending on the exposition to different cell wall-active antibiotics. Cells were grown in TSB medium supplemented with 100 µM IPTG and 50 µg/ml erythromycin until the late exponential phase and then exposed to the 10x MIC of the respective antibiotic for 10 min at 37 °C. Per antibiotic, each 50 cells of three independent experiments were quantified. An FR greater than 2 shows the preferred binding of the fluorescent conjugate to the cell septum while values equal or less than 2 indicate the dissemination throughout the cell surface. Points represent the mean of each individual experiment. The line shows the combined mean of three independent experiments ± SD. ns $P > 0.05$ (unpaired t-test, GraphPad Prism V9.5.1.733). GFP-PBP2 was equally distributed to the cell surface in the untreated control as with vancomycin, teixobactin, ampicillin, and ramoplanin. The FR of moenomycin-treated cells was slightly higher than 2 indicating a preferential localization to the division septum. However, this increment was not significant with regard to the control sample. Scale bar: 2 µm.

3.1.10 Deletion of LCP enzymes affects the autolytic activity

To investigate the interplay between LCP proteins and the major autolysin Atl, the PG hydrolase activities of *S. aureus* MSSA1112 wildtype and related *lcp*-deletion strains were examined. In the absence of WTAs, *S. aureus* cells were shown to become more susceptible to autolysis (Oshida *et al*., 1995, Heilmann *et al*., 1997), suggesting a possible connection between the autolysin Atl and WTA-attaching LCP enzymes. The SA113 Δ*tarO* mutant, which is devoid of WTAs like the Δ*lcpABC* triple mutant, was previously shown to possess an increased autolytic activity possibly due to enhanced binding levels of the amidase domain alone and in combination with a portion of the propeptide (approx. 65 kDa) (Schlag *et al*., 2010).

The zymogram revealed distinct differences in the lytic band profiles of *S. aureus* MSSA1112 and the related *lcp*-depleted strains. For the wildtype strain, bands representing the full-length Pro-Atl (P1), the Pro-AM fragment (P3), and the single amidase domain (AM) were detectable (Figure 46A). The P3 and AM forms were clearly reduced in the Δ*lcp* single and triple mutants, whereby the latter was barely visible in the Δ*lcpB*, Δ*lcpC*, and Δ*lcpABC* mutants. Only in the Δ*lcpABC* triple mutant, the full-length P1 form was less active than in the other strains. The lysis patterns of the Δ*lcpA* and Δ*lcpB* mutants included a band representing the combined AM and GM domains without the propeptide (P2). The signal was weaker in Δ*lcpB* and not detectable for any other strain. As expected, the isolated GM domain could not be identified in the zymogram, because the protein is only marginally active with *S. aureus* cell wall as substrate (Heilmann *et al*., 1997). Notably, the AM fragment adjunct to only a portion of the propeptide as described by Schlag *et al*. (2010) was not observed for the strains tested.

Taken together, it could be demonstrated by zymography that the production and/or binding of Atl to the cell wall of *S. aureus* MSSA1112 and consequently the hydrolysis of the PG substrate is affected in the absence of LCP enzymes. Future experiments are needed to determine the expression levels of *atl* in wildtype and *lcp*-depleted strains, *e.g*., by real-time PCR.

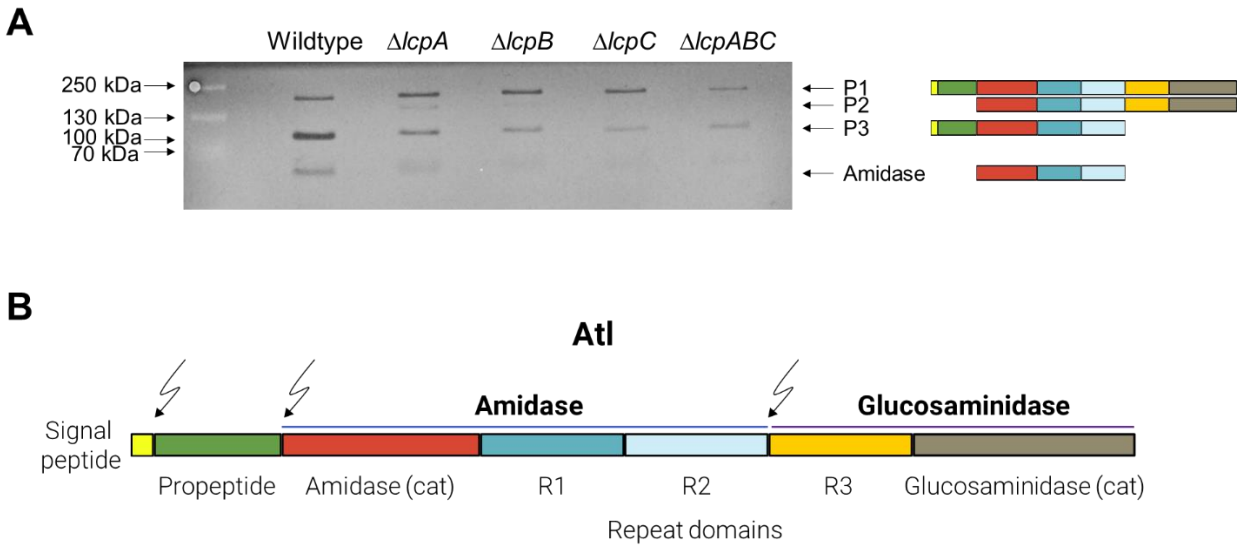

Figure 46: Zymogram of *S. aureus* MSSA1112 and respective LCP-deprived mutant strains. (A) Extracts of late-exponential grown cells were subjected to SDS-PAGE using a 4-10% Bis-Tris acrylamide gel containing autoclaved *S. aureus* NCTC8325 cells as cell wall substrate. The gel was incubated overnight at 37 °C prior to staining with methylene blue. Hydrolyzed cell wall became visible as clear bands that can be attributed to the autolysin Atl as followed: P1 (signal peptide, propeptide, amidase, and glucosaminidase), P2 (amidase and glucosaminidase), P3 (signal peptide, propeptide, and amidase), and the single amidase. *lcp* deletion mutant strains showed an altered autolysin profile with reduced levels of Atl cleavage products P3 and amidase compared to the wildtype strain. Representative result of three independent experiments. (B) Structural arrangement of the autolysin Atl in *S. aureus*. Posttranslational processing sites are indicated by arrows. cat: catalytic domain.

Chapter 2: Corallorazine A targets the DNA-dependent RNA polymerase

Corallorazines constitute a novel group of natural products with a biosynthetic gene cluster that has been shown to be widely distributed amongst diverse bacterial genera (Dreckmann *et al*., manuscript in preparation). Using agar diffusion assays against various bacteria and fungi, Schmitz *et al*. (2014) could not detect any antimicrobial effects. In this part, we re-evaluated the antibacterial activity of corallorazine A and identified the antibiotic target pathway.

3.2.1 Corallorazine A shows antibacterial activity

Corallorazine A displayed a moderate activity (4-32 µg/ml) against Gram-positive bacteria, including methicillin-sensitive (MSSA) and -resistant (MRSA) staphylococci (Table 5).

Table 5: MIC values of corallorazine A against selected Gram-positive and Gram-negative bacteria. Data are representative of three or more independent experiments.

Strain	MIC [µg/ml]
Staphylococcus aureus SG511 (MSSA)	16
Staphylococcus aureus RN4220 (MSSA)	32
Staphylococcus aureus HG003 (MSSA)	32
Staphylococcus aureus Mu50 (VISA, rifampin^{R})	8
Staphylococcus aureus COL (MRSA)	4-8
Enterococcus faecalis BM4223 (VRE)	16
Bacillus subtilis 168	128
Escherichia coli I-112768	> 64
Escherichia coli MB5746	16

The vancomycin-intermediate *S*. *aureus* strain Mu50, which is resistant to rifampin, was susceptible to the lipodipeptide (MIC 8 µg/ml), whereas the growth of rod-shaped *B*. *subtilis* was only marginally affected by corallorazine A (MIC 128 µg/ml). The endpoint MIC of *E*. *coli* I-112768 (> 64 µg/ml) could not be exactly determined due to compound shortness. However, if the outer membrane permeability was increased as in *E*. *coli* MB5746, the strain was significantly more

susceptible to corallorazine A, pointing towards the outer membrane of Gram-negative bacteria as a physical barrier for the antibiotic.

3.2.2 Corallorazine A inhibits the transcription

To elucidate the mode of action of corallorazine A, selected *B. subtilis* β-galactosidase gene expression bioreporters were exposed to the compound (Figure 47). These strains contained plasmid-encoded promoters of major biosynthesis pathways, including DNA (P_{yorB}), RNA (P_{yvgS}), protein (P_{yhel}), and cell wall (P_{ypuA}), that are fused to a *lacZ* operon. 6 µg of corallorazine A induced the P_{yvgS} promoter as indicated by the blue circle around the inhibition zone due to the β-galactosidase-mediated hydrolysis of the X-gal substrate present in the agar plate. The P_{ypuA}-*lacZ* reporter strain also showed a weak blue halo around the inhibition zone, indicating cell wall biosynthesis as an alternative target pathway.

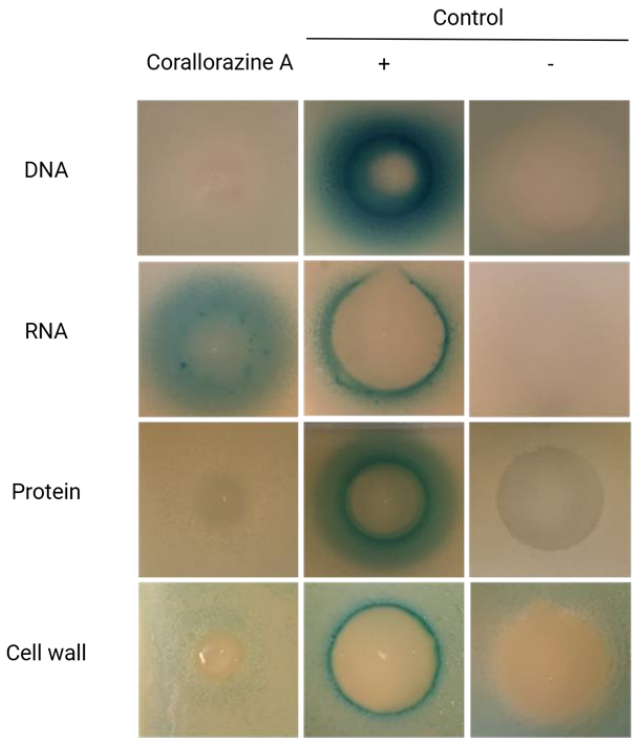

Figure 47: Corallorazine A interferes with the bacterial RNA biosynthesis pathway. The selected bioreporter strains harbored plasmid-encoded biosynthesis-specific promoter-*lacZ* fusions (DNA (P_{yorB}), RNA (P_{yvgS}), protein (P_{yhel}) or cell wall (P_{ypuA})). If the respective promotor is induced, *lacZ* is expressed and the gene product hydrolyzes agar-contained X-gal as displayed by a blue circle around the inhibition zone. Antibiotics with known target vancomycin, ciprofloxacin, rifampin, and clindamycin were used as positive controls, vancomycin (for protein bioreporter) and clindamycin (for DNA, RNA, and cell wall reporter) served as negative controls. Representative result of two independent experiments.

To confirm RNA biosynthesis as the targeted pathway, *S. aureus* RN4220 antisense strains of essential genes involved in bacterial transcription and translation were analyzed for an increased susceptibility to corallorazine A (Table 6). The tested strains, which were engineered by Donald *et al*. (2009), harbor plasmids carrying antisense RNA fragments that are directed against selected genes under control of a conditional, xylose-inducible promoter. Upon induction, the gene expression of a targeted protein is down-regulated and the target-depleted cells become susceptible to a compound in case it inhibits the specific pathway. The β-lactam ampicillin served as a negative control. Corallorazine A showed a strong effect on the RNA polymerase β-subunit (*rpoC*) and the 30S ribosomal protein S5 (*rpsE*) antisense clones, whereas the susceptibility of the RNA polymerase sigma factor (*sigA*) and the translation initiation factor IF-1 (*infA*) antisense clones remained unaffected.

Table 6: Selected clones with reduced expression of genes involved in transcription and translation exhibit an increased susceptibility to corallorazine A. Antisense mechanisms were used to down-regulate the expression of target genes. The β-lactam antibiotic ampicillin served as negative control. Data are representative of two independent experiments.

Gene	Function	Fold increase in susceptibility	
		Corallorazine A	Ampicillin
Transcription			
rpoC	RNA polymerase β' subunit	1.96	1.12
sigA	RNA polymerase σ factor	1.04	0.84
Translation			
rpsE	30S ribosomal protein S5	1.85	1.28
infA	translation initiation factor IF-1	0.99	0.84

To verify bacterial transcription as the antibiotic target pathway, the effect of corallorazine A on the DNA-dependent RNA polymerase (RNAP) from *E. coli* was studied *in vitro*. ΦX174 RF DNA served as template and the transcribed RNAs were visualized by gel electrophoresis (Figure 48). RNA molecules of different length appeared as a smear (positive control, lane 1) while the untranscribed DNA template was visible as distinct bands (control without RNAP, lane 2). The

ansamycin rifampin, which is known to bind the RNAP β-subunit and thereby sterically blocks the elongation of the RNA transcript (Campbell *et al*., 2001), was used as a positive control. Following the reduction of the smear with increasing amounts of corallorazine A, the inhibition of RNAP activity correlated with the used compound quantity, confirming previous results that corallorazine A targets the bacterial transcription and more precisely the bacterial RNAP. However, rifampin is much more potent than corallorazine A as RNAP inhibitor, because complete inhibition of transcription was achieved through addition of 0.03 nmol of rifampin (equivalent to 25 ng) while 40 nmol of corallorazine A (equivalent to 10 µg) were needed to obtain the same effect.

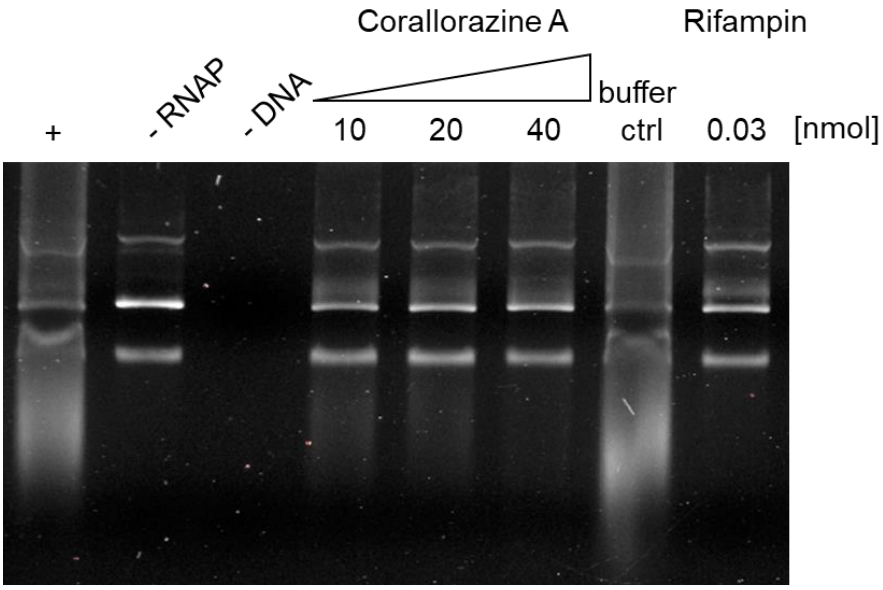

Figure 48: Corallorazine A inhibits the *E. coli* DNA-dependent RNA polymerase (RNAP)-catalyzed *in vitro* transcription. *In vitro* transcribed RNAs were mixed with GelRed (Biotium, Fremont, USA) and visualized by 1% (w/v) agarose gel electrophoresis in 1x TAE buffer at 100 V. ΦX174 RF DNA was used as transcription template. Corallorazine A interfered quantitatively with the polymerase activity, pointing towards the RNA polymerase as a target structure. The ansamycin antibiotic rifampin was used as an inhibition control. The buffer control contained the same amount of DMSO as used in the 10 nmol corallorazine A sample. Representative result of three independent experiments.

4. Discussion

Chapter 1: Moenomycin offers more than the inhibition of PG glycosyltransferases

The Gram-positive bacterium *S. aureus* is a commensal of the human nasal mucosa but has the potential to elicit life-threatening infections in immunocompromised patients. Once a newly discovered, promising antibiotic is approved, the organism may develop resistance mechanisms and spread these to other species within healthcare facilities and the community (Foster *et al*., 2017, Guo *et al*., 2020, Mlynarczyk-Bonikowska *et al*., 2022). Valuable reserve antibiotic agents listed by the WHO AWaRe classification (WHO Access, Watch, Reserve classification of antibiotics for evaluation and monitoring of use, 2021) have been proven to become increasingly ineffective (Tsiodras *et al*., 2001, van Hal *et al*., 2011, Chen *et al*., 2015, Yousefi *et al*., 2017). In order to reverse this unsettling trend, we must continuously develop new anti-infectives and optimize existing ones, besides improving the global hygiene standards and avoiding antibiotic mis- and overuse. We also need more understanding of the cellular antibiotic mechanisms to identify new targets in the bacterial metabolism and outsmart threatening resistance strategies.

The encapsulation and the decoration of the PG scaffold with WTAs are powerful tools that *S. aureus* uses to protect itself against host immune defense mechanisms and a broad range of antibiotics (Rajagopal & Walker, 2017). Since LCP proteins have been shown to catalyze the attachment of these anionic glycopolymers to PG (Chan *et al*., 2013 & 2014, Gale *et al*., 2017, Schaefer *et al*., 2017, Rausch *et al*., 2019), they constitute a promising target for the development of antibacterial agents or drug combinations.

4.1.1 Elucidation of the LCP enzyme acceptor substrate

LCP enzymes are magnesium-dependent phosphosugar transferases catalyzing the attachment of anionic glycopolymers to most commonly the C_6 hydroxyl of Mur*N*Ac moieties of the PG mesh via a phosphodiester linkage (Kawai *et al*., 2011, Chan *et al*., 2013 & 2014, Gale *et al*., 2017, Schaefer *et al*., 2017, Larson & Yother, 2017). However, the precise identity of the acceptor substrate remains elusive, because different publications come to divergent conclusions. The ultimate PG

precursor lipid II, nascent (uncross-linked), and mature (cross-linked) PG are being discussed as potential substrates (Kawai *et al*., 2011, Gale *et al*., 2017, Schaefer *et al*., 2017, Rausch *et al*., 2019).

Rausch *et al*. (2019) demonstrated the *in vitro* hydrolysis of the first three lipid-linked capsule precursors by *S*. *aureus* LcpC and the subsequent transfer of the phosphosugar unit onto lipid II. Even so, LCP enzymes have been suggested to possess overlapping substrate specificities as the transfer of WTA precursors to nascent PG was shown to be catalyzed by LcpA, LcpB, and LcpC *in vitro* (Schaefer *et al*., 2017). Moreover, only the abrogation of all three enzymes prevented the attachment of WTAs and CPs to the acceptor substrate and the overexpression of each *lcp* gene in *trans* could restore the WTA and CP levels to some extent (Chan *et al*., 2013 & 2014). While LcpC is supposed to be the major ligase in CP attachment, LcpA was shown to be the primary WTA transferase (Chan *et al*., 2013 & 2014, Schaefer *et al*., 2017).

Crystallization studies (Li *et al*., 2020) and 3D structure predictions of LcpA in complex with a WTA donor substrate (this work) unveiled a giant hydrophobic pocket in its center, which opens towards the extracellular space (Figure 49). A similar conformation has been found for the homologous LCP proteins in *B*. *subtilis*, TagT, TagU, and TagV (Kawai *et al*., 2011, Li *et al*., 2020). Artificial intelligence-based ligand-binding site predictions of LcpA place the undecaprenyl residue of the precursor lipid III_{WTA} inside the pocket and the pyrophosphate and sugar units at the exit (Figure 49B, left and middle) (this work). The actual attachment reaction to the PG scaffold is thought to take place in the groove at the opening of the pocket, which is encompassed by the four flexible loop regions A, B, C, and D (Figure 49A & B) (Kawai *et al*., 2011, Eberhardt *et al*., 2012, Schaefer *et al*., 2018, Li *et al*., 2020). Here, the pyrophosphate residue is stabilized by positively charged arginine residues within the active site, which are highly conserved among LCP homologs (Kawai *et al*., 2011, Siegel *et al*., 2019, Pan *et al*., 2021) and assumed to be aligned by a magnesium ion located adjacent to the proposed PG binding site surrounded by the loops A, C, and D (Figure 49B, right) (Li *et al*., 2020). This binding conformation was confirmed by crystallographic studies conducted by Li *et al*. (2020) featuring C_{40}-PP–Glc*N*Ac captured in the elongated cavity. The crystal structures of homologous TagT from *B*. *subtilis* and Cps2A from *S*. *pneumoniae* also revealed polyprenol(pyro)phosphate ligands bound in a similar orientation to their substrate binding site (Kawai *et al*., 2011, Eberhardt *et al*., 2012, Schaefer *et al*., 2018, Li *et al*., 2020).

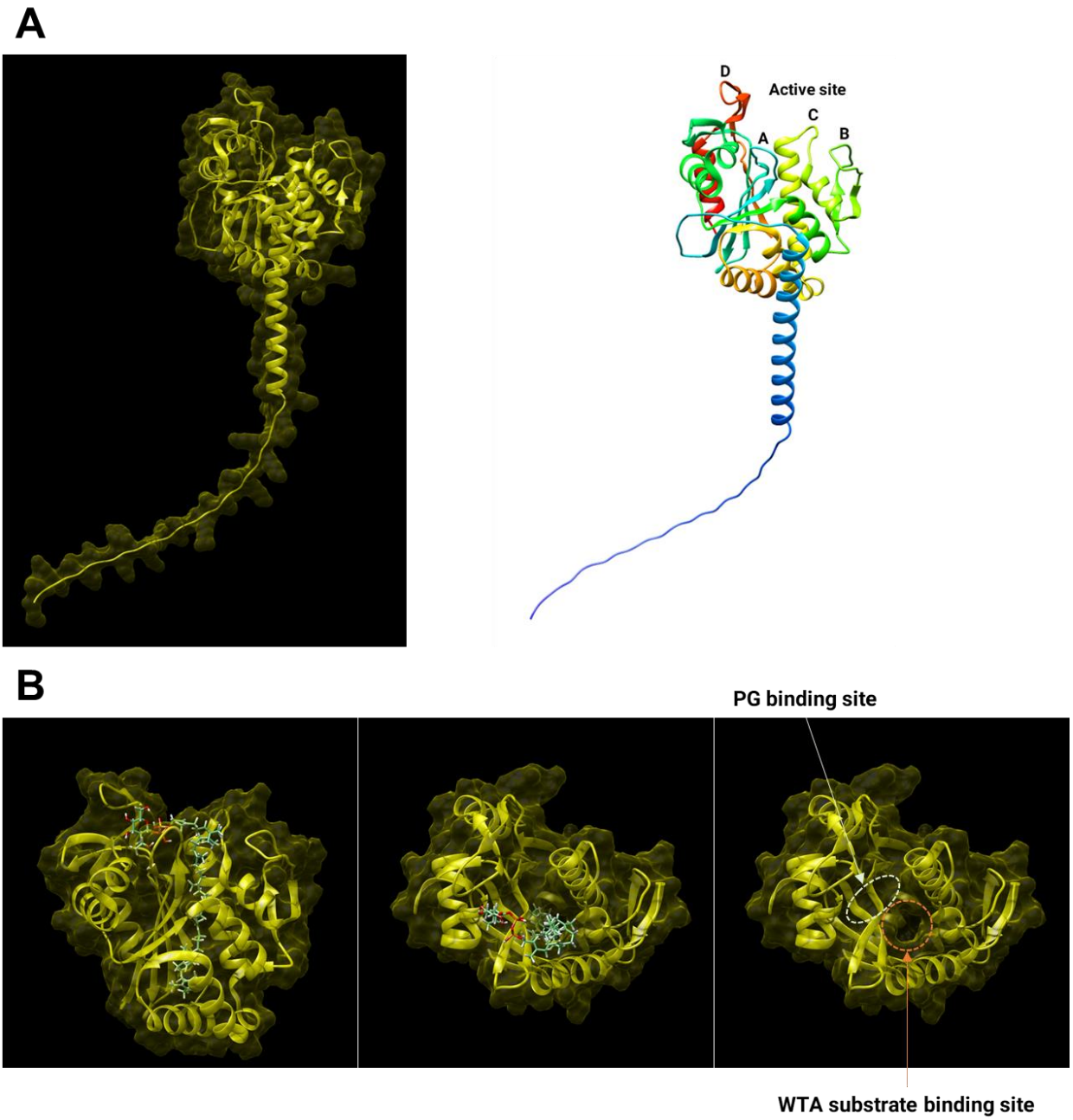

Figure 49: Structural prediction for full-length LcpA and the binding of lipid III_{WTA} to truncated LcpA from *S. aureus*. (A) Predicted structure of LcpA provided by Alphafold (identifier AF-Q99Q02-F1, date accessed July 02, 2023, Jumper *et al*., 2021). The active site is surrounded by four loops (A to D) as depicted on the right. For orientation, the different secondary structures are displayed in diverse colors. (B) Crystal structure of truncated LcpA (PDB identifier 6UEX, Lu *et al*., 2020) in complex with the bound WTA precursor lipid III_{WTA}. The lipid is depicted in sticks with heteroatoms colored by type (carbon, green; hydrogen, white; nitrogen, blue; oxygen, red; phosphorous, orange). The ligand binding predictions were compiled by Jan-Martin Daniel (Institute for Pharmaceutical Microbiology, University of Bonn) with UCSF Chimera V1.17.1 software (Pettersen *et al*., 2008). Side view and top view of the lipid-binding pocket of short-length LcpA harboring lipid III_{WTA} (left and middle). The lipid carrier is buried in the hydrophobic pocket, while the pyrophosphate residue is located in the entrance, the putative active site. The top view on LcpA without the bound substrate (right) highlights the central cavity (the putative WTA substrate binding site, orange) and the putative PG binding site (white) as suggested by Li *et al*. (2020).

For the crystallization experiments, the truncated LCP enzymes were heterologously overproduced in *E. coli*. Cell lysis was performed by homogenization or sonication that could have contributed to the accessibility of the possibly membrane-embedded polyprenol-lipids to the LCPs. Yet, it is unclear how the lipid-bound substrates are relocated *in vivo* from the outer cytoplasmic leaflet into the cavity of membrane-bound LCP enzymes given the circumstance that there is no membrane-directed opening in the proteins as indicated by the crystal structures (Kawai *et al*., 2011, Eberhardt *et al*., 2012, Schaefer *et al*., 2018, Li *et al*., 2020). The catalytic domain of other integral lipid II-interacting membrane proteins, including *S. aureus* PBP2 and SgtB, is located near the substrate site to facilitate the immediate processing of the donor (Figure 50) (Lovering *et al*., 2007, Huang *et al*., 2012). It is important to note that the LCP crystal structures were not accomplished in the natural lipid environment of the proteins and the transmembrane domains were missing. Both factors could have influenced the observed LCP protein conformation (Guo, 2020).

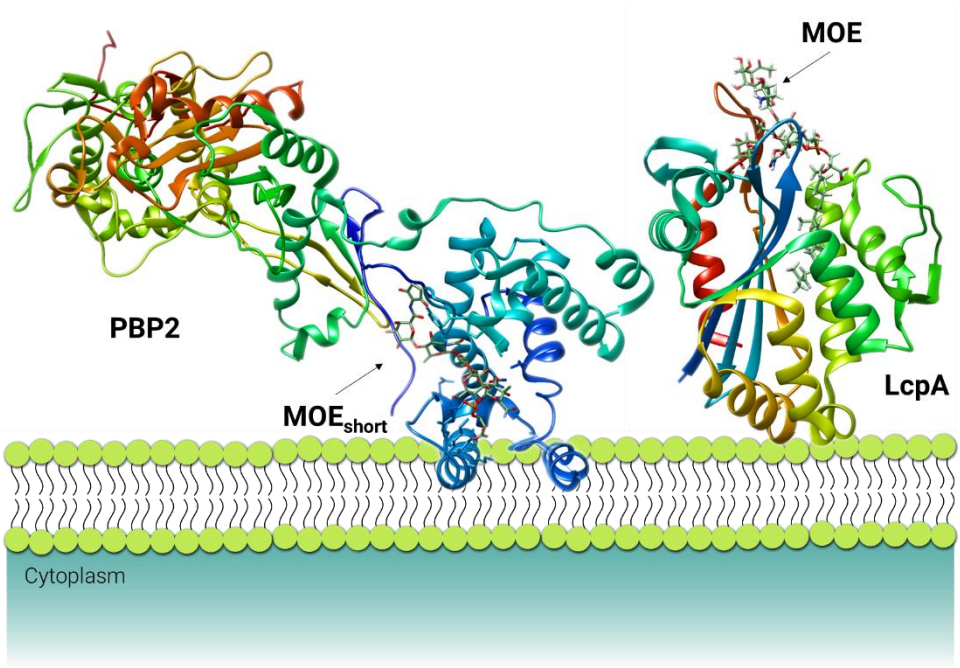

Figure 50: Crystal structures of truncated PBP2 and LcpA from *S. aureus* with moenomycin. For orientation, the different secondary structures are displayed in diverse colors. The antibiotic is depicted in sticks with elements colored by type (carbon, green; hydrogen, white; nitrogen, blue; oxygen, red; phosphorous, orange). (Left) Ribbon structure of truncated PBP2 bound to moenomycin with missing C_{25}-isoprenoid residue (PDB identifier 2OLV, Lovering *et al*., 2007). The PG glycosyltransferase domain is suggested to be partially immersed into the cytoplasmic membrane bilayer to reach its substrate. Here, shortened moenomycin occupies the donor substrate site. (Right) Ribbon structure of truncated LcpA (PDB identifier 6UEX, Lu *et al*., 2020) in combination with full-length moenomycin as proposed by ligand binding predictions compiled by Jan-Martin Daniel (Institute for Pharmaceutical Microbiology, University of Bonn) with UCSF Chimera V1.17.1 software (Pettersen *et al*., 2008). The antibiotic is thought to access the protein via the active site groove which opens to the extracellular space.

If the results of the crystal structure analysis and 3D structure predictions reflect the actual protein conformation found *in vivo*, the lipid-linked WTA and CP donor substrates would have to be translocated out of the cytoplasmic membrane and in the hydrophobic pocket of LcpA. Afterwards, the byproduct C_{55}-P would have to be inserted back into the membrane to be available for the next cycle of PG, WTA, or CP biosynthesis. Indeed, lipid-transfer proteins catalyzing the extraction and non-vesicular trafficking of membrane-embedded lipids have been found in prokaryotes (Lev, 2010, Wong *et al*., 2019). A common example is the lipopolysaccharide transport pathway in *E. coli* with the enzyme cascade LptABCDEFG transferring lipopolysaccharides from the inner to the outer membrane (Sperandeo *et al*., 2017). In *S. aureus*, the regulator protein CapA1, which is part of the tyrosine kinase complex CapA1B1 and coordinates capsular biosynthesis by protein phosphorylation (Rausch *et al*., 2019), has been suggested to actively assist the LCP reaction by passing WTA or capsule precursors to the phosphodiesterases and returning C_{55}-P into the membrane (Li *et al*., 2020). CapA1 has been demonstrated to interact with both lipid III_{WTA} and lipid I_{cap}, catalyzing the hydrolysis of the phosphodiester bond. Its presence in the LcpC-catalyzed CP attachment reaction resulted, moreover, in an increased product yield (Rausch *et al*., 2019). If the activity of CapA1 is essential at the intersection between the cytoplasmic membrane and the active site of LCPs, other Gram-positive bacteria would also possess structurally related proteins. Indeed, potential homologs of CapA1 can be found in *S. pneumoniae* (CpsC, 30.00% protein sequence identity) and *B. subtilis* (TkmA, 37.61%), among others (supplementary Figure 61). TkmA has been demonstrated to be involved in biofilm formation (Gao *et al*., 2015), but a direct connection to glycopolymer precursors could not be found in the literature. LCP enzymes have been shown to associate with the MreB cytoskeleton in the rod-shaped *B. subtilis* (Kawai *et al*., 2011). Therefore, alternative candidates for the assistance of the phosphodiesterases may also be connected to the filamental structure. In the spherical *S. aureus*, the cytoskeleton is restricted to the ring-like FtsZ scaffold guiding multiprotein complexes at the division site (Margolin, 2009).

If the obtained crystal structures of LCP enzymes (Kawai *et al*., 2011, Eberhardt *et al*., 2012, Schaefer *et al*., 2018, Li *et al*., 2020) are inaccurate due to, *e.g*., distorted charge conditions caused by the abrogation of the transmembrane domain or the non-native environment during crystallization (Guo, 2020), a conceivable alternative conformation includes a membrane-directed

opening of the hydrophobic pocket as seen in PBP2 and SgtB (Lovering *et al*., 2007, Huang *et al*., 2012) to reach the lipid-bound donor substrate directly.

While Rausch *et al*. (2019) was in preparation, our group discovered that LcpA does not only hydrolyze the first WTA precursor lipid III_{WTA} but also the PG precursor lipid II *in vitro* (Figures 18 & 19), a capability not shared by LcpB or LcpC (Figure 20). If the hydrolysis of lipid II is also catalyzed by LcpA *in vivo*, this circumstance would most likely exclude the PG precursor as WTA and CP acceptor, because LcpA would hydrolyze its own substrate. The HPLC separation of membrane lipids from *S*. *aureus* Newman wildtype and the Δ*lcpA* single mutant did not reveal a significant difference regarding the level of lipid II (Figures 21 & 22), suggesting that the hydrolysis of lipid II by LcpA does not occur *in vivo*.

Using the acceptor substrate lipid II, the attachment of anionic glycopolymers by LCP enzymes could occur prior to the polymerization of glycan chains. In contrast to LcpA, LcpC has not been shown to hydrolyze lipid II *in vitro* but to transfer the phosphosugar units of the first three lipid-linked capsule precursors to lipid II and the adducts could be polymerized by the glycosyltransferase PBP2 (Rausch *et al*., 2019). In contrast, regarding the ligation of WTAs, the use of lipid II as acceptor could be aggravated by the negative charge of the WTA chain consisting of repeating ribitol phosphate units since the modification of WTAs with D-alanine residues has been shown to occur after the glycopolymers were attached to the PG scaffold (Neuhaus & Baddiley, 2003). The overall negative charge of undecorated WTAs could impair the polymerization of the adduct by PBP2, *e.g*., by repelling the putative catalytic residues E114 and E171 (Lovering *et al*., 2007). The LCP-catalyzed transfer of WTAs and CPs could also occur after the polymerization of glycan strands to nascent or mature PG. Schaefer *et al*. (2017) could reconstitute the ligation of WTA precursors to nascent PG by LcpA, LcpB, and LcpC *in vitro* but not to lipid II. However, the work group used WTA and PG precursors synthesized from a short-chain carrier lipid and LCP enzymes without a transmembrane domain. Moreover, the importance of nascent PG *in vivo* is still under debate. Gale *et al*. (2017) demonstrated the redundancy of the *B*. *subtilis* LCP homologs TagT, TagU, and TagV catalyzing the attachment of WTA precursors to mature peptidoglycan *in vitro*. They were not successful in using lipid II as an acceptor substrate while, similar to Schaefer *et al*. (2017), assaying truncated LCP proteins.

Altogether the acceptor substrate specificity of LCP enzymes remains elusive. Schaefer *et al*. (2017) proposed that the acceptor substrate located in the putative PG binding site requires the positioning of the Mur*N*Ac residue between adjacent Glc*N*Ac residues. This assumption contradicts the observation made by Rausch *et al*. (2019) that the disaccharide unit of lipid II is sufficient for the transfer of CP precursors. Considering lipid II as an acceptor substrate, the negative charge of the pyrophosphate residues of lipid II and the donor substrate could repel each other. Individual differences in the structures of LCP enzymes, such as the positioning of positively charged arginine residues in or close to the acceptor binding site, could equalize the electrical charge and facilitate the acceptance of lipid II as acceptor substrate.

To conclude, future studies are required in order to establish the capability of LCP enzymes to discriminate against PG, WTA, and CP intermediates *in vitro* and *in vivo*.

4.1.2 The interruption of the WTA biosynthesis pathway at various stages affects the cell wall homeostasis differently

Depending on the biosynthetic stage, the inhibition of the WTA pathway in *S*. *aureus* triggers different cellular consequences. While deletions in the later steps of the WTA production are lethal, the early-acting *tarO* and *tarA* are conditionally essential genes. The accumulation of lipid-linked WTA precursors limiting the available carrier lipid for the essential PG biosynthesis is thought to cause cell death (Sewell & Brown, 2014).

The absence of WTA precursors in *S*. *aureus* through the deletion of *tarO*, which encodes for the initial WTA glycosyltransferase (Soldo *et al*., 2002a), severely affects the PG biosynthesis machinery (Figure 51). As a consequence, the percentage of peptides in cross-links is decreased although similar PBP4 levels as in the parental strain are present. In the absence of WTAs, PBP4 delocalizes and equally disperses over the cell surface (Atilano *et al*., 2010). It has been argued that septally localized WTA precursors are needed for a proper localization of PBP4 to the division site, because no direct protein-protein interaction between PBP4 and TarO could be demonstrated and TarO is recruited earlier to the septum than PBP4 (Atilano *et al*., 2010). More recent evidence (Lu *et al*., 2023), confirmed by microscopy studies conducted in this work, has revealed that the bifunctional PBP2 also delocalizes in the Δ*tarO* background. With both, MOE-BDP and Bocillin FL,

the FR values of the SA113 Δ*tarO* mutant were significantly decreased compared to those of the parental strain (Figures 37 & 39). As PBP2 loses its normal function when delocalized (Pinho & Errington, 2005) and more Vancomycin-FITC bound to the D-Ala-D-Ala residues of PG stem peptides at the cell septum in the absence of TarO (Figure 41), the ultimate PG precursor lipid II may not have accumulated at the division site.

The hydrolysis of PG is also impaired with the abrogation of WTAs. As demonstrated by Schlag *et al*. (2010), the amidase domain of the autolysin Atl loses its septal localization in the Δ*tarO* background and ties in higher amounts to the bacterial cell envelope, rendering the cells more susceptible to detergent-induced autolysis. Similar to PBP4, the authors have suggested WTA precursors as mediators and mature, PG-attached WTAs as a repellent for the recruitment of Atl-derived autolysins to the division site. In contrast, LTAs seem to function as receptor molecules directing the autolysin to the emerging cell septum (Zoll *et al*., 2012).

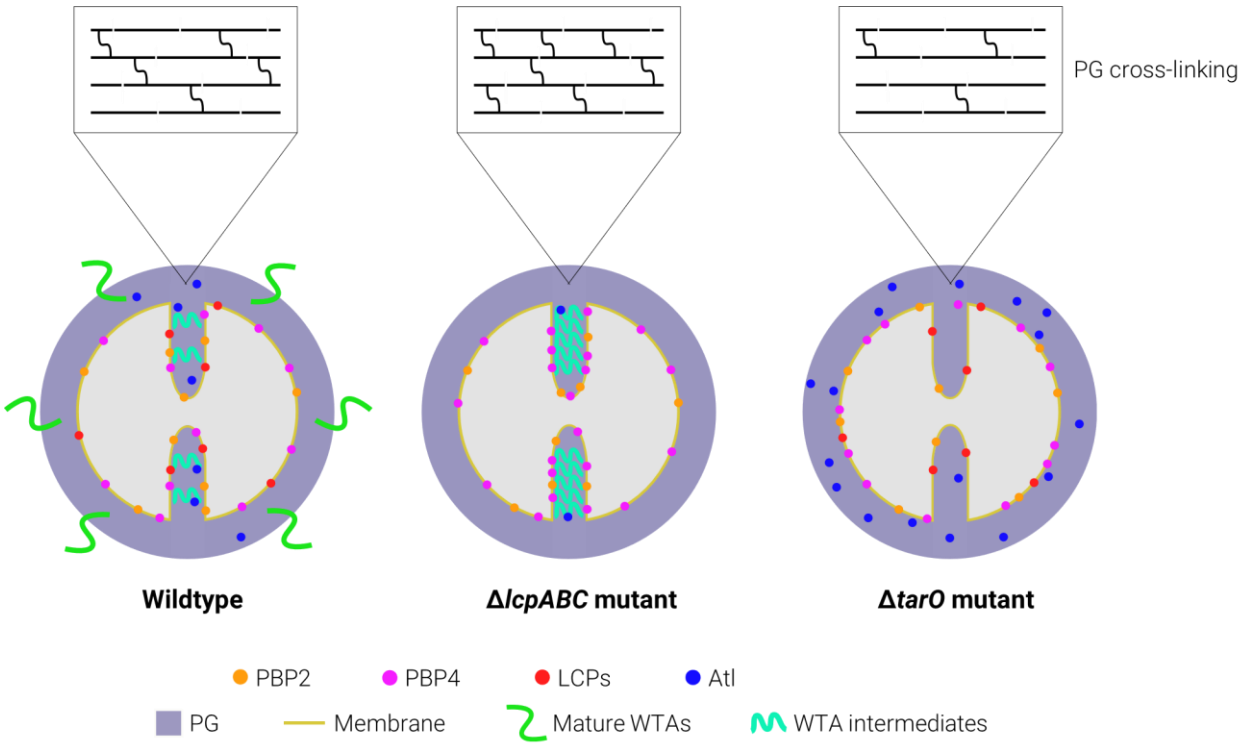

Figure 51: Model for the cellular localization of membrane proteins in *S. aureus* wildtype in comparison to the Δ*lcpABC* and Δ*tarO* null mutants. With the deprivation of LCP enzymes, *S. aureus* cannot attach anionic glycopolymers to the PG scaffold and intermediates of the WTA biosynthetic pathway accumulate predominantly at the cell septum. As the production of PBP4 is enhanced, the percentage of peptides in cross-links is increased. At the same time, the binding of catalytic Atl domains to the cell wall is reduced. In the absence of TarO, the biosynthesis of WTAs is initially prevented. Premature WTAs, which are suspected to attract PBP2, PBP4, and autolysins to the division site (Atilano *et al*., 2010, Schlag *et al*., 2010, Lu *et al*., 2023), are missing and the respective enzyme delocalize into the peripheral membrane leading to a decreased PG cross-linking.

Although LCP enzymes catalyze the ultimate step of the WTA biosynthesis, the deletion of the corresponding genes in *S. aureus* is not lethal but associated with severe morphological defects similar to those seen for the Δ*tarO* null mutant. However, while the TarO-depleted strain is barely impaired in growth, the MSSA1112 Δ*lcpABC* triple mutant showed a reduced viability (Chan *et al*., 2014). Presumably, the biosynthesis of WTAs continues in the Δ*lcpABC* triple mutant leading to the accumulation of dead-end intermediates that eventually reduces the cellular pool of C_{55}-P. This assumption is further supported by the observation that the Δ*lcpABC* triple mutant is highly sensitive to the polypeptide antibiotic bacitracin, which inhibits the dephosphorylation of C_{55}-PP (Dengler *et al*., 2012). Due to the release of WTAs and CPs to the medium of LCP-deprived cells, CapA1 has been suggested to ensure the viability of this strain by hydrolyzing the final precursors as part of a rescue mechanism (Chan *et al*., 2013 & 2014, Rausch *et al*., 2019). Of note, the mentioned literature offers no information about potential background mutations in the Δ*lcpABC* triple mutant. In contrast to *S. aureus*, the disruption of all LCP-encoding genes in *B. subtilis* is lethal (Kawai *et al*., 2011). Similar observations were made, among others, for *Corynebacterium glutamicum*, *Lactococcus lactis*, and *Streptococcus mutans*, in which at least one functional *lcp* homolog is essential for bacterial growth or survival (Bitoun *et al*., 2013, Baumgart *et al*., 2016, Sadovskaya *et al*., 2017).

The late-stage interruption of the WTA biosynthesis pathway in *S. aureus* by the abrogation of LCP enzymes affects the cell wall homeostasis differently than the disruption of the early-acting gene *tarO*. In contrast, the Δ*lcpABC* triple mutant possessed a considerable higher amount (approx. 10%) of highly cross-linked PG than the parental strain (Figure 32) and an increased production of PBP4 (Figure 33), which is mainly responsible for an enhanced cross-linking (Łeski & Tomasz, 2005, Memmi *et al*., 2008). A highly cross-linked PG may provide additional structural rigidity to the bacterial cell wall, especially if the PG mesh is not stabilized by the attachment of anionic glycopolymers and the cellular potential to form a thick PG layer is compromised. The latter hypothesis is based on the assumption that the formation of WTA precursors continues in LCP-depleted cells limiting the availability of the carrier lipid C_{55}-P to PG biosynthesis. The Δ*lcpABC* triple mutant showed a fourfold increased sensitivity (MIC 16 µg/ml) to tunicamycin compared to the parental strain (MIC 128 µg/ml) (Table 2). Due to the likely reduced PG biosynthesis, the mutant strain seemed to be more affected by the inhibitor targeting the PG translocase MraY.

Future studies need to focus on the distribution of PBPs in the Δ*lcp* null background and address the question if PBP4 is attracted to the division site by the accumulation of premature WTAs.

Zymogram analysis of LCP-deficient mutants performed in this work (Figure 46) revealed that either the activity of Atl-derived autolysins is reduced or lower amounts are associated with the cell wall. The latter would contradict the hypothesis of Schlag *et al*. (2010) that more processed Atl enzymes bind to the cell wall in the absence of mature WTAs. *S*. *aureus* Δ*atl* null mutants are highly affected in the formation of daughter cells and tend to form cell aggregates (Biswas *et al*., 2006). However, a reduced amount of active Atl in the Δ*lcpABC* triple mutant did not seem to contribute to the highly retarded cell growth of this strain since the hydrolytic profiles of the MSSA1112 Δ*lcp* single mutants were comparable and their growth was not affected compared to the parental strain (data not shown).

Although provoking different cellular responses, the disruption of at least one LCP enzyme or TarO in *S*. *aureus* has been demonstrated to induce the cell wall stress stimulon (CWSS), a combination of dozens of genes regulated by the VraSR two-component system in response to cell envelope perturbations caused by cell wall targeting antibiotics. Triggering this sensor system improves the cellular tolerance against antibacterial substances that jeopardize the integrity of the cell wall (Belcheva & Golemi-Kotra, 2008, Dengler *et al*., 2012, Lu *et al*., 2023). Strikingly, the precise identity of the VraSR regulon activator remains elusive, even if Lu *et al*. (2023) provided evidence that the accumulation of either lipid-linked PG or WTA precursors can induce the CWSS in *S*. *aureus*. This finding is consistent with the stimulation of the system in the absence of either TarO and the increased availability of carrier lipid for PG biosynthesis or, in case WTA biosynthesis continues in LCP-deficient cells, LCP enzymes (Dengler *et al*., 2012, Lu *et al*., 2023).

4.1.3 How moenomycin interacts with LCP enzymes in *S*. *aureus*

Moenomycin is a phosphoglycolipid antibiotic that is known to interfere with the activity of PG glycosyltransferases by binding to the donor substrate site. Thereby, the antibiotic prevents the translocation of the growing glycan polymer to membrane-bound lipid II and blocks the biosynthesis of new carbohydrate chains to maintain and expand the PG scaffold (Lovering *et al*., 2007 & 2008, Yuan *et al*., 2008, Fuse *et al*., 2010). The molecular structure of moenomycin

resembles, to a certain degree, that of lipid-linked PG precursors: a 25-carbon isoprenoid chain is tethered, via an ether bond, to the C_2 hydroxyl group of 3-phosphoglyceric acid that is further connected, by a phosphodiester linkage, to a tetrasaccharide core with various substitutions. The lipid chain is essential for the intercalation of the natural product into the cytoplasmic membrane, ensuring its antibacterial activity (Ostash & Walker, 2010). As expected, while binding to *S. aureus* PBP2, the orientation of moenomycin is similar to that of the glycan chain substrate: the positioning of the two sugars adjacent to the 3-phosphoglyceric acid residue overlaps with the location of the disaccharide unit of lipid II close to the putative catalytic residue E114, while the pyrophosphate is surrounded by positively charged moieties (Lovering *et al*., 2007). Moenomycin-resistant mutants of *S. aureus* have been found to possess a point mutation (either Y196D or P234Q) in the active site of PBP2, which, however, is not located in the vicinity of the presumed pharmacophore of the antibiotic consisting of the pyrophosphate with the adjoining disaccharide (Rebets *et al*., 2014).

In this work, moenomycin was shown to inhibit the hydrolysis of both the WTA precursor lipid III_{WTA} and the PG intermediate lipid II by LcpA (Figures 18 & 19). This finding presents the first evidence of an additional cellular target for moenomycin in *S. aureus* apart from PBP2 and the monofunctional glycosyltransferases SgtA and SgtB. To further investigate the nature of the protein-inhibitor interaction, different techniques were used to conduct affinity measurements including FA and SDS-PAGE. All three LCP proteins from *S. aureus* were shown to interact with the antibiotic directly and specifically (Figures 26 to 28). However, as reflected by the moderately differential MIC results of moenomycin against various LCP-depleted strains (Table 2), the LCP enzyme family has to be considered an off-target of the antibiotic, because the bactericidal effect seems to be mainly caused by the inhibition of essential PG glycosyltransferases.

Moenomycin is a potent inhibitor whose activity depends on the C_{25}-isoprenoid chain, because the lipid tail must be inserted into the membrane to occupy efficiently the donor site of PG glycosyltransferases and inhibit the polymerization of glycan chains (Ostash *et al*., 2022). In contrast to this suggested binding conformation in PG glycosyltransferases, ligand-binding site predictions place the isoprene unit of the antibiotic in the hydrophobic pocket of LcpA and the pharmacophore in the active site region (Figure 52). This positioning is similar to the proposed binding orientation of lipid III_{WTA} in the donor binding site of LcpA (Figure 49). Since little is known

about the nature of the acceptor binding site in LCPs, this location cannot be excluded as moenomycin binding site. At the time this thesis is written, endeavors to acquire high-resolution crystal structures of the LcpA-moenomycin complex are in progress.

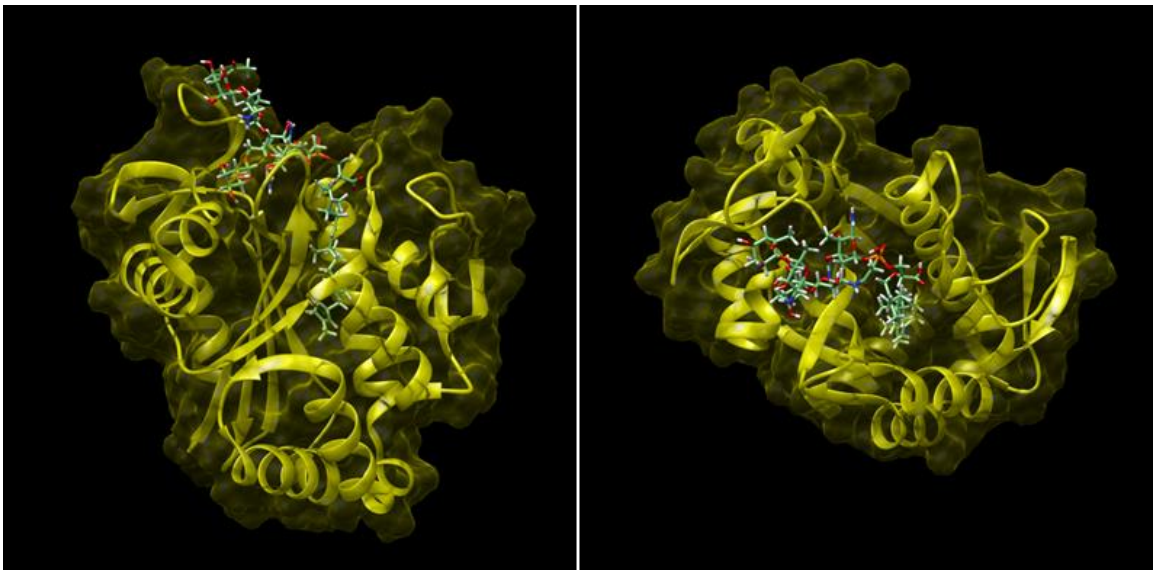

Figure 52: Structural prediction for the binding of moenomycin to truncated LcpA from *S. aureus*. The antibiotic is depicted in sticks with heteroatoms colored by type (carbon, green; hydrogen, white; nitrogen, blue; oxygen, red; phosphorous, orange). The ligand binding predictions were compiled by Jan-Martin Daniel (Institute for Pharmaceutical Microbiology, University of Bonn) with UCSF Chimera V1.17.1 software (Pettersen *et al*., 2008). To facilitate the calculations, the modeling was performed with a moenomycin A derivative missing the A ring, which is *in vivo* tenfold less active than the potent parent molecule (Ostash & Walker, 2010). Side view (left) and top view (right) of the lipid-binding pocket of short-length LcpA (PDB identifier 6UEX, Lu *et al*., 2020). The phosphoglycolipid is supposed to penetrate the hydrophobic cavity of LcpA with its isoprene unit and occupy the active site, which is surrounded by four flexible loops, with its pyrophosphate and sugar units preventing the catalytic activity of the enzyme.

In binding studies, the FA decreased when the LcpA-MOE-BDP complex was challenged by increasing concentrations of lipid II, indicating that MOE-BDP and the PG precursor target the same binding site within the LcpA protein (Figure 28B). This result also confirms that the interaction between LCP enzymes and MOE-BDP is based on non-covalent interactions, an observation that can also be deduced from the nature of the active site residues, that is unfavorable for the covalent binding of a pyrophosphate-containing substrate due to a missing nucleophile (Li *et al*., 2020).

By incubating the purified enzymes with the fluorescently labeled antibiotic and subsequent separation by SDS-PAGE, it was demonstrated that the proteins form a complex with MOE-BDP (Figure 26). Full-length as well as short variants of LcpA, LcpB, and LcpC were able to interact with

the fluorescent agent, indicating that the presence of the transmembrane domain is not relevant for binding. Cheng *et al*. (2008) demonstrated that the truncated versions of PBPs, however, possess lower binding affinities for the antibiotic. Therefore, the significance of the transmembrane domain needs to be examined in future studies. FA assays further showed that, as judged from the dissociation constant K_D, the affinity of the bifunctional PBP2 and the monofunctional glycosyltransferases SgtA and SgtB for MOE-BDP were substantially higher than that of LCPs (Table 3). Using fluorescein-labeled moenomycin, Cheng *et al*. (2008) determined a K_D value of 0.03 ± 0.03 µM for PBP2 in a FA-based assay, which is in good agreement with the results obtained in this work (K_D value of 0.10 ± 0.02 µM). The literature offers no K_D values for SgtA and SgtB, but *in vitro* PG glycosyltransferase inhibition assays have revealed an IC_{50} of 6 nM for soluble SgtB with moenomycin A, confirming that the antibiotic is effective in a nanomolar range (Gampe *et al*., 2013). While other workgroups were not successful in the reconstitution of the glycosyltransferase activity of SgtA *in vitro* (Rebets *et al*., 2014), the protein was active in assays performed in this work despite the rather poor protein purity after size-exclusion chromatography (supplementary Figures 58 & 59).

4.1.4 Unraveling the effect of moenomycin on *S. aureus* cells

Of the three LCP enzymes produced by *S. aureus*, LcpA stands out in various respects. The K_D value determined by FA measurements for LcpA was half the one for LcpB and LcpC (Table 3). Moreover, in microscopy studies, the binding of MOE-BDP to LcpA-deprived *S. aureus* MSSA1112 cells was significantly decreased compared to the parental strain (Figure 37). A different localization behavior was further observed for GFP-labeled LcpA, which, in contrast to LcpB and LcpC, was recruited to the cell division site in the presence of moenomycin (Figures 42 to 44). Other antibiotics targeting the cell wall in *S. aureus*, including vancomycin, teixobactin, ampicillin, and ramoplanin, did not alter the localization of LcpA. The microscopy studies in this work were performed using the MSSA strain RN4220 due to its efficient transformability with foreign DNA (Waldron & Lindsay, 2006, Veiga & Pinho, 2009). Since this strain does not produce a polysaccharide capsule, the potential of anionic glycopolymer attachment catalyzed by LCP enzymes is restricted to the PG-linkage of WTAs. Although displaying semi-redundant functions,

LcpA is likely the major WTA transferase in *S. aureus* (Schaefer *et al*., 2017, Chan *et al*., 2013 & 2014). If the cells are exposed to moenomycin, the antibiotic may initially reach and inhibit the LCP enzymes located in the cell periphery. As part of a stress response, newly synthesized LcpA could accumulate at the division site in order to maintain WTA biosynthesis, which is suggested to occur mainly at the cell septum (Figure 53) (Bhavsar *et al*., 2005, Formstone *et al*., 2008, Atilano *et al*., 2010). In this work, the localization of fluorescently labeled proteins was investigated after a 10 min treatment period. It is possible that GFP-LcpB and GFP-LcpC are recruited to the division site at a later time. These LCP enzymes may play a secondary role under the given conditions, since the examined strain did not produce a polysaccharide capsule (Kreiswirth *et al*., 1983, Wann *et al*., 1999).

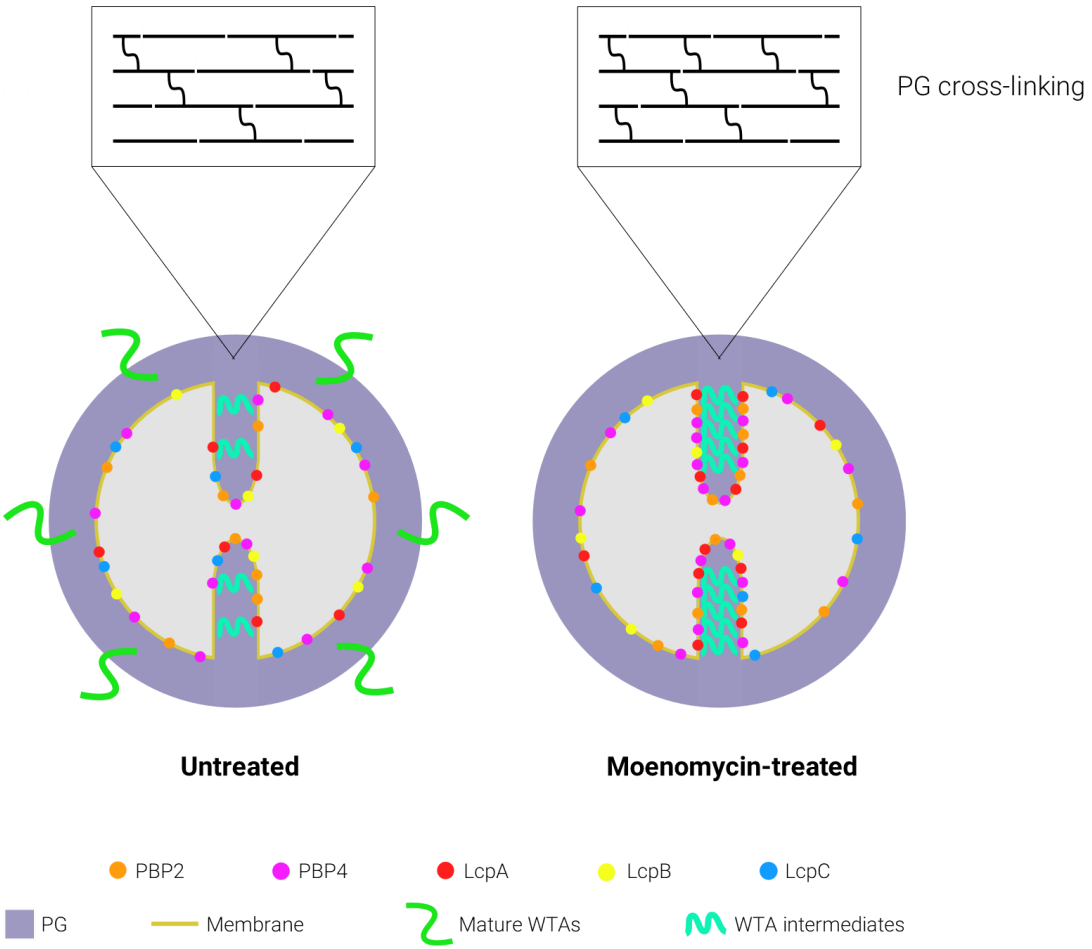

Figure 53: Model for the cellular localization of membrane proteins in *S. aureus* before and after exposure to moenomycin. The phosphoglycolipid supposedly inhibits, in addition to the transglycosylation of lipid II by PBP2 and monoglycosyltransferases, the attachment of WTAs by binding to LCP enzymes. WTA intermediates accumulate at the division site and mediate the recruitment of PBP2, PBP4 and LcpA to the septum, resulting in an increased degree of PG cross-linkage.

In addition to GFP-LcpA, also PBP4-YFP was recruited to the septum after the cells were treated with moenomycin, while for GFP-labeled PBP2, the FR value was not significantly higher than the threshold of 2 (Figures 35 & 45). Nevertheless, this result may, very carefully interpreted, indicate a positive trend towards septal recruitment. Given that *gfp-pbp2* was under the control of an IPTG-inducible promoter in this work, the overproduced fusion protein was most likely additionally integrated into the peripheral membrane distorting the basal FR value of the untreated control. In contrast, Pinho & Errington (2005) claimed that if the *gfp* gene is fused to chromosomal *pbp2* and expressed under the control of the P_{xyl} promoter, the fusion product GFP-PBP2 would predominantly localize to the septum and the localization could be influenced by the disposability of the PBP2 substrate lipid II. However, this result was not based on the calculation of the respective FR values and no statistical analysis was performed. Recently, our group could confirm the septal localization of GFP-PBP2 in the strain generated by Pinho & Errington (2005) through the analysis of convolved average projections (Puls *et al*., 2023). The divergent observations regarding the septal recruitment of GFP-PBP2 in the absence of antibiotics could result from the usage of different expression promoters or analysis methods and demands further experimental investigations.

With moenomycin inhibiting the activity of LcpA at the division site, premature WTAs supposedly accumulate and direct additional PBP4 and most likely PBP2 to the septum. While PBP4 is also active at the peripheral cell wall to maintain the aging PG scaffold, PBP2 has to localize to the division site to fulfill its essential PG glycosyltransferase activity (Gautam *et al*., 2015, Pinho & Errington, 2005). However, in the presence of moenomycin, PBP2 can only act as a transpeptidase (Ostash & Walker, 2010). In accordance with the results obtained by microscopy, the percentage of cross-linked peptides in *S*. *aureus* Newman wildtype PG was enhanced by approximately 6% after the administration of moenomycin (Figure 34). Moreover, the overall production of PBPs was stimulated compared to the untreated control (Figure 33A), which may be associated with the initiated cell wall stress response. By induction kinetics of the *vraX* promoter, it has been demonstrated that the natural product antibiotic gradually triggers the CWSS to a peak response after 60 min (Dengler *et al*., 2011). Unpublished data obtained by Jan-Samuel Puls (Institute for Pharmaceutical Microbiology, University of Bonn) show that the incorporation of the fluorescent D-amino acid probe HADA (7-hydroxycoumarincarbonylamino-D-alanine) by PBP4 at the cell

septum proceeds for at least 30 min after the exposure of the cells to moenomycin, while vancomycin and fosfomycin have already completely inhibited PG biosynthesis by then. After 90 min, the activity of PBP4 comes to a standstill and the cells predominantly remain in the assembly state with a thoroughly formed septum (data not shown, manuscript in preparation). Concordantly, a killing assay performed in this work revealed that the bactericidal effect of the antibiotic is initiated in a time-delayed manner (Figure 25). Approximately 2 h after the application of the phosphoglycolipid, the viable cell counts declined in the MSSA1112 wildtype strain. A similar observation has been made both for *S*. *aureus* ATCC 29213 and *S*. *epidermidis* ATCC 12228 (Baizman *et al*., 2000). By measuring the incorporation of [^{14}C]-lysine into the PG of *E*. *faecalis*, Baizman *et al*. (2000) could not detect an inhibition of the *in vivo* PG biosynthesis within 60 min after the exposure of the cells to moenomycin. The deferred action of the antibiotic is possibly caused by its molecular structure. To inhibit PG glycosyltransferases, the isoprenoid chain of moenomycin has to be integrated into the cytoplasmic membrane (Ostash *et al*., 2022). In contrast, considering the active site conformation of LCP enzymes facing the extracellular space and the expected binding orientation of the phosphoglycolipid within the hydrophobic pocket of the phosphodiesterases, the antibiotic likely inhibits laterally localized LCP enzymes instantly upon cell exposure. However, to reach the target enzymes that are located in the forming cell septum, moenomycin has either to overcome the cytoplasmic membrane or to find its way to the divisome by moving passively with the constricting cell envelope, which is expected to be a time-consuming process. Membranal structures constitute a solid physical barrier for the phosphoglycolipid as reflected by the MICs against Gram-negative bacteria, that are 100 to 1000-fold higher than the working concentrations against Gram-positive bacteria (Ostash & Walker, 2010). In this context, it has to be considered that the outer face of the outer membrane in Gram-negative bacteria is decorated with lipopolysaccharides that are cross-bridged by the interaction with divalent cations and form an effective permeability barrier for hydrophobic antibiotics (Savage, 2001, Nikaido, 2003). Nonetheless, moenomycin aggregates into micelles in aqueous solutions and easily integrates into lipid bilayers (Lantzsch *et al*., 1998, Anikin *et al*., 1999). Due to its hydrophobicity, it seems unlikely that the isoprenoid chain of the antibiotic is extracted from the cytoplasmic membrane once it is integrated and then reintegrated into the septum. In accordance, MOE-BDP was found to localize mainly in the lateral cell wall of *S*. *aureus* Newman wildtype (Figure 37).

Besides the interruption of the PG biosynthesis pathway leading to the predominantly found cell cycle arrest in the assembly state, moenomycin could also impair the PG hydrolysis. *S. aureus* strains have been shown to be less susceptible to autolysis if exposed to subinhibitory concentrations of moenomycin (Antignac *et al.*, 2007). In line with the hypothesis that the antibiotic inhibits LCP enzymes in *vivo*, LCP-deficient strains were demonstrated to have less active Atl-derived enzymes bound to the cell wall (Figure 46).

To mediate the cellular division into two identical daughter cells, a myriad of enzymes involved in both PG biosynthesis and hydrolysis allies to form the highly coordinated divisome complex. As the main representative, FtsZ forms a septal ring marking the future division site, that serves as a scaffold for early- and late-stage divisomal proteins including PBPs (Attaibi & den Blaauwen, 2022). The WTA biosynthesis apparatus is expected to be engaged in this well-orchestrated multiprotein factory, but the direct spatial connection linking the enzymes of the PG and WTA machineries has long remained elusive. Protein elutions of heterologously expressed *S. aureus* LcpA, LcpB, and LcpC, that had not been further purified by gelfiltration, always contained, in contrast to an empty vector control, a contaminating carboxypeptidase from *E. coli* (data not shown), indicating that the phosphodiesterases most probably interact with certain PBP motives. Moreover, recent evidence highlights GpsB as a coordinator of cell division by regulating FtsZ polymerization and directly interacting with FtsZ (Eswara *et al.*, 2018, Sacco *et al.*, 2022, preprint, Sutton *et al.*, 2023, preprint), EzrA (Steele *et al.*, 2011), PBP4, TarO, and TarG (Sacco *et al.*, 2022 preprint, Hammond *et al.*, 2022). GpsB is highly conserved in Gram-positive bacteria and essential in *S. aureus* as well as *S. pneumoniae* but dispensable in *B. subtilis* (Santiago *et al.*, 2015, Halbedel & Lewis, 2019, Hammond *et al.*, 2019). By forming an unusual dimer, the soluble protein associates with the inner face of the cytoplasmic membrane (Sacco *et al.*, 2022, preprint).

Moenomycin was demonstrated to inhibit the hydrolysis of lipid III_{WTA} *in vitro* (Figure 18). However, to provide evidence that the phosphoglycolipid affects the WTA biosynthesis *in vivo* is challenging. 30 min after the addition of the antibiotic, *S. aureus* Newman cells were shown to possess significantly less WTAs, but, at the same time, the PG content was reduced by a similar percentage, which likely limits possible attachment sites for anionic glycopolymers (Figure 36).

In MRSA strains, the equipment of the cell wall with WTAs has been proven to be essential for β-lactam resistance (Hartman & Tomasz, 1984, Matsuhashi *et al.*, 1986, Brown *et al.*, 2012, Farha

et al., 2013). Accordingly, the exposure to low levels of tunicamycin renders otherwise resistant strains susceptible to oxacillin (Campbell *et al*., 2011). Indeed, both MRSA strains USA300 and COL were shown to become sensitive to the β-lactam in the presence of moenomycin (supplementary Figure 60). However, this was not particularly surprising given the fact that an active PBP2 glycosyltransferase domain is required for the expression of β-lactam resistance in *S*. *aureus* (Pinho *et al*., 2001). The combination of moenomycin and β-lactams was further tested against MSSA strains and found to act synergistically in MSSA1112 wildtype and the SA113 Δ*tarO* null mutant (Figures 29 & 31). In contrast, no synergism could be detected in the LCP-deficient MSSA1112 strain referring to LCP enzymes as a complementary target for the phosphoglycolipid in the parental and the TarO-deprived strain (Figure 30). Considering that the latter presumably still produces LCP enzymes that do not fulfill an active function since the biosynthesis of WTAs is abrogated, it cannot be excluded that the synergism is based on other cellular processes in this strain.

Taken together, the antibiotic effectiveness of moenomycin is not solely based on the inhibition of essential PG glycosyltransferases but on the additional interaction with LCP enzymes in Gram-positive bacteria, rendering the phosphoglycolipid a powerful template for antibiotic drug design.

Chapter 2: Corallorazine A extends the small portfolio of RNAP inhibitors

The emerging antibiotic resistance crisis causes an exponential increase in hospitalizations, medical costs, and mortality worldwide (WHO, 2021). Simultaneously, pharmaceutical companies withdraw from the search for novel anti-infectives, because they are discouraged by high-risk investments and low long-term profit opportunities (Dutescu & Hillier, 2021). It is estimated that by 2050, about ten million people could die annually of hard-to-treat infections caused by antibiotic resistant pathogens (O'Neill, 2014). If no urgently required actions are taken, the world is expected to be reset to a pre-antibiotic era. To counter this appalling development, it is essential to understand how bacterial resistance mechanisms work and to find possibilities to overcome them. Interestingly, the sources of new compounds against resistant bacteria are often other microorganisms (Schäberle *et al*., 2014a, Quinn *et al*., 2020).

In consequence of the high bacterial density in their geobiotic habitat and their preferentially stationary lifestyle in slime sheets, myxobacteria produce numerous bioactive substances to maintain their ecological niche against opponents and are, therefore, a rich source of promising antimicrobial compounds (Reichenbach *et al*., 2001). *C. coralloides* B035 is an organism that has already acquired prominence for producing the bacterial DNA-dependent RNA polymerase (RNAP) inhibitor corallopyronin A that is of major interest in fighting human filarial infections (Irschik *et al*., 1985, Krome *et al*., 2022). Another secondary metabolite synthesized by this bacterium, corallorazine A, constitutes a new group of natural products and could contribute to fill the gap of effective compounds fighting resistant pathogens.

4.2.1 Corallorazines form a new group of natural product antibiotics

Corallorazine A was found to be the final product of the corallorazine biosynthesis pathway while corallorazine B and C are supposed to be intermediates. The compound owns an unusual structure consisting of the two amino acid residues dehydroalanine and glycine that are connected by a semiaminal bond to form a piperazine ring, which is, in turn, linked to an uncommon aliphatic acyl chain by an amide bond (Figure 8) (Schmitz *et al*., 2014). Corallorazine A shares structural similarities with a biosynthetic byproduct of phenylahistin, a diketopiperazine metabolite produced by the ascomycete *Aspergillus ustus* and inhibitor of tubulin polymerization

in eukaryotic cells (Figure 54). However, the dipeptide backbone of the byproduct is composed of a L-phenylalanine and an isoprenylated dehydrohistidine moiety and, in contrast to corallorazines, not connected to an acyl chain (Kanoh *et al*., 1997 & 1999, Schmitz *et al*., 2014). A closer related structure was found in the secondary metabolite cyrmenin A, a fungicide that is produced by the myxobacteria *Cystobacter armeniaca* and *Archangium gephyra* and known to interrupt mitochondrial respiration by interfering with the cytochrome bc_1 complex (Leibold *et al*., 2004). Its dipeptide core contains also dehydroalanine, but, unlike corallorazine A, the second amino acid residue is an *O*-methylated dihydroserine. Another resembling feature is the linkage of the lipophilic chain via an amide bond that contains a (2*E*,4*Z*)-dodecadienoic acid residue in cyrmenin A but a (2*E*,4*Z*)-iso-octa-2,4-dienoic acid residue in corallorazines (Leibold *et al*., 2004, Schmitz *et al*., 2014).

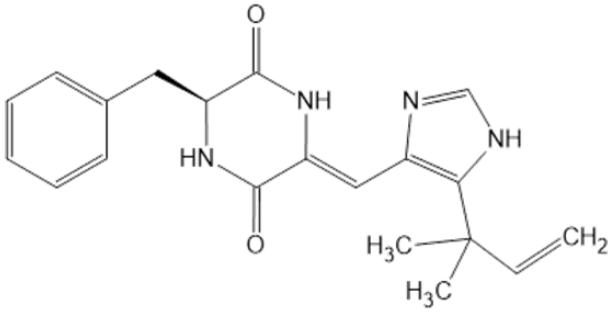

A) Phenylahistin

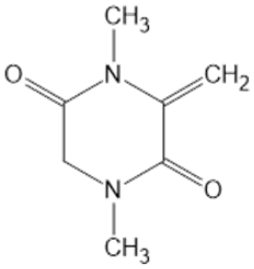

B) Byproduct of phenylahistin biosynthesis

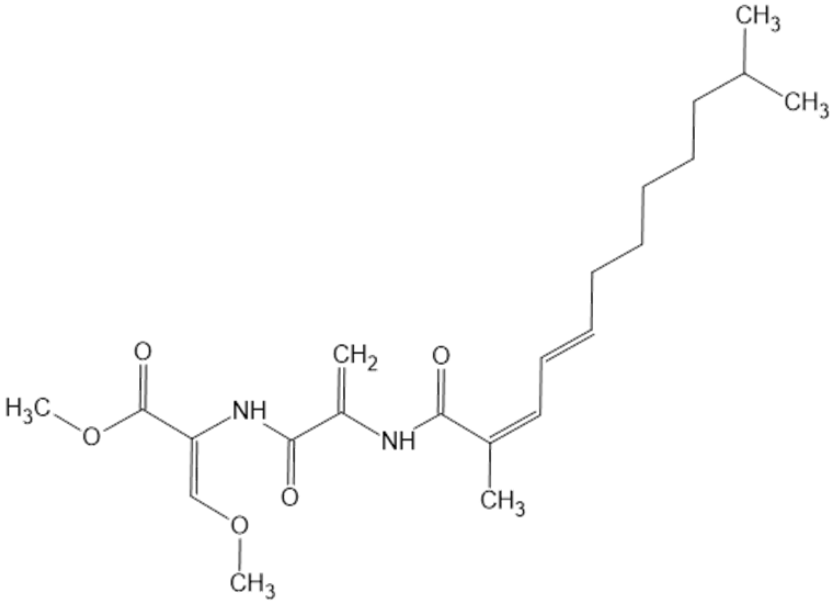

C) Cyrmenin A

Figure 54: Structures of (A) phenylahistin, (B) its biosynthesis byproduct, and (C) cyrmenin A, which possess structural resemblance to corallorazine A.

Corallorazine A showed moderate antibiotic activity against Gram-positive bacteria, especially the MRSA strain COL (Table 5). *S. aureus* belongs to the so-called ESKAPE pathogens, an acronym for *Enterococcus faecium*, *Staphylococcus aureus*, *Klebsiella pneumoniae*, *Acinetobacter baumannii*, *Pseudomonas aeruginosa*, and *Enterobacter* spp., a group of bacterial species with increased multi-drug resistance (Tommasi *et al*., 2015). Commonly used antibiotics become progressively ineffective to treat infections caused by these pathogens and corallorazine A could be a potential candidate to treat MRSA infections.

In Gram-negative bacteria, the outer membrane constitutes a mechanical barrier for the penetration of hydrophobic compounds, such as corallorazine A. The core region of the outer membrane lipopolysaccharides presents a protective shield against lipophilic compounds, providing intrinsic resistance (Delcour, 2008). Indeed, as shown by MIC determinations, the *E. coli* strain MB5746 with an increased outer membrane permeability was more susceptible to corallorazine A than the strain I-122768 with an intact membrane. Therefore, the simultaneous administration of membrane permeabilizing substances (*e.g.*, polymyxin B, Tris/EDTA) could enhance the antibiotic effect of corallorazine A on Gram-negative bacteria (Vaara, 1992, Delcour, 2008). Another approach to improve the activity could be the shortening of the acyl chain. However, other hydrophobic antibiotics, *e.g.*, moenomycins, are impaired in their biological activity if the length of their lipid chain is reduced (Adachi *et al*., 2006). In addition, moenomycins have a poor bioavailability and a hemolytic activity that is potentially ascribed to the lipid tail (Figure 7) (Adachi *et al*., 2006, Pfaller *et al*., 2006, Ostash & Walker, 2010). Effects that may also be assigned to corallorazine A in further studies.

In order to produce corallorazine A on a large scale, Dreckmann *et al*. (manuscript in preparation) have already successfully reconstituted the biosynthesis pathway *in vitro*.

4.2.2. Corallorazine A in comparison with other RNAP inhibitors

In this work, corallorazine A was shown to inhibit the *in vitro* activity of the *E. coli* DNA-dependent RNA polymerase (RNAP). This protein enables the highly coordinated process of transcription, the initial step of gene expression. The shape of the bacterial RNAP resembles a crab claw with the protruding large subunits β and β' forming a central cleft that contains the active site including a

catalytic magnesium-ion (Figures 55 & 57). Two identical smaller α-subunits form the distal base, whereby each α-subunit collaborates with another β-subunit via the N-terminal domain (αNTD). In addition, the α-subunits possess a C-terminal domain (αCTD) for the interaction with upstream promoter DNA and proteogenic regulatory factors (Ebright *et al*., 2000). The RNAP core enzyme is completed by the smallest subunit ω that binds to β' as a chaperone and is responsible for RNAP assembly and stabilization (Mathew & Chatterji, 2006). To initiate bacterial transcription, the core enzyme associates with the factor sigma (σ) that allows specific promoter recognition to form the RNAP holoenzyme (Gruber & Gross, 2003). In the base region close to the active site, the switch region encompassing five sections regulates the movement of the β'-clamp. It governs the opening of the claw-like RNAP structure to grant the incoming DNA strand access to the active-center cleft and coordinates the closing of the "pincer" to keep the DNA in place for unwinding (Srivastava *et al*., 2011, Artsimovitch *et al*., 2012, Chakraborty *et al*., 2012).

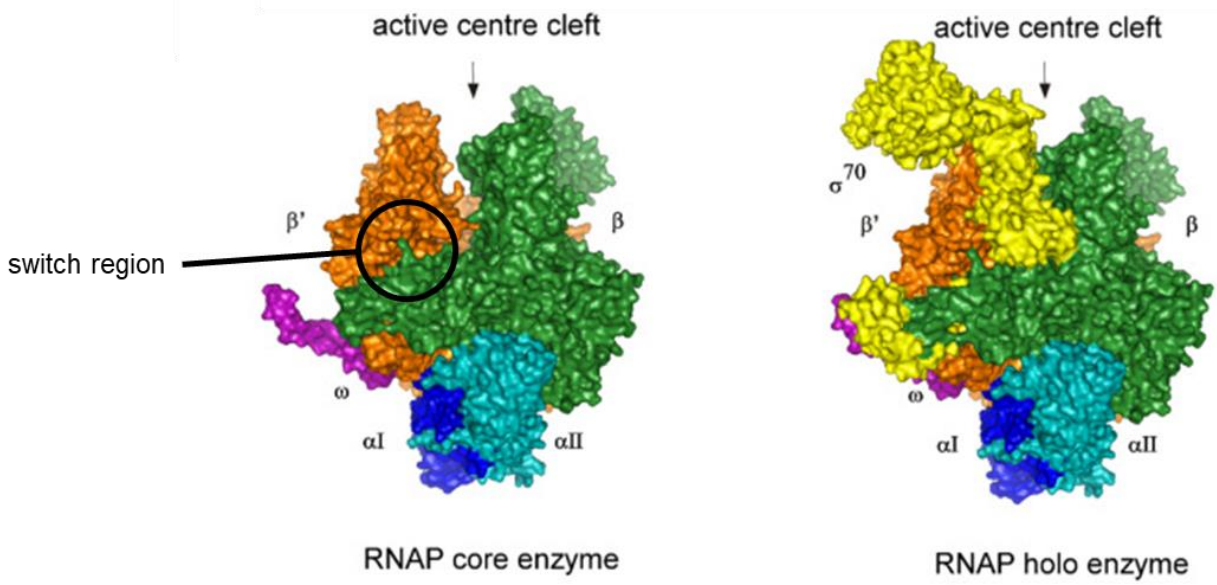

Figure 55: Structure of the bacterial RNAP. The RNAP of prokaryotes is composed of different subunits forming a clamp-like shape. Subunits β' and β build a pincer with ω as a stabilizing chaperone for β' while two identical α-subunits provide the base. The σ-factor completes the RNAP holoenzyme and enables specific promoter recognition. The switch region (circle) controls the movement of the β'-clamp (figure adapted from Mazumder & Kapanidis, 2019).

The RNAP represents an attractive target for antimicrobials and particularly broad-spectrum antibiotics, because of its essentiality and highly conserved structure in bacteria. Although homolog, the eukaryotic RNAP has diverged from the bacterial RNAP, allowing a selective therapy approach with a minor risk for cytotoxicity (Ma *et al*., 2016). To this day, only two groups of RNAP inhibitors are approved for therapeutic treatment, namely the members and derivatives of the rifamycins, including rifampin, and fidaxomicin (lipiarmycin) (Figure 56) (Kirsch *et al*., 2022).

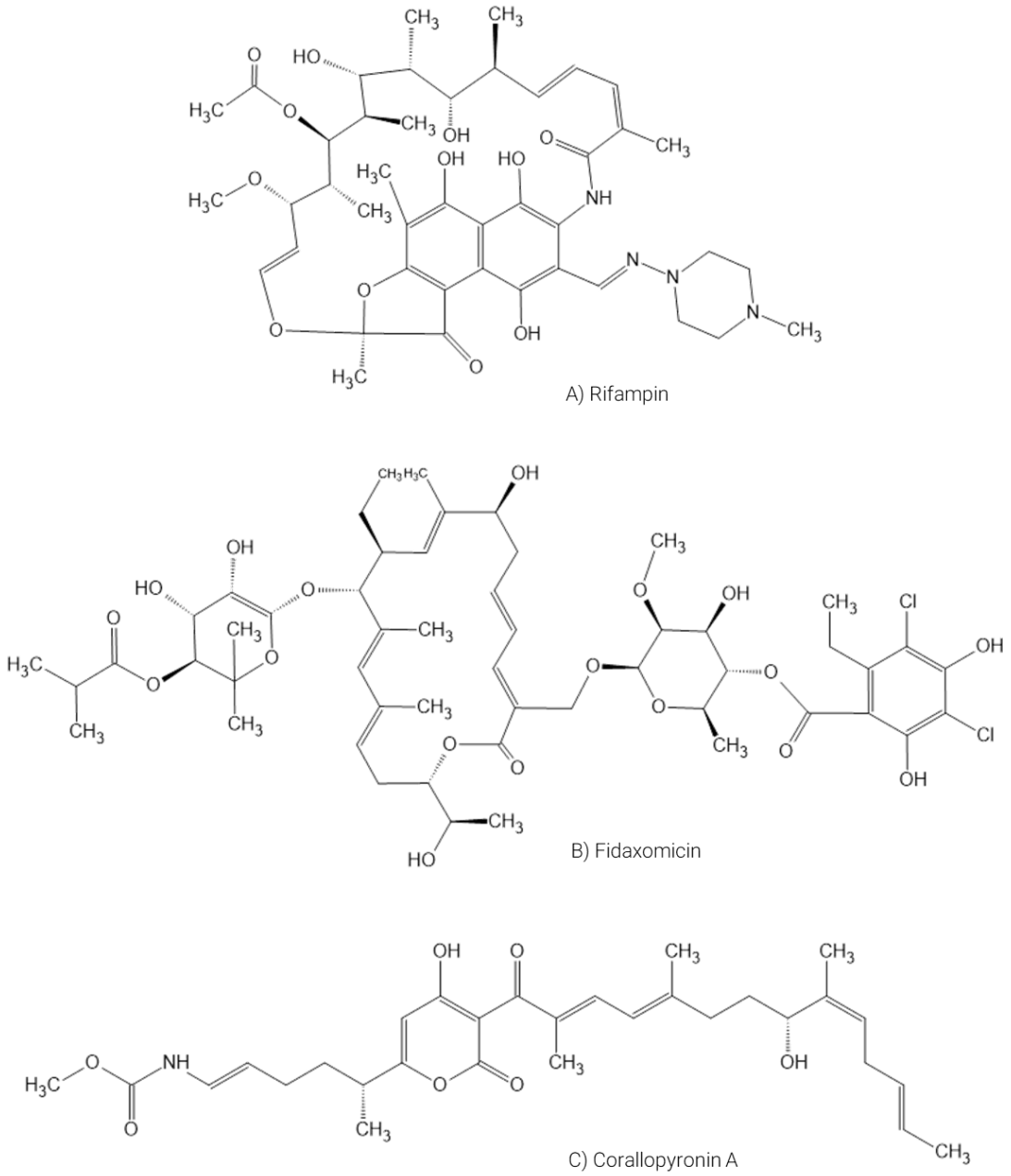

Figure 56: Structures of the RNAP inhibitors (A) rifampin and (B) fidaxomicin, which are approved for medical use, and the drug candidate (C) corallopyronin A.

The ansamycin rifampin is the most prominent representative of RNAP inhibitors. Discovered in 1965 as a secondary metabolite of *Amycolatopsis mediterranei*, rifampin binds to the β-subunit of the RNAP in proximity to the active site and interferes with the RNA elongation after the second or third nucleotide of the growing RNA transcript (Figure 57) (Campbell *et al*., 2001). In conjunction with other anti-infectives, the antibiotic is used to treat, *e.g*., active and latent tuberculosis infections, anthrax, leprosy, and streptococcal and staphylococcal infections (Sensi, 1983, Centers for Disease Control and Prevention, 2001, American Academy of Pediatrics, 2006). Nevertheless, since the therapeutic treatment of particularly mycobacterial infections requires several months, the infection strain is prone to develop resistance to rifampin that predominantly includes mutations in the β-subunit-encoding *rpoB* gene (American Academy of Pediatrics, 2006, Goldstein, 2014).

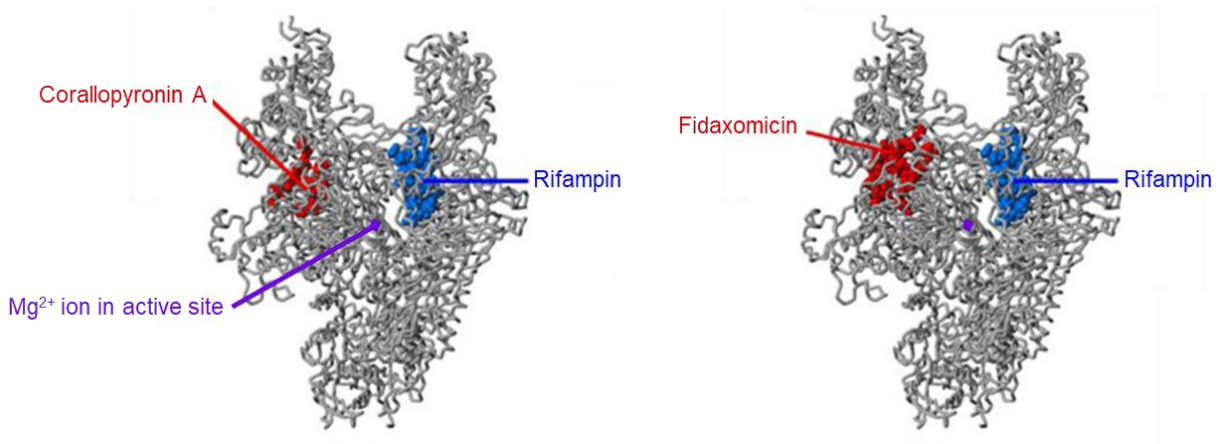

Figure 57: Inhibitor target sites of the bacterial RNAP. The RNAP-inhibitors corallopyronin A and fidaxomicin bind each to a different position within the switch region of the β'-subunit, whereas the binding site of rifampin is located in the β-subunit. The catalytic magnesium ion is marked in purple (adapted from Srivastava *et al*., 2011).

MIC determinations conducted in this work (Table 5) revealed that the vancomycin-intermediate *S. aureus* Mu50 strain, which is resistant to rifampin, was, indeed, susceptible to corallorazine A. This result points to a different target structure than the rifampin-binding site. Moreover, if the expression of *rpoC*, which encodes for the β'-subunit, was reduced, the test strain became more susceptible to corallorazine A, suggesting the switch region as a possible target site. A similar effect in the susceptibility to corallorazine A was observed for the downregulation of the 30S ribosomal subunit 5S-encoding gene *rpsE*, although no interference with the protein

biosynthesis pathway could be demonstrated using *B. subtilis* β-galactosidase reporter assays (Figure 47). However, the accuracy of antisense-induced strain sensitivity profiling is restricted, because different biosynthetic pathways and proteins may influence each other (Donald *et al*., 2009, Chiriac *et al*., 2015).

In direct comparison, rifampin possessed a superior antibacterial activity compared to corallorazine A in *in vitro* transcription studies including *E. coli* RNAP (Figure 48). Approximately the 1300-fold molar amount of corallorazine A was needed to reach the same level of transcriptional inhibition as shown by rifampin. In line with this observation, the *S. aureus* strain SG511 was found to be distinctly less susceptible to corallorazine A than to rifampin with MIC values of 32 µg/ml (Table 5) and 0.004 µg/ml (Dietrich *et al*., 2021), respectively.

Another approved RNAP inhibitor is the macrocyclic fidaxomicin, which is produced by the actinomycetes *Dactylosporangium aurantiacum* and *Actinoplanes deccanensisis* and mainly active against Gram-positive bacteria. The narrow-spectrum antibiotic is used to treat *Clostridioides difficile*-associated diarrhea and inhibits the early transcription by binding to the β' switch-2 region (Figure 57) (Parenti *et al*., 1975, Swanson *et al*., 1991, Hardesty & Juang, 2011, Goldstein *et al*., 2012, Artsimovitch *et al*., 2012, Venugopal & Johnson, 2012, Sears *et al*., 2013, Lee & Borukhov, 2016). The drug candidate corallopyronin A, which is currently undergoing preclinical trials, also binds to the β'-switch-2 region preventing clamp motion (Figure 57). However, the exact target site differs and no cross-resistance to fidaxomicin was detectable (Srivastava *et al*., 2011, Lee & Borukhov, 2016). For fidaxomicin as well as for corallopyronin A, no cross-resistance with rifampin has been reported due to their different target sites within the RNAP (Goldstein *et al*., 2014, Krome *et al*., 2022).

As already mentioned, corallopyronin A and corallorazine A are produced by the same myxobacterium, *C. coralloides*, and have been suggested to target the same structure in prey organisms (Irschik *et al*., 1985, this work). If the bacterium is challenged for its ecological niche and the competitor develops resistance to corallopyronin A, it would be energetically disadvantageous to produce a second compound that has already proven to be ineffective. However, these overlapping target sites are not mutually exclusive. Depending on, *e.g.*, environmental conditions such as temperature, humidity, and resource availability as well as the nature of the target organism, the biosynthesis of one compound could be favorable. Similar to

corallorazine A, corallopyronin A has been demonstrated to possess a relatively low binding affinity to *E. coli* RNAP with regard to rifampin. The α-pyrone antibiotic revealed a 50% inhibitory concentration of 0.73 ± 0.2 µM, while rifampin displayed an average IC_{50} of 11.5 ± 1.1 nM (Mariner *et al*., 2011). Nevertheless, corallopyronin A is highly effective against endobacterial *Wolbachia* and a promising candidate for the treatment of human filarial infections (Krome *et al*., 2022).

Considering that test systems from different bacterial strains (*S. aureus* antisense strains (Table 6), *B. subtilis* β-galactosidase reporter (Figure 47), purified *E. coli* RNAP (Figure 48)), which differ in their susceptibility to corallorazine A (Table 5), were used to reveal the antibiotic target site of corallorazine A, additional experimental methods are required to examine a possible inhibition of the bacterial ribosome. Even though the antibacterial potency of corallorazine A seemed to be less compared to rifampin, derivates of the lipodipeptide with advanced features could render this compound a promising drug candidate.

5. Appendix

5.1 Supplementary figures and tables

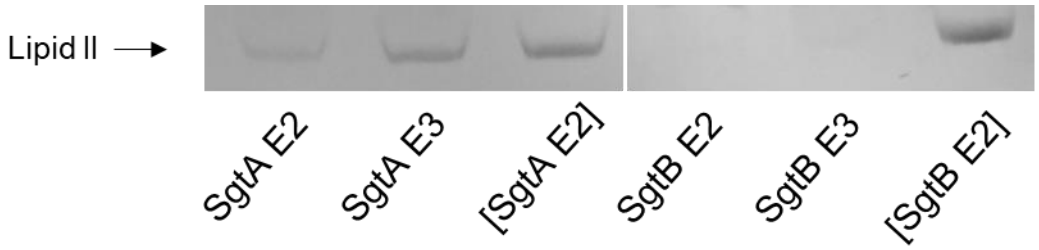

Figure 58: *In vitro* activity test of purified full-length SgtA and SgtB. Purified lipid II was incubated with hexahistidine-tagged SgtA and SgtB from *S. aureus*. Following extraction with BuOH/PyrAc, samples were separated by TLC and developed using Hanessian's stain. In the negative control, the enzyme was added simultaneously with the organic solvents after the incubation period. Hydrolysis was displayed by reduction of the lipid II substrate band. E2: Elution fraction 2, E3: Elution fraction 3. Representative results of three independent experiments.

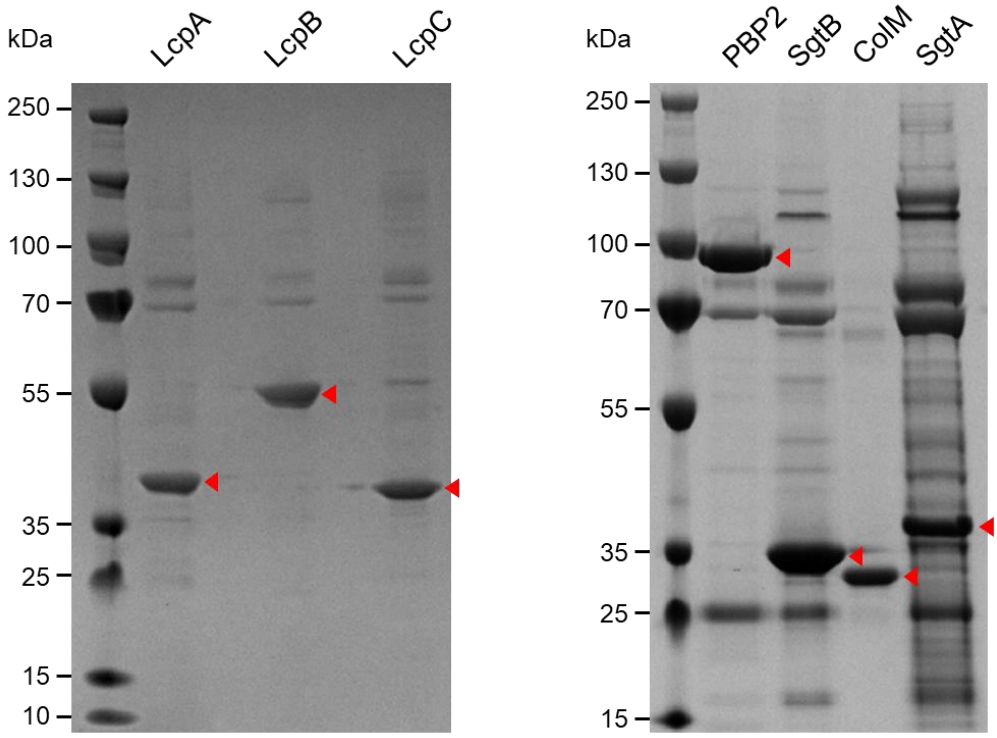

Figure 59: SDS-PAGE of purified proteins used for FA experiments. Final protein purity after gel filtration assessed by PageBlue stained 4 -12% Bis-Tris acrylamide SDS-PAGE. Approximately 5 µg was applied on gel. Despite gel filtration, the eluate of the monoglycosyltransferase SgtA exhibited many contaminating proteins. A Bocillin assay revealed no contamination by PBPs in the protein solutions of LcpA, LcpB, and LcpC (data not shown). Arrows indicate the respective protein band. Representative results of three independent purifications.

Table 7: MIC values of *S. aureus* Newman for fluorescently labeled cell wall targeting antibiotics. The table shows representative data of three or more independent experiments.

Strain	MIC (µg/ml)			
	MOE-BDP	Bocillin FL	Vancomycin-FITC	Rhodamine B-Ramoplanin
Newman wildtype	2	0.5	4	4

Table 8: MIC values of *S. aureus* RN4220 strains producing GFP-tagged LCP and PBP enzymes for moenomycin and other cell wall targeting antibiotics. The table shows representative data of three or more independent experiments.

Strain	MIC (µg/ml)				
	Moenomycin	Vancomycin	Teixobactin	Ramoplanin	Ampicillin
RN4220 pCQ11-*gfp-lcpA*	0.25	4	2	1	0.125
RN4220 pCQ11-*gfp-lcpB*	0.125	2	2	1	0.0625
RN4220 pCQ11-*gfp-lcpC*	0.125	2	2	1	0.0625
RN4220 pCQ11-*gfp-pbp2*	0.25	4	2	1	0.125
RN4220 pCQ11-*yfp-pbp4*	0.125				

Table 9: Checkerboard assay results of moenomycin in combination with antibiotics of other classes against the MRSA strains USA300 and COL. A fractional inhibitory concentration (FIC) of <0.5 indicates synergism while a value of 0.5-4 suggests an unremarkable additive effect or no increase in inhibitory activity when the two compounds are combined (Lorian, 2005). With moenomycin, both strains were sensitized to the β-lactam oxacillin. Chloramphenicol displayed antagonistic activity in combination with the phosphoglycolipid, while ciprofloxacin did not affect the MIC of moenomycin against USA300. Synergy was observed for moenomycin and the glycopeptide vancomycin. The table shows representative data of three independent experiments.

Antibiotic	Class	USA300		COL	
		FIC	Interaction	FIC	Interaction
Oxacillin	β-lactam	0.125	synergistic	0.25	synergistic
Chloramphenicol	other	4.016	antagonistic		
Ciprofloxacin	fluoroquinolone	1.001	indifferent		
Vancomycin	glycopeptide	0.375	synergistic		

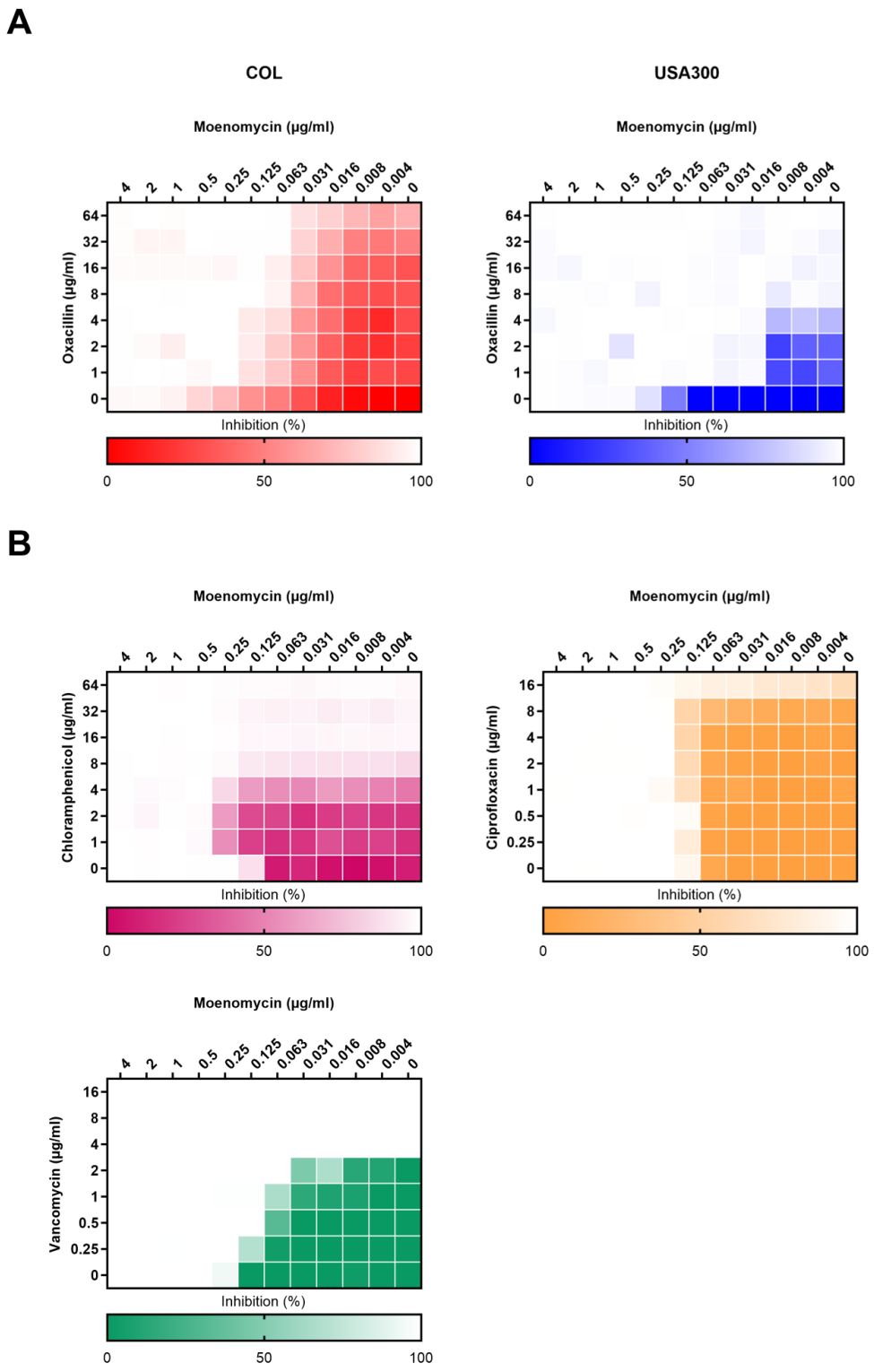

Figure 60: The effect of moenomycin in combination with different class antibiotics against methicillin-resistant *S. aureus* (MRSA) strains. (A) Both *S. aureus* COL and USA300 became susceptible to the β-lactam antibiotic oxacillin in the presence of moenomycin. (B) The MRSA strain USA300 was further tested with other classes of antibiotics. Chloramphenicol increased the inhibitory effect of moenomycin, while ciprofloxacin had no effect. For the combination with vancomycin, a synergistic effect was observed. Representative results of three independent experiments.

```
                          1         10        20        30        40        50
S.aureus_N315_Cap5A       MESTLEL....TKIKEVLQKNLKILIILPLLFLIISAIVTFFVLSPKYQANTQIL.VNQT
B.subtilis_168_TkmA       MGESTSL....KEILSTLTKRILLIMIVTAAATAAGGLISFFALTPIYENSTQIL.VNQS
S.pneumoniae_D39_Cps4C    MKEQNTIEIDVFQLFKTLWKRKLMILLVALVTGAGAFAYSTFIVKPEYTSTTRIYVVNRN

                             60        70        80        90       100       110
S.aureus_N315_Cap5A       KGDNPQFMAQEVQSNIQLVNTYKEIVKSPRILDEVSKDLNDKYSPSKLSSMLTITNQENT
B.subtilis_168_TkmA       KNERKEVQFNDVQTNLQLINTYNVIIKSPAILDEVIKEMGLSMTSQELNDKITVSSEQDS
S.pneumoniae_D39_Cps4C    QGDKSGLTNQDLQAGSYLVKDYREIILSQDALEKVATNLKLDMPAKTLASKVQVTVPTDT

                            120       130       140       150       160       170
S.aureus_N315_Cap5A       QLINIQVKSGHKQDSEKIANSFAKVTSKQIPKIMSVDNVSILSKADGTA..VKVAPKTVV
B.subtilis_168_TkmA       QVVNISVRDENAETAAHIANTIASVFQDKITSIMNVDNVSILSKAEVSEHPSPVSPKPLL
S.pneumoniae_D39_Cps4C    RIVSISVKDKQPEEASRIANSLREVAVEKIVAVTRVSDVTTLEEARPAT..TPSSPNVRR

                            180       190       200       210       220
S.aureus_N315_Cap5A       NLIGAFFLGLVVALIYIFFKVIFDKRIKDEEDVEKELGLPVLGSIQKFN..........
B.subtilis_168_TkmA       NIAIAFAAGLAGSIGLAFLLEHLDNTIKSEEQLESLLDIPVLGTVSTIANEQKTAKTLQG
S.pneumoniae_D39_Cps4C    NSLFGFLGGAVVTVIAVLLIELFDTRVKRPEDIEDVLQIPLLGLVPDLDKMK.......

S.aureus_N315_Cap5A       .............
B.subtilis_168_TkmA       FQSEKTGSGHFGA
S.pneumoniae_D39_Cps4C    .............
```

Figure 61: Amino acid sequence analysis of *S. aureus* N315 CapA1. Sequence alignment of *S. aureus* N315 CapA1 (Uniprot accession A0A0H3JSH5) with *B. subtilis* 168 TkmA (A0A6M3ZHD8) and *S. pneumoniae* D39 CpsC (Q9ZII7). Conserved residues among all three sequences are highlighted in red. Similarities are framed by blue boxes. The sequence identity scores against CapA1 from *S. aureus* N315 were 37.61% (*B. subtilis* 168 TkmA) and 30.00% (*S. pneumoniae* D39 CpsC), respectively. Figure was generated using the ESPript 3 server (Robert *et al*., 2014).

6. References

Adachi M, Zhang Y, Leimkuhler C, Sun B, LaTour JV, Kahne DE. Degradation and reconstruction of moenomycin A and derivatives: dissecting the function of the isoprenoid chain. J Am Chem Soc. 2006 Nov 1;128(43):14012-3.

American Academy of Pediatrics. 2006 Red Book: Report of the Committee on Infectious Diseases. 27th ed. Elk Grove Village, IL: American Academy of Pediatrics; 2006.

Andersen KR, Leksa NC, Schwartz TU. Optimized E. coli expression strain LOBSTR eliminates common contaminants from His-tag purification. Proteins. 2013 Nov;81(11):1857-61.

Anikin A, Buchynskyy A, Kempin U, Stembera K, Welzel P, Lantzsch G. Membrane Anchoring and Intervesicle Transfer of a Derivative of the Antibiotic Moenomycin A. Angew Chem Int Ed Engl. 1999 Dec 16;38(24):3703-3707.

Antignac A, Sieradzki K, Tomasz A. Perturbation of cell wall synthesis suppresses autolysis in Staphylococcus aureus: evidence for coregulation of cell wall synthetic and hydrolytic enzymes. J Bacteriol. 2007 Nov;189(21):7573-80.

Antimicrobial Resistance Collaborators. Global burden of bacterial antimicrobial resistance in 2019: a systematic analysis. Lancet. 2022 Feb 12;399(10325):629-655.

Araki Y, Ito E. Linkage units in cell walls of gram-positive bacteria. Crit Rev Microbiol. 1989;17(2):121-35.

Arenas T, Osorio A, Ginez LD, Camarena L, Poggio S. Bacterial cell wall quantification by a modified low-volume Nelson-Somogyi method and its use with different sugars. Can J Microbiol. 2022 Apr;68(4):295-302.

Arias Del Angel JA, Escalante AE, Martínez-Castilla LP, Benítez M. An evo-devo perspective on multicellular development of myxobacteria. J Exp Zool B Mol Dev Evol. 2017;328(1–2):165–178.

Artsimovitch I, Seddon J, Sears P. Fidaxomicin is an inhibitor of the initiation of bacterial RNA synthesis. Clin Infect Dis. 2012 Aug;55 Suppl 2(Suppl 2):S127-31.

Atilano ML, Pereira PM, Yates J, Reed P, Veiga H, Pinho MG, Filipe SR. Teichoic acids are temporal and spatial regulators of peptidoglycan cross-linking in Staphylococcus aureus. Proc Natl Acad Sci U S A. 2010 Nov 2;107(44):18991-6.

Attaibi M, den Blaauwen T. An Updated Model of the Divisome: Regulation of the Septal Peptidoglycan Synthesis Machinery by the Divisome. Int J Mol Sci. 2022 Mar 24;23(7):3537.

Baddiley J, Buchanan JG, Martin RO, Rajbhandary UL. Teichoic acid from the walls of Staphylococcus aureus H. 2. Location of phosphate and alanine residues. Biochem J. 1962 Oct;85(1):49-56.

Badurina DS, Zolli-Juran M, Brown ED. CTP:glycerol 3-phosphate cytidylyltransferase (TarD) from Staphylococcus aureus catalyzes the cytidylyl transfer via an ordered Bi-Bi reaction mechanism with micromolar K(m) values. Biochim Biophys Acta. 2003 Mar 21;1646(1-2):196-206.

Baizman ER, Branstrom AA, Longley CB, Allanson N, Sofia MJ, Gange D, Goldman RC. Antibacterial activity of synthetic analogues based on the disaccharide structure of moenomycin, an inhibitor of bacterial transglycosylase. Microbiology (Reading). 2000 Dec;146 Pt 12:3129-3140.

Ballhausen B, Kriegeskorte A, Schleimer N, Peters G, Becker K. The mecA homolog mecC confers resistance against β-lactams in Staphylococcus aureus irrespective of the genetic strain background. Antimicrob Agents Chemother. 2014 Jul;58(7):3791-8.

Barna JC, Williams DH. The structure and mode of action of glycopeptide antibiotics of the vancomycin group. Annu Rev Microbiol. 1984;38:339-57.

Barreteau H, Kovac A, Boniface A, Sova M, Gobec S, Blanot D. Cytoplasmic steps of peptidoglycan biosynthesis. FEMS Microbiol Rev. 2008 Mar;32(2):168-207.

Barreteau H, Magnet S, El Ghachi M, Touzé T, Arthur M, Mengin-Lecreulx D, Blanot D. Quantitative high-performance liquid chromatography analysis of the pool levels of undecaprenyl phosphate and its derivatives in bacterial membranes. J Chromatogr B Analyt Technol Biomed Life Sci. 2009 Jan 15;877(3):213-20.

Barreteau H, Bouhss A, Gérard F, Duché D, Boussaid B, Blanot D, Lloubès R, Mengin-Lecreulx D, Touzé T. Deciphering the catalytic domain of colicin M, a peptidoglycan lipid II-degrading enzyme. J Biol Chem. 2010 Apr 16;285(16):12378-89.

Barrett D, Leimkuhler C, Chen L, Walker D, Kahne D, Walker S. Kinetic characterization of the glycosyltransferase module of Staphylococcus aureus PBP2. J Bacteriol. 2005 Mar;187(6):2215-7.

Baumgart M, Schubert K, Bramkamp M, Frunzke J. Impact of LytR-CpsA-Psr Proteins on Cell Wall Biosynthesis in Corynebacterium glutamicum. J Bacteriol. 2016 Oct 21;198(22):3045-3059.

Belaaouaj A, Kim KS, Shapiro SD. Degradation of outer membrane protein A in Escherichia coli killing by neutrophil elastase. Science. 2000 Aug 18;289(5482):1185-8.

Belcheva A, Golemi-Kotra D. A close-up view of the VraSR two-component system. A mediator of Staphylococcus aureus response to cell wall damage. J Biol Chem. 2008 May 2;283(18):12354-64.

Belcheva A, Verma V, Korenevsky A, Fridman M, Kumar K, Golemi-Kotra D. Roles of DNA sequence and sigma A factor in transcription of the vraSR operon. J Bacteriol. 2012 Jan;194(1):61-71.

Benson TE, Marquardt JL, Marquardt AC, Etzkorn FA, Walsh CT. Overexpression, purification, and mechanistic study of UDP-N-acetylenolpyruvylglucosamine reductase. Biochemistry. 1993 Mar 2;32(8):2024-30.

Bera A, Herbert S, Jakob A, Vollmer W, Götz F. Why are pathogenic staphylococci so lysozyme resistant? The peptidoglycan O-acetyltransferase OatA is the major determinant for lysozyme resistance of Staphylococcus aureus. Mol Microbiol. 2005 Feb;55(3):778-87.

Bera A, Biswas R, Herbert S, Götz F. The presence of peptidoglycan O-acetyltransferase in various staphylococcal species correlates with lysozyme resistance and pathogenicity. Infect Immun. 2006 Aug;74(8):4598-604.

Bera A, Biswas R, Herbert S, Kulauzovic E, Weidenmaier C, Peschel A, Götz F. Influence of wall teichoic acid on lysozyme resistance in Staphylococcus aureus. J Bacteriol. 2007 Jan;189(1):280-3.

Bernal P, Zloh M, Taylor PW. Disruption of D-alanyl esterification of Staphylococcus aureus cell wall teichoic acid by the {beta}-lactam resistance modifier (-)-epicatechin gallate. J Antimicrob Chemother. 2009 Jun;63(6):1156-62.

Bhavsar AP, Truant R, Brown ED. The TagB protein in Bacillus subtilis 168 is an intracellular peripheral membrane protein that can incorporate glycerol phosphate onto a membrane-bound acceptor in vitro. J Biol Chem. 2005 Nov 4;280(44):36691-700.

Biswas R, Voggu L, Simon UK, Hentschel P, Thumm G, Götz F. Activity of the major staphylococcal autolysin Atl. FEMS Microbiol Lett. 2006 Jun;259(2):260-8.

Biswas R, Martinez RE, Göhring N, Schlag M, Josten M, Xia G, Hegler F, Gekeler C, Gleske AK, Götz F, Sahl HG, Kappler A, Peschel A. Proton-binding capacity of Staphylococcus aureus wall teichoic acid and its role in controlling autolysin activity. PLoS One. 2012;7(7):e41415.

Bitoun JP, Liao S, McKey BA, Yao X, Fan Y, Abranches J, Beatty WL, Wen ZT. Psr is involved in regulation of glucan production, and double deficiency of BrpA and Psr is lethal in Streptococcus mutans. Microbiology (Reading). 2013 Mar;159(Pt 3):493-506.

Blumberg PM, Strominger JL. Interaction of penicillin with the bacterial cell: penicillin-binding proteins and penicillin-sensitive enzymes. Bacteriol Rev. 1974 Sep;38(3):291-335.

Boes A, Olatunji S, Mohammadi T, Breukink E, Terrak M. Fluorescence anisotropy assays for high throughput screening of compounds binding to lipid II, PBP1b, FtsW and MurJ. Sci Rep. 2020 Apr 14;10(1):6280.

Bouhss A, Mengin-Lecreulx D, Blanot D, van Heijenoort J, Parquet C. Invariant amino acids in the Mur peptide synthetases of bacterial peptidoglycan synthesis and their modification by site-directed mutagenesis in the UDP-MurNAc:L-alanine ligase from Escherichia coli. Biochemistry. 1997 Sep 30;36(39):11556-63.

Bouhss A, Crouvoisier M, Blanot D, Mengin-Lecreulx D. Purification and characterization of the bacterial MraY translocase catalyzing the first membrane step of peptidoglycan biosynthesis. J Biol Chem. 2004 Jul 16;279(29):29974-80.

Bouhss A, Trunkfield AE, Bugg TD, Mengin-Lecreulx D. The biosynthesis of peptidoglycan lipid-linked intermediates. FEMS Microbiol Rev. 2008 Mar;32(2):208-33.

Bradford MM. A rapid and sensitive method for the quantitation of microgram quantities of protein utilizing the principle of protein-dye binding. Anal Biochem. 1976 May 7;72:248-54.

Brown S, Zhang YH, Walker S. A revised pathway proposed for Staphylococcus aureus wall teichoic acid biosynthesis based on in vitro reconstitution of the intracellular steps. Chem Biol. 2008 Jan;15(1):12-21.

Brown S, Meredith T, Swoboda J, Walker S. Staphylococcus aureus and Bacillus subtilis W23 make polyribitol wall teichoic acids using different enzymatic pathways. Chem Biol. 2010 Oct 29;17(10):1101-10.

Brown S, Xia G, Luhachack LG, Campbell J, Meredith TC, Chen C, Winstel V, Gekeler C, Irazoqui JE, Peschel A, Walker S. Methicillin resistance in Staphylococcus aureus requires glycosylated wall teichoic acids. Proc Natl Acad Sci U S A. 2012 Nov 13;109(46):18909-14.

Brown S, Santa Maria JP Jr, Walker S. Wall teichoic acids of gram-positive bacteria. Annu Rev Microbiol. 2013;67:313-36.

Brumfitt W, Hamilton-Miller J. Methicillin-resistant Staphylococcus aureus. N Engl J Med. 1989 May 4;320(18):1188-96.

Bui NK, Eberhardt A, Vollmer D, Kern T, Bougault C, Tomasz A, Simorre JP, Vollmer W. Isolation and analysis of cell wall components from Streptococcus pneumoniae. Anal Biochem. 2012 Feb 15;421(2):657-66.

Büttner FM, Zoll S, Nega M, Götz F, Stehle T. Structure-function analysis of Staphylococcus aureus amidase reveals the determinants of peptidoglycan recognition and cleavage. J Biol Chem. 2014 Apr 18;289(16):11083-11094.

Campbell EA, Korzheva N, Mustaev A, Murakami K, Nair S, Goldfarb A, Darst SA. Structural mechanism for rifampicin inhibition of bacterial rna polymerase. Cell. 2001 Mar 23;104(6):901-12.

Campbell J, Singh AK, Santa Maria JP Jr, Kim Y, Brown S, Swoboda JG, Mylonakis E, Wilkinson BJ, Walker S. Synthetic lethal compound combinations reveal a fundamental connection between wall teichoic acid and peptidoglycan biosyntheses in Staphylococcus aureus. ACS Chem Biol. 2011 Jan 21;6(1):106-16.

Campbell J, Singh AK, Swoboda JG, Gilmore MS, Wilkinson BJ, Walker S. An antibiotic that inhibits a late step in wall teichoic acid biosynthesis induces the cell wall stress stimulon in Staphylococcus aureus. Antimicrob Agents Chemother. 2012 Apr;56(4):1810-20.

Campos MA, Vargas MA, Regueiro V, Llompart CM, Albertí S, Bengoechea JA. Capsule polysaccharide mediates bacterial resistance to antimicrobial peptides. Infect Immun. 2004 Dec;72(12):7107-14.

Cegelski L, Kim SJ, Hing AW, Studelska DR, O'Connor RD, Mehta AK, Schaefer J. Rotational-echo double resonance characterization of the effects of vancomycin on cell wall synthesis in Staphylococcus aureus. Biochemistry. 2002 Oct 29;41(43):13053-8.

Centers for Disease Control and Prevention (CDC). Update: Investigation of bioterrorism-related anthrax and interim guidelines for exposure management and antimicrobial therapy, October 2001. MMWR Morb Mortal Wkly Rep. 2001 Oct 26;50(42):909-19. Erratum in: MMWR Morb Mortal Wkly Rep 2001 Nov 2;50(43):962.

Chakraborty A, Wang D, Ebright YW, Korlann Y, Kortkhonjia E, Kim T, Chowdhury S, Wigneshweraraj S, Irschik H, Jansen R, Nixon BT, Knight J, Weiss S, Ebright RH. Opening and closing of the bacterial RNA polymerase clamp. Science. 2012 Aug 3;337(6094):591-5.

Chambers HF, Sachdeva M. Binding of beta-lactam antibiotics to penicillin-binding proteins in methicillin-resistant Staphylococcus aureus. J Infect Dis. 1990 Jun;161(6):1170-6.

Chambers HF, Deleo FR. Waves of resistance: Staphylococcus aureus in the antibiotic era. Nat Rev Microbiol. 2009 Sep;7(9):629-41.

Chan YG, Frankel MB, Dengler V, Schneewind O, Missiakas D. Staphylococcus aureus mutants lacking the LytR-CpsA-Psr family of enzymes release cell wall teichoic acids into the extracellular medium. J Bacteriol. 2013 Oct;195(20):4650-9.

Chan YG, Kim HK, Schneewind O, Missiakas D. The capsular polysaccharide of Staphylococcus aureus is attached to peptidoglycan by the LytR-CpsA-Psr (LCP) family of enzymes. J Biol Chem. 2014 May 30;289(22):15680-90.

Chatterjee AN. Use of bacteriophage-resistant mutants to study the nature of the bacteriophage receptor site of Staphylococcus aureus. J Bacteriol. 1969 May;98(2):519-27.

Chaudhuri RR, Allen AG, Owen PJ, Shalom G, Stone K, Harrison M, Burgis TA, Lockyer M, Garcia-Lara J, Foster SJ, Pleasance SJ, Peters SE, Maskell DJ, Charles IG. Comprehensive identification of essential Staphylococcus aureus genes using Transposon-Mediated Differential Hybridisation (TMDH). BMC Genomics. 2009 Jul 1;10:291.

Chen CJ, Huang YC, Chiu CH. Multiple pathways of cross-resistance to glycopeptides and daptomycin in persistent MRSA bacteraemia. J Antimicrob Chemother. 2015 Nov;70(11):2965-72.

Chen L, Walker D, Sun B, Hu Y, Walker S, Kahne D. Vancomycin analogues active against vanA-resistant strains inhibit bacterial transglycosylase without binding substrate. Proc Natl Acad Sci U S A. 2003 May 13;100(10):5658-63.

Cheng TJ, Sung MT, Liao HY, Chang YF, Chen CW, Huang CY, Chou LY, Wu YD, Chen YH, Cheng YS, Wong CH, Ma C, Cheng WC. Domain requirement of moenomycin binding to bifunctional transglycosylases and development of high-throughput discovery of antibiotics. Proc Natl Acad Sci U S A. 2008 Jan 15;105(2):431-6.

Chevance FF, Hughes KT. Coordinating assembly of a bacterial macromolecular machine. Nat Rev Microbiol. 2008 Jun;6(6):455-65.

Chiriac AI, Kloss F, Krämer J, Vuong C, Hertweck C, Sahl HG. Mode of action of closthioamide: the first member of the polythioamide class of bacterial DNA gyrase inhibitors. J Antimicrob Chemother. 2015 Sep;70(9):2576-88.

Chung BC, Zhao J, Gillespie RA, Kwon DY, Guan Z, Hong J, Zhou P, Lee SY. Crystal structure of MraY, an essential membrane enzyme for bacterial cell wall synthesis. Science. 2013 Aug 30;341(6149):1012-1016.

CLSI. Performance standards for antimicrobial susceptibility testing. In: CLSI supplement M100. 29th ed. Wayne PA: Clinical and Laboratory Standards Institute; 2019.

Collins LV, Kristian SA, Weidenmaier C, Faigle M, Van Kessel KP, Van Strijp JA, Götz F, Neumeister B, Peschel A. Staphylococcus aureus strains lacking D-alanine modifications of teichoic acids are highly susceptible to human neutrophil killing and are virulence attenuated in mice. J Infect Dis. 2002 Jul 15;186(2):214-9.

da Costa TM, de Oliveira CR, Chambers HF, Chatterjee SS. PBP4: A New Perspective on Staphylococcus aureus β-Lactam Resistance. Microorganisms. 2018 Jun 22;6(3):57.

de Jonge BL, Chang YS, Gage D, Tomasz A (1992): Peptidoglycan composition of a highly methicillin-resistant Staphylococcus aureus strain. The role of penicillin binding protein 2A. J Biol Chem. 1992 Jun 5;267(16):11248-54.

Delcour AH. Outer membrane permeability and antibiotic resistance. Biochim Biophys Acta. 2009 May;1794(5):808-16.

D'Elia MA, Pereira MP, Chung YS, Zhao W, Chau A, Kenney TJ, Sulavik MC, Black TA, Brown ED. Lesions in teichoic acid biosynthesis in Staphylococcus aureus lead to a lethal gain of function in the otherwise dispensable pathway. J Bacteriol. 2006a Jun;188(12):4183-9.

D'Elia MA, Millar KE, Beveridge TJ, Brown ED. Wall teichoic acid polymers are dispensable for cell viability in Bacillus subtilis. J Bacteriol. 2006b Dec;188(23):8313-6.

D'Elia MA, Millar KE, Bhavsar AP, Tomljenovic AM, Hutter B, Schaab C, Moreno-Hagelsieb G, Brown ED. Probing teichoic acid genetics with bioactive molecules reveals new interactions among diverse processes in bacterial cell wall biogenesis. Chem Biol. 2009a May 29;16(5):548-56.

D'Elia MA, Henderson JA, Beveridge TJ, Heinrichs DE, Brown ED. The N-acetylmannosamine transferase catalyzes the first committed step of teichoic acid assembly in Bacillus subtilis and Staphylococcus aureus. J Bacteriol. 2009b Jun;191(12):4030-4.

Dengler V, Meier PS, Heusser R, Berger-Bächi B, McCallum N. Induction kinetics of the Staphylococcus aureus cell wall stress stimulon in response to different cell wall active antibiotics. BMC Microbiol. 2011 Jan 20;11:16.

Dengler V, Meier PS, Heusser R, Kupferschmied P, Fazekas J, Friebe S, Staufer SB, Majcherczyk PA, Moreillon P, Berger-Bächi B, McCallum N. Deletion of hypothetical wall teichoic acid ligases in Staphylococcus aureus activates the cell wall stress response. FEMS Microbiol Lett. 2012 Aug;333(2):109-20.

Dietrich A, Steffens U, Sass P, Bierbaum G. The hypersusceptible antibiotic screening strain Staphylococcus aureus SG511-Berlin harbors multiple mutations in regulatory genes. Int J Med Microbiol. 2021 Dec;311(8):151545.

Donald RG, Skwish S, Forsyth RA, Anderson JW, Zhong T, Burns C, Lee S, Meng X, LoCastro L, Jarantow LW, Martin J, Lee SH, Taylor I, Robbins D, Malone C, Wang L, Zamudio CS, Youngman PJ, Phillips JW. A Staphylococcus aureus fitness test platform for mechanism-based profiling of antibacterial compounds. Chem Biol. 2009 Aug 28;16(8):826-36.

Dramsi S, Magnet S, Davison S, Arthur M. Covalent attachment of proteins to peptidoglycan. FEMS Microbiol Rev. 2008 Mar;32(2):307-20.

Dreckmann T, Wirtz DA, Fritz L, Kaiser CF, Bouhired SM, Schneider T, Koenig GM, Cruesemann M. Biosynthesis of the corallorazines, a widespread class of antibiotic cyclic lipodipeptides. In preparation.

Du X, Larsen J, Li M, Walter A, Slavetinsky C, Both A, Sanchez Carballo PM, Stegger M, Lehmann E, Liu Y, Liu J, Slavetinsky J, Duda KA, Krismer B, Heilbronner S, Weidenmaier C, Mayer C, Rohde H, Winstel V, Peschel A. Staphylococcus epidermidis clones express Staphylococcus aureus-type wall teichoic acid to shift from a commensal to pathogen lifestyle. Nat Microbiol. 2021 Jun;6(6):757-768.

Dutescu IA, Hillier SA. Encouraging the Development of New Antibiotics: Are Financial Incentives the Right Way Forward? A Systematic Review and Case Study. Infect Drug Resist. 2021 Feb 5;14:415-434.

Duthie ES, Lorenz LL. Staphylococcal coagulase; mode of action and antigenicity. J Gen Microbiol. 1952 Feb;6(1-2):95-107.

Dyke KG, Jevons MP, Parker MT. Penicillinase production and intrinsic resistance to penicillins in Staphylococcus aures. Lancet. 1966 Apr 16;1(7442):835-8.

Eberhardt A, Hoyland CN, Vollmer D, Bisle S, Cleverley RM, Johnsborg O, Håvarstein LS, Lewis RJ, Vollmer W. Attachment of capsular polysaccharide to the cell wall in Streptococcus pneumoniae. Microb Drug Resist. 2012 Jun;18(3):240-55.

Ebright RH. RNA polymerase: structural similarities between bacterial RNA polymerase and eukaryotic RNA polymerase II. J Mol Biol. 2000 Dec 15;304(5):687-98.

Economou NJ, Cocklin S, Loll PJ. High-resolution crystal structure reveals molecular details of target recognition by bacitracin. Proc Natl Acad Sci U S A. 2013 Aug 27;110(35):14207-12.

Egan AJF, Errington J, Vollmer W. Regulation of peptidoglycan synthesis and remodelling. Nat Rev Microbiol. 2020 Aug;18(8):446-460.

El Ghachi M, Bouhss A, Blanot D, Mengin-Lecreulx D. The bacA gene of Escherichia coli encodes an undecaprenyl pyrophosphate phosphatase activity. J Biol Chem. 2004 Jul 16;279(29):30106-13.

El Ghachi M, Derbise A, Bouhss A, Mengin-Lecreulx D. Identification of multiple genes encoding membrane proteins with undecaprenyl pyrophosphate phosphatase (UppP) activity in Escherichia coli. J Biol Chem. 2005 May 13;280(19):18689-95.

Ellwood DC. The wall content and composition of Bacillus substilis var. niger grown in a chemostat. Biochem J. 1970 Jul;118(3):367-73.

Endl J, Seidl PH, Fiedler F, Schleifer KH. Determination of cell wall teichoic acid structure of staphylococci by rapid chemical and serological screening methods. Arch Microbiol. 1984 Mar;137(3):272-80.

Entenza JM, Vouillamoz J, Glauser MP, Moreillon P. Levofloxacin versus ciprofloxacin, flucloxacillin, or vancomycin for treatment of experimental endocarditis due to methicillin-susceptible or -resistant Staphylococcus aureus. Antimicrob Agents Chemother. 1997 Aug;41(8):1662-7.

Eswara PJ, Brzozowski RS, Viola MG, Graham G, Spanoudis C, Trebino C, Jha J, Aubee JI, Thompson KM, Camberg JL, Ramamurthi KS. An essential Staphylococcus aureus cell division protein directly regulates FtsZ dynamics. Elife. 2018 Oct 2;7:e38856.

EUCAST Definitive Document Methods for the determination of susceptibility of bacteria to antimicrobial agents. Terminology. Clin Microbiol Infect. 1998 May;4(5):291.

Fang X, Tiyanont K, Zhang Y, Wanner J, Boger D, Walker S. The mechanism of action of ramoplanin and enduracidin. Mol Biosyst. 2006 Jan;2(1):69-76.

Farha MA, Leung A, Sewell EW, D'Elia MA, Allison SE, Ejim L, Pereira PM, Pinho MG, Wright GD, Brown ED. Inhibition of WTA synthesis blocks the cooperative action of PBPs and sensitizes MRSA to β-lactams. ACS Chem Biol. 2013 Jan 18;8(1):226-33.

Figueiredo TA, Sobral RG, Ludovice AM, Almeida JM, Bui NK, Vollmer W, de Lencastre H, Tomasz A. Identification of genetic determinants and enzymes involved with the amidation of glutamic acid residues in the peptidoglycan of Staphylococcus aureus. PLoS Pathog. 2012 Jan;8(1):e1002508.

Finland M. Emergence of antibiotic-resistant bacteria. N Engl J Med. 1955 Nov 24;253(21):909-22; contd.

Fisher LM, Lawrence JM, Josty IC, Hopewell R, Margerrison EE, Cullen ME. Ciprofloxacin and the fluoroquinolones. New concepts on the mechanism of action and resistance. Am J Med. 1989 Nov 30;87(5A):2S-8S.

Flores-Kim J, Dobihal GS, Fenton A, Rudner DZ, Bernhardt TG. A switch in surface polymer biogenesis triggers growth-phase-dependent and antibiotic-induced bacteriolysis. Elife. 2019 Apr 9;8:e44912.

Formstone A, Carballido-López R, Noirot P, Errington J, Scheffers DJ. Localization and interactions of teichoic acid synthetic enzymes in Bacillus subtilis. J Bacteriol. 2008 Mar;190(5):1812-21.

Forsyth RA, Haselbeck RJ, Ohlsen KL, Yamamoto RT, Xu H, Trawick JD, Wall D, Wang L, Brown-Driver V, Froelich JM, C KG, King P, McCarthy M, Malone C, Misiner B, Robbins D, Tan Z, Zhu Zy ZY, Carr G, Mosca DA, Zamudio C, Foulkes JG, Zyskind JW. A genome-wide strategy for the identification of essential genes in Staphylococcus aureus. Mol Microbiol. 2002 Mar;43(6):1387-400.

Foster TJ. Antibiotic resistance in Staphylococcus aureus. Current status and future prospects. FEMS Microbiol Rev. 2017 May 1;41(3):430-449.

Frankel MB, Schneewind O. Determinants of murein hydrolase targeting to cross-wall of Staphylococcus aureus peptidoglycan. J Biol Chem. 2012 Mar 23;287(13):10460-10471.

Fuse S, Tsukamoto H, Yuan Y, Wang TS, Zhang Y, Bolla M, Walker S, Sliz P, Kahne D. Functional and structural analysis of a key region of the cell wall inhibitor moenomycin. ACS Chem Biol. 2010 Jul 16;5(7):701-11.

Gale RT, Li FKK, Sun T, Strynadka NCJ, Brown ED. B. subtilis LytR-CpsA-Psr Enzymes Transfer Wall Teichoic Acids from Authentic Lipid-Linked Substrates to Mature Peptidoglycan In Vitro. Cell Chem Biol. 2017 Dec 21;24(12):1537-1546.e4.

Gallo P, Fabbrocino S, Serpe L, Fiori M, Civitareale C, Stacchini P. Determination of the banned growth promoter moenomycin A in feed stuffs by liquid chromatography coupled to electrospray ion trap mass spectrometry. Rapid Commun Mass Spectrom. 2010 Apr 15;24(7):1017-24.

Gampe CM, Tsukamoto H, Doud EH, Walker S, Kahne D. Tuning the moenomycin pharmacophore to enable discovery of bacterial cell wall synthesis inhibitors. J Am Chem Soc. 2013 Mar 13;135(10):3776-9.

Gao T, Greenwich J, Li Y, Wang Q, Chai Y. The Bacterial Tyrosine Kinase Activator TkmA Contributes to Biofilm Formation Largely Independently of the Cognate Kinase PtkA in Bacillus subtilis. J Bacteriol. 2015 Nov;197(21):3421-32.

Gautam S, Kim T, Spiegel DA. Chemical probes reveal an extraseptal mode of cross-linking in Staphylococcus aureus. J Am Chem Soc. 2015 Jun 17;137(23):7441-7.

Gerlach D, Guo Y, De Castro C, Kim SH, Schlatterer K, Xu FF, Pereira C, Seeberger PH, Ali S, Codée J, Sirisarn W, Schulte B, Wolz C, Larsen J, Molinaro A, Lee BL, Xia G, Stehle T, Peschel A. Methicillin-resistant Staphylococcus aureus alters cell wall glycosylation to evade immunity. Nature. 2018 Nov;563(7733):705-709.

Ghuysen JM, Strominger JL. Structure of the cell wall of Staphylococcus aureus, strain Copenhagen. II. Separation and structure of disaccharides. Biochemistry. 1963 Sep-Oct;2:1119-25.

Ginsberg C, Zhang YH, Yuan Y, Walker S. In vitro reconstitution of two essential steps in wall teichoic acid biosynthesis. ACS Chem Biol. 2006 Feb 17;1(1):25-8.

Glauner B, Höltje JV, Schwarz U. The composition of the murein of Escherichia coli. J Biol Chem. 1988 Jul 25;263(21):10088-95.

Glauner B. Separation and quantification of muropeptides with high-performance liquid chromatography. Anal Biochem. 1988 Aug 1;172(2):451-64.

Goffin C, Ghuysen JM. Multimodular penicillin-binding proteins: an enigmatic family of orthologs and paralogs. Microbiol Mol Biol Rev. 1998 Dec;62(4):1079-93.

Goldstein BP. Resistance to rifampicin: a review. J Antibiot (Tokyo). 2014 Sep;67(9):625-30.

Goldstein EJ, Babakhani F, Citron DM. Antimicrobial activities of fidaxomicin. Clin Infect Dis. 2012 Aug;55 Suppl 2(Suppl 2):S143-8.

Graumann PL. Dynamics of bacterial cytoskeletal elements. Cell Motil Cytoskeleton. 2009 Nov;66(11):909-14.

Graves-Woodward K, Pratt RF. Interactions of soluble penicillin-binding protein 2a of methicillin-resistant Staphylococcus aureus with moenomycin. Biochemistry. 1999 Aug 10;38(32):10533-42.

Gross M, Cramton SE, Götz F, Peschel A. Key role of teichoic acid net charge in Staphylococcus aureus colonization of artificial surfaces. Infect Immun. 2001 May;69(5):3423-6.

Gruber TM, Gross CA. Multiple sigma subunits and the partitioning of bacterial transcription space. Annu Rev Microbiol. 2003;57:441-66.

Grzegorzewicz AE, de Sousa-d'Auria C, McNeil MR, Huc-Claustre E, Jones V, Petit C, Angala SK, Zemanová J, Wang Q, Belardinelli JM, Gao Q, Ishizaki Y, Mikušová K, Brennan PJ, Ronning DR, Chami M, Houssin C, Jackson M. Assembling of the Mycobacterium tuberculosis Cell Wall Core. J Biol Chem. 2016 Sep 2;291(36):18867-79.

Guo Y, Song G, Sun M, Wang J, Wang Y. Prevalence and Therapies of Antibiotic-Resistance in Staphylococcus aureus. Front Cell Infect Microbiol. 2020 Mar 17;10:107.

Guo Y. Be Cautious with Crystal Structures of Membrane Proteins or Complexes Prepared in Detergents. Crystals (Basel). 2020 Feb;10(2):86.

Halbedel S, Lewis RJ. Structural basis for interaction of DivIVA/GpsB proteins with their ligands. Mol Microbiol. 2019 Jun;111(6):1404-1415.

Hall MJ, Middleton RF, Westmacott D. The fractional inhibitory concentration (FIC) index as a measure of synergy. J Antimicrob Chemother. 1983 May;11(5):427-33.

Halliday J, McKeveney D, Muldoon C, Rajaratnam P, Meutermans W. Targeting the forgotten transglycosylases. Biochem Pharmacol. 2006 Mar 30;71(7):957-67.

Hammond LR, White ML, Eswara PJ. ¡vIVA la DivIVA! J Bacteriol. 2019 Oct 4;201(21):e00245-19.

Hammond LR, Sacco MD, Khan SJ, Spanoudis C, Hough-Neidig A, Chen Y, Eswara PJ. GpsB Coordinates Cell Division and Cell Surface Decoration by Wall Teichoic Acids in Staphylococcus aureus. Microbiol Spectr. 2022 Jun 29;10(3):e0141322.

Hanson BR, Runft DL, Streeter C, Kumar A, Carion TW, Neely MN. Functional analysis of the CpsA protein of Streptococcus agalactiae. J Bacteriol. 2012 Apr;194(7):1668-78.

Hardesty JS, Juang P. Fidaxomicin: a macrocyclic antibiotic for the treatment of Clostridium difficile infection. Pharmacotherapy. 2011 Sep;31(9):877-86.

Harms H, Klöckner A, Schrör J, Josten M, Kehraus S, Crüsemann M, Hanke W, Schneider T, Schäberle TF, König GM. Antimicrobial Dialkylresorcins from Marine-Derived Microorganisms: Insights into Their Mode of Action and Putative Ecological Relevance. Planta Med. 2018 Dec;84(18):1363-1371.

Harrison J, Lloyd G, Joe M, Lowary TL, Reynolds E, Walters-Morgan H, Bhatt A, Lovering A, Besra GS, Alderwick LJ. Lcp1 Is a Phosphotransferase Responsible for Ligating Arabinogalactan to Peptidoglycan in Mycobacterium tuberculosis. mBio. 2016 Aug 2;7(4):e00972-16.

Harry W. Lewis & Christopher J. Moody (13 Jun 1989). Experimental Organic Chemistry: Principles and Practice (Illustrated ed.). WileyBlackwell. pp. 159–173. ISBN 9780632020171.

Hartman BJ, Tomasz A. Low-affinity penicillin-binding protein associated with beta-lactam resistance in Staphylococcus aureus. J Bacteriol. 1984 May;158(2):513-6.

Hayashi K. A rapid determination of sodium dodecyl sulfate with methylene blue. Anal Biochem. 1975 Aug;67(2):503-6.

Healy VL, Lessard IA, Roper DI, Knox JR, Walsh CT. Vancomycin resistance in enterococci: reprogramming of the D-ala-D-Ala ligases in bacterial peptidoglycan biosynthesis. Chem Biol. 2000 May;7(5):R109-19.

Heaslet H, Shaw B, Mistry A, Miller AA. Characterization of the active site of S. aureus monofunctional glycosyltransferase (Mtg) by site-directed mutation and structural analysis of the protein complexed with moenomycin. J Struct Biol. 2009 Aug;167(2):129-35.

Heilmann C, Hussain M, Peters G, Götz F. Evidence for autolysin-mediated primary attachment of Staphylococcus epidermidis to a polystyrene surface. Mol Microbiol. 1997 Jun;24(5):1013-24.

Henze U, Sidow T, Wecke J, Labischinski H, Berger-Bächi B. Influence of femB on methicillin resistance and peptidoglycan metabolism in Staphylococcus aureus. J Bacteriol. 1993 Mar;175(6):1612-20.

Henze UU, Berger-Bächi B. Staphylococcus aureus penicillin-binding protein 4 and intrinsic beta-lactam resistance. Antimicrob Agents Chemother. 1995 Nov;39(11):2415-22.

Heptinstall S, Archibald AR, Baddiley J. Teichoic acids and membrane function in bacteria. Nature. 1970 Feb 7;225(5232):519-21.

Herbert S, Ziebandt AK, Ohlsen K, Schäfer T, Hecker M, Albrecht D, Novick R, Götz F. Repair of global regulators in Staphylococcus aureus 8325 and comparative analysis with other clinical isolates. Infect Immun. 2010 Jun;78(6):2877-89.

Heß N, Waldow F, Kohler TP, Rohde M, Kreikemeyer B, Gómez-Mejia A, Hain T, Schwudke D, Vollmer W, Hammerschmidt S, Gisch N. Lipoteichoic acid deficiency permits normal growth but impairs virulence of Streptococcus pneumoniae. Nat Commun. 2017 Dec 12;8(1):2093.

Höltje JV. Growth of the stress-bearing and shape-maintaining murein sacculus of Escherichia coli. Microbiol Mol Biol Rev. 1998 Mar;62(1):181-203.

Howden BP, Davies JK, Johnson PD, Stinear TP, Grayson ML. Reduced vancomycin susceptibility in Staphylococcus aureus, including vancomycin-intermediate and heterogeneous vancomycin-intermediate strains: resistance mechanisms, laboratory detection, and clinical implications. Clin Microbiol Rev. 2010 Jan;23(1):99-139.

Howlett AC. The cannabinoid receptors. Prostaglandins Other Lipid Mediat. 2002 Aug;68-69:619-31.

Hsieh PY, Meng FC, Guo CW, Hu KH, Shih YL, Cheng WC. Harnessing Fluorescent Moenomycin A Antibiotics for Bacterial Cell Wall Imaging Studies. Chembiochem. 2021 Dec 10;22(24):3462-3468.

Hu Y, Chen L, Ha S, Gross B, Falcone B, Walker D, Mokhtarzadeh M, Walker S. Crystal structure of the MurG:UDP-GlcNAc complex reveals common structural principles of a superfamily of glycosyltransferases. Proc Natl Acad Sci U S A. 2003 Feb 4;100(3):845-9.

Huang CY, Shih HW, Lin LY, Tien YW, Cheng TJ, Cheng WC, Wong CH, Ma C. Crystal structure of Staphylococcus aureus transglycosylase in complex with a lipid II analog and elucidation of peptidoglycan synthesis mechanism. Proc Natl Acad Sci U S A. 2012 Apr 24;109(17):6496-501.

Huber G, Schacht U, Weidenmüller HL, Schmidt-Thomé J, Duphorn J, Tschesche R. Meonomycin, a new antibiotic. II. Characterization and chemistry. Antimicrob Agents Chemother (Bethesda). 1965;5:737-42.

Hübscher J, Lüthy L, Berger-Bächi B, Stutzmann Meier P. Phylogenetic distribution and membrane topology of the LytR-CpsA-Psr protein family. BMC Genomics. 2008 Dec 19;9:617.

Hübscher J, McCallum N, Sifri CD, Majcherczyk PA, Entenza JM, Heusser R, Berger-Bächi B, Stutzmann Meier P. MsrR contributes to cell surface characteristics and virulence in Staphylococcus aureus. FEMS Microbiol Lett. 2009 Jun;295(2):251-60.

Inoue A, Murata Y, Takahashi H, Tsuji N, Fujisaki S, Kato J. Involvement of an essential gene, mviN, in murein synthesis in Escherichia coli. J Bacteriol. 2008 Nov;190(21):7298-301.

International Standard. ISO 20776-1. Susceptibility Testing of Infectious Agents and Evaluation of Performance of Antimicrobial Susceptibility Test Devices—Part 1: Broth Micro-Dilution Reference Method for Testing the In Vitro Activity of Antimicrobial AGENTS Against Rapidly Growing Aerobic Bacteria Involved in Infectious Diseases. 2nd ed. International Organization for Standardization; Geneva, Switzerland: 2019

.

Iordanescu S, Surdeanu M. Two restriction and modification systems in Staphylococcus aureus NCTC8325. J Gen Microbiol. 1976 Oct;96(2):277-81.

Irschik H, Jansen R, Höfle G, Gerth K, Reichenbach H. The corallopyronins, new inhibitors of bacterial RNA synthesis from Myxobacteria. J Antibiot (Tokyo). 1985 Feb;38(2):145-52.

Jousselin A, Manzano C, Biette A, Reed P, Pinho MG, Rosato AE, Kelley WL, Renzoni A. The Staphylococcus aureus Chaperone PrsA Is a New Auxiliary Factor of Oxacillin Resistance Affecting Penicillin-Binding Protein 2A. Antimicrob Agents Chemother. 2015 Dec 28;60(3):1656-66.

Jumper J, Evans R, Pritzel A, Green T, Figurnov M, Ronneberger O, Tunyasuvunakool K, Bates R, Žídek A, Potapenko A, Bridgland A, Meyer C, Kohl SAA, Ballard AJ, Cowie A, Romera-Paredes B, Nikolov S, Jain R, Adler J, Back T, Petersen S, Reiman D, Clancy E, Zielinski M, Steinegger M, Pacholska M, Berghammer T, Bodenstein S, Silver D, Vinyals O, Senior AW, Kavukcuoglu K, Kohli P, Hassabis D. Highly accurate protein structure prediction with AlphaFold. Nature. 2021 Aug;596(7873):583-589.

Kanoh K, Kohno S, Asari T, Harada T, Katada J, Muramatsu M, Kawashima H, Sekiya H, Uno I. (−)-Phenylahistin: A new mammalian cell cycle inhibitor produced by aspergillus ustus. Bioorganic & Medicinal Chemistry Letters 7 (1997): 2847-2852.

Kanoh K, Kohno S, Katada J, Takahashi J, Uno I. (-)-Phenylahistin arrests cells in mitosis by inhibiting tubulin polymerization. J Antibiot (Tokyo). 1999 Feb;52(2):134-41.

Kato J, Fujisaki S, Nakajima K, Nishimura Y, Sato M, Nakano A. The Escherichia coli homologue of yeast RER2, a key enzyme of dolichol synthesis, is essential for carrier lipid formation in bacterial cell wall synthesis. J Bacteriol. 1999 May;181(9):2733-8.

Kawai Y, Marles-Wright J, Cleverley RM, Emmins R, Ishikawa S, Kuwano M, Heinz N, Bui NK, Hoyland CN, Ogasawara N, Lewis RJ, Vollmer W, Daniel RA, Errington J. A widespread family of bacterial cell wall assembly proteins. EMBO J. 2011 Sep 30;30(24):4931-41.

Kern T, Giffard M, Hediger S, Amoroso A, Giustini C, Bui NK, Joris B, Bougault C, Vollmer W, Simorre JP. Dynamics characterization of fully hydrated bacterial cell walls by solid-state NMR: evidence for cooperative binding of metal ions. J Am Chem Soc. 2010 Aug 11;132(31):10911-9.

Kim JO, Weiser JN. Association of intrastrain phase variation in quantity of capsular polysaccharide and teichoic acid with the virulence of Streptococcus pneumoniae. J Infect Dis. 1998 Feb;177(2):368-77.

King BF, Wilkinson BJ. Binding of human immunoglobulin G to protein A in encapsulated Staphylococcus aureus. Infect Immun. 1981 Sep;33(3):666-72.

Kirsch SH, Haeckl FPJ, Müller R. Beyond the approved: target sites and inhibitors of bacterial RNA polymerase from bacteria and fungi. Nat Prod Rep. 2022 Jun 22;39(6):1226-1263.

Kloos WE, Schleifer KH. Simplified scheme for routine identification of human Staphylococcus species. J Clin Microbiol. 1975 Jan;1(1):82-8.

Kobayashi K, Ehrlich SD, Albertini A, Amati G, Andersen KK, Arnaud M, Asai K, Ashikaga S, Aymerich S, Bessieres P, Boland F, Brignell SC, Bron S, Bunai K, Chapuis J, Christiansen LC, Danchin A, Débarbouille M, Dervyn E, Deuerling E, Devine K, Devine SK, Dreesen O, Errington J, Fillinger S, Foster SJ, Fujita Y, Galizzi A, Gardan R, Eschevins C, Fukushima T, Haga K, Harwood CR, Hecker M, Hosoya D, Hullo MF, Kakeshita H, Karamata D, Kasahara Y, Kawamura F, Koga K, Koski P, Kuwana R, Imamura D, Ishimaru M, Ishikawa S, Ishio I, Le Coq D, Masson A, Mauël C, Meima R, Mellado RP, Moir A, Moriya S, Nagakawa E, Nanamiya H, Nakai S, Nygaard P, Ogura M, Ohanan T, O'Reilly M, O'Rourke M, Pragai Z, Pooley HM, Rapoport G, Rawlins JP, Rivas LA, Rivolta C, Sadaie A, Sadaie Y, Sarvas M, Sato T, Saxild HH, Scanlan E, Schumann W, Seegers JF, Sekiguchi J, Sekowska A, Séror SJ, Simon M, Stragier P, Studer R, Takamatsu H, Tanaka T, Takeuchi M, Thomaides HB, Vagner V, van Dijl JM, Watabe K, Wipat A, Yamamoto H, Yamamoto M, Yamamoto Y, Yamane K, Yata K, Yoshida K, Yoshikawa H, Zuber U, Ogasawara N. Essential Bacillus subtilis genes. Proc Natl Acad Sci U S A. 2003 Apr 15;100(8):4678-83.

Koch HU, Haas R, Fischer W. The role of lipoteichoic acid biosynthesis in membrane lipid metabolism of growing Staphylococcus aureus. Eur J Biochem. 1984 Jan 16;138(2):357-63.

Koch HU, Döker R, Fischer W. Maintenance of D-alanine ester substitution of lipoteichoic acid by reesterification in Staphylococcus aureus. J Bacteriol. 1985 Dec;164(3):1211-7.

Kodali S, Galgoci A, Young K, Painter R, Silver LL, Herath KB, Singh SB, Cully D, Barrett JF, Schmatz D, Wang J. Determination of selectivity and efficacy of fatty acid synthesis inhibitors. J Biol Chem. 2005 Jan 14;280(2):1669-77.

Kojima N, Araki Y, Ito E. Structure of the linkage units between ribitol teichoic acids and peptidoglycan. J Bacteriol. 1985 Jan;161(1):299-306.

Kreiswirth BN, Löfdahl S, Betley MJ, O'Reilly M, Schlievert PM, Bergdoll MS, Novick RP. The toxic shock syndrome exotoxin structural gene is not detectably transmitted by a prophage. Nature. 1983 Oct 20-26;305(5936):709-12.

Krome AK, Becker T, Kehraus S, Schiefer A, Gütschow M, Chaverra-Muñoz L, Hüttel S, Jansen R, Stadler M, Ehrens A, Pogorevc D, Müller R, Hübner MP, Hesterkamp T, Pfarr K, Hoerauf A, Wagner KG, König GM. Corallopyronin A: antimicrobial discovery to preclinical development. Nat Prod Rep. 2022 Sep 21;39(9):1705-1720.

Kunst F, Ogasawara N, Moszer I, Albertini AM, Alloni G, Azevedo V, Bertero MG, Bessières P, Bolotin A, Borchert S, Borriss R, Boursier L, Brans A, Braun M, Brignell SC, Bron S, Brouillet S, Bruschi CV, Caldwell B, Capuano V, Carter NM, Choi SK, Cordani JJ, Connerton IF, Cummings NJ, Daniel RA, Denziot F, Devine KM, Düsterhöft A, Ehrlich SD, Emmerson PT, Entian KD, Errington J, Fabret C, Ferrari E, Foulger D, Fritz C, Fujita M, Fujita Y, Fuma S, Galizzi A, Galleron N, Ghim SY, Glaser P, Goffeau A, Golightly EJ, Grandi G, Guiseppi G, Guy BJ, Haga K, Haiech J, Harwood CR, Hènaut A, Hilbert H, Holsappel S, Hosono S, Hullo MF, Itaya M, Jones L, Joris B, Karamata D, Kasahara Y, Klaerr-Blanchard M, Klein C, Kobayashi Y, Koetter P, Koningstein G, Krogh S, Kumano M, Kurita K, Lapidus A, Lardinois S, Lauber J, Lazarevic V, Lee SM, Levine A, Liu H, Masuda S, Mauël C, Médigue C, Medina N, Mellado RP, Mizuno M, Moestl D, Nakai S, Noback M, Noone D, O'Reilly M, Ogawa K, Ogiwara A, Oudega B, Park SH, Parro V, Pohl TM, Portelle D, Porwollik S, Prescott AM, Presecan E, Pujic P, Purnelle B, Rapoport G, Rey M, Reynolds S, Rieger M, Rivolta C, Rocha E, Roche B, Rose M, Sadaie Y, Sato T, Scanlan E, Schleich S, Schroeter R, Scoffone F, Sekiguchi J, Sekowska A, Seror SJ, Serror P, Shin BS, Soldo B, Sorokin A, Tacconi E, Takagi T, Takahashi H, Takemaru K, Takeuchi M, Tamakoshi A, Tanaka T, Terpstra P, Togoni A, Tosato V, Uchiyama S, Vandebol M, Vannier F, Vassarotti A, Viari A, Wambutt R, Wedler H, Weitzenegger T, Winters P, Wipat A, Yamamoto H, Yamane K, Yasumoto K, Yata K, Yoshida K, Yoshikawa HF, Zumstein E, Yoshikawa H, Danchin A. The complete genome sequence of the gram-positive bacterium Bacillus subtilis. Nature. 1997 Nov 20;390(6657):249-56.

Kuroda M, Ohta T, Uchiyama I, Baba T, Yuzawa H, Kobayashi I, Cui L, Oguchi A, Aoki K, Nagai Y, Lian J, Ito T, Kanamori M, Matsumaru H, Maruyama A, Murakami H, Hosoyama A, Mizutani-Ui Y, Takahashi NK, Sawano T, Inoue R, Kaito C, Sekimizu K, Hirakawa H, Kuhara S, Goto S, Yabuzaki J, Kanehisa M, Yamashita A, Oshima K, Furuya K, Yoshino C, Shiba T, Hattori M, Ogasawara N, Hayashi H, Hiramatsu K. Whole genome sequencing of meticillin-resistant Staphylococcus aureus. Lancet. 2001 Apr 21;357(9264):1225-40.

Lade H, Kim JS. Molecular Determinants of β-Lactam Resistance in Methicillin-Resistant Staphylococcus aureus (MRSA): An Updated Review. Antibiotics (Basel). 2023 Aug 24;12(9):1362.

Laemmli UK. Cleavage of structural proteins during the assembly of the head of bacteriophage T4. Nature. 1970 Aug 15;227(5259):680-5.

Lakowicz, J. R. Principles of fluorescence spectroscopy. Third Edition edn, Springer US, (2010).

Lantzsch G, Binder H, Heerklotz H, Welzel P, Klose G. Aggregation Behavior of the Antibiotic Moenomycin A in Aqueous Solution. Langmuir 1998 Jul 3;14(15):4095-4104.

Laux C, Peschel A, Krismer B. Staphylococcus aureus Colonization of the Human Nose and Interaction with Other Microbiome Members. Microbiol Spectr. 2019 Mar;7(2).

Larson TR, Yother J. Streptococcus pneumoniae capsular polysaccharide is linked to peptidoglycan via a direct glycosidic bond to β-D-N-acetylglucosamine. Proc Natl Acad Sci U S A. 2017 May 30;114(22):5695-5700.

Lazarevic V, Margot P, Soldo B, Karamata D. Sequencing and analysis of the Bacillus subtilis lytRABC divergon: a regulatory unit encompassing the structural genes of the N-acetylmuramoyl-L-alanine amidase and its modifier. J Gen Microbiol. 1992 Sep;138(9):1949-61.

Lazarevic V, Karamata D. The tagGH operon of Bacillus subtilis 168 encodes a two-component ABC transporter involved in the metabolism of two wall teichoic acids. Mol Microbiol. 1995 Apr;16(2):345-55.

Lazarevic V, Abellan FX, Möller SB, Karamata D, Mauël C. Comparison of ribitol and glycerol teichoic acid genes in Bacillus subtilis W23 and 168: identical function, similar divergent organization, but different regulation. Microbiology (Reading). 2002 Mar;148(Pt 3):815-24.

Leclercq R, Derlot E, Weber M, Duval J, Courvalin P. Transferable vancomycin and teicoplanin resistance in Enterococcus faecium. Antimicrob Agents Chemother. 1989 Jan;33(1):10-5.

Lee J, Borukhov S. Bacterial RNA Polymerase-DNA Interaction-The Driving Force of Gene Expression and the Target for Drug Action. Front Mol Biosci. 2016 Nov 9;3:73.

Lee W, Schaefer K, Qiao Y, Srisuknimit V, Steinmetz H, Müller R, Kahne D, Walker S. The Mechanism of Action of Lysobactin. J Am Chem Soc. 2016 Jan 13;138(1):100-3.

Leibold, T., Sasse, F., Reichenbach, H. and Höfle, G. (2004), Cyrmenins, Novel Antifungal Peptides Containing a Nitrogen-Linked β-Methoxyacrylate Pharmacophore: Isolation and Structural Elucidation. Eur. J. Org. Chem., 2004: 431-435.

Lenoir D, Tschesche R, Wucherpfennig W, Huber G, Weidenmüller HL. Moenomycin A: further characterization and chemistry. Antimicrob Agents Chemother (Bethesda). 1969;9:144-7.

Łeski TA, Tomasz A. Role of penicillin-binding protein 2 (PBP2) in the antibiotic susceptibility and cell wall cross-linking of Staphylococcus aureus: evidence for the cooperative functioning of PBP2, PBP4, and PBP2A. J Bacteriol. 2005 Mar;187(5):1815-24.

Lev S. Non-vesicular lipid transport by lipid-transfer proteins and beyond. Nat Rev Mol Cell Biol. 2010 Oct;11(10):739-50.

Li FKK, Rosell FI, Gale RT, Simorre JP, Brown ED, Strynadka NCJ. Crystallographic analysis of Staphylococcus aureus LcpA, the primary wall teichoic acid ligase. J Biol Chem. 2020 Feb 28;295(9):2629-2639.

Lin JT, Connelly MB, Amolo C, Otani S, Yaver DS. Global transcriptional response of Bacillus subtilis to treatment with subinhibitory concentrations of antibiotics that inhibit protein synthesis. Antimicrob Agents Chemother. 2005 May;49(5):1915-26.

Ling LL, Schneider T, Peoples AJ, Spoering AL, Engels I, Conlon BP, Mueller A, Schäberle TF, Hughes DE, Epstein S, Jones M, Lazarides L, Steadman VA, Cohen DR, Felix CR, Fetterman KA, Millett WP, Nitti AG, Zullo AM, Chen C, Lewis K. A new antibiotic kills pathogens without detectable resistance. Nature. 2015 Jan 22;517(7535):455-9. Erratum in: Nature. 2015 Apr 16;520(7547):388.

Livingstone PG, Morphew RM, Whitworth DE. Myxobacteria are able to prey broadly upon clinically-relevant pathogens, exhibiting a prey range which cannot be explained by phylogeny. Front Microbiol. 2017;8:1593.

Lorian 5th edition, Chapter 9 (2005) Antimicrobial Combinations, in Antibiotics In Laboratory Medicine, pp. 365-441. Lippincott Williams and Wilkins, Philadelphia, PA.

Lovering AL, de Castro LH, Lim D, Strynadka NC. Structural insight into the transglycosylation step of bacterial cell-wall biosynthesis. Science. 2007 Mar 9;315(5817):1402-5.

Lovering AL, De Castro L, Strynadka NC. Identification of dynamic structural motifs involved in peptidoglycan glycosyltransfer. J Mol Biol. 2008 Oct 31;383(1):167-77.

Lu Y, Chen F, Zhao Q, Cao Q, Chen R, Pan H, Wang Y, Huang H, Huang R, Liu Q, Li M, Bae T, Liang H, Lan L. Modulation of MRSA virulence gene expression by the wall teichoic acid enzyme TarO. Nat Commun. 2023 Mar 22;14(1):1594.

Ma C, Yang X, Lewis PJ. Bacterial Transcription as a Target for Antibacterial Drug Development. Microbiol Mol Biol Rev. 2016 Jan 13;80(1):139-60.

Maidhof H, Reinicke B, Blümel P, Berger-Bächi B, Labischinski H. femA, which encodes a factor essential for expression of methicillin resistance, affects glycine content of peptidoglycan in methicillin-resistant and methicillin-susceptible Staphylococcus aureus strains. J Bacteriol. 1991 Jun;173(11):3507-13.

Manat G, Roure S, Auger R, Bouhss A, Barreteau H, Mengin-Lecreulx D, Touzé T. Deciphering the metabolism of undecaprenyl-phosphate: the bacterial cell-wall unit carrier at the membrane frontier. Microb Drug Resist. 2014 Jun;20(3):199-214.

Margolin W. Sculpting the bacterial cell. Curr Biol. 2009 Sep 15;19(17):R812-22.

Mariner K, McPhillie M, Trowbridge R, Smith C, O'Neill AJ, Fishwick CW, Chopra I. Activity of and development of resistance to corallopyronin A, an inhibitor of RNA polymerase. Antimicrob Agents Chemother. 2011 May;55(5):2413-6.

Marquardt JL, Siegele DA, Kolter R, Walsh CT. Cloning and sequencing of Escherichia coli murZ and purification of its product, a UDP-N-acetylglucosamine enolpyruvyl transferase. J Bacteriol. 1992 Sep;174(17):5748-52.

Mascher T, Margulis NG, Wang T, Ye RW, Helmann JD. Cell wall stress responses in Bacillus subtilis: the regulatory network of the bacitracin stimulon. Mol Microbiol. 2003 Dec;50(5):1591-604.

Mascher T, Zimmer SL, Smith TA, Helmann JD. Antibiotic-inducible promoter regulated by the cell envelope stress-sensing two-component system LiaRS of Bacillus subtilis. Antimicrob Agents Chemother. 2004 Aug;48(8):2888-96.

Massidda O, Kariyama R, Daneo-Moore L, Shockman GD. Evidence that the PBP 5 synthesis repressor (psr) of Enterococcus hirae is also involved in the regulation of cell wall composition and other cell wall-related properties. J Bacteriol. 1996 Sep;178(17):5272-8.

Mathew R, Chatterji D. The evolving story of the omega subunit of bacterial RNA polymerase. Trends Microbiol. 2006 Oct;14(10):450-5.

Matsuhashi M, Song MD, Ishino F, Wachi M, Doi M, Inoue M, Ubukata K, Yamashita N, Konno M. Molecular cloning of the gene of a penicillin-binding protein supposed to cause high resistance to beta-lactam antibiotics in Staphylococcus aureus. J Bacteriol. 1986 Sep;167(3):975-80.

Mazumder A, Kapanidis AN. Recent Advances in Understanding σ70-Dependent Transcription Initiation Mechanisms. J Mol Biol. 2019 Sep 20;431(20):3947-3959.

Memmi G, Filipe SR, Pinho MG, Fu Z, Cheung A. Staphylococcus aureus PBP4 is essential for beta-lactam resistance in community-acquired methicillin-resistant strains. Antimicrob Agents Chemother. 2008 Nov;52(11):3955-66.

Mengin-Lecreulx D, Texier L, Rousseau M, van Heijenoort J. The murG gene of Escherichia coli codes for the UDP-N-acetylglucosamine: N-acetylmuramyl-(pentapeptide) pyrophosphoryl-undecaprenol N-acetylglucosamine transferase involved in the membrane steps of peptidoglycan synthesis. J Bacteriol. 1991 Aug;173(15):4625-36.

Meredith TC, Swoboda JG, Walker S. Late-stage polyribitol phosphate wall teichoic acid biosynthesis in Staphylococcus aureus. J Bacteriol. 2008 Apr;190(8):3046-56.

Miroux B, Walker JE. Over-production of proteins in Escherichia coli: mutant hosts that allow synthesis of some membrane proteins and globular proteins at high levels. J Mol Biol. 1996 Jul 19;260(3):289-98.

Mistretta N, Brossaud M, Telles F, Sanchez V, Talaga P, Rokbi B. Glycosylation of Staphylococcus aureus cell wall teichoic acid is influenced by environmental conditions. Sci Rep. 2019 Mar 1;9(1):3212.

Mlynarczyk-Bonikowska B, Kowalewski C, Krolak-Ulinska A, Marusza W. Molecular Mechanisms of Drug Resistance in Staphylococcus aureus. Int J Mol Sci. 2022 Jul 22;23(15):8088.

Monk IR, Shah IM, Xu M, Tan MW, Foster TJ. Transforming the untransformable: application of direct transformation to manipulate genetically Staphylococcus aureus and Staphylococcus epidermidis. mBio. 2012 Mar 20;3(2):e00277-11.

Murakami K, Fujimura T, Doi M. Nucleotide sequence of the structural gene for the penicillin-binding protein 2 of Staphylococcus aureus and the presence of a homologous gene in other staphylococci. FEMS Microbiol Lett. 1994 Apr 1;117(2):131-6.

Mullis K, Faloona F, Scharf S, Saiki R, Horn G, Erlich H. Specific enzymatic amplification of DNA in vitro: the polymerase chain reaction. Cold Spring Harb Symp Quant Biol. 1986;51 Pt 1:263-73.

Münch D, Roemer T, Lee SH, Engeser M, Sahl HG, Schneider T. Identification and in vitro analysis of the GatD/MurT enzyme-complex catalyzing lipid II amidation in Staphylococcus aureus. PLoS Pathog. 2012 Jan;8(1):e1002509.

Nathenson SG, Ishimoto N, Anderson JS, Strominger JL. Enzymatic synthesis and immunochemistry of alpha- and beta-N-acetylglucosaminylribitol linkages in teichoic acids from several strains of Staphylococcus aureus. J Biol Chem. 1966 Feb 10;241(3):651-8.

Naumova IB, Shashkov AS, Tul'skaya EM, Streshinskaya GM, Kozlova YI, Potekhina NV, Evtushenko LI, Stackebrandt E. Cell wall teichoic acids: structural diversity, species specificity in the genus Nocardiopsis, and chemotaxonomic perspective. FEMS Microbiol Rev. 2001 May;25(3):269-84.

Nega M, Tribelli PM, Hipp K, Stahl M, Götz F. New insights in the coordinated amidase and glucosaminidase activity of the major autolysin (Atl) in Staphylococcus aureus. Commun Biol. 2020 Nov 20;3(1):695.

Neuhaus FC, Baddiley J. A continuum of anionic charge: structures and functions of D-alanyl-teichoic acids in gram-positive bacteria. Microbiol Mol Biol Rev. 2003 Dec;67(4):686-723.

Nilsson IM, Lee JC, Bremell T, Rydén C, Tarkowski A. The role of staphylococcal polysaccharide microcapsule expression in septicemia and septic arthritis. Infect Immun. 1997 Oct;65(10):4216-21.

Nikaido H. Molecular basis of bacterial outer membrane permeability revisited. Microbiol Mol Biol Rev. 2003 Dec;67(4):593-656.

Nomura R, Nakaminami H, Takasao K, Muramatsu S, Kato Y, Wajima T, Noguchi N. A class A β-lactamase produced by borderline oxacillin-resistant Staphylococcus aureus hydrolyses oxacillin. J Glob Antimicrob Resist. 2020 Sep;22:244-247.

Novick R. Properties of a cryptic high-frequency transducing phage in Staphylococcus aureus. Virology. 1967 Sep;33(1):155-66.

Olivares-Illana V, Meyer P, Bechet E, Gueguen-Chaignon V, Soulat D, Lazereg-Riquier S, Mijakovic I, Deutscher J, Cozzone AJ, Laprévote O, Morera S, Grangeasse C, Nessler S. Structural basis for the regulation mechanism of the tyrosine kinase CapB from Staphylococcus aureus. PLoS Biol. 2008 Jun 10;6(6):e143.

O'Neill J. Review on Antimicrobial Resistance Antimicrobial Resistance: Tackling a crisis for the health and wealth of nations. London: Review on Antimicrobial Resistance; 2014. Available from: https://amr-review.org/sites/default/files/AMR%20Review%20Paper%20-%20Tackling%20a%20crisis%20for%20the%20health%20and%20wealth%20of%20nations_1.pdf. Date accessed: November 16, 2023.

Ophir T, Gutnick DL. A role for exopolysaccharides in the protection of microorganisms from desiccation. Appl Environ Microbiol. 1994 Feb;60(2):740-5.

Oshida T, Sugai M, Komatsuzawa H, Hong YM, Suginaka H, Tomasz A. A Staphylococcus aureus autolysin that has an N-acetylmuramoyl-L-alanine amidase domain and an endo-beta-N-acetylglucosaminidase domain: cloning, sequence analysis, and characterization. Proc Natl Acad Sci U S A. 1995 Jan 3;92(1):285-9.

Ostash B, Doud EH, Lin C, Ostash I, Perlstein DL, Fuse S, Wolpert M, Kahne D, Walker S. Complete characterization of the seventeen step moenomycin biosynthetic pathway. Biochemistry. 2009 Sep 22;48(37):8830-41.

Ostash B, Walker S. Moenomycin family antibiotics: chemical synthesis, biosynthesis, and biological activity. Nat Prod Rep. 2010 Nov;27(11):1594-617.

Ostash B, Makitrynskyy R, Yushchuk O, Fedorenko V. Structural diversity, bioactivity, and biosynthesis of phosphoglycolipid family antibiotics: Recent advances. BBA Adv. 2022 Nov 17;2:100065.

Ou LT, Marquis RE. Electromechanical interactions in cell walls of gram-positive cocci. J Bacteriol. 1970 Jan;101(1):92-101.

Over B, Heusser R, McCallum N, Schulthess B, Kupferschmied P, Gaiani JM, Sifri CD, Berger-Bächi B, Stutzmann Meier P. LytR-CpsA-Psr proteins in Staphylococcus aureus display partial functional redundancy and the deletion of all three severely impairs septum placement and cell separation. FEMS Microbiol Lett. 2011 Jul;320(2):142-51.

Pan T, Guan J, Li Y, Sun B. LcpB Is a Pyrophosphatase Responsible for Wall Teichoic Acid Synthesis and Virulence in Staphylococcus aureus Clinical Isolate ST59. Front Microbiol. 2021 Dec 16;12:788500. Erratum in: Front Microbiol. 2023 Jul 04;14:1229396.

Parenti F, Pagani H, Beretta G. Lipiarmycin, a new antibiotic from Actinoplanes. I. Description of the producer strain and fermentation studies. J Antibiot (Tokyo). 1975 Apr;28(4):247-52.

Parenti F, Beretta G, Berti M, Arioli V. Teichomycins, new antibiotics from Actinoplanes teichomyceticus Nov. Sp. I. Description of the producer strain, fermentation studies and biological properties. J Antibiot (Tokyo). 1978 Apr;31(4):276-83.

Park JT. Uridine-5'-pyrophosphate derivatives. II. A structure common to three derivatives. J Biol Chem. 1952 Feb;194(2):885-95.

Park JT, Shaw DR, Chatterjee AN, Mirelman D, Wu T. Mutants of staphylococci with altered cell walls. Ann N Y Acad Sci. 1974 Jul 31;236(0):54-62.

Pasquina LW, Santa Maria JP, Walker S. Teichoic acid biosynthesis as an antibiotic target. Curr Opin Microbiol. 2013 Oct;16(5):531-7.

Patin D, Boniface A, Kovač A, Hervé M, Dementin S, Barreteau H, Mengin-Lecreulx D, Blanot D. Purification and biochemical characterization of Mur ligases from Staphylococcus aureus. Biochimie. 2010 Dec;92(12):1793-800.

Percy MG, Gründling A. Lipoteichoic acid synthesis and function in gram-positive bacteria. Annu Rev Microbiol. 2014;68:81-100.

Pereira MP, D'Elia MA, Troczynska J, Brown ED. Duplication of teichoic acid biosynthetic genes in Staphylococcus aureus leads to functionally redundant poly(ribitol phosphate) polymerases. J Bacteriol. 2008 Aug;190(16):5642-9.

Pereira SF, Henriques AO, Pinho MG, de Lencastre H, Tomasz A. Role of PBP1 in cell division of Staphylococcus aureus. J Bacteriol. 2007 May;189(9):3525-31.

Pérez J, Moraleda-Muñoz A, Marcos-Torres FJ, Muñoz-Dorado J. Bacterial predation: 75 years and counting! Environ Microbiol. 2016;18(3):766–779.

Peschel A, Otto M, Jack RW, Kalbacher H, Jung G, Götz F. Inactivation of the dlt operon in Staphylococcus aureus confers sensitivity to defensins, protegrins, and other antimicrobial peptides. J Biol Chem. 1999 Mar 26;274(13):8405-10.

Peschel A, Vuong C, Otto M, Götz F. The D-alanine residues of Staphylococcus aureus teichoic acids alter the susceptibility to vancomycin and the activity of autolytic enzymes. Antimicrob Agents Chemother. 2000 Oct;44(10):2845-7.

Pettersen EF, Goddard TD, Huang CC, Couch GS, Greenblatt DM, Meng EC, Ferrin TE. UCSF Chimera--a visualization system for exploratory research and analysis. J Comput Chem. 2004 Oct;25(13):1605-12.

Pfaller MA. Flavophospholipol use in animals: positive implications for antimicrobial resistance based on its microbiologic properties. Diagn Microbiol Infect Dis. 2006 Oct;56(2):115-21.

Pinho MG, de Lencastre H, Tomasz A. Cloning, characterization, and inactivation of the gene pbpC, encoding penicillin-binding protein 3 of Staphylococcus aureus. J Bacteriol. 2000 Feb;182(4):1074-9.

Pinho MG, de Lencastre H, Tomasz A. An acquired and a native penicillin-binding protein cooperate in building the cell wall of drug-resistant staphylococci. Proc Natl Acad Sci U S A. 2001 Sep 11;98(19):10886-91.

Pinho MG, Errington J. Recruitment of penicillin-binding protein PBP2 to the division site of Staphylococcus aureus is dependent on its transpeptidation substrates. Mol Microbiol. 2005 Feb;55(3):799-807.

Pinho MG, Kjos M, Veening JW. How to get (a)round: mechanisms controlling growth and division of coccoid bacteria. Nat Rev Microbiol. 2013 Sep;11(9):601-14.

Pless DD, Neuhaus FC. Initial membrane reaction in peptidoglycan synthesis. Lipid dependence of phospho-n-acetylmuramyl-pentapeptide translocase (exchange reaction). J Biol Chem. 1973 Mar 10;248(5):1568-76.

Pöhlmann-Dietze P, Ulrich M, Kiser KB, Döring G, Lee JC, Fournier JM, Botzenhart K, Wolz C. Adherence of Staphylococcus aureus to endothelial cells: influence of capsular polysaccharide, global regulator agr, and bacterial growth phase. Infect Immun. 2000 Sep;68(9):4865-71.

Puls JS, Brajtenbach D, Schneider T, Kubitscheck U, Grein F. Inhibition of peptidoglycan synthesis is sufficient for total arrest of staphylococcal cell division. Sci Adv. 2023 Mar 22;9(12):eade9023.

Pushkaran AC, Nataraj N, Nair N, Götz F, Biswas R, Mohan CG. Understanding the Structure-Function Relationship of Lysozyme Resistance in Staphylococcus aureus by Peptidoglycan O-Acetylation Using Molecular Docking, Dynamics, and Lysis Assay. J Chem Inf Model. 2015 Apr 27;55(4):760-70.

Qamar A, Golemi-Kotra D. Dual roles of FmtA in Staphylococcus aureus cell wall biosynthesis and autolysis. Antimicrob Agents Chemother. 2012 Jul;56(7):3797-805.

Qi ZD, Lin Y, Zhou B, Ren XD, Pang DW, Liu Y. Characterization of the mechanism of the Staphylococcus aureus cell envelope by bacitracin and bacitracin-metal ions. J Membr Biol. 2008 Sep-Oct;225(1-3):27-37.

Qiao Y, Lebar MD, Schirner K, Schaefer K, Tsukamoto H, Kahne D, Walker S. Detection of lipid-linked peptidoglycan precursors by exploiting an unexpected transpeptidase reaction. J Am Chem Soc. 2014 Oct 22;136(42):14678-81.

Quinn GA, Banat AM, Abdelhameed AM, Banat IM. Streptomyces from traditional medicine: sources of new innovations in antibiotic discovery. J Med Microbiol. 2020 Aug;69(8):1040-1048.

Rahman MM, Hunter HN, Prova S, Verma V, Qamar A, Golemi-Kotra D. The Staphylococcus aureus Methicillin Resistance Factor FmtA Is a d-Amino Esterase That Acts on Teichoic Acids. mBio. 2016 Feb 9;7(1):e02070-15.

Rajagopal M, Walker S. Envelope Structures of Gram-Positive Bacteria. Curr Top Microbiol Immunol. 2017;404:1-44.

Rammelkamp CH, Maxon T. Resistance of Staphylococcus aureus to the Action of Penicillin. Proceedings of the Society for Experimental Biology and Medicine. 1942;51(3):386-389.

Rausch M, Deisinger JP, Ulm H, Müller A, Li W, Hardt P, Wang X, Li X, Sylvester M, Engeser M, Vollmer W, Müller CE, Sahl HG, Lee JC, Schneider T. Coordination of capsule assembly and cell wall biosynthesis in Staphylococcus aureus. Nat Commun. 2019 Mar 29;10(1):1404.

Rebets Y, Lupoli T, Qiao Y, Schirner K, Villet R, Hooper D, Kahne D, Walker S. Moenomycin resistance mutations in Staphylococcus aureus reduce peptidoglycan chain length and cause aberrant cell division. ACS Chem Biol. 2014 Feb 21;9(2):459-67.

Reed P, Veiga H, Jorge AM, Terrak M, Pinho MG. Monofunctional transglycosylases are not essential for Staphylococcus aureus cell wall synthesis. J Bacteriol. 2011 May;193(10):2549-56.

Reichenbach H. Myxobacteria, producers of novel bioactive substances. J Ind Microbiol Biotechnol. 2001 Sep;27(3):149-56.

Reichmann NT, Cassona CP, Gründling A. Revised mechanism of D-alanine incorporation into cell wall polymers in Gram-positive bacteria. Microbiology (Reading). 2013 Sep;159(Pt 9):1868-1877.

Reichmann NT, Tavares AC, Saraiva BM, Jousselin A, Reed P, Pereira AR, Monteiro JM, Sobral RG, VanNieuwenhze MS, Fernandes F, Pinho MG. SEDS-bPBP pairs direct lateral and septal peptidoglycan synthesis in Staphylococcus aureus. Nat Microbiol. 2019 Aug;4(8):1368-1377.

Rick PD, Hubbard GL, Kitaoka M, Nagaki H, Kinoshita T, Dowd S, Simplaceanu V, Ho C. Characterization of the lipid-carrier involved in the synthesis of enterobacterial common antigen (ECA) and identification of a novel phosphoglyceride in a mutant of Salmonella typhimurium defective in ECA synthesis. Glycobiology. 1998 Jun;8(6):557-67.

Roberson EB, Firestone MK. Relationship between Desiccation and Exopolysaccharide Production in a Soil Pseudomonas sp. Appl Environ Microbiol. 1992 Apr;58(4):1284-91.

Robert X, Gouet P. Deciphering key features in protein structures with the new ENDscript server. Nucl. Acids Res. 2014 42(W1), W320-W324.

Rocchetta HL, Burrows LL, Pacan JC, Lam JS. Three rhamnosyltransferases responsible for assembly of the A-band D-rhamnan polysaccharide in Pseudomonas aeruginosa: a fourth transferase, WbpL, is required for the initiation of both A-band and B-band lipopolysaccharide synthesis. Mol Microbiol. 1998 Jun;28(6):1103-19.

Rogers HJ, Perkins HR, Ward JB. Microbial Cell Walls and Membranes. London: Chapman and Hall; 1980.

Rohrer S, Ehlert K, Tschierske M, Labischinski H, Berger-Bächi B. The essential Staphylococcus aureus gene fmhB is involved in the first step of peptidoglycan pentaglycine interpeptide formation. Proc Natl Acad Sci U S A. 1999 Aug 3;96(16):9351-6.

Rossi J, Bischoff M, Wada A, Berger-Bächi B. MsrR, a putative cell envelope-associated element involved in Staphylococcus aureus sarA attenuation. Antimicrob Agents Chemother. 2003 Aug;47(8):2558-64.

Rouser G, Fkeischer S, Yamamoto A. Two dimensional then layer chromatographic separation of polar lipids and determination of phospholipids by phosphorus analysis of spots. Lipids. 1970 May;5(5):494-6.

Ruiz N. Bioinformatics identification of MurJ (MviN) as the peptidoglycan lipid II flippase in Escherichia coli. Proc Natl Acad Sci U S A. 2008 Oct 7;105(40):15553-7.

Sacco MD, Hammond LR, Noor RE, Bhattacharya D, Madsen JJ, Zhang X, Butler SG, Kemp MT, Jaskolka-Brown AC, Khan SJ, Gelis I, Eswara PJ, Chen Y. Staphylococcus aureus FtsZ and PBP4 bind to the conformationally dynamic N-terminal domain of GpsB. bioRxiv 2022.10.25.513704.

Sadovskaya I, Vinogradov E, Courtin P, Armalyte J, Meyrand M, Giaouris E, Palussière S, Furlan S, Péchoux C, Ainsworth S, Mahony J, van Sinderen D, Kulakauskas S, Guérardel Y, Chapot-Chartier MP. Another Brick in the Wall: a Rhamnan Polysaccharide Trapped inside Peptidoglycan of Lactococcus lactis. mBio. 2017 Sep 12;8(5):e01303-17.

Sambrook J, Russel DW (2001). Molecular Cloning: A Laboratory Manual 3rd Ed. Cold Spring Harbor Laboratory Press. Cold Spring Harbor, NY.

Sanger F, Nicklen S, Coulson AR. DNA sequencing with chain-terminating inhibitors. Proc Natl Acad Sci U S A. 1977 Dec;74(12):5463-7.

Santiago M, Matano LM, Moussa SH, Gilmore MS, Walker S, Meredith TC. A new platform for ultra-high density Staphylococcus aureus transposon libraries. BMC Genomics. 2015 Mar 29;16(1):252.

Sass P, Bierbaum G. Native graS mutation supports the susceptibility of Staphylococcus aureus strain SG511 to antimicrobial peptides. Int J Med Microbiol. 2009 Jun;299(5):313-22.

Sauvage E, Kerff F, Terrak M, Ayala JA, Charlier P. The penicillin-binding proteins: structure and role in peptidoglycan biosynthesis. FEMS Microbiol Rev. 2008 Mar;32(2):234-58. Erratum in: FEMS Microbiol Rev. 2008 May;32(3):556.

Savage PB. Multidrug-resistant bacteria: overcoming antibiotic permeability barriers of gram-negative bacteria. Ann Med. 2001 Apr;33(3):167-71.

Schäberle TF, Lohr F, Schmitz A, König GM. Antibiotics from myxobacteria. Nat Prod Rep. 2014a Jul;31(7):953-72.

Schäberle TF, Schiefer A, Schmitz A, König GM, Hoerauf A, Pfarr K. Corallopyronin A - a promising antibiotic for treatment of filariasis. Int J Med Microbiol. 2014b Jan;304(1):72-8.

Schaefer K, Matano LM, Qiao Y, Kahne D, Walker S. In vitro reconstitution demonstrates the cell wall ligase activity of LCP proteins. Nat Chem Biol. 2017 Apr;13(4):396-401.

Schaefer K, Owens TW, Kahne D, Walker S. Substrate Preferences Establish the Order of Cell Wall Assembly in Staphylococcus aureus. J Am Chem Soc. 2018 Feb 21;140(7):2442-2445.

Schlag M, Biswas R, Krismer B, Kohler T, Zoll S, Yu W, Schwarz H, Peschel A, Götz F. Role of staphylococcal wall teichoic acid in targeting the major autolysin Atl. Mol Microbiol. 2010 Feb;75(4):864-73.

Schleifer KH, Kandler O. Peptidoglycan types of bacterial cell walls and their taxonomic implications. Bacteriol Rev. 1972 Dec;36(4):407-77.

Schneider T, Senn MM, Berger-Bächi B, Tossi A, Sahl HG, Wiedemann I. In vitro assembly of a complete, pentaglycine interpeptide bridge containing cell wall precursor (lipid II-Gly5) of Staphylococcus aureus. Mol Microbiol. 2004 Jul;53(2):675-85.

Schneider T, Sahl HG. An oldie but a goodie - cell wall biosynthesis as antibiotic target pathway. Int J Med Microbiol. 2010a Feb;300(2-3):161-9.

Schneider T, Sahl HG. Lipid II and other bactoprenol-bound cell wall precursors as drug targets. Curr Opin Investig Drugs. 2010b Feb;11(2):157-64.

Sears P, Ichikawa Y, Ruiz N, Gorbach S. Advances in the treatment of Clostridium difficile with fidaxomicin: a narrow spectrum antibiotic. Ann N Y Acad Sci. 2013 Jul;1291:33-41.

Sensi P. History of the development of rifampin. Rev Infect Dis. 1983 Jul-Aug;5 Suppl 3:S402-6.

Severin A, Tabei K, Tenover F, Chung M, Clarke N, Tomasz A. High level oxacillin and vancomycin resistance and altered cell wall composition in Staphylococcus aureus carrying the staphylococcal mecA and the enterococcal vanA gene complex. J Biol Chem. 2004 Jan 30;279(5):3398-407.

Sewell EW, Brown ED. Taking aim at wall teichoic acid synthesis: new biology and new leads for antibiotics. J Antibiot (Tokyo). 2014 Jan;67(1):43-51.

Sham LT, Butler EK, Lebar MD, Kahne D, Bernhardt TG, Ruiz N. Bacterial cell wall. MurJ is the flippase of lipid-linked precursors for peptidoglycan biogenesis. Science. 2014 Jul 11;345(6193):220-2.

Sidders AE, Kedziora KM, Arts M, Daniel JM, de Benedetti S, Beam JE, Bui DT, Parsons JB, Schneider T, Rowe SE, Conlon BP. Antibiotic-induced accumulation of lipid II synergizes with antimicrobial fatty acids to eradicate bacterial populations. Elife. 2023 Mar 6;12:e80246.

Siegel SD, Amer BR, Wu C, Sawaya MR, Gosschalk JE, Clubb RT, Ton-That H. Structure and Mechanism of LcpA, a Phosphotransferase That Mediates Glycosylation of a Gram-Positive Bacterial Cell Wall-Anchored Protein. mBio. 2019 Feb 19;10(1):e01580-18. Erratum in: MBio. 2019 Apr 16;10(2).

Silhavy TJ, Kahne D, Walker S. The bacterial cell envelope. Cold Spring Harb Perspect Biol. 2010 May;2(5):a000414.

Singh SB, Phillips JW, Wang J. Highly sensitive target-based whole-cell antibacterial discovery strategy by antisense RNA silencing. Curr Opin Drug Discov Devel. 2007 Mar;10(2):160-6.

Snowden MA, Perkins HR, Wyke AW, Hayes MV, Ward JB. Cross-linking and O-acetylation of newly synthesized peptidoglycan in Staphylococcus aureus H. J Gen Microbiol. 1989 Nov;135(11):3015-22.

Sobhanifar S, Worrall LJ, Gruninger RJ, Wasney GA, Blaukopf M, Baumann L, Lameignere E, Solomonson M, Brown ED, Withers SG, Strynadka NC. Structure and mechanism of Staphylococcus aureus TarM, the wall teichoic acid α-glycosyltransferase. Proc Natl Acad Sci U S A. 2015 Feb 10;112(6):E576-85.

Soldo B, Lazarevic V, Karamata D. tagO is involved in the synthesis of all anionic cell-wall polymers in Bacillus subtilis 168. Microbiology (Reading). 2002a Jul;148(Pt 7):2079-2087.

Soldo B, Lazarevic V, Pooley HM, Karamata D. Characterization of a Bacillus subtilis thermosensitive teichoic acid-deficient mutant: gene mnaA (yvyH) encodes the UDP-N-acetylglucosamine 2-epimerase. J Bacteriol. 2002b Aug;184(15):4316-20.

Song MD, Wachi M, Doi M, Ishino F, Matsuhashi M. Evolution of an inducible penicillin-target protein in methicillin-resistant Staphylococcus aureus by gene fusion. FEBS Lett. 1987 Aug 31;221(1):167-71.

Sperandeo P, Martorana AM, Polissi A. The lipopolysaccharide transport (Lpt) machinery: A nonconventional transporter for lipopolysaccharide assembly at the outer membrane of Gram-negative bacteria. J Biol Chem. 2017 Nov 3;292(44):17981-17990

Spinosa MR, Progida C, Talà A, Cogli L, Alifano P, Bucci C. The Neisseria meningitidis capsule is important for intracellular survival in human cells. Infect Immun. 2007 Jul;75(7):3594-603.

Srivastava A, Talaue M, Liu S, Degen D, Ebright RY, Sineva E, Chakraborty A, Druzhinin SY, Chatterjee S, Mukhopadhyay J, Ebright YW, Zozula A, Shen J, Sengupta S, Niedfeldt RR, Xin C, Kaneko T, Irschik H, Jansen R, Donadio S, Connell N, Ebright RH. New target for inhibition of bacterial RNA polymerase: 'switch region'. Curr Opin Microbiol. 2011 Oct;14(5):532-43.

Staubitz P, Neumann H, Schneider T, Wiedemann I, Peschel A. MprF-mediated biosynthesis of lysylphosphatidylglycerol, an important determinant in staphylococcal defensin resistance. FEMS Microbiol Lett. 2004 Feb 9;231(1):67-71.

Steele VR, Bottomley AL, Garcia-Lara J, Kasturiarachchi J, Foster SJ. Multiple essential roles for EzrA in cell division of Staphylococcus aureus. Mol Microbiol. 2011 Apr;80(2):542-55.

Stefanović C, Hager FF, Schäffer C. LytR-CpsA-Psr Glycopolymer Transferases: Essential Bricks in Gram-Positive Bacterial Cell Wall Assembly. Int J Mol Sci. 2021 Jan 18;22(2):908.

Stembera K, Vogel S, Buchynskyy A, Ayala JA, Welzel P. A surface plasmon resonance analysis of the interaction between the antibiotic moenomycin A and penicillin-binding protein 1b. Chembiochem. 2002 Jun 3;3(6):559-65.

Stryjewski ME, Corey GR. Methicillin-resistant Staphylococcus aureus: an evolving pathogen. Clin Infect Dis. 2014 Jan;58 Suppl 1:S10-9.

Sung MT, Lai YT, Huang CY, Chou LY, Shih HW, Cheng WC, Wong CH, Ma C. Crystal structure of the membrane-bound bifunctional transglycosylase PBP1b from Escherichia coli. Proc Natl Acad Sci U S A. 2009 Jun 2;106(22):8824-9.

Sutton JAF, Carnell OT, Lafage L, Gray J, Biboy J, Gibson JF, Pollitt EJG, Tazoll SC, Turnbull W, Hajdamowicz NH, Salamaga B, Pidwill GR, Condliffe AM, Renshaw SA, Vollmer W, Foster SJ. Staphylococcus aureus cell wall structure and dynamics during host-pathogen interaction. PLoS Pathog. 2021 Mar 31;17(3):e1009468.

Sutton JAF, Cooke M, Tinajero-Trejo M, Wacnik K, Salamaga B, Portman-Ross C, Lund VA, Hobbs JK, Foster SJ. The roles of GpsB and DivIVA in Staphylococcus aureus growth and division. bioRxiv 2023.06.16.545239.

Swanson RN, Hardy DJ, Shipkowitz NL, Hanson CW, Ramer NC, Fernandes PB, Clement JJ. In vitro and in vivo evaluation of tiacumicins B and C against Clostridium difficile. Antimicrob Agents Chemother. 1991 Jun;35(6):1108-11.

Taguchi A, Welsh MA, Marmont LS, Lee W, Sjodt M, Kruse AC, Kahne D, Bernhardt TG, Walker S. FtsW is a peptidoglycan polymerase that is functional only in complex with its cognate penicillin-binding protein. Nat Microbiol. 2019 Apr;4(4):587-594.

Tan S, Ludwig KC, Müller A, Schneider T, Nodwell JR. The Lasso Peptide Siamycin-I Targets Lipid II at the Gram-Positive Cell Surface. ACS Chem Biol. 2019 May 17;14(5):966-974.

Taylor CM, Roberts IS. Capsular polysaccharides and their role in virulence. Contrib Microbiol. 2005;12:55-66.

Thakker M, Park JS, Carey V, Lee JC. Staphylococcus aureus serotype 5 capsular polysaccharide is antiphagocytic and enhances bacterial virulence in a murine bacteremia model. Infect Immun. 1998 Nov;66(11):5183-9.

Tipper DJ, Strominger JL, Ensign JC. Structure of the cell wall of Staphylococcus aureus, strain Copenhagen. VII. Mode of action of the bacteriolytic peptidase from Myxobacter and the isolation of intact cell wall polysaccharides. Biochemistry. 1967 Mar;6(3):906-20.

Tomita S, Irisawa T, Tanaka N, Nukada T, Satoh E, Uchimura T, Okada S. Comparison of components and synthesis genes of cell wall teichoic acid among Lactobacillus plantarum strains. Biosci Biotechnol Biochem. 2010;74(5):928-33.

Tommasi R, Brown DG, Walkup GK, Manchester JI, Miller AA. ESKAPEing the labyrinth of antibacterial discovery. Nat Rev Drug Discov. 2015 Aug;14(8):529-42. Erratum in: Nat Rev Drug Discov. 2015 Sep;14(9):662.

Tong SY, Davis JS, Eichenberger E, Holland TL, Fowler VG Jr. Staphylococcus aureus infections: epidemiology, pathophysiology, clinical manifestations, and management. Clin Microbiol Rev. 2015 Jul;28(3):603-61.

Torii M, Kabat EA, Bezer AE. Separation of teichoic acid of Staphylococcus aureus into two immunologically distinct specific polysaccharides with alpha- and beta-N-acetylglucosaminyl linkages respectively. Antigenicity of teichoic acids in man. J Exp Med. 1964 Jul 1;120(1):13-29.

Torikata A, Yoshikawa H, Katayama T, Arai M, Nakahara M, Kitano N. Pholipomycin, a new member of phosphoglycolipid antibiotics. III. Biological properties. J Antibiot (Tokyo). 1977 Dec;30(12):1060-3.

Tsiodras S, Gold HS, Sakoulas G, Eliopoulos GM, Wennersten C, Venkataraman L, Moellering RC, Ferraro MJ. Linezolid resistance in a clinical isolate of Staphylococcus aureus. Lancet. 2001 Jul 21;358(9277):207-8.

Turner NA, Sharma-Kuinkel BK, Maskarinec SA, Eichenberger EM, Shah PP, Carugati M, Holland TL, Fowler VG Jr. Methicillin-resistant Staphylococcus aureus: an overview of basic and clinical research. Nat Rev Microbiol. 2019 Apr;17(4):203-218.

Typas A, Banzhaf M, Gross CA, Vollmer W. From the regulation of peptidoglycan synthesis to bacterial growth and morphology. Nat Rev Microbiol. 2012 Feb;10(2):123-36.

Tzianabos AO, Wang JY, Lee JC. Structural rationale for the modulation of abscess formation by Staphylococcus aureus capsular polysaccharides. Proc Natl Acad Sci U S A. 2001 Jul 31;98(16):9365-70.

Vaara M. Agents that increase the permeability of the outer membrane. Microbiol Rev. 1992 Sep;56(3):395-411.

van Dalen R, Peschel A, van Sorge NM. Wall Teichoic Acid in Staphylococcus aureus Host Interaction: (Trends in Microbiology. In press. Trends Microbiol. 2020 Oct;28(10):869. Erratum for: Trends Microbiol. 2020 Jun 12.

van Hal SJ, Paterson DL, Gosbell IB. Emergence of daptomycin resistance following vancomycin-unresponsive Staphylococcus aureus bacteraemia in a daptomycin-naïve patient--a review of the literature. Eur J Clin Microbiol Infect Dis. 2011 May;30(5):603-10.

van Heijenoort Y, van Heijenoort J. Biosynthesis of the peptidoglycan of Escherichia coli K-12: properties of the in vitro polymerization by transglycosylation. FEBS Lett. 1980 Feb 11;110(2):241-4.

van Heijenoort Y, Leduc M, Singer H, van Heijenoort J. Effects of moenomycin on Escherichia coli. J Gen Microbiol. 1987 Mar;133(3):667-74.

Vandooren J, Geurts N, Martens E, Van den Steen PE, Opdenakker G. Zymography methods for visualizing hydrolytic enzymes. Nat Methods. 2013 Mar;10(3):211-20.

Veiga H, Pinho MG. Inactivation of the SauI type I restriction-modification system is not sufficient to generate Staphylococcus aureus strains capable of efficiently accepting foreign DNA. Appl Environ Microbiol. 2009 May;75(10):3034-8.

Venugopal AA, Johnson S. Fidaxomicin: a novel macrocyclic antibiotic approved for treatment of Clostridium difficile infection. Clin Infect Dis. 2012 Feb 15;54(4):568-74.

Vergara-Irigaray M, Maira-Litrán T, Merino N, Pier GB, Penadés JR, Lasa I. Wall teichoic acids are dispensable for anchoring the PNAG exopolysaccharide to the Staphylococcus aureus cell surface. Microbiology (Reading). 2008 Mar;154(Pt 3):865-877.

Vinogradov E, Sadovskaya I, Li J, Jabbouri S. Structural elucidation of the extracellular and cell-wall teichoic acids of Staphylococcus aureus MN8m, a biofilm forming strain. Carbohydr Res. 2006 May 1;341(6):738-43.

Vogel S, Stembera K, Hennig L, Findeisen M, Giesa S, Welzel P, Lampilas M. Moenomycin analogues with modified lipid side chains from indium-mediated Barbier-type reactions. Tetrahedron. 2001a May 7;57(19):4139–46.

Vogel S, Stembera K, Hennig L, Findeisen M, Giesa S, Welzel P, Tillier C, Bonhomme C, Lampilas M. Moenomycin analogues with long-chain amine lipid parts from reductive aminations. Tetrahedron. 2001b May 7;57(19):4147–60.

Volke F, Waschipky R, Pampel A, Donnerstag A, Lantzsch G, Pfeiffer H, Richter W, Klose G, Welzel P. Characterisation of antibiotic moenomycin A interaction with phospholipid model membranes. Chem Phys Lipids. 1997 Feb 28;85(2):115-23.

Vollmer W, Blanot D, de Pedro MA. Peptidoglycan structure and architecture. FEMS Microbiol Rev. 2008 Mar;32(2):149-67.

Vollmer W. Structural variation in the glycan strands of bacterial peptidoglycan. FEMS Microbiol Rev. 2008 Mar;32(2):287-306.

Vollmer W, Seligman SJ. Architecture of peptidoglycan: more data and more models. Trends Microbiol. 2010 Feb;18(2):59-66.

Waldron DE, Lindsay JA. Sau1: a novel lineage-specific type I restriction-modification system that blocks horizontal gene transfer into Staphylococcus aureus and between S. aureus isolates of different lineages. J Bacteriol. 2006 Aug;188(15):5578-85.

Wallhausser KH, Nesemann G, Prave P, Steigler A. Moenomycin, a new antibiotic. I. Fermentation and isolation. Antimicrob Agents Chemother (Bethesda). 1965;5:734-6.

Walsh CT. Enzymes in the D-alanine branch of bacterial cell wall peptidoglycan assembly. J Biol Chem. 1989 Feb 15;264(5):2393-6.

Wang H, Gill CJ, Lee SH, Mann P, Zuck P, Meredith TC, Murgolo N, She X, Kales S, Liang L, Liu J, Wu J, Santa Maria J, Su J, Pan J, Hailey J, Mcguinness D, Tan CM, Flattery A, Walker S, Black T, Roemer T. Discovery of wall teichoic acid inhibitors as potential anti-MRSA β-lactam combination agents. Chem Biol. 2013 Feb 21;20(2):272-84.

Wann ER, Dassy B, Fournier JM, Foster TJ. Genetic analysis of the cap5 locus of Staphylococcus aureus. FEMS Microbiol Lett. 1999 Jan 1;170(1):97-103.

Ward JB. Teichoic and teichuronic acids: biosynthesis, assembly, and location. Microbiol Rev. 1981 Jun;45(2):211-43.

Weidenmaier C, Kokai-Kun JF, Kristian SA, Chanturiya T, Kalbacher H, Gross M, Nicholson G, Neumeister B, Mond JJ, Peschel A. Role of teichoic acids in Staphylococcus aureus nasal colonization, a major risk factor in nosocomial infections. Nat Med. 2004 Mar;10(3):243-5.

Weidenmaier C, Peschel A. Teichoic acids and related cell-wall glycopolymers in Gram-positive physiology and host interactions. Nat Rev Microbiol. 2008 Apr;6(4):276-87.

Weidenmaier C, Lee JC. Structure and Function of Surface Polysaccharides of Staphylococcus aureus. Curr Top Microbiol Immunol. 2017;409:57-93.

Weissman KJ, Müller R. Myxobacterial secondary metabolites: bioactivities and modes-of-action. Nat Prod Rep. 2010 Sep;27(9):1276-95.

Welzel P. Syntheses around the transglycosylation step in peptidoglycan biosynthesis. Chem Rev. 2005 Dec;105(12):4610-60.

Wenzel SC, Müller R. The impact of genomics on the exploitation of the myxobacterial secondary metabolome. Nat Prod Rep. 2009 Nov;26(11):1385-407.

WHO. Prioritization of pathogens to guide discovery, research and development of new antibiotics for drug-resistant bacterial infections, including tuberculosis. World Health Organization. 2017. https://apps.who.int/iris/handle/10665/311820. Lizenz: CC BY-NC-SA 3.0 IGO. Date accessed: April 25, 2023.

WHO. Antimicrobial resistance. World Health Organization. [updated 2021 Nov 17; retrieved 2023 Feb 19]. Available from https://www.who.int/news-room/fact-sheets/detail/antimicrobial-resistance. Date accessed: November 16, 2023.

WHO Access, Watch, Reserve (AWaRe) classification of antibiotics for evaluation and monitoring of use, 2021. Geneva: World Health Organization; 2021 (WHO/MHP/HPS/EML/2021.04). Licence: CC BY-NC-SA 3.0 IGO.

Wieser M, Denner EB, Kämpfer P, Schumann P, Tindall B, Steiner U, Vybiral D, Lubitz W, Maszenan AM, Patel BK, Seviour RJ, Radax C, Busse HJ. Emended descriptions of the genus Micrococcus, Micrococcus luteus (Cohn 1872) and Micrococcus lylae (Kloos et al. 1974). Int J Syst Evol Microbiol. 2002 Mar;52(Pt 2):629-37.

Wilkinson BJ, Holmes KM. Staphylococcus aureus cell surface: capsule as a barrier to bacteriophage adsorption. Infect Immun. 1979 Feb;23(2):549-52.

Winstel V, Sanchez-Carballo P, Holst O, Xia G, Peschel A. Biosynthesis of the unique wall teichoic acid of Staphylococcus aureus lineage ST395. mBio. 2014 Apr 8;5(2):e00869.

Wisseman CL Jr, Smadel JE, Hahn FE, Hopps HE. Mode of action of chloramphenicol. I. Action of chloramphenicol on assimilation of ammonia and on synthesis of proteins and nucleic acids in Escherichia coli. J Bacteriol. 1954 Jun;67(6):662-73.

Workman SD, Strynadka NCJ. A Slippery Scaffold: Synthesis and Recycling of the Bacterial Cell Wall Carrier Lipid. J Mol Biol. 2020 Aug 21;432(18):4964-4982.

Wong LH, Gatta AT, Levine TP. Lipid transfer proteins: the lipid commute via shuttles, bridges and tubes. Nat Rev Mol Cell Biol. 2019 Feb;20(2):85-101.

Wyke AW, Ward JB, Hayes MV, Curtis NA. A role in vivo for penicillin-binding protein-4 of Staphylococcus aureus. Eur J Biochem. 1981 Oct;119(2):389-93.

Xia G, Kohler T, Peschel A. The wall teichoic acid and lipoteichoic acid polymers of Staphylococcus aureus. Int J Med Microbiol. 2010a Feb;300(2-3):148-54.

Xia G, Maier L, Sanchez-Carballo P, Li M, Otto M, Holst O, Peschel A. Glycosylation of wall teichoic acid in Staphylococcus aureus by TarM. J Biol Chem. 2010b Apr 30;285(18):13405-15.

Yamada S, Sugai M, Komatsuzawa H, Nakashima S, Oshida T, Matsumoto A, Suginaka H. An autolysin ring associated with cell separation of Staphylococcus aureus. J Bacteriol. 1996 Mar;178(6):1565-71.

Yang F, Gao S, Yan J, Lin X, van der Veen S. Moenomycin is broadly active against multidrug-resistant Neisseria gonorrhoeae and clears an infection from a murine vaginal tract infection model. J Antimicrob Chemother. 2022 Aug 25;77(9):2461-2469.

Yokoyama K, Mizuguchi H, Araki Y, Kaya S, Ito E. Biosynthesis of linkage units for teichoic acids in gram-positive bacteria: distribution of related enzymes and their specificities for UDP-sugars and lipid-linked intermediates. J Bacteriol. 1989 Feb;171(2):940-6.

Yother J. Capsules of Streptococcus pneumoniae and other bacteria: paradigms for polysaccharide biosynthesis and regulation. Annu Rev Microbiol. 2011;65:563-81.

Yousefi M, Fallah F, Arshadi M, Pourmand MR, Hashemi A, Pourmand G. Identification of tigecycline- and vancomycin-resistant Staphylococcus aureus strains among patients with urinary tract infection in Iran. New Microbes New Infect. 2017 May 24;19:8-12.

Yuan Y, Fuse S, Ostash B, Sliz P, Kahne D, Walker S. Structural analysis of the contacts anchoring moenomycin to peptidoglycan glycosyltransferases and implications for antibiotic design. ACS Chem Biol. 2008 Jul 18;3(7):429-36.

Zapun A, Contreras-Martel C, Vernet T. Penicillin-binding proteins and beta-lactam resistance. FEMS Microbiol Rev. 2008 Mar;32(2):361-85.

Zhao G, Meier TI, Kahl SD, Gee KR, Blaszczak LC. BOCILLIN FL, a sensitive and commercially available reagent for detection of penicillin-binding proteins. Antimicrob Agents Chemother. 1999 May;43(5):1124-8.

Zoll S, Pätzold B, Schlag M, Götz F, Kalbacher H, Stehle T. Structural basis of cell wall cleavage by a staphylococcal autolysin. PLoS Pathog. 2010 Mar 12;6(3):e1000807.

Zoll S, Schlag M, Shkumatov AV, Rautenberg M, Svergun DI, Götz F, Stehle T. Ligand-binding properties and conformational dynamics of autolysin repeat domains in staphylococcal cell wall recognition. J Bacteriol. 2012 Aug;194(15):3789-802.

Zullo AM, Chen C, Lewis K. A new antibiotic kills pathogens without detectable resistance. Nature. 2015 Jan 22;517(7535):455-9. Erratum in: Nature. 2015 Apr 16;520(7547):388.